

**THE CHEMISTRY OF FULLERENES, POLYMERS, AND HOST/GUEST
INTERACTIONS**

Daniel Vernon Schoonover

Dissertation submitted to the faculty of the Virginia Polytechnic Institute and State University in
partial fulfillment of the requirements for the degree of

Doctor of Philosophy

In

Chemistry

Harry W. Gibson

Harry C. Dorn

Richard D. Gandour

Alan R. Esker

December 15, 2014

Blacksburg, Virginia

Keywords: fullerene, endohedral metallofullerene, host/guest, ionomer, polymer, purification,
isothermal titration calorimetry, imidazolium, paraquat, cryptand, pseudorotaxane

Copyright 2014

THE CHEMISTRY OF FULLERENES, POLYMERS, AND HOST/GUEST INTERACTIONS

Daniel Vernon Schoonover

ABSTRACT

The exploitation of the relationship between the chemical and physical properties of materials is the hallmark of advancing science throughout the world. The basic understanding of how and why molecules react and interact with each other in different environments allows for the discovery and implementation of new materials and devices that not only advance the state of human life but continually change the planet. The work described in this dissertation generally falls under three diverse categories: functionalization of fullerenes, investigation of host/guest interactions in solution, and the synthesis and characterization of ion containing polymers.

The separation and functionalization of fullerenes is a recent and exciting area of research. The separation methods outlined are intended to increase the availability of endohedral metallofullerenes by decreasing their cost of production. Functionalized fullerene species were achieved through Bingel and Prato reactions to provide materials with novel functional groups. These materials may be further utilized in photovoltaic or other organic electronic devices.

The characterization of noncovalent interactions between different molecules in solution is the focus of supramolecular chemistry. Isothermal Titration Calorimetry stands out as one of the best, among the many methods used to elucidate the characteristics of these systems. The binding of bis-imidazolium and paraquat guests with macrocyclic host molecules has been explored in this work. The measurements of the association constants for these systems will aid in the ongoing synthesis of new host/guest systems.

Ion containing polymers were synthesized and characterized for their use in electroactive devices. Imidazolium containing polymers with bulky anions were synthesized on low glass transition polymer chains. These materials had enhanced ion conductivity and may eventually be used in electronic actuator materials.

Dedication

Dedication is an appropriate word in the context of doctoral work. Without dedication and perseverance there is no hope of extricating oneself from the confines of graduate study. However, these things alone cannot suffice to deliver a student from his formal studies. Here I need to thank God, and my family, and friends, all of whom, stood with me during my sojourn here in the Gibson research group. Without the faith and optimism that I have received from these, I would never have come to this point. It is because of all of you that I can end my time here successfully and move on. My faith in the Almighty has been bolstered by this experience, and I eagerly await my next calling in life. I particularly want to thank my parents, Dianne and Elliott Schoonover for all of their love, support, and encouragement. My friends, the members of the research group, who offered knowledge and were eager to help me, particularly Hanlie Wessels who I hope will share the rest of my life. To all these people, and many more, I can only offer my most sincere and heartfelt thanks and gratitude, for helping me finish this work. Thank you.

Acknowledgements

Several people kindly and generously gave of their time and expertise in order that the following work could come to fruition. Kim Harich provided MALDI TOF analysis of fullerene derivatives. Hunter Champion completed cyclic voltammetry measurements on fullerene derivatives as well as constructing and characterizing a photovoltaic device with some of the fullerene derivatives with the help of Dr. R. Heflin and his students here at Virginia Tech. Jonathan Reid provided endohedral metallo fullerene containing soot and other materials, as well as a wealth of chromatographic knowledge. Dr. Minjae Lee and Dr. Manav Gupta both of the Gibson research group provided both materials and guidance in research. Finally Dr. U Hyeok Choi, and Mr. Renxuan Xie of the Colby research group at Penn State University provided dielectric spectroscopy measurements on imidazolium containing ion conductive materials. I would also like to thank the National Science Foundation, the National Institute of Standards and Technology, and the Virginia Tech Institute for Critical Technology and Applied Science for funding some of the research contained in this work.

Table of Contents

Part I: Fullerene Chemistry

Chapter 1: Introduction to Fullerenes	1
Chapter 2: Separation and Purification of Trimetallic Nitride Templated (TNT) Endohedral Metalofullerenes (EMF) Employing Exohedral Functionalization	27
Chapter 3: Prato Functionalization of Fullerenes	73
Chapter 4: Bingel Functionalization of Fullerenes	99

Part II: Host/Guest Chemistry

Chapter 5: Introduction to Isothermal Titration Microcalorimetry.....	113
Chapter 6: Complexation Behavior of Bisimidazolium Salts.....	130
Chapter 7: ITC Analysis of Polymeric Materials	158

Part III: Polymer Chemistry

Chapter 8: Synthesis of Imidazolium-Based Ion Conductive Polymers.....	178
Chapter 9: Removal of Tosyl Chloride from Solution Using Cellulosic Materials	204
Chapter 10: Conclusions and Future Work.....	219
Appendix: Size Exclusion Chromatography Instrumentation	A-1

List of Figures

Chapter 1: Introduction to Fullerenes

Figure 1.1 Structure of I_h $Sc_3N@C_{80}$1

Figure 1.2 Magnevist MRI contrast agent.3

Figure 1.3 Structure of coranulene.....9

Figure 1.4 HPLC stationary phase functional groups.14

Chapter 2: Separation and Purification of Trimetallic Nitride Templated (TNT)
Endohedral Metalofullerenes (EMF) Employing Exohedral Functionalization

Figure 2.1. Structure of C_{60} (left) $Sc_3N@C_{80}$ (right).27

Figure 2.2. HPLC chromatogram of a stock solution of fullerenes extracted from
Kratchmer-Huffman reactor soot (toluene, PYE functionalized silica gel, 1.0 mL/min).....29

Figure 2.3 Stacked chromatograms from initial furan extractions. The $Sc_3N@C_{80}$ is seen
at 17 minutes, C_{60} and C_{70} peaks are at 5 and 8 minutes respectively HPLC: 1.0 mL/min
toluene pyrene functionalized silica.....32

Figure 2.4. Stacked chromatogram showing the extracted fullerene and PAH material
after sonication for 4 hours with different solutions of furan and met35

Figure 2.5. Plot of various fullerenes extracted using different mixtures of furan and
methanol normalized by the amounts extracted with toluene.....36

Figure 2.6 Stacked chromatographic plot showing the functionalization of empty cage fullerenes and their coalescence into large peaks shortly after the void volume (approx. 3 mL). HPLC: pyrene functionalized silica, toluene 1.0 mL/min.39

Figure 2.7. Plot showing the area fraction of C₆₀ (black), C₇₀ (red), and Sc₃N@C₈₀ (blue) chromatographic peaks as the number of equivalents of cyclopentadiene increased. ... 40

Figure 2.8. Stacked chromatographic plot illustrating the purification steps for Sc₃N@C₈₀. Stock solution (green) was treated with cyclopentadiene (blue). The treated mixture was separated on silica gel to remove most of the functional material (red). Finally the mixture was purified by a single pass on the HPLC (black). HPLC: pyrene functionalized silica, toluene 1.0 mL/min.....41

Figure 2.9. MALDI TOF mass spectrum of purified Sc₃N@C₈₀. This material was obtained after cyclopentadiene treatment and one HPLC separation. The molecular weight of Sc₃N@C₈₀ is 1109 Da.....42

Figure 2.10. Stacked chromatographic plot showing the reversibility of the reaction with C₆₀. Fullerene extract was functionalized with cyclopentadiene and then subjected to different levels of vacuum and heat. Heating to 150 °C under 0.1 mm Hg reversed the reaction and gave peaks matching the starting materials. HPLC: pyrene functionalized silica, toluene 1 mL/min.43

Figure 2.11. Stacked chromatograms showing the functionalization of empty cage fullerenes with anthracene. The peaks for C₆₀ (5.6 min.) and C₇₀ (8.2 min) decrease in area over two days. HPLC: pyrene functionalized silica, toluene 1.0 mL/min.45

Figure 2.12. Plot of the relative peak areas of C_{60} (black), C_{70} (red), and $Sc_3N@C_{80}$ (blue) during the functionalization reaction with anthracene. The peak areas for both of the major empty cage fullerenes decrease over time, while the TNT EMF peak remains constant. This indicates that the Diels-Alder reaction is selective for the empty cage fullerenes.47

Figure 2.13. Stacked chromatographic traces of fullerene extract as it is reacted with isoprene over time. The peaks for C_{60} (5.8 min) and C_{70} (8.0 min) decrease in size and disappear entirely over time. The peak in the last two traces at 6 min. is not C_{60} but is probably the mono-adduct of C_{70} . HPLC: pyrene functionalized silica, toluene 1 mL/min.....49

Figure 2.14. Plot of the peak areas of C_{60} (black), C_{70} (red), and $Sc_3N@C_{80}$ (blue) relative to their initial areas, over time during the reaction with isoprene. The reactivity of C_{60} as compared to C_{70} is much higher. Most of the C_{60} peak area is gone by the end of the first day. The $Sc_3N@C_{80}$ peak area remains constant during the entire time.51

Figure 2.15. Stacked chromatograms showing the removal of mainly C_{60} by functionalization with furfuryl alcohol. HPLC: toluene 1 mL/min, pyrene functionalized silica.53

Figure 2.16. Mass spectrum of the crude reaction product of C_{60} and DETA.....56

Figure 2.17. Stacked chromatographic plots showing the conversion of empty cage fullerenes, after reaction with DETA, to amine functionalized material that elutes shortly after the void volume (approximately 3 minutes). The extent of conversion increases as

the number of equivalents of DETA increase. HPLC: pyrene functionalized silica, toluene 1 mL/min.....57

Figure 2.18. Plot of the chromatographic peak areas of C₆₀ (black), C₇₀ (red), and Sc₃N@C₈₀ (blue) as the molar equivalents of DETA in the reaction increase. The C₆₀ and C₇₀ peak areas decrease faster than the Sc₃N@C₈₀ peak.58

Figure 2.19. Stacked chromatograms showing the functionalization and removal (by precipitation) of empty cage fullerenes over time. The chromatogram for 12 hours of reaction time (violet) shows only small amounts of poly(aromatic hydrocarbon)s in addition to the Sc₃N@C₈₀ peak. HPLC: pyrene functionalized silica, toluene 1.0 mL/min.....59

Figure 2.20. Plot of chromatographic peak area for C₆₀ (black), C₇₀ (red), and Sc₃N@C₈₀ (blue). The empty cage peaks disappeared quickly over time due to reaction with DETA while the Sc₃N@C₈₀ peak retained much of its area. An excess of DETA (10 molar equivalents) was used for this study.60

Figure 2.21. MALDI TOF spectrum of the crude product of the reaction of C₆₀ and dimethyl sodium.....61

Figure 2.22. Stacked chromatograms showing the removal of fullerenes from solution after reacting with dimethyl sodium, precipitation and filtering. HPLC: pyrene functionalized silica, toluene 1.0 mL/min.....63

Chapter 3: Prato Functionalization of Fullerenes

Figure 3.1. HPLC trace of the reaction mixture of sarcosine and 4-(2'-hydroxyethoxy)benzaldehyde and C₆₀. The C₆₀ peak is at 14.9 minutes and the adduct peak is at 20 minutes (PYE functionalized silica 0.5 mL/min toluene).....76

Figure 3.2. HPLC trace of the purified reaction product of 4-(2'-hydroxyethoxy)benzaldehyde and sarcosine with C₆₀. Residual C₆₀ is seen at 12 minutes, the product at 18 minutes, and residual solvent at 7 minutes (PYE functionalized silica, 0.5 mL/min toluene).....77

Figure 3.3. ¹H NMR spectrum for the purified product of the reaction of 4-(2'-hydroxyethoxy)benzaldehyde, sarcosine and C₆₀ (CDCl₃ 500 MHz).78

Figure 3.4. MALDI TOF MS for the isolated product of the reaction of 4-(2'-hydroxyethoxy)benzaldehyde, sarcosine and C₆₀ (M+ = m/z 913 Da for C₇₁H₁₅NO₂)......79

Figure 3.5. HPLC trace of the reaction mixture from the reaction of 4-(3'-hydroxypropoxy)benzaldehyde, sarcosine and C₆₀. The peak for C₆₀ is seen at 12 minutes, and the adduct peak is at 17.5 minutes (PYE functionalized silica, 0.5 mL/min toluene).81

Figure 3.6. HPLC trace of the purified product of the reaction of 4-(3'-hydroxypropoxy)benzaldehyde, sarcosine and C₆₀ (PYE functionalized silica 0.5 mL/min toluene).82

Figure 3.7. ¹H NMR spectrum of the product of the reaction of 4-(3'-hydroxypropoxy)benzaldehyde, sarcosine and C₆₀ (CDCl₃, 500 MHz).83

Figure 3.8. MALDI TOF MS of the product of the reaction of 4-(3'-hydroxypropoxy)benzaldehyde, sarcosine and C ₆₀ . M ⁺ = m/z 927 Da (C ₇₂ H ₁₇ NO ₂).	84
Figure 3.9. Cyclic voltammogram traces for mono- (dark blue), bis- (light blue) and tris-3-(4'-(1''-methylpyrrolidin-2''-yl)phenoxy)propan-1-ol adducts of C ₆₀ (red).	85
Figure 3.10. Current/voltage plot for a photovoltaic device constructed from tris-3-(4'-(1''-methylpyrrolidin-2''-yl)phenoxy)propan-1-ol adduct of C ₆₀ and P3HT, illuminated with AM 1.5 light before and after annealing the device at 110 °C.	87
Figure 3.11. HPLC chromatogram of the propiolate product derived from 3-(4'-(1''-methylpyrrolidin-2''-yl)phenoxy)propan-1-ol Functionalized C ₆₀ . Pyrene functionalized silica, toluene 0.5 mL/min.	89
Figure 3.12. ¹ H NMR spectra showing the propiolate ester of 3-(4'-(1''-methylpyrrolidin-2''-yl)phenoxy)propan-1-ol Functionalized C ₆₀ . The presence of the alkynyl proton at 2.86 ppm indicates the product. (CDCl ₃ , 500 MHz).....	90
Figure 3.15. MALDI TOF MS of the C ₆₀ propiolate ester product. M ⁺ = m/z 979 Da for C ₂₇ H ₁₇ NO ₃	91
Figure 3.16. HPLC chromatogram of C ₆₀ propiolate ester (PYE functionalized silica, toluene 0.5 mL/min).....	93
Figure 3.17. HPLC chromatogram for the click reaction mixture of C ₆₀ propiolate and 1,4-bis(azidomethyl)benzene (PYE functionalized silica, toluene 0.5 mL/min.).....	94

Chapter 4: Bingel Functionalization of Fullerenes

Figure 4.1. MALDI TOF MS of the mono-adduct of Meldrum's acid and C₆₀ indicating the degradation products of the adduct and the presence of C₆₀ ketene.103

Figure 4.2. HPLC chromatogram showing the major dimer product from thermal decomposition of C₆₀ Meldrum's acid adduct at 26.9 minutes. The other major peak at 10.8 minutes is residual starting material.105

Figure 4.3. MALDI TOF MS for the C₆₀ dimer product showing several degradation products as well as the dimer at m/z 1519 Da (M-1)⁺.106

Figure 4.4. ¹³C NMR spectrum for the dimer synthesized from C₆₀ Meldrum's acid mono-adduct
.....107

Figure 4.5. MALDI TOF MS of the fullerene polymer made from the C₆₀ Meldrum's acid bis-adduct showing up to six repeat units.109

Chapter 5: Introduction to Isothermal Titration Microcalorimetry

Figure 5.1. Cutaway drawing and diagram of the inside of the Microcal MCS ITC instrument.
.....115

Figure 5.2. Cutaway drawing of the ITC titration cell including the working volume V_o and the volume ejected (ΔV), after every injection of titrant.118

Figure 5.3. Plot of the ITC scaling factor vs. the volumetric heat capacity of the solvent used to calibrate the instrument.126

Figure 5.4. Enthalpogram of a timed pulse experiment showing 5 pulses of different heating rates, and the linear plot of their integrated energies. Different heating rates are used in order to determine the linearity of the response coefficient over the heating range of the instrument.

.....127

Chapter 6: Complexation Behavior of Bisimidazolium Salts

Figure 6.1. Chemical structures of the butylene bisimidazolium **G3(PF₆)₂** and dibenzo-24-crown-8.135

Figure 6.2. Enthalpogram for the binding of **G3(PF₆)₂** (806.5 mM) and dibenzo-24-crown-8 (30.2 mM) in acetone at 25 °C.136

Figure 6.3. Chemical structures of propylene linked bisimidazolium **G4(PF₆)₂** and dibenzo-24-crown-8.137

Figure 6.4. Enthalpogram for propylene linked bisimidazolium **G4(PF₆)₂** (802.4 mM) and dibenzo-24-crown-8 (30.2 mM) in acetone at 25 °C.138

Figure 6.5. Chemical structures of ethylene linked bisimidazolium **G5 (PF₆)₂** and dibenzo-24-crown-8.139

Figure 6.6. Enthalpogram for the binding of ethylene linked bisimidazolium **G5 (PF₆)₂** (393.7 mM) and dibenzo-24-crown-8 (15.2 mM) in acetone at 25 °C.140

Figure 6.7. Chemical structures of phenylene bisimidazolium **G1(PF₆)₂** and dibenzo-24-crown-8.

.....	141
Figure 6.8. Enthalpogram for phenylene bisimidazolium G1(PF₆)₂ (25.96 mM) and dibenzo-24-crown 8 (1.09 mM) in acetone at 25 °C.	142
Figure 6.9. Chemical structures of phenylene bisimidazolium G1(PF₆)₂ and dibenzo-30-crown 10.....	143
Figure 6.10. Enthalpogram for the binding of phenylene bisimidazolium G1(PF₆)₂ (25.96 mM) and dibenzo-30-crown-10 (1.05 mM) in acetone at 25 °C.	144
Figure 6.11. Chemical structures of phenylene bisimidazolium G1(PF₆)₂ and dibenzo-30-crown-10 based cryptand.	145
Figure 6.12. Enthalpogram for the binding of phenylene bisimidazolium G1(PF₆)₂ (27.46 mM) and dibenzo-30-crown-10 based cryptand (0.978 mM) in acetone at 25 °C.	146
Figure 6.13. Chemical structures of xylene bisimidazolium guest G2(PF₆)₂ and dibenzo-24-crown-8.	147
Figure 6.14. Enthalpogram for the interaction of xylene bisimidazolium guest G2(PF₆)₂ (27.19 mM) and dibenzo-24-crown-8 (1.09 mM) in acetone at 25 °C.	148
Figure 6.15. Chemical structures of xylylene bisimidazolium guest G2(PF₆)₂ and dibenzo-30-crown-10.....	149
Figure 6.16. Enthalpogram for the binding of the xylylene bisimidazolium guest G2(PF₆)₂ (27.19 mM) and dibenzo-30-crown-10 (1.05 mM) in acetone at 25 °C.	150

Figure 6.17. Chemical structures of xylylene bisimidazolium guest **G2(PF₆)₂** and dibenzo-30-crown-10-based cryptand.151

Figure 6.18. Enthalpogram for the binding of the xylylene bisimidazolium guest **G2(PF₆)₂** (26.35 mM) with dibenzo-30-crown-10 cryptand (0.977 mM) in acetone at 25 °C.152

Chapter 7: Isothermal Titration Calorimetric (ITC) Analysis of Polymeric Materials

Figure 7.1. Plot of the predicted degree of polymerization versus the association constant between host and guest chain ends, and the concentration of the chain ends [H] in an AB monomer system.160

Figure 7.2. Enthalpogram for the binding titration of bis(*meta* phenylene)-32-crown 10 centered polystyrene and paraquat terminated polystyrene in acetone at 25 °C. Reprinted (adapted) with permission from Lee, M.; Schoonover, D.; Gibson, H. W., *Polymer Preprints (American Chemical Society, Division of Polymer Chemistry)* **2008**, 49, 107-108. Copyright 2009 American Chemical Society.166

Figure 7.3. Enthalpogram for the ITC titration of bis meta phenylene-32-crown 10 with paraquat terminated poly(methyl methacrylate), in acetone at 25 °C.....168

Figure 7.4. Enthalpogram for the titration of polyviologen with dibenzo-30-crown 10 in acetone at 25 °C169

Figure 7.5. Enthalpogram for the ITC titration of paraquat terminated polystyrene with dibenzo-30-crown-10 based cryptand in chloroform at 25 °C.171

Figure 7.6. Stacked plot of the association constants (blue) and change in Gibbs free energy (red) for the titrations of paraquat terminated polystyrene and dibenzo-30-crown-10 based cryptand.173

Figure 7.7. Stacked plot of the changes in enthalpy (red) and changes in entropy (blue) for titrations involving paraquat terminated polystyrene and dibenzo-30-crown-10 based cryptand.174

Chapter 8: Synthesis of Imidazolium-Based Ion Conductive Polymers

Figure 8.1. DSC trace for the monomer **RM4** with a T_g of -69 °C. All monomers had similarly low T_g values. Second heat cycle shown.185

Figure 8.2. DC conductivity vs. inverse temperature for all four monomers.186

Figure 8.3 Stacked SEC chromatogram showing the relative retention times for monomer RM1 and polymer RP1. The monomer shows less retention than the polymer, indicating that the SEC conditions are not suitable for the polymer.188

Figure 8.4. DC conductivity α_{DC} plotted against inverse temperature for the four ROMP polymers.189

Figure 8.5. HRMS spectrum of (1R,2S,4R)-2-(2'-(2''-(2'''-(Tosyloxy)ethoxy)ethoxy)ethoxy)ethyl bicyclo[2.2.1]hept-5-ene-2-carboxylate (6) monomer precursor.192

Figure 8.6. HRMS of monomer RM 01.....195

Figure 8.7. HRMS for monomer RM 02.....196

Figure 8.8. HRMS for monomer RM 03.....197

Figure 8.9. HRMS for monomer RM 04.....198

Chapter 9: Removal of Tosyl Chloride from Solution using Cellulosic Materials

Figure 9.1. Stacked ¹H NMR plot showing a mixture (1:10) of anthracene and tosyl chloride (top red spectrum) and the nearly complete removal of tosyl chloride from anthracene (bottom blue spectrum) after sonication with pyridine and cellulose (filter paper). ¹H NMR CDCl₃ 500 MHz.

.....208

Appendix A: Size Exclusion Chromatography Instrumentation

Figure A.1. Generic plot showing the exclusion and permeation limits of SEC columns. ...A-2

Figure A.2. Component schematic of the Gibson lab SEC instrument including liquid and electric connections.....A-3

Figure A.3. Superimposed calibration chromatograms with toluene flow marker peak.A-7

Figure A.4. Calibration curve for column Set 01.....A-8

Figure A.5. Calibration curve for column Set 02.....	A-9
Figure A.6. Calibration curve for column Set 03.....	A-10
Figure A.7. Calibration curve for column Set 04.....	A-11
Figure A.8. Calibration curve for column Set 05.....	A-12
Figure A.9. Calibration curve for column Set 06.....	A-13
Figure A.10. Calibration curve for column Set 07.....	A-14
Figure A.11. Calibration curve for column Set 08.....	A-16

List of Tables

Chapter 3: Prato Reaction of Fullerenes

Table 3.1. Reduction half potentials for C₆₀, mono-, bis-, and tris-3-(4'-(1''-methylpyrrolidin-2''-yl)phenoxy)propan-1-ol adducts of C₆₀. Scan rate 250 mV/sec, Ag/AgCl reference electrode. All values are relative to ferrocene/ferrocinium couple.86

Table 3.2. Characteristics of the two photovoltaic cells made with the tris-adduct of C₆₀ under AM 1.5 conditions.88

Chapter 7: Isothermal Titration Calorimetric (ITC) Analysis of Polymeric Materials

Table 7.1. Binding parameters for the titration of paraquat terminated polystyrene with dibenzo-30-crown-10 based cryptand in chloroform at 25 °C.172

Chapter 8: Synthesis of Imidazolium-Based Ion Conductive Polymers

Table 8.1. T_g and conductivity values measured for ROMP monomers of different tail length as described in Scheme 8.1184

Table 8.2. T_g, αDC, and molecular weights of the four polymers shown in Scheme 9.2. ¹H NMR in CD₃CN, 400 MHz. Mn determined by comparison of imidazolium 2H peak and the benzyl end group peaks. Error in Mn values: ± 10 %.....187

Table 9.1. Primary hydroxyl content effect on tosyl chloride removal. Equivalents are based upon the anhydroglucose repeat unit. Initial tosyl chloride and anthracene concentrations 100 and 10 mM respectively.209

Table 9.2. Pyridine content effect on removal of tosyl chloride from solution. Hydroxyl equivalents are based on anhydroglucose repeat unit. Initial tosyl chloride and anthracene concentrations 100 and 10 mM respectively.209

Table 9.3. Tosyl chloride removal by different types of cellulosic materials. Initial tosyl chloride and anthracene concentrations 100 and 10 mM respectively.211

Table 9.4. Alcoholic and phenolic materials tosylated by different methods and purified using pyridine and cellulose for the removal of tosyl chloride.
.....212

Chapter One

Introduction to Fullerenes

Since their discovery as an additional allotrope of pure carbon, fullerenes and their derivatives have been studied for their potential promise in many different fields, due to their chemical and electronic properties.¹⁻² The all-carbon fullerene molecules generally consist of sp^2 hybridized carbon atoms, and have the formula C_{2X} , where $X \geq 30$. This describes the standard “empty cage” fullerenes. Endohedral fullerenes are species in which an element (or elements) has (have) been introduced inside the carbon shell. These elements are isolated inside the carbon cage and thus cannot interact directly with the environment outside the fullerene. Most work to date has incorporated metal atoms to form endohedral metallofullerenes (EMF). The nomenclature for these EMFs is generally presented in the form of $A@C_X$ where A is the endohedral species, and x is the number of carbons in the fullerene cage.

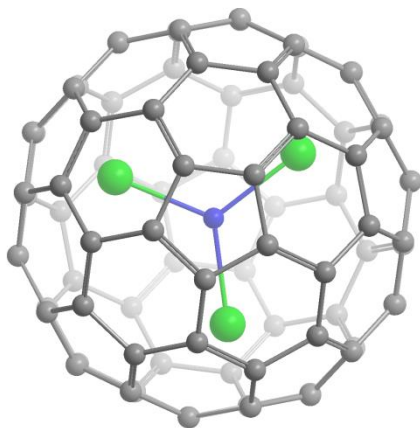


Figure 1.1 Structure of $I_h Sc_3N@C_{80}$.

The incorporation of transition metals and lanthanides has been explored for a number of reasons.³⁻⁶ Transition metals such as Sc have different electronic properties, including a large

number of oxidation states. Since the scandium species is more easily available, it is often used as a model for exploration of new synthetic routes. Other metal heteroatoms such as lanthanides can provide further functionality. Magnetically active elements such as gadolinium, and even radioactive elements, can be introduced into the endohedral environment. Standard EMF species contain one to three metal atoms inside the fullerene cage. A special class of EMF was first synthesized by Dorn's group and called the trimetallic nitride templated (TNT) EMF.⁷ In this case three metal atoms and one nitrogen atom are present inside the fullerene cage. The trimetallic nitride species, which is only stable in the arc environment, has been shown to template the synthesis of a C₈₀ cage. An example of this species, Sc₃N@C₈₀ is shown in Figure 1.1.

The TNT EMF moieties are being investigated for a number of biomedical applications. By placing different lanthanide atoms inside fullerene cages, the heteroatoms are isolated from the environment outside of the cage. Thus these elements can then be introduced into biological systems without direct interaction of the heteroatoms and the host entity. The earliest and most promising application of this type of system is the use of gadolinium based TNT EMFs as MRI contrast agents. The paramagnetic properties of gadolinium complexes brighten an MRI image in the area to which they are introduced. MRI contrast agents such as Magnevist, shown in Figure 1.2, allow *in vivo* water molecules to couple with the gadolinium center. Image enhancement is accomplished by increasing the relaxivity of adjacent hydrogen nuclei through short distance coupling. Current NMR contrast agents incorporate gadolinium complexes with various ligands to ensure aqueous solubility and low reactivity of the toxic Gd species with biological systems.

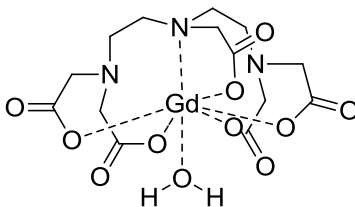


Figure 1.2 Magnevist MRI contrast agent.

There are still, however, concerns about the toxicity of gadolinium complexes in the human body.⁸⁻⁹ Use of EMF species as a container for gadolinium nuclei has the advantage of totally isolating the gadolinium inside the fullerene shell. While the distance between the gadolinium in the EMF and the outside water molecules is increased, coupling interactions can be maintained. This shortcoming is also abated by the fact that there are three gadolinium nuclei present in a TNT EMF. The close proximity of these three nuclei amplifies the overall effectiveness of the gadolinium inside the TNT EMF as an MRI contrast agent. Several, very effective MRI contrast agents have been synthesized from $Gd_3N@C_{80}$.¹⁰⁻¹⁴

Synthesis of Fullerenes

There will be four methods of synthesis of fullerenes discussed in this chapter. These methods include solar and laser vaporization of graphite, electric arc discharge, and radio frequency induced plasma. Solar vaporization is different from laser vaporization in that solar vaporization uses a continuous spectrum of light as opposed to a discrete wavelength used in laser vaporization. Flamant et al. describe scaling up a solar reactor process.¹⁵ In this work, a graphite target was vaporized using solar flux in an argon environment. The fullerenes produced in this work should therefore be considered entirely empty cage species. Despite the lack of any templating or catalytic species, such as trimetallic nitride templates like Fe_3N , the average fullerene content of the vaporized soot produced was as high as 5% fullerenes. The authors did

not separate the different fullerene species present, so no further quantification was given. However, with the lack of heteroatoms, or templating agents, the majority of the product was probably C₆₀ and C₇₀.¹⁵ The advantage of solar vaporization is that the light used to effect the vaporization of the graphite target can contain less light in the UV region, which tends to degrade or hinder the formation of fullerenes.¹⁶ These experiments are completed in high energy solar furnaces at high temperatures. Experiments at the National Renewable Energy Lab have produced C₆₀ with a solar powered furnace.² The group doing this work also hopes to use the furnace reactor with three dimensional (cylindrical) graphite samples to increase the effectiveness of the vaporization in the furnace.

Laser vaporization, also called laser ablation, of graphite substrates can also be used to synthesize fullerenes.¹⁶⁻²² These methods generally use discrete wavelengths of light to excite, and vaporize carbon atoms. The use of laser light sources adds more control to the synthetic procedure. Synthetic variables include the wavelength and intensity of light used. The temperature of the carbon substrate can be controlled by pulsing the laser light.¹⁹ This high level of control over the synthetic environment can render some very interesting results. Mordkovich et al.²⁰ have been able to synthesize multiwalled fullerenes using laser vaporization of carbon materials already containing fullerenes. These multishell fullerenes are analogues to multiwalled nanotubes. The authors speculate on the mechanisms responsible for the formation of both the multiwalled, and single walled fullerenes by observing the percentages of their products under different synthetic conditions. They propose that atomization or fragmentation of the carbon source occurs at the surface during the laser vaporization process, while the formation of fullerenes and other products occurs in the plume or cloud of vapor that is produced. They also indicate that the size and shape of the reaction chamber can affect the formation of fullerene

products. If the chamber is small, the incoming laser light may have to pass through the vapor cloud on a subsequent pulse, depending on the pulse frequency. In a large chamber though, the vapor cloud tends to diffuse quickly, and there is not as much re-irradiation of the material in the vapor cloud. The authors also note that the formation of fullerene products is a function of the pressure in the reaction chamber.¹⁹ This experimental variable, like the size and shape of the chamber, can also affect the residence time of reactant carbon species in the vapor cloud. These two variables, the chamber size and pressure, seem to be related such that the larger the chamber, the less dependent the synthesis is on the pressure.²⁰ Laser ablation methods have also been used for the production of EMF species. Neeb et al.²¹ used metal doped carbon to produce EMF species with Sc, Y, La, Ce, and Gd. The EMF species were seen to contain either one or two metal atoms. These singly and doubly populated fullerenes were produced in an inert atmosphere. Researchers in the Czech Republic synthesized fullerenes with a near infrared laser system.¹⁶ The main point of this work was to determine if fullerenes could be synthesized by excitation in that region, without UV radiation. The authors note the high decomposition rates of fullerenes under UV radiation, and thus managed to produce a synthetic route to a fullerene product without the use of the higher energy radiation.

Electric arc vaporization of carbon is the method of fullerene synthesis currently employed by the Dorn group at Virginia Tech.²³ Like laser ablation, this process can be optimized to give the maximum amount of fullerene products. Unfortunately, the electric arc discharge tends to give off a large amount of UV radiation. UV radiation, as noted by Laska et al.,¹⁶ has the ability to degrade fullerenes. The Krättschmer-Huffman generator is the instrument used. A direct current potential is applied between two graphite electrodes. At a suitably high potential, dielectric breakdown occurs and an arc is generated between the electrodes. The

graphite, while electrically conductive, is vaporized by resistance heating of the surface where the arc occurs. In this process the cathode electrode is consumed during the experiment. This process allows one to control most of the same experimental variables as in the laser experiments. Since the reaction occurs in a closed vessel, the atmosphere can be externally controlled. Controlling the pressure in the reactor allows the optimization of fullerene production. Different gases can also be introduced to the reactor vessel in varying percentages. The introduction of nitrogen gas to the reaction chamber enabled the Dorn group to discover the first trimetallic nitride templated (TNT) EMF species.²³ The arc potential and distance between the electrodes are inversely related such that at a given current level, the farther the electrode tips are from each other, the higher the potential needed to generate the arc. All of these experimental variables are controllable, making the Krätschmer-Huffman generator a reasonably reliable apparatus for the synthesis of fullerene species. While it does not have some of the selective features of laser vaporization, the cost of equipment and maintenance greatly favor the arc reactor. If in the future there is a need for large scale production of fullerenes, the arc discharge generator would probably be the apparatus of choice for industrial applications. Fullerene production on any scale is difficult. The total yield of fullerene and polyaromatic hydrocarbons from the arc reactor is generally between 5 and 15% of the total mass of graphite consumed. Larger fullerenes and EMF species generally constitute a small percentage of the total fullerene product. The smaller cage fullerenes such as C₆₀ and C₇₀ are produced in the most abundance, with large cage and EMF species constituting about 10% or less of the total fullerene content (typically 0.5 to 1.5 %).²⁴⁻²⁵

Radio frequency produced plasma is yet another synthetic method for the production of fullerenes. There are a number of advantages of this method over those described previously.

Ideally an RF plasma source could be run continuously, and may be able to run with several different types of carbon sources. Additionally, the characteristics of the plasma plume generated by this method are much easier to control. In the paper written by Wang et al. fullerenes were synthesized using an RF plasma torch, and different carbon feedstocks.²⁶ In this case, solid carbon materials were used as feedstocks, but using this type of method could enable the use of liquid carbon sources. Amorphous carbon doped with a nickel catalyst was used by Cota-Sanchez et al. to produce C₆₀ and C₇₀ in a similar manner.²⁷ There are thus a number of possible advantages to the use of RF induction plasma for the synthesis of fullerenes.

In 1999 the Dorn group presented the synthesis of a new kind of EMF species, the trimetallic nitride templated (TNT) EMF. These endohedral metallofullerenes contained an ion comprised of three metal atoms and a centrally bonded nitrogen atom. The trimetallic nitride is almost always surrounded by a C₈₀ cage of either I_h or D_{5h} symmetry. The selectivity of the trimetallic nitride for cage size, and larger rates of production of the TNT species leads to the assertion that the trimetallic nitride is somehow a templating agent for the formation of the surrounding C₈₀ fullerene. Endohedral metallofullerene species have been previously synthesized by a number of groups, but in general, the rate of production of the EMF species and the selectivity of both cage identity and endohedral content are not supportive of a templated synthetic mechanism. In addition to the increased production of TNT EMF species as evidence of a templated reaction, there is the fact that the interior trimetallic nitride ion is not stable outside the C₈₀ cage structure. The synthesis of these new molecules draws on a number of experimental factors, as well as standard engineering controls. Since these fullerene products are made in such small quantities, the synthetic conditions must be strictly controlled in order to maximize production. During synthesis, a graphite electrode is consumed to produce vaporized

carbon and subsequently a sooty solid that contains solvent extractable fullerene species. The consumed electrode in this case must contain two of the three reactants for the synthesis. In practice, a graphite tube is created by drilling a hole through the center of a graphite rod. This tube is then filled with a heterogeneous mixture of graphite powder, and the metal that is to be placed inside the fullerene cage. Pure metallic sources are generally not used, but are substituted with oxides of the appropriate metal. Mixtures of different metal oxides have been used, and an alloy of gadolinium and nickel has been suggested as a metal source.²⁸ Another substituent of the filling mixture is iron nitride (Fe_3N), which appears to be a catalyst for all fullerene production. In order to produce TNT EMF species, there must be a source of nitrogen to complete the trimetallic nitride templating agent. Again, the trimetallic nitride is an unstable species, and thus does not exist outside the fullerene cage, or the carbon vapor cloud. Nitrogen is introduced into the atmosphere of the reactor as the diatomic gas. Nitrogen gas is generally inert; however, inside the high energy environment in which fullerenes form, it can be converted into the central trimetallic nitride moiety. The nitrogen and metallic components are present in optimized percentages. An excess of the metal species will lead to side reactions and production of nanotube species above a maximum level of TNT EMF production. Therefore, the metal content of the graphite electrode is limited, so that only fullerene species are produced. The bulk of the atmosphere is comprised of inert helium, and the bulk of the filling mixture is comprised of carbon powder. The atmospheric pressure of the reactor is an important synthetic variable. If the pressure is not high enough there will be little or no production of TNT species, as there will not be an effectively high enough concentration of nitrogen to form the templating agent. The final synthetic variable available is the arc potential. The potential is controlled by the current being passed, and the distance between the electrodes. The reactor uses a constant current

generator in the form of an arc welding machine to provide electric current. A feedback controlled mechanical device then varies the distance between the electrode tips to maintain a constant voltage. All of these variables must be carefully controlled and optimized to produce the largest amounts of TNT EMF species for use in further experimentation.

Synthesis of fullerenes by the previous methods is generally also accompanied by the co-synthesis of polyaromatic hydrocarbon (PAH) species. These species are generally considered to be fullerene shell fragments, and are thus similar to completed fullerene shells. The PAH species of particular interest to fullerene chemistry is the corannulene moiety. This molecule or fragment consists of five six-membered rings arranged such that there are two bonded concentric aromatic rings, one with five carbons, and one with 15 carbons.

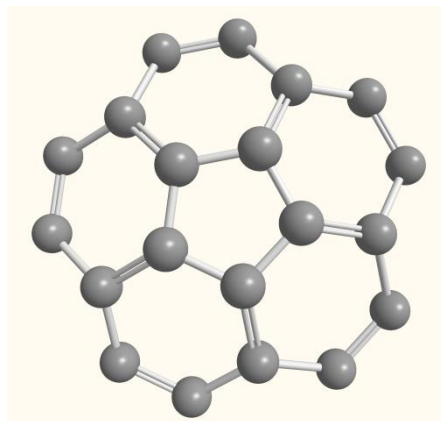


Figure 1.3 Structure of corannulene.

The corannulene molecule (Figure 1.3) consisting of sp^2 hybridized carbons is not planar. Geometric bond length limitations force the low energy conformation of this molecule to be concave instead of planar. This type of fragment is seen in fullerene structures, and leads to the curvature of the fullerene molecule. Corannulene has been synthetically available much longer than fullerenes. The molecule was synthesized by Barth et al. from methyl 4,5-

methylenephenanthrene-3-carboxylate in 1965.²⁹ The synthetic method used by this group was very long and complex. It includes two ring closure reactions as well as elimination steps needed to remove different functional groups.²⁹ The synthesis reported by Barth et al. is a standard wet chemical synthetic method. There have been bench methods reported for corannulene synthesis.³⁰ Solution phase chemistry has the distinct advantage of being easily scalable, and productive on a macroscopic scale. Starting materials for these reactions are generally inexpensive and available. The only true drawback to solution phase synthesis of corannulenes is the fact that the synthetic reactions available are extensive and time consuming. These reactions are difficult to accomplish because the corannulene molecule is not planar. The aromatic substrates used to synthesize corannulenes are generally planar anthracene and phenanthrene derivatives. Forcing these planar systems to deflect into the concave corannulene system through ring closure reactions tends to be very difficult. This was investigated by a number of groups.^{29, 31} One interesting synthetic method involved a larger ring analogue, and generated corannulene using a ring contraction reaction. There is a much faster and simpler method for corannulene synthesis. Just like fullerene species, corannulenes can be synthesized by pyrolytic or vaporization methods. There are numerous pyrolytic synthetic methods.³²⁻³⁵ However, like fullerene synthesis, large scale synthesis of corannulenes via pyrolytic methods is very difficult. These high energy reactions are able to introduce curvature into planar aromatic systems as they are being degraded. Thus the formation of corannulene species during high energy pyrolysis reactions is easier to accomplish. Unfortunately, without preordering the reactants, or some sort of templating mechanism, the production percentage of corannulenes from pyrolytic methods tends to be very low. The other drawback of pyrolytic methods may be cost. Like fullerene synthesis, pyrolysis reactions require special reaction chambers and

equipment. The need for specialized equipment is another reason that solution phase synthetic methods may be favored over pyrolysis, as they generally only require the use of standard laboratory glassware. Beyond the ability of corannulene to model the basic unit of curvature in fullerene systems, it is a useful model for exploring the electronic properties of fullerene cages. Complexation studies using corannulene and different metals may help to elucidate the interactions between fullerene cages and endo- and exo-hedral metallofullerenes. As polyaromatic systems, corannulenes are able to accept or donate electrons from their extended π -orbital system. Studies of complexation reactions of corannulene molecules with metals such as Ni, Pt, Li, Ir, and Ru have been reported.³⁶⁻³⁸ Since the active π orbitals used for these complexation reactions exist on both the convex and concave surfaces of the corannulene, complexation of a metal species can occur on either surface. Aprahamian et al.³⁷ suggest that in the complexation of corannulene molecules with lithium, there is the possibility of the transfer of up to 4 electrons from the lithium atoms to the corannulene. They propose that the complexation of four lithium atoms by a corannulene molecule occurs with two lithium atoms bound to each surface of the corannulene. They also report the possibility of three dimensional stacking of these complexes to give four lithium molecules sandwiched between two corannulenes. This type of work is important to increase the understanding of the interaction between endohedral metal atoms and the fullerene cages that surround them.

After the synthesis of fullerene species by any of the previously mentioned methods, it is necessary to isolate and purify the particular species that is being studied. The product of graphite vaporization is a mixture of different fullerene species, in amounts and densities depending on the conditions in the reactor. In the absence of reactive metals or gases, empty cage fullerenes can be produced with the majority of the product consisting of C₆₀ and C₇₀. If

there are metals present, endohedral species can be produced, generally with one or two metal atoms inside the fullerene shell. Finally, if nitrogen is added to the reactor, TNT EMF species can be produced. In each case of an added reactant, the constituent mixture of products will generally contain all previous constituents as well as any possible new species. The exception, however, may be the production of TNT EMF species which does not seem to produce significant amounts of other EMF species, possibly because of the templating reaction that occurs with the trimetallic nitride species. All species are thus mixed together in the bulk of the vaporization product, which consists of unreacted, or amorphous carbon soot. The first and seemingly simplest task for purification of any fullerene species is removal of the bulk amorphous carbon soot. Soot removal is usually accomplished by selectively extracting the fullerene and PAH products from the soot. Soxhlet extraction is generally the most effective method. Suitable extraction solvents include toluene, xylene, hexane, benzene and an azeotropic mixture of carbon disulfide and methanol.³⁹⁻⁴⁰ As fullerene species are unsaturated nonpolar species, preferred solvents are understandably similar. Toluene and xylene, despite their high boiling points, are generally accepted as the Soxhlet solvent of choice. Hexane and the azeotrope of carbon disulfide and methanol have much lower boiling points. Therefore, they might seem preferable; however, the solvents are highly volatile, and great care must be taken to minimize solvent loss. Fullerenes are generally insoluble in other common organic solvents. This includes alcohols, ethers, ketones, and aldehydes. Pure fullerenes are also insoluble in aqueous systems. PAH species are soluble in ethers and ketones, however, and this can lead to their selective extraction from fullerene species.⁴¹⁻⁴² Uncommon solvents for fullerenes include 1,3-substituted dienes. Diene species such as cyclopentadiene, isoprene, and furfuryl alcohol can be used to dissolve fullerenes as will be shown in the second chapter of this work. The

conjugated diene moiety found in these molecules is apparently similar enough to the aromatic fullerene shell to allow solubility. Unfortunately, even in a reasonable solvent the total solubility of fullerenes tends to be low. Experimentally, the solubility limit of fullerene species in toluene is approximately 3 to 4 mg/ml.²⁵ This is one of the reasons that Soxhlet extraction of the produced soot is extremely important. The low solubility of fullerenes and the small number of solvents that can be used also limit the number of reaction environments that can be used to functionalize fullerenes. Enhancements in solubility and solvent selection can be made by synthesizing derivatives of fullerene species. This approach to extraction and purification will be discussed further in Chapter 2.

Once the fullerene and PAH products have been separated from the original soot, separation of the different fullerene species is the next step in purification. Traditionally, separation of fullerene species has been accomplished by use of liquid chromatographic methods. On the analytical scale, samples can be separated by both HPLC and TLC methods. TLC separation of fullerene extracts can provide qualitative information about the products generated. The method is fast and simple. Unfortunately, TLC provides no meaningful quantitative information about product formation.⁴³ Though it requires more equipment and time, the better method for analysis of fullerene extracts is HPLC. HPLC analysis of extract samples can provide reliable quantitative information about the constituents and relative amounts of different species. Most HPLC methods for the separation of fullerenes are normal phase separations with a solvent that is the same or similar to the extraction solvent. Stationary phases are usually pyrene (PYE), or the Buckyprep (Figure 1.4) type that employ π - π interactions to effect separation. Synthetic yields for fullerene synthesis are generally very low, and the small sample size and low detection limit of HPLC using a UV-Vis detector are well suited.

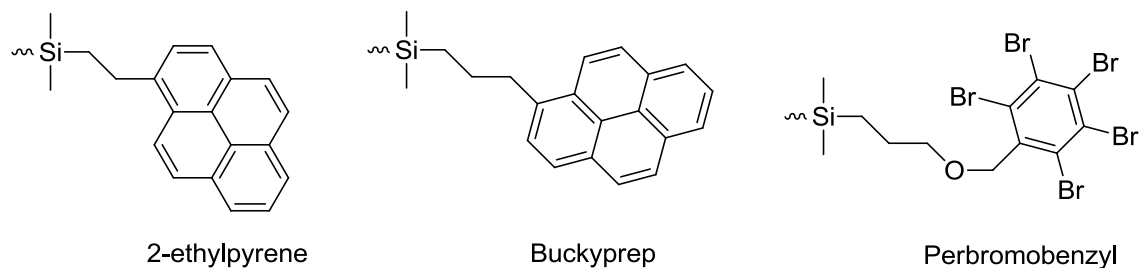


Figure 1.4 HPLC stationary phase functional groups.

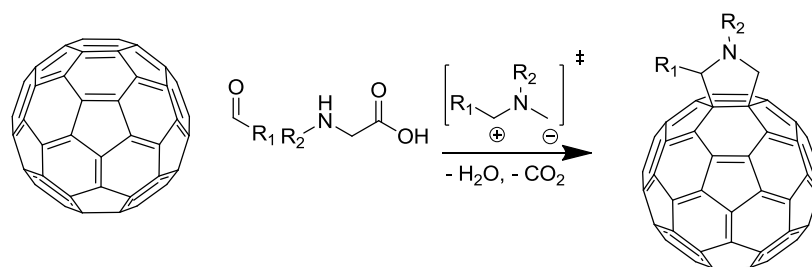
Once the fullerenes have been extracted from the soot, and quantified by analytical scale HPLC, the remainder of the synthetic products must be separated and isolated. Separation is also generally accomplished by chromatographic methods. On the preparative scale, two chromatographic methods are well suited for this type of separation. Larger scale low pressure liquid chromatography can be used to separate fullerenes. This method uses a normal phase silica gel column, and a mixed solvent system. Elution times are long, and the amount of solvent used is very large; however, this method can be used to separate large amounts of fullerenes from complex mixtures. Since the amount of fullerenes produced from any one or a set of reactions is very small, preparative scale HPLC is also an option for product separation. The same normal phase separation system as the analytical scale is used. Generally, multiple passes through the HPLC will purify enough material that further experiments can be accomplished.

Fullerenes are generally insoluble in aqueous media.. Fullerenes and other organic species can be dissolved in aqueous systems containing surfactant agents with a concentration exceeding the critical micelle concentration. Surfactants are amphiphilic molecules with a hydrophilic head group and a hydrophobic tail. In an aqueous solution, they form ordered clusters with the head units in contact with the water, and the tail units on the inside. These

clusters, called micelles, thus generate small volumes of stable, nonpolar, organic environments in a bulk aqueous media. Work done by Treubig and Brown has shown that fullerenes C₆₀ and C₇₀ can be stabilized and dissolved in an aqueous micellar system using sodium dodecylsulfate (SDS) as a surfactant.⁴² The authors noted that C₆₀ was slightly soluble in the micellar system, and that C₇₀ would also dissolve if some C₆₀ was also present. Capillary electrophoresis was then used to separate the fullerenes by differences in their mass to charge ratio. While these results assume a number of conditions, such as a static micelle size and aggregation number, the separation data indicate a good separation.⁴² Micellar solvent systems can also be used in chromatographic methods. Different groups have reported success separating organic media using reverse phase chromatography with micellar mobile phases.⁴⁴⁻⁴⁷ In reverse phase chromatography, an aqueous mobile phase is used with a nonpolar organic stationary phase. The partitioning of organic molecules, including fullerenes, inside and outside the micelles in the mobile phase, and their different interactions with the stationary phase, make reverse phase micellar liquid chromatography a reasonable system for the separation of different organic species.⁴⁴⁻⁴⁶ Micellar chromatography has not been applied to fullerene systems; however, the use of aqueous systems for their separation may be promising in the future. While standard reverse phase micellar chromatography on fullerene systems has not been reported, the use of micellar electrokinetic chromatography (MEKC) has been reported by Treubig and Brown.⁴² In this separation system, standard chromatographic conditions apply. There is a stationary phase and mobile phase, and the solute partitioning characteristics of different constituents becomes the method for their separation. There is also an additional separation regime, analogous to capillary electrophoresis, in which an electric potential is applied to the column. The data produced by the MEKC is analogous to the chromatogram produced by a standard HPLC separation. The added

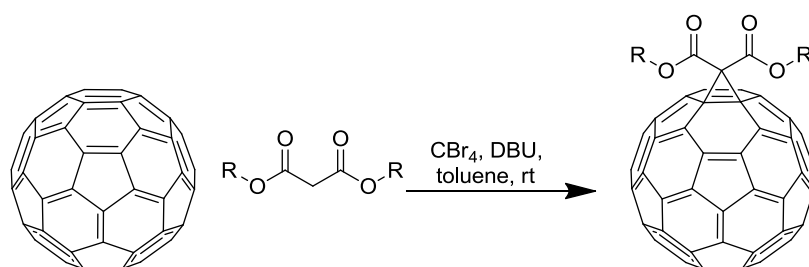
functionality of this system is that column selectivity can be adjusted not only by the standard methods of stationary and mobile phase identity, but also by the electrostatic potential applied to the column.⁴² This type of separation may become very useful in the separation of EMF and TNT EMF species, which have been shown to exhibit electron transfer from the endohedral metal atoms to the fullerene shell.

One of the most promising areas of application for TNT EMF species is the use of gadofullerenes as MRI contrast agents.^{6, 48} The magnetic properties of the gadolinium atom make it active in experiments using NMR, including the medical MRI application. By encapsulating the gadolinium atoms in a fullerene shell, they become chemically inaccessible, yet will interact with surrounding NMR active nuclei. Gadolinium EMF species can improve the contrast and subsequent quality of MRI images by decreasing the relaxation time of hydrogen nuclei in close proximity to the fullerene shell. By reducing the relaxivity of these hydrogen nuclei, higher quality images can be generated in a shorter amount of time.⁴⁸ Unfortunately, as noted earlier, fullerenes are insoluble in aqueous, and thus biological, systems. Fullerene species such as Gd₃@C₈₀ must be functionalized with hydrophilic groups in order to become soluble in aqueous systems. Toth et al. working with Gd@C₆₀ hydroxylated the fullerene, and synthesized a deca-adduct and a carboxylic acid.⁴⁸ The authors noted that introduction of the gadofullerene derivatives to aqueous solutions significantly reduced hydrogen relaxivity. They also showed that the hydrogen relaxivity could be changed by varying the pH of the aqueous solution.⁴⁸ This makes sense because the hydroxyl and carboxylic hydrogens should both be able to dissociate from the fullerene molecule depending on the solution pH. Other functionalization reactions intended for the production of water soluble fullerenes include the Prato reaction and the Bingel reactions.



Scheme 1.1 Generic Prato reaction.

The Prato reaction shown in Scheme 1.1 is a 1,3-dipolar cycloaddition of an azomethine ylide to the fullerene shell.⁴⁹⁻⁵⁴ In this reaction an aldehyde and an amino acid are employed to form adducts.⁵² The addition of amino acid type functional groups can make the fullerene adducts water soluble.⁵⁰ The Prato reaction may be important in forming fullerene adducts used for biological applications because a number of different amino acid functional moieties can be used.⁵² The bis-adducts of TNT EMF species has been recently reported as well as the thermal control of their isomerization.⁵⁵⁻⁵⁷



Scheme 1.2 Generic Bingel reaction.

The Bingel reaction (Scheme 1.2), reported by Ge et al. on the C₈₀ TNT EMF, also holds promise as a water soluble functionalization reaction capable of producing poly(ethylene glycol) (PEG), and dendritic functionalized fullerenes.⁵⁸ This reaction has been used to functionalize empty cage and endohedral species. Functionalized malonates, or malonate salts have been

reacted with fullerene moieties to produce mono- and bis-adducts.^{52, 59-60} The reaction usually generates a cyclopropyl link between the fullerene and the malonate.⁶¹ This type of reaction was originally thought to be ineffective when using TNT EMF species, but that was disproved by Echegoyen et al.^{25, 62-66}

Fullerenes in aqueous systems, depending on their functionality, tend to have amphiphilic properties. The large fullerene cage may be considered the hydrophobic head unit with a hydrophilic functionalized tail. These models are most applicable for the PEG and dendritic functional systems. Therefore, functionalized fullerenes tend to form aggregates in aqueous media in the form of micelles. Aggregation of EMF species may or may not be favorable, depending on the level of micellization. The effects of the ionic composition of aqueous media on the relaxivity induced by Gd@C₆₀ were measured by Laus et al.⁶⁷ They found that increasing the ionic strength or salt concentration of the aqueous solution had the effect of dissociating the EMF aggregates, and lowering the relaxivity of adjacent hydrogen nuclei.⁶⁷ Conversely, Brant et al. found that adding electrolytes to aqueous suspensions of C₆₀ clusters had the effect of causing those clusters to precipitate.⁶⁸ For non-functionalized fullerenes in aqueous suspension, the addition of dissociated ions into an aqueous medium should have the effect of enhancing the polarity of the solvent, and causing the nonpolar fullerenes to aggregate on a larger scale and phase separate. With the functionalized fullerenes, the opposite is probably true. Since aggregation of these molecules can probably be attributed to the hydrophobic nature of the fullerene cage, adding electrolytic species to the water will serve to stabilize the hydrophilic substituent, and make individual molecules less soluble. This addition has the effect, for EMF species, of lowering the CMC. For monometallic EMF species, aggregation is very important. Relaxivity depends on the number and proximity of the gadolinium atoms present. Therefore,

aggregates of monometallic EMF species will have greater relaxivity than single molecules.⁶⁷ TNT EMF species contain three gadolinium atoms inside the fullerene. This means that aggregation of these species in aqueous systems should be much less important than monometallic EMF species.

Functionalization of fullerene species, as a means for easier separation, has become an area of interest. Since fullerenes are made in such low yields, and the formation of endohedral species is much lower still, efficient separation is extremely important. Perhaps one of the most efficient separation methods discussed by Dorn et al. is the separation of TNT EMF species using Merrifield resin.⁶⁹ This group reported using two different methods with this material. It can be used as a large scale low pressure liquid chromatography column packing, or in a stir and filter approach. The Merrifield resin, a crosslinked chloromethylated polystyrene, is functionalized with cyclopentadiene units by the addition of sodium cyclopentadiene to the chloromethyl moieties. This arrangement ideally functionalizes the solid surface with cyclopentadiene reactive groups. When a solution of fullerene species is introduced to the solid, the empty cage fullerenes preferentially react, and bond with the cyclopentadiene groups. The reaction is a Diels-Alder 4+2 addition, in which the cyclopentadiene is the diene, and the empty fullerene cage is the dieneophile. TNT EMF species have been shown to be nearly unreactive in Diels-Alder additions, compared to empty cage species. The difference in reactivity may be attributed to the charge transfer of electrons from the trimetallic nitride species to the fullerene cage. Different groups have shown that the C₈₀ fullerene cage is electronically stabilized by the transfer of electrons from the endohedral species.^{3, 5} Electrochemical studies support the hypothesis that the endohedral trimetallic nitride species transfers as many as 6 electrons to the C₈₀ fullerene cage.^{3, 70-73} The electron transfer to the fullerene cage makes it a poor dieneophile.

In the classical Diels-Alder reaction, the diene species used should be comparatively electron-rich, and the dieneophile species should be electron-poor.⁷⁴ Since the cyclopentadiene on the Merrifield resin would have to react with the fullerene cage, the TNT EMF species with its 6 extra electrons would make a comparatively electron-rich dieneophile, and is hence unreactive. The empty cage fullerenes, however, are suitably electron-poor. This, coupled with their high polarizability, makes them much more suitable dieneophiles. Thus, when a mixture of fullerene species is introduced in solution to the solid phase Merrifield resin, the empty cage fullerenes selectively react with the resin, and become immobilized. Separation of the EMF species is accomplished by washing the unreacted species out of the slurry with an appropriate solvent.^{23, 69} Other functionalization methods can be used to expedite the separation of fullerene species. Continuing with the use of the Diels-Alder reaction, adducts of empty cage fullerenes and different dienes can be selectively soluble in different solvents. Functionalization with dienes such as cyclopentadiene, anthracenes, and isoprene yield adduct species that are similar to other PAH species, and are thus soluble in either acetone or diethyl ether. Functionalized species can then be removed by solvent extraction. Work by Bolskar and Alford predicts that EMF species can be selectively extracted by oxidation.⁷⁵ The authors propose that the extra electrons present on the fullerene shell, due to electron transfer from the endohedral metal, should make endohedral species much easier to oxidize. Using oxidizing agents such as Lewis acids, they were able to selectively isolate a number of endohedral species as salts in polar organic solvents.⁷⁵ This prediction was later proven by Stevenson et al. who used Lewis acids such as AlCl_3 and MgCl_2 to rapidly purify TNT EMF species.⁷⁶⁻⁷⁸

In conclusion, the separation and isolation of TNT EMF species is a very important area of study. There are many possible applications for derivatives of these molecules.

Unfortunately, one of the largest problems with any fullerene species is availability of material. Synthetic methods are not selective, and yields of these materials are very low. Traditional separation of TNT EMF species by HPLC produces high purity materials, but it is a time and resource intensive method. Separation by functionalization may eventually provide fast and inexpensive methods to procure high purity TNT EMF samples.

References:

1. Kiang, C. H.; Van Loosdrecht, P. H. M.; Beyers, R.; Salem, J. R.; Bethune, D. S.; Goddard, W. A., III; Dorn, H. C.; Burbank, P.; Stevenson, S., *Surface Review and Letters* **1996**, *3*, 765-769.
2. Winston, R.; Jenkins, D.; O'Gallagher, J.; Lando, M.; Bernstein, H., *Renewable Energy* **1994**, *5*, 368-72.
3. Anderson, M. R.; Dorn, H. C.; Stevenson, S.; Burbank, P. M.; Gibson, J. R., *Journal of the American Chemical Society* **1997**, *119*, 437-438.
4. Fatouros P, P.; Corwin F, D.; Chen, Z.-J.; Broaddus W, C.; Tatum J, L.; Kettenmann, B.; Ge, Z.; Gibson H, W.; Russ J, L.; Leonard A, P.; Duchamp J, C.; Dorn H, C., *Radiology* **2006**, *240*, 756-64.
5. Heflin, J. R.; Marciu, D.; Figura, C.; Wang, S.; Burbank, P.; Stevenson, S.; Dorn, H. C., *Applied Physics Letters* **1998**, *72*, 2788-2790.
6. Iezzi, E. B.; Duchamp, J. C.; Fletcher, K. R.; Glass, T. E.; Dorn, H. C., *Nano Letters* **2002**, *2*, 1187-1190.
7. Stevenson, S.; Fowler, P. W.; Heine, T.; Duchamp, J. C.; Rice, G.; Glass, T.; Harich, K.; Hajdu, E.; Bible, R.; Dorn, H. C., *Nature (London)* **2000**, *408*, 427-428.
8. Perazella, M. A., *Clinical Journal of the American Society of Nephrology* **2009**, *4*, 461-469.
9. Thomsen, H. S.; Morcos, S. K.; Dawson, P., *Clinical radiology* **2006**, *61*, 905-6.
10. Cui, R.; Li, J.; Huang, H.; Zhang, M.; Guo, X.; Chang, Y.; Li, M.; Dong, J.; Sun, B.; Xing, G., *Nano Research* **2014**, Ahead of Print.

11. Kong, K. V.; De Liao, L.; Goh, D.; Thakor, N. V.; Olivo, M., *Journal of Nanomedicine & Nanotechnology* **2014**, *5*, 1000223/1-1000223/11.
12. Shu, C.-Y.; Wang, C.-R., *RSC Drug Discovery Series* **2012**, *15*, 261-284.
13. Zhang, J.; Stevenson, S.; Dorn, H. C., *Accounts of Chemical Research* **2013**, *46*, 1548-1557.
14. Zhang, J.; Ye, Y.; Chen, Y.; Pregot, C.; Li, T.; Balasubramaniam, S.; Hobart, D. B.; Zhang, Y.; Wi, S.; Davis, R. M.; Madsen, L. A.; Morris, J. R.; LaConte, S. M.; Yee, G. T.; Dorn, H. C., *Journal of the American Chemical Society* **2014**, *136*, 2630-2636.
15. Flamant, G.; Robert, J. F.; Marty, S.; Gineste, J. M.; Giral, J.; Rivoire, B.; Laplaze, D., *Energy* **2004**, *29*, 801-809.
16. Laska, L.; Krasa, J.; Juha, L.; Hamplova, V.; Soukup, L., *Carbon* **1996**, *34*, 363-8.
17. Ajie, H.; Alvarez, M. M.; Anz, S. J.; Beck, R. D.; Diedrich, F.; Fostiropoulos, K.; Huffman, D. R.; Kratschmer, W.; Rubin, Y.; Schriver, K. E.; Sensharma, D.; Whetten, R. L., *Journal of Physics Chemistry* **1990**, *94*, 8630-8633.
18. Armand, X.; Herlin, N.; Voicu, I.; Cauchetier, M., *Journal of Physics and Chemistry of Solids* **1997**, *58*, 1853-1859.
19. Kasuya, D.; Kokai, F.; Takahashi, K.; Yudasaka, M.; Iijima, S., *Chemical Physical Letters* **2001**, *337*, 25-30.
20. Mordkovich, V. Z.; Maezawa, T.; Takeuchi, Y., *Fullerenes, Nanotubes, and Carbon Nanostructures* **2004**, *12*, 11-16.
21. Neeb, M.; Klingeler, R.; Bechthold, P. S.; Kann, G.; Wirth, I.; Eisebitt, S.; Eberhardt, W., *Applied Physics A: Material Science Proceedings* **2001**, *72*, 289-293.
22. Ohkawara, Y.; Shinada, T.; Fukada, Y.; Ohshio, S.; Saitoh, H., *Journal of Materials Science* **2003**, *30*, 2447-2453.
23. Dorn, H. C.; Iezzi, E. B.; Stevenson, S.; Balch, A. L.; Dunchamp, J. C., *Developments in Fullerene Science* **2002**, *3*, 121-131.
24. Bancu, M.; Rai, A. K.; Cheng, P.; Gilardi, R. D.; Scott, L. T., *Synlett* **2004**, 173-176.
25. Chen, N.; Ortiz, A. L.; Echegoyen, L., *RSC Nanoscience & Nanotechnology* **2012**, *20*, 12-65.

26. Wang, C.; Imahori, T.; Tanaka, Y.; Sakuta, T.; Takikawa, H.; Matsuo, H., *Thin Solid Films* **2001**, *390*, 31-36.
27. Cota-Sanchez, G.; Soucy, G.; Huczko, A.; Lange, H., *Carbon* **2005**, *43*, 3153-3166.
28. Wang, X.; Zuo, T.; Olmstead, M. M.; Duchamp, J. C.; Glass, T. E.; Cromer, F.; Balch, A. L.; Dorn, H. C., *Journal of the American Chemical Society* **2006**, *128*, 8884-8889.
29. Barth, W. E.; Lawton, R. G., *Journal of the American Chemical Society* **1966**, *88*, 380-1.
30. Lawton, R. G.; Barth, W. E., *Journal of the American Chemical Society* **1971**, *93*, 1730-45.
31. Sygula, A.; Xu, G.; Marcinow, Z.; Rabideau, P. W., *Tetrahedron* **2001**, *57*, 3637-3644.
32. Crowley, C.; Taylor, R.; Kroto, H. W.; Walton, D. R. M.; Cheng, P.-C.; Scott, L. T., *Synthetic Metals* **1996**, *77*, 17-22.
33. Hagen, S.; Christoph, H.; Zimmerman, G., *Tetrahedron* **1995**, *51*, 6961-70.
34. Liu, C. Z.; Rabideau, P. W., *Tetrahedron Lett.* **1996**, *37*, 3437-3440.
35. Scott, L. T.; Hashemi, M. M.; Meyer, D. T.; Warren, H. B., *Journal of the American Chemical Society* **1991**, *113*, 7082-4.
36. Alvarez, C. M.; Angelici, R. J.; Sygula, A.; Sygula, R.; Rabideau, P. W., *Organometallics* **2003**, *22*, 624-626.
37. Aprahamian, I.; Eisenberg, D.; Hoffman, R. E.; Sternfeld, T.; Matsuo, Y.; Jackson, E. A.; Nakamura, E.; Scott, L. T.; Sheradsky, T.; Rabinovitz, M., *Journal of the American Chemical Society* **2005**, *127*, 9581-9587.
38. Vecchi, P. A.; Alvarez, C. M.; Ellern, A.; Angelici, R. J.; Sygula, A.; Sygula, R.; Rabideau, P. W., *Angewandte Chemie International Edition* **2004**, *43*, 4497-4500.
39. Diener, M. D.; Alford, J. M., *Nature (London)* **1998**, *393*, 668-671.
40. Takehara, H.; Fujiwara, M.; Arikawa, M.; Diener, M. D.; Alford, J. M., *Carbon* **2005**, *43*, 311-319.
41. Boyd, T. J.; Schrock, R. R., *Macromolecules* **1999**, *32*, 6608-6618.
42. Truebig, J. M.; Brown, P. R., *Journal of Chromatography A* **2000**, *873*, 257-267.
43. Armstrong, D. W.; Terrill, R. Q., *Analytical Chemistry* **1979**, *51*, 2160-2163.

44. Armstrong, D. W.; Nome, F., *Analytical Chemistry* **1981**, *53*, 1662-1666.
45. Arunyanart, M.; Love, L. J. C., *Analytical Chemistry* **1984**, *56*, 1557-1561.
46. Khaledi, M. G.; Strasters, J. K.; Rodgers, A. H.; Breyer, E. D., *Analytical Chemistry* **1990**, *62*, 130-136.
47. Moroi, Y.; Yoshida, N., *Langmuir* **1997**, *13*, 3909-3912.
48. Toth, E.; Bolskar, R. D.; Borel, A.; Gonzalez, G.; Helm, L.; Merbach, A. E.; Sitharaman, B.; Wilson, L. J., *Journal of the American Chemical Society* **2005**, *127*, 799-805.
49. Cai, T.; Ge, Z.; Iezzi, E. B.; Glass, T. E.; Harich, K.; Gibson, H. W.; Dorn, H. C., *Chemical Communications* **2005**, 3594-3596.
50. Da Ros, T.; Prato, M., *Journal of Organic Chemistry* **1996**, *61*, 9070-9072.
51. Alvarez, A.; Ochoa, E.; Verdecia, Y.; Suarez, M.; Sola, M.; Martin, N., *Journal of Organic Chemistry* **2005**, *70*, 3256-3262.
52. Cox, C. T., Jr.; Cooper, M. M., *Journal of Chemical Education* **2006**, *83*, 99-100.
53. Sokolov, V. I.; Abramova, N. V.; Khrushcheva, N. S.; Peregudova, S. M., *Russian Chemical Bulletin (Translation of Izvestiya Akademii Nauk, Seriya Khimicheskaya)* **2003**, *52*, 2764-2765.
54. Wei, X.-w.; Avent, A. G.; Boltalina, O. V.; Street, J. M.; Taylor, R., *Journal of the Chemical Society, Perkin Transactions 2* **2002**, 47-52.
55. Aroua, S.; Garcia-Borras, M.; Bolter, M. F.; Osuna, S.; Yamakoshi, Y., *Journal of the American Chemical Society* **2015**, *137*, 58-61.
56. Aroua, S.; Garcia-Borras, M.; Osuna, S.; Yamakoshi, Y., *Chemistry - A European Journal* **2014**, *20*, 14032-14039.
57. Aroua, S.; Yamakoshi, Y., *Journal of the American Chemical Society* **2012**, *134*, 20242-20245.
58. Ge, Z.; Dorn, H. C.; Phillips, J. P. Pegylation and hydroxylation of trimetallic nitride endohedral metallofullerenes. 2005-US10219 2005097807, 20050325., 2005.
59. Ball, G. E.; Burley, G. A.; Chaker, L.; Hawkins, B. C.; Williams, J. R.; Keller, P. A.; Pyne, S. G., *Journal of Organic Chemistry* **2005**, *70*, 8572-8574.
60. Burley, G. A.; Keller, P. A.; Pyne, S. G.; Ball, G. E., *Journal of Organic Chemistry* **2002**, *67*, 8316-8330.

61. Wei, X.-W.; Avent, A. G.; Boltalina, O. V.; Darwish, A. D.; Fowler, P. W.; Sandall, J. P. B.; Street, J. M.; Taylor, R., *Journal of the Chemical Society, Perkin Transactions 2* **2002**, 41-46.
62. Alegret, N.; Chaur, M. N.; Santos, E.; Rodriguez-Forteza, A.; Echegoyen, L.; Poblet, J. M., *Journal of Organic Chemistry* **2010**, *75*, 8299-8302.
63. Elliott, B.; Cardona, C. M.; Ortiz, A.; Dorn, H. C.; Echegoyen, L., *Abstracts, 56th Southeast Regional Meeting of the American Chemical Society, Research Triangle Park, NC, United States, November 10-13 \2004*, GEN-313.
64. Garcia-Borras, M.; Osuna, S.; Swart, M.; Luis, J. M.; Echegoyen, L.; Sola, M., *Chemical Communications (Cambridge, United Kingdom)* **2013**, *49*, 8767-8769.
65. Lukoyanova, O.; Wang, H.; Gibson, H.; Herranz, M.; Echegoyen, L., *Abstracts, 55th Southeast Regional Meeting of the American Chemical Society, Atlanta, GA, United States, November 16-19, 2003* **2003**, 16.
66. Pinzon, J. R.; Zuo, T.; Echegoyen, L., *Chemistry - A European Journal* **2010**, *16*, 4864-4869, S4864/1-S4864/15.
67. Laus, S.; Sitharaman, B.; Toth, E.; Bolskar, R. D.; Heim, L.; Asokan, S.; Wong, M. S.; Wilson, L. J.; Merbach, A. E., *Journal of the American Chemical Society* **2005**, *127*, 9368-9369.
68. Brant, J.; Lecoanet, H.; Wiesner, M. R., *J. of Nanoparticle Res.* **2005**, *7*, 545-553.
69. Ge, Z.; Duchamp, J. C.; Cai, T.; Gibson, H. W.; Dorn, H. C., *Journal of the American Chemical Society* **2005**, *127*, 16292-8.
70. Anderson, M. R.; Dorn, H. C.; Stevenson, S. A., *Carbon* **2000**, *38*, 1663-1670.
71. Burbank, P.; Gibson Harry, W.; Dorn Harry, C.; Anderson, M., *J. Electroanalytical Chemistry* **1996**, *417*, 1-4.
72. Krause, M.; Wong, J.; Dunsch, L., *Chemistry* **2005**, *11*, 706-11.
73. Ioffe, I. N.; Ievlev, A. S.; Boltalina, O. V.; Sidorov, L. N.; Dorn, H. C.; Stevenson, S.; Rice, G., *Mass Spectrometry* **2002**, *213*, 183-189.
74. Fringuelli, F.; Taticci, A., *Dienes and the Diels-Alder reaction*. Wiley and Sons. Inc.: New York, 1990.
75. Bolskar, R. D.; Alford, J. M., *Chemical Communications* **2003**, 1292-3.

76. Stevenson, S.; Rottinger, K. A., *Inorganic Chemistry* **2013**, 52, 9606-9612.
77. Akiyama, K.; Hamano, T.; Nakanishi, Y.; Takeuchi, E.; Noda, S.; Wang, Z.; Kubuki, S.; Shinohara, H., *Journal of the American Chemical Society* **2012**, 134, 9762-9767.
78. Edelmann, F. T., *Coordination Chemistry Reviews* **2015**, 284, 124-205.

Chapter Two

Separation and Purification of Trimetallic Nitride Templated (TNT) Endohedral Metallofullerenes (EMF) Employing Exohedral Functionalization

Introduction

The subset of fullerenes described as trimetallic nitride templated endohedral metallofullerenes (TNT EMFs) discovered by Dorn et al.¹ hold the potential to be very important chemical starting materials in the future. This type of fullerene has been proposed for uses in the areas of medical imaging,²⁻⁹ medical therapeutics¹⁰⁻²⁰ and organic photovoltaics.^{12, 21-25} Unfortunately, the synthesis and purification of these materials is not trivial, and currently limits their availability.²⁶⁻²⁷ The efficient separation of TNT EMFs from soot-containing fullerenes, and specifically from other empty cage fullerenes, is the purpose for the work contained in this chapter.

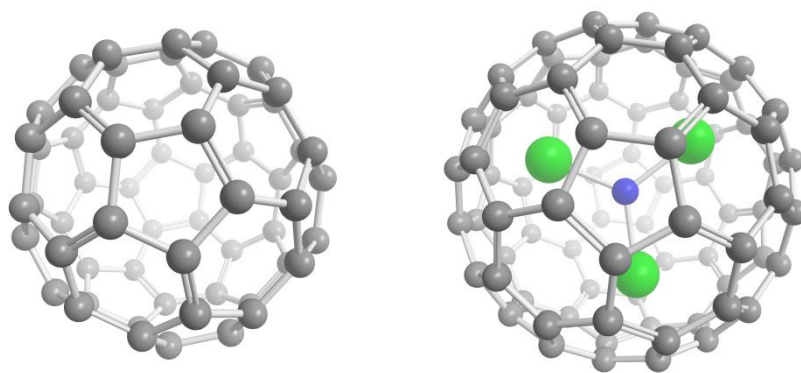


Figure 2.2. Structure of C_{60} (left) $Sc_3N@C_{80}$ (right).

TNT EMFs of the general form $A_3N@C_{80}$ where A = transition, lanthanide, or actinide metal are the focus of this chapter. They differ from empty cage fullerenes in that

they contain one nitrogen, and three metal atoms inside the fullerene cage, as seen in Figure 2.1. Specifically soot containing $\text{Sc}_3\text{N@C}_{80}$ was used as a representative of this class of materials. $\text{Sc}_3\text{N@C}_{80}$ is one of the most abundant TNT EMF species. The fullerene containing soot was extracted with toluene. The chromatogram shown in Figure 2.2 depicts the assortment of fullerenes produced in the Kratchmer-Huffman reactor. The major substituents of the mixture are C_{60} and C_{70} which elute at 6 and 8 minutes respectively. Polycyclic aromatic hydrocarbons elute between 3 and 5 minutes. Larger empty cage fullerenes, and smaller endohedral metallo fullerenes elute between 9 and 15 minutes. The compound of interest, $\text{Sc}_3\text{N@C}_{80}$ elutes at approximately 17 minutes.

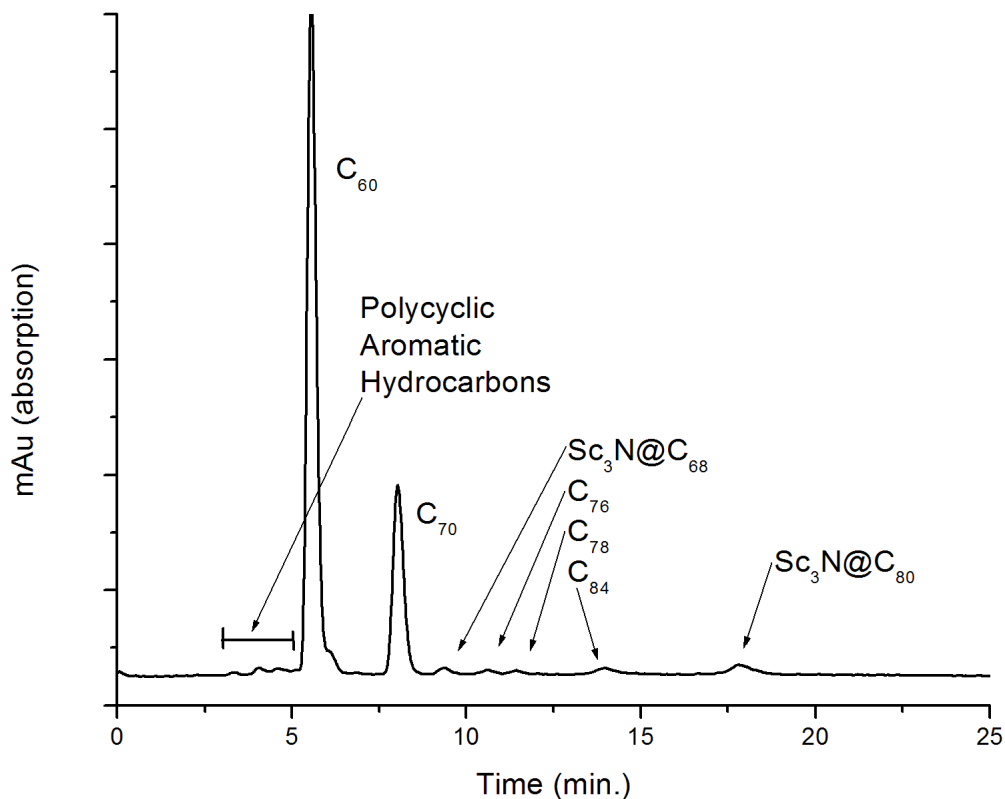


Figure 2.2. HPLC chromatogram of a stock solution of fullerenes extracted from Kratchmer-Huffman reactor soot (toluene, PYE functionalized silica gel, 1.0 mL/min).

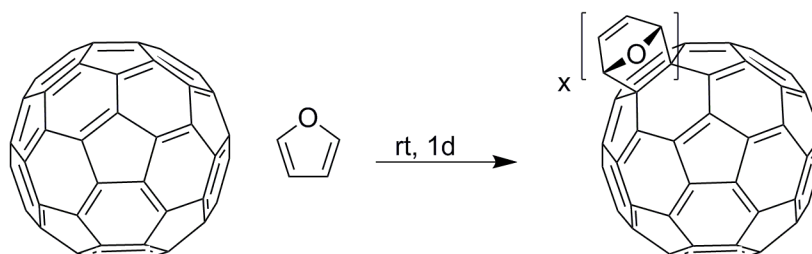
There are currently a number of methods used to separate TNT EMF species from empty cage fullerenes. Two previously reported methods are the use of functionalized Merrifield resin described by Dorn et al.²⁸ and the use of amino-functionalized silica gel described by Stevenson et al.²⁹ These methods take advantage of the lower reactivity of TNT EMF species relative to empty cage fullerenes. Therefore, using Sc₃N@C₈₀ as a model system is applicable here, as it is one of the most reactive TNT EMF's which are all less reactive than empty cage fullerenes. Any reactive separation that works for this molecule should work well for other TNT EMF's. The limitations of the published systems are their cost, speed, and difficulty of recyclability. Reported in this chapter is

the separation of TNT EMF species from empty cage fullerenes based on differences in reactivity. The general approach was to functionalize most or all of the empty cage species, and remove them using simple chromatography or precipitation. Several reactions of common reagents with empty cage fullerenes were examined. The reactions were evaluated on the basis of their speed, selectivity, and the ease or difficulty of separating the functionalized material. Two distinct types of reactions were used; either Diels-Alder, or nucleophilic addition type reactions. The current state of the art in the separation of TNT EMF's employs the reaction of the endohedral species with Lewis acids to form precipitates. Filtration and subsequent removal of the salts provides TNT EMF materials in high purity.³⁰⁻³⁴

Diels-Alder reactions

1. Functionalization and separation with furan

Empty cage fullerenes are particularly good diene substrates for Diels–Alder reactions. The reactivity of C_{60} with dienes is similar to that of maleic anhydride or maleimides.³⁵ Consequently, relatively poorly reactive dienes such as furan react with empty cage fullerenes. Two different types of experiments were conducted to determine if the Diels-Alder reaction with furan could be used to separate empty cage fullerenes from $Sc_3N@C_{80}$. Soot extract was reacted with furan, and fullerene containing soot was extracted with furan.



Scheme 2.1. Reaction of empty cage fullerenes with furan.

The stacked chromatograms in Figure 2.3 show the stock solution chromatographic trace, furan extract at room temperature, and the Soxhlet furan extract after one day. The splitting of the C_{60} and C_{70} peaks indicates that mono-adducts are being formed, and are soluble in furan. After the soot was extracted with furan, it was extracted with toluene. The relative concentration of $Sc_3N@C_{80}$ increased significantly; however, there was still a large amount of empty cage fullerenes in the toluene extracted

sample. In this case the selectivity was good, but the time and efficiency of the pre-extraction with furan were poor.

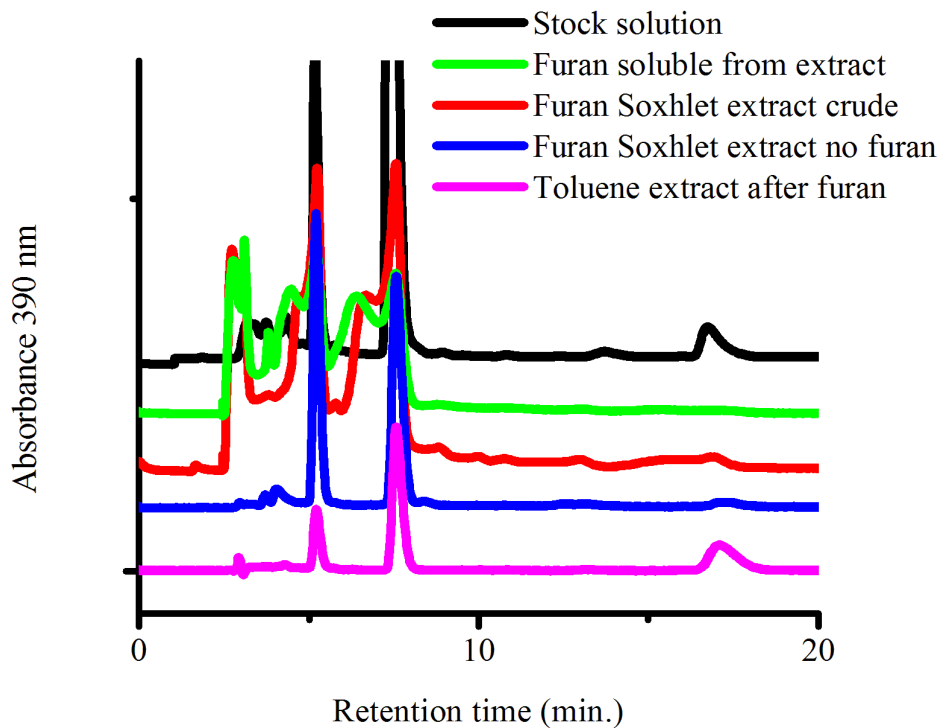


Figure 3.3 Stacked chromatograms from initial furan extractions. The $Sc_3N@C_{80}$ is seen at 17 minutes, C_{60} and C_{70} peaks are at 5 and 8 minutes respectively HPLC: 1.0 mL/min toluene pyrene functionalized silica.

Functionalization and separation of empty cage fullerenes using furan were initially explored by reacting fullerene extract with pure furan. In Figure 2.3, the top trace (black) shows the separation of a toluene extract of fullerene containing soot. The major peaks were assigned using data from the paper by Ge et al.,³⁶ since the same type of column was used. The major peaks of interest are C_{60} which appears near 6.6 minutes of retention time, C_{70} which appears near 8.9 minutes of retention time, and $Sc_3N@C_{80}$ which appears near 17.5 minutes of retention time. The empty cage fullerenes C_{60} and

C_{70} make up over 90 % of the extracted fullerene material, and consequently the area fractions of their peaks are tracked to determine how much of those materials have been removed. After the toluene had been removed, the residue was stirred with furan at room temperature for a day. The resulting solution was separated using the same HPLC conditions to give the second trace (green) in Figure 2.3. This trace shows the splitting of the empty C_{60} , and C_{70} peaks at 5.5, and 8.5 minutes, respectively. Soxhlet extraction of fullerene-containing soot was performed, and the extract solution was separated to give the third trace (red) in Figure 2.2. This trace shows more functionalized material as well as some $Sc_3N@C_{80}$ at 16.7 minutes. After removing the furan solvent, the residue was dissolved in toluene and separated to give the fourth trace (blue) in Figure 2.3. This trace shows the reversal of the Diels-Alder reaction with the C_{60} and C_{70} peaks, and a small amount of $Sc_3N@C_{80}$. Finally, the furan extracted soot was extracted with toluene, and the resulting solution was separated to produce the fifth trace (purple) in Figure 2.3. This trace shows peaks for C_{60} , C_{70} , and other empty cage fullerenes, as well as a larger peak for $Sc_3N@C_{80}$. In this case, since all of the extracted solutions were not treated the same way, it is difficult to quantify exactly how much of the empty cage material was removed compared to $Sc_3N@C_{80}$. In the original toluene extract solution the TNT EMF peak area was 5.0 % of the total peak area for the chromatogram. The second trace does not appear to contain any TNT EMF material, but did not contain much empty cage material either. The Soxhlet extraction with furan removed material that was only 0.7 % TNT EMF, while leaving behind extractable material that was 25.7 % TNT EMF. This indicates that pre-extraction of fullerene soot with furan does selectively remove empty cage fullerenes. This process is not very fast, as it takes two days to extract the fullerenes from soot.

In an effort to optimize the separation, a series of extractions from fullerene-containing soot was undertaken using mixtures of furan and methanol. The use of methanol with furan was intended to increase the selectivity of the extraction. Generally fullerenes are insoluble in methanol, but the furan adducts could be soluble. In order to hasten the extractions, they were performed in an ultrasonic bath. Sonication has been shown to increase the speed of Diels-Alder reactions, particularly in volatile solvents.³⁷⁻⁴⁰ A series of extractions was performed using mixtures of furan and methanol with fullerene-containing soot. The samples were sonicated for four hours and then the supernatant liquid was extracted and characterized by HPLC. The resulting HPLC traces are shown in Figure 2.4.

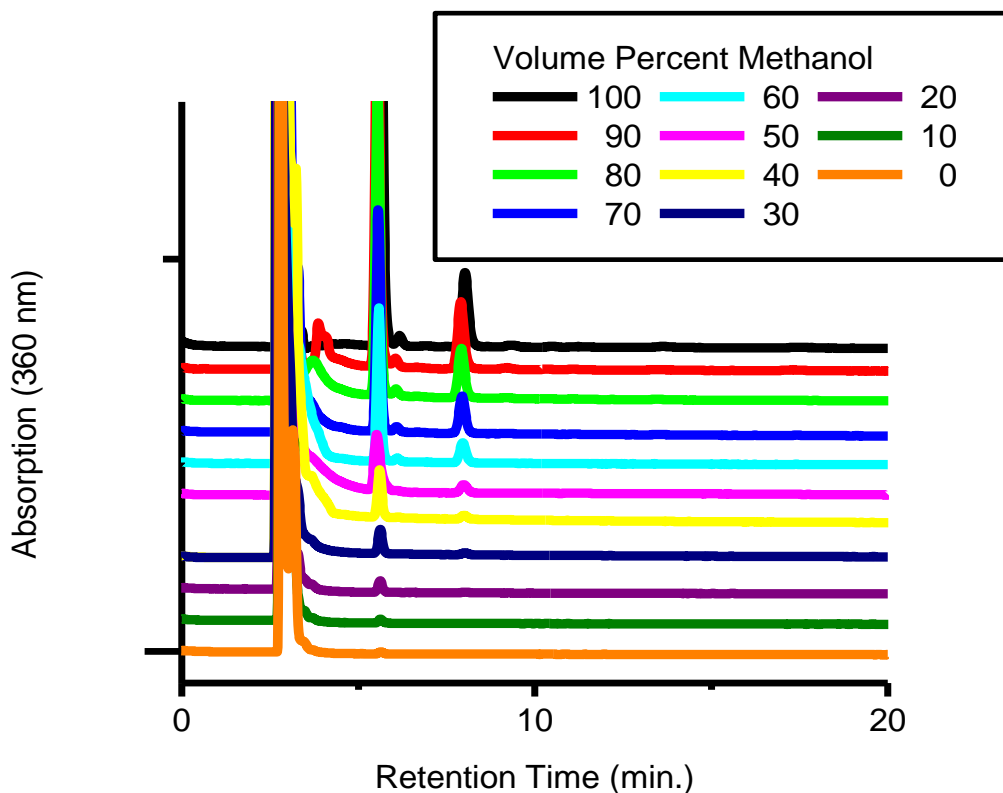


Figure 2.4. Stacked chromatogram showing the extracted fullerene and PAH material after sonication for 4 hours with different solutions of furan and methanol. HPLC: pyrene functionalized silica, toluene 1.0 mL/min.

The stacked chromatograms in Figure 2.4 show that as the concentration of methanol in the extraction solvent increases, the amount of fullerenes extracted decreases. Peaks of note in the chromatograms are poly(aromatic hydrocarbon)s at 3.1 minutes, C₆₀ at 5.7 minutes, and C₇₀ at 8.5 minutes. The peak for Sc₃N@C₈₀ is very small and not visible in the figure above, but upon magnification it can be seen at 17.5 minutes. The chromatograms at the bottom of the figure, corresponding to high levels of methanol, show only the removal of poly(aromatic hydrocarbon)s. Therefore, extraction

with a mostly methanol mixture is useful for removal of non-fullerene species. Empty cage and TNT EMF species were removed using only up to 20 % methanol. The peak areas of the C_{60} , C_{70} , and $Sc_3N@C_{80}$ peaks, compared to a toluene extraction are shown in the plot in Figure 2.5.

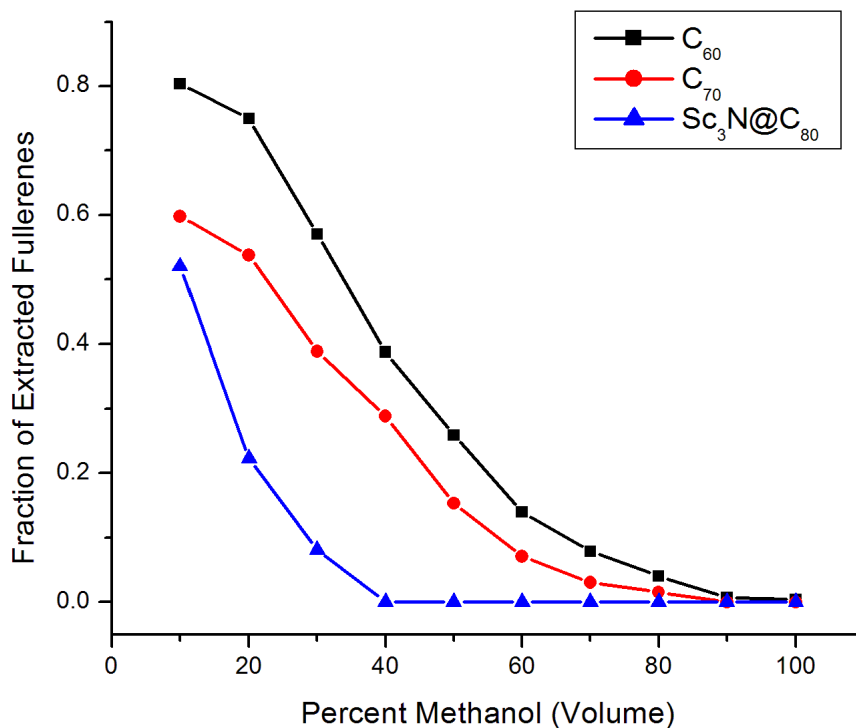


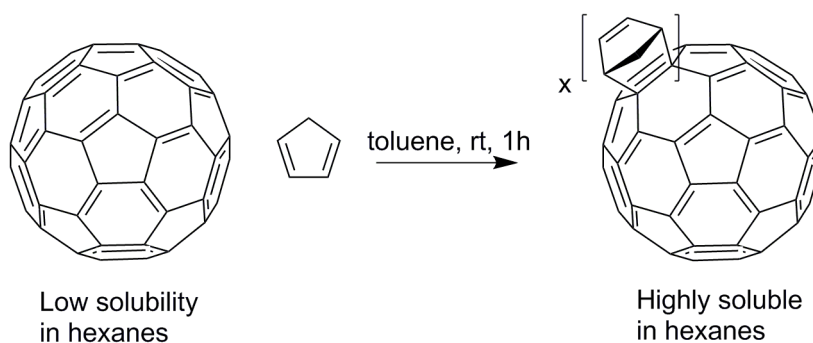
Figure 2.5. Plot of various fullerenes extracted using different mixtures of furan and methanol normalized by the amounts extracted with toluene.

The plot in Figure 2.5 shows the fraction of fullerenes extracted by the different mixtures of furan and methanol, relative to an extraction with toluene. The amounts of all fullerenes drop rapidly as the volume percentage of methanol is increased. Methanol is therefore an excellent non-solvent for unfunctionalized fullerenes. Unfortunately, the selectivity of the solvent mixtures for empty cage fullerenes over TNT EMF species is

poor. The TNT EMF species are less soluble than empty cage fullerenes as the concentration of methanol increases, but the overall solubility of fullerenes is drastically decreased. This method is not selective enough to be of use for the purification of TNT EMF species.

B. Functionalization and separation with cyclopentadiene

The Diels-Alder reaction between fullerene C_{60} and cyclopentadiene is known.^{28, 41-44} In this case, the reaction is very favorable due to the fact that C_{60} is a very good dienophile, and cyclopentadiene is a very good diene. The reaction between the two, with an excess of cyclopentadiene, very quickly gives the hexa-adduct. This reaction took less than an hour. Since the additions to the fullerene cage occur across the 6,6-double bonds between two five-membered rings, the addition product elutes soon after the void volume (approximately 3 mL) on a pyrene (PYE) functionalized silica HPLC column due to the decreased interaction between the stationary phase and the fullerene subunit.



Scheme 2.2. Functionalization of empty cage fullerenes using cyclopentadiene.

Using Diels-Alder cycloaddition for fullerene separation is already known in the case of cyclopentadiene (CP)-functionalized Merrifield resin as reported by Dorn et al.²⁸ The limitations of this method are the cost of the parent resin, and the adverse conditions of using the cyclopentadienyl anion to functionalize the resin. However, cyclopentadiene itself is inexpensive and readily available. A second advantage of the reaction of empty cage fullerenes with cyclopentadiene itself, as opposed to the resin supported analog, is that in solution the concentration of the reactive diene can be more easily controlled. In the case of the functionalized resin, the diene moieties may dimerize over time and reduce the overall efficiency of the medium. By using freshly cracked and distilled cyclopentadiene for the functionalization reaction the amount and condition of the diene can be controlled.

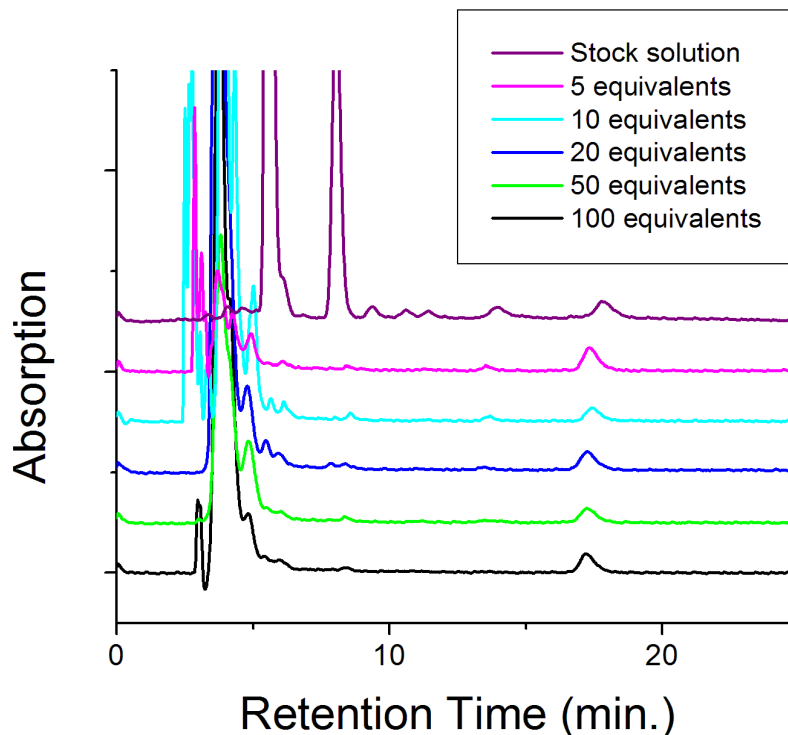


Figure 2.6 Stacked chromatographic plot showing the functionalization of empty cage fullerenes and their coalescence into large peaks shortly after the void volume (approx. 3 mL). HPLC: pyrene functionalized silica, toluene 1.0 mL/min.

Initial experiments began by reacting cyclopentadiene with a toluene solution of fullerenes extracted from soot. The extract solution and cyclopentadiene were stirred together in different molar ratios based on the concentrations of C_{60} and C_{70} in the extract solution. The reaction solutions were treated equally so that their chromatograms could be compared. The stacked chromatograms in Figure 2.6 show the conversion of C_{60} and C_{70} , with peaks at 5.6 and 8.1 minutes, into functionalized material with peaks at approximately 4.1 minutes. The functionalized materials have a much weaker interaction with the pyrene functionalized stationary phase and therefore elute shortly after the void volume. The peak for $Sc_3N@C_{80}$ appears at 17.5 minutes and remains

fairly constant in area during the reaction of the empty cage fullerenes. The peak identities for the major peaks were confirmed by MALDI TOF mass spectrometry; smaller peaks in the stock solution were identified as larger empty cage fullerenes

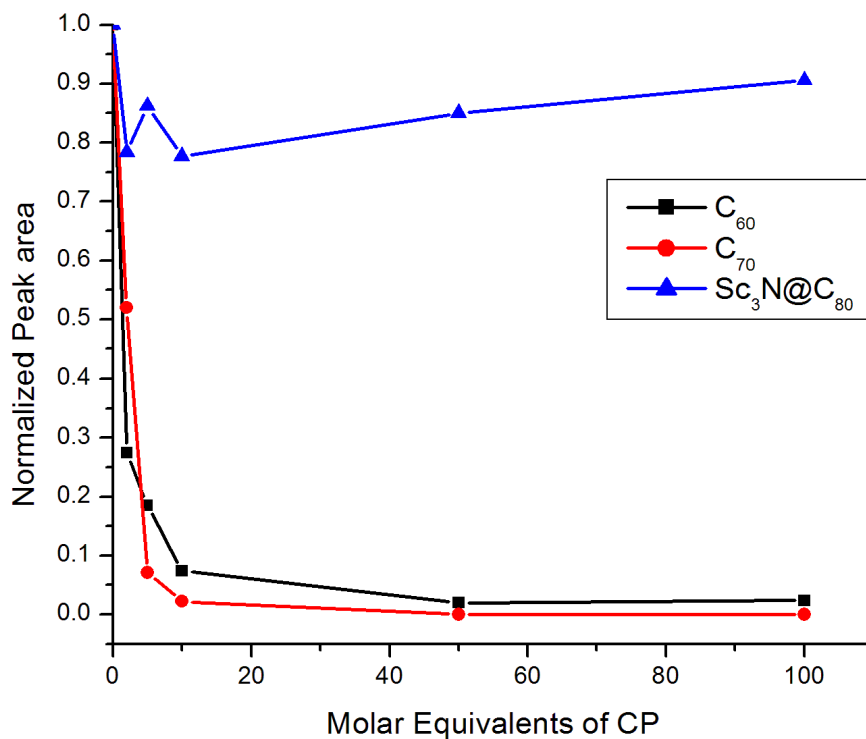


Figure 2.7. Plot showing the area fraction of C₆₀ (black), C₇₀ (red), and Sc₃N@C₈₀ (blue) chromatographic peaks as the number of equivalents of cyclopentadiene increased.

The plot in Figure 2.7 shows the area fraction of the C₆₀, C₇₀, and Sc₃N@C₈₀ peaks compared to their original peak areas, as the molar equivalents of CP are increased. The rapid disappearance of C₆₀ and C₇₀ peaks and the near constant area of Sc₃N@C₈₀ peak, show that this functionalization method is selective for empty cage fullerenes.

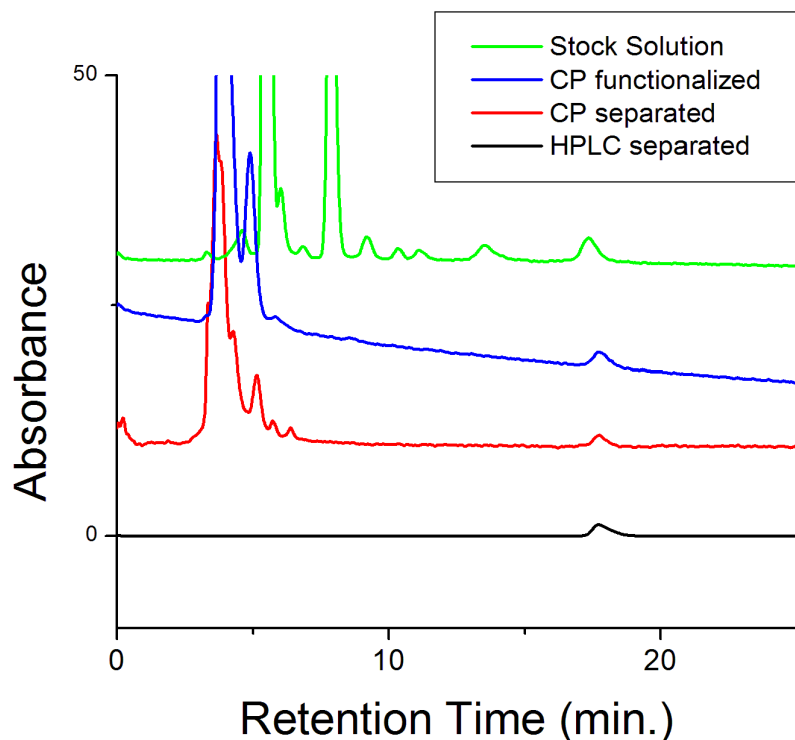


Figure 2.8. Stacked chromatographic plot illustrating the purification steps for $\text{Sc}_3\text{N@C}_{80}$. Stock solution (green) was treated with cyclopentadiene (blue). The treated mixture was separated on silica gel to remove most of the functional material (red). Finally the mixture was purified by a single pass on the HPLC (black). HPLC: pyrene functionalized silica, toluene 1.0 mL/min.

The functionalized fullerenes were then removed by simple column chromatographic separation on silica gel using hexanes and toluene. The stacked chromatograms in Figure 2.8 show the original stock solution, functionalized empty cage fullerenes, separated functionalized materials, and the final sample of $\text{Sc}_3\text{N@C}_{80}$ purified by HPLC. It is important to note that like other separation methods based on the reactivity of TNT EMF molecules, final purification is accomplished by HPLC. This is not to say that reactive separation is ineffective, but it generally cannot produce highly

purified samples in a single treatment. The MALDI TOF mass spectrum of the final sample is shown in Figure 2.9, identifying it as pure $\text{Sc}_3\text{N@C}_{80}$.

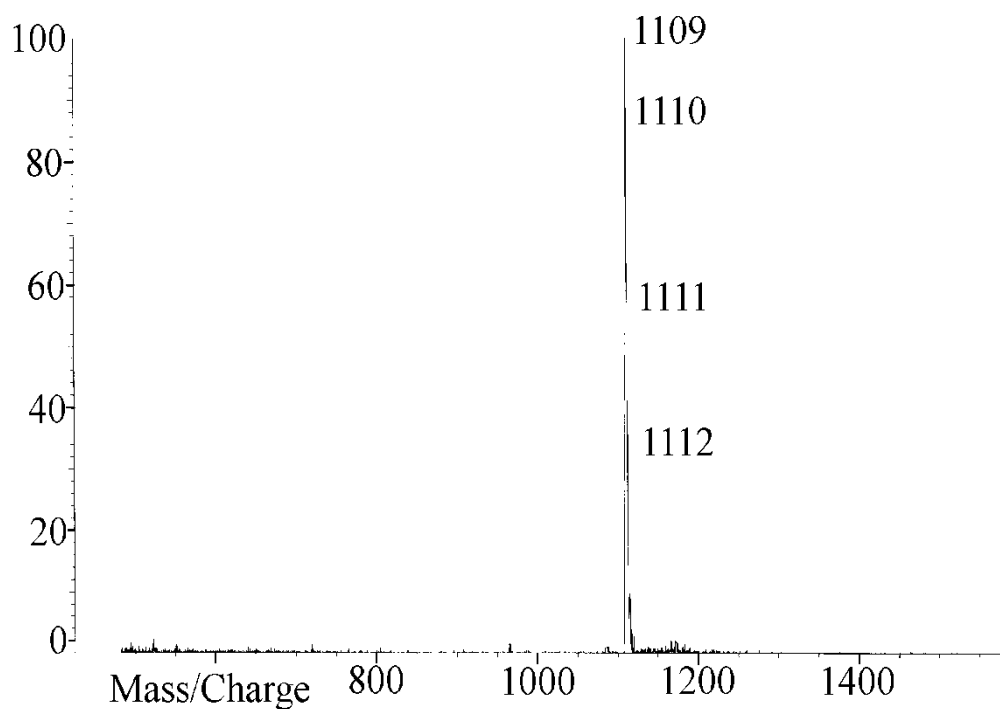


Figure 2.9. MALDI TOF mass spectrum of purified $\text{Sc}_3\text{N@C}_{80}$. This material was obtained after cyclopentadiene treatment and one HPLC separation. The molecular weight of $\text{Sc}_3\text{N@C}_{80}$ is 1109 Da.

The recoverability of the empty cage fullerenes and functionalizing reagents was also explored. The retro-reaction of cyclopentadiene functionalized materials was explored by heating them under vacuum and then characterizing the resulting mixture by HPLC. Reversal of cyclopentadiene functionalization was effective using vacuum (~ 0.1

mm Hg) and high temperature (150 °C) as seen in Figure 2.10. The recovery of the functionalizing reagent in the case of Diels-Alder reactions is theoretically possible via condensation of the diene, but it may be difficult for small quantities of materials.

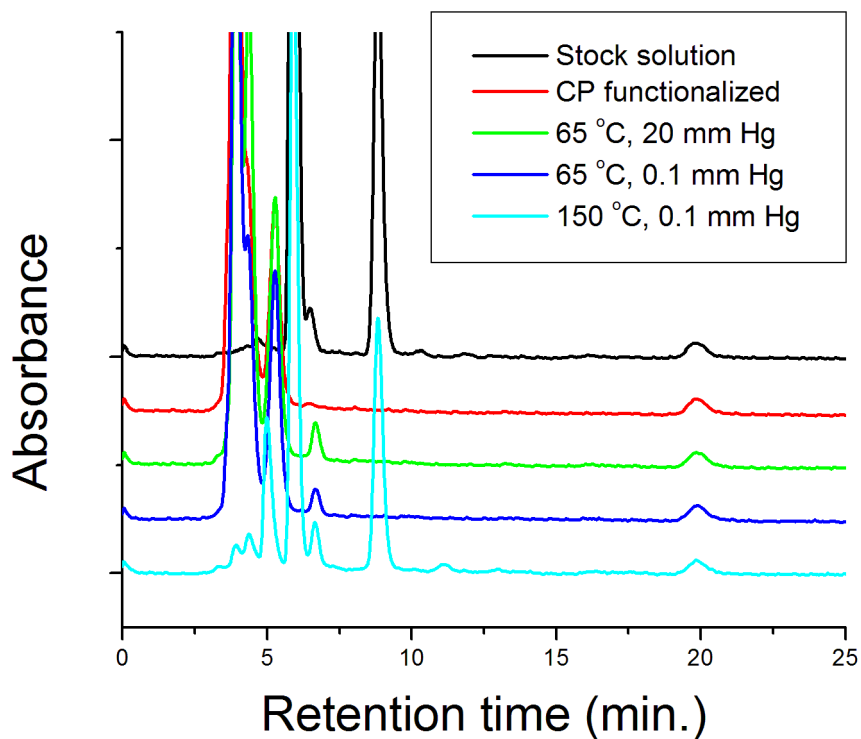


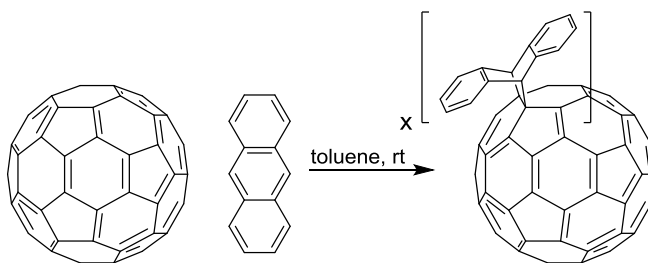
Figure 2.10. Stacked chromatographic plot showing the reversibility of the reaction with C₆₀. Fullerene extract was functionalized with cyclopentadiene and then subjected to different levels of vacuum and heat. Heating to 150 °C under 0.1 mm Hg reversed the reaction and gave peaks matching the starting materials. HPLC: pyrene functionalized silica, toluene 1 mL/min.

Figure 2.10 shows chromatograms for the original stock solution, the solution after CP functionalization, and then after three different heating/vacuum regimes. Initially the functionalized material was heated at 65 °C on a rotary evaporator, under

vacuum provided by a water aspirator (~20 mm Hg), these conditions did not noticeably change the resulting chromatogram. Then the functionalized material was heated at the same temperature under vacuum provided by a vacuum pump (~0.1 mm Hg). This again did not change the resulting chromatogram. Finally the functionalized material was heated to approximately 150 °C with a heat gun, and vacuum was provided by a vacuum pump. The resulting chromatogram for this sample contains peaks for the unfunctionalized C₆₀, and C₇₀ and the recovery was high. This shows that with high heat and vacuum the functionalization with CP is reversible.

C. Functionalization and separation using anthracene

Following the work done in the Dorn group with 9-methylantracene functionalization, we proposed the reaction with unsubstituted anthracene as it is less expensive. The reaction of empty cage fullerenes such as C₆₀ with anthracene is shown in Scheme 2.3 below.



Scheme 2.4 Reaction of empty cage fullerenes with

Initial experiments showed that the anthracene Diels-Alder reaction is selective for the functionalization of empty cage fullerenes over TNT EMF species. Unfortunately, the separation of the functionalized material and anthracene from the reaction mixture was initially problematic. More recent attempts with this work have

focused on flash chromatographic separation of the functionalized fullerenes from the TNT EMF's.

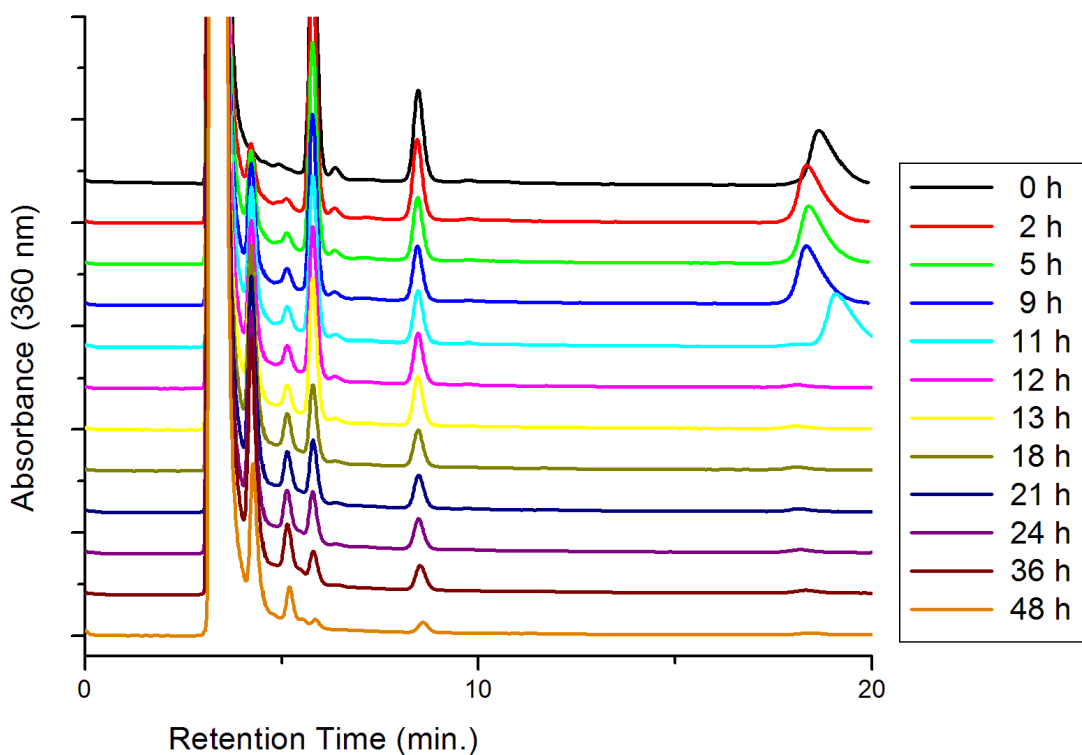


Figure 2.11. Stacked chromatograms showing the functionalization of empty cage fullerenes with anthracene. The peaks for C₆₀ (5.6 min.) and C₇₀ (8.2 min) decrease in area over two days. HPLC: pyrene functionalized silica, toluene 1.0 mL/min.

The stacked chromatograms in Figure 2.11 show the functionalization of empty cage fullerenes over time using 20 equivalents of anthracene. The peaks for C₆₀ (5.8 min.) and C₇₀ (8.2 min) decrease in area over 48 hours, while the peaks for Sc₃N@C₈₀

(18.5 min) remain nearly the same intensity until the last sample. The chromatograms are interesting in the very large anthracene peak that is seen at approximately 3.6 minutes. While it is simple to assign the reduction of area in the empty cage fullerene peaks to the formation of adducts, the very large anthracene peak overshadows the peaks generated by the functionalized material. There is also a peak that initially occurs at the same retention volume as $\text{Sc}_3\text{N@C}_{80}$. This may be an impurity in the anthracene, or some sort of multi-adduct. By the time 11 hours had passed, this peak moved to a higher elution time at approximately 22 minutes. The characteristics of anthracene functionalization are that the reaction is slower than CP and DETA, and the adducts and diene need to be removed in order to purify the sample. The separation of this mixture was originally done with

diethyl ether on silica gel. This type of separation is difficult to achieve.

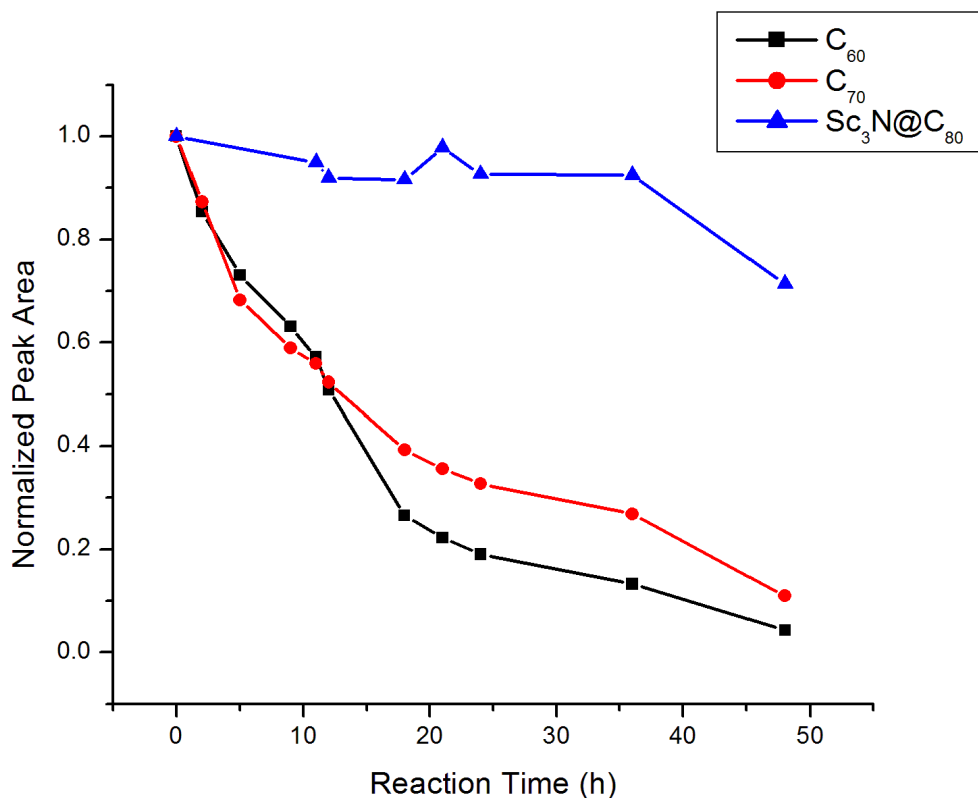
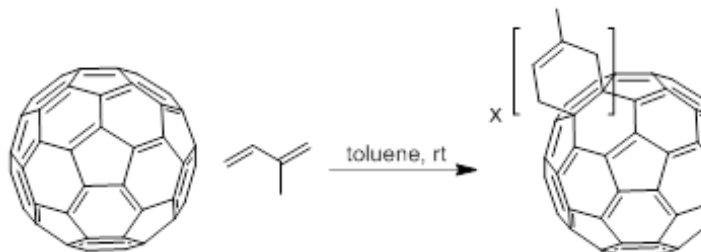


Figure 2.12. Plot of the relative peak areas of C₆₀ (black), C₇₀ (red), and Sc₃N@C₈₀ (blue) during the functionalization reaction with anthracene. The peak areas for both of the major empty cage fullerenes decrease over time, while the TNT EMF peak remains constant. This indicates that the Diels-Alder reaction is selective for the empty cage fullerenes.

The plot in Figure 2.12 shows the disappearance of the C₆₀ and C₇₀ peaks over time. The Sc₃N@C₈₀ peak remains approximately the same intensity. If it was not for the difficulty in separating the reaction mixture, and the slow speed of this reaction, it would be comparable to CP functionalization. The selectivity of this reaction is better than CP functionalization, but the time it takes and the final separation leave much to be desired.

D. Functionalization with isoprene

Functionalization with isoprene is an interesting prospect for the separation of TNT EMF species from empty cage fullerenes. The reaction of C_{60} with isoprene is shown below in Scheme 2.4.



Scheme 2.4. Reaction of empty cage fullerenes with isoprene

Isoprene has a low boiling point and, therefore, is readily removed from the reaction mixture. Unfortunately, compared to the other dienes, like cyclopentadiene or anthracene, the geometry of the two double bonds is not fixed and, therefore, the reaction of empty cage fullerenes with isoprene is much slower.

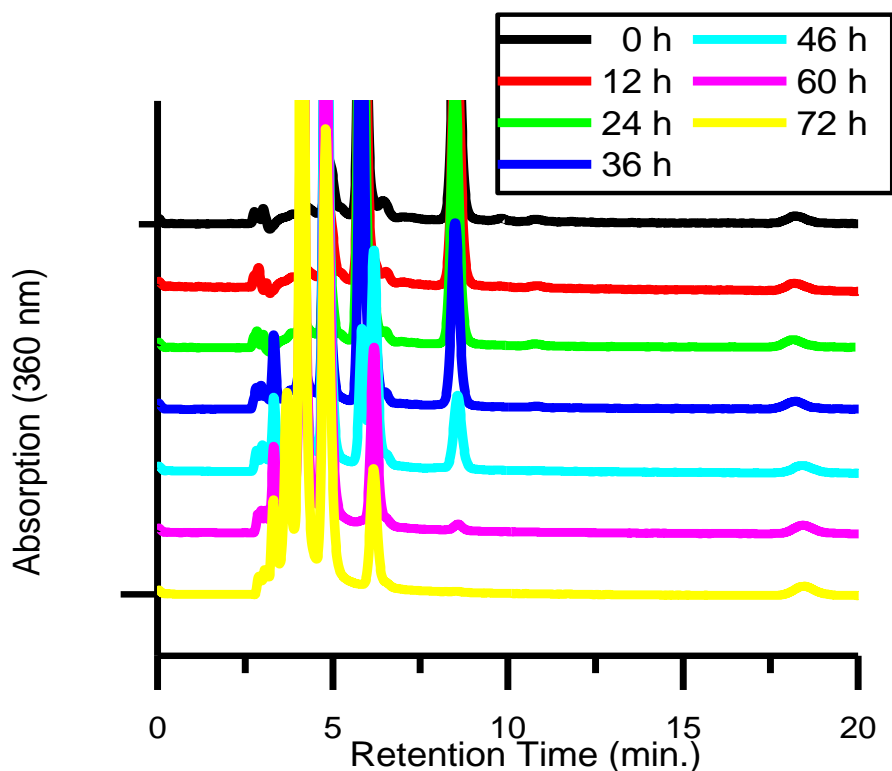


Figure 2.13. Stacked chromatographic traces of fullerene extract as it is reacted with isoprene over time. The peaks for C_{60} (5.8 min) and C_{70} (8.0 min) decrease in size and disappear entirely over time. The peak in the last two traces at 6 min. is not C_{60} but is probably the mono-adduct of C_{70} . HPLC: pyrene functionalized silica, toluene 1 mL/min.

The stacked chromatograms in Figure 2.13 show the functionalization of empty cage fullerenes using isoprene. The reaction was characterized by HPLC for three days until the major empty cage constituents (C_{60} and C_{70}) were both functionalized. The peaks at approximately 6 minutes in the last two traces are not C_{60} as they are in the initial traces, but are probably the mono adduct of C_{70} . The cleanliness of the chromatograms generated from the isoprene reaction, and the ease with which the diene is removed make the isoprene reaction desirable as a method for separating TNT EMFs.

However, the length of time it takes to run the functionalization reaction makes this method prohibitive. Another problem with this separation routine is that the flash chromatographic method for separating the functionalized material from the TNT EMFs involves the use of diethyl ether and silica gel. These conditions make this separation more difficult than the hexanes/toluene system used for cyclopentadiene. The need for the ether column is probably due to the fact that most of the reaction products are mono-adducts. This means that there is less difference between the functionalized materials and the unreacted TNT EMFs.

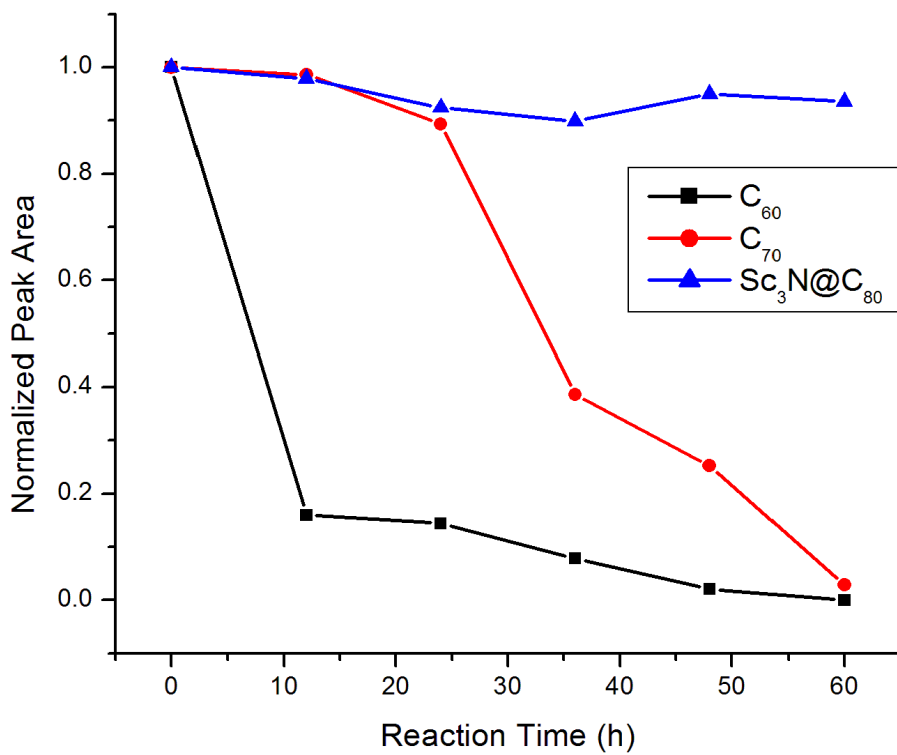
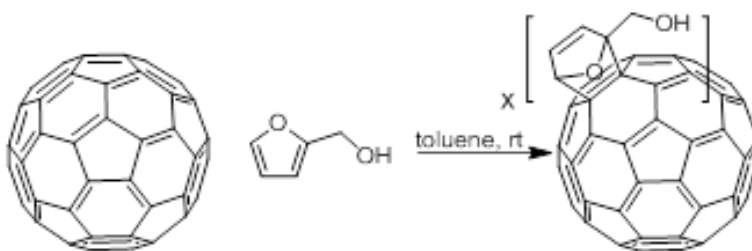


Figure 2.14. Plot of the peak areas of C_{60} (black), C_{70} (red), and $Sc_3N@C_{80}$ (blue) relative to their initial areas, over time during the reaction with isoprene. The reactivity of C_{60} as compared to C_{70} is much higher. Most of the C_{60} peak area is gone by the end of the first day. The $Sc_3N@C_{80}$ peak area remains constant during the

Figure 2.14 shows the area fraction of the empty cage peaks (C_{60} , C_{70}), and the TNT EMF peak as the reaction time increases. The $Sc_3N@C_{80}$ peak remains consistently above 95 % of its original area, while the empty cage peaks both decrease to zero after three days. This plot further illustrates that the functionalization reaction with isoprene is very selective for TNT EMF species, but the speed of the reaction and the separation conditions make this separation method less desirable.

E. Functionalization with furfuryl alcohol

The reaction of furfuryl alcohol with empty cage fullerenes was also marginally successful. It was hoped that the addition of the hydroxymethyl group at the 2-position would lend more electron density to the furanyl diene. This may have helped marginally, but it also made the diene very difficult to remove from solution due to the increase in its boiling point. Ideally, the reaction would have produced fullerene multi-adducts that were water soluble and could be removed by washing with water.



Scheme 2.5. Reaction of empty cage fullerenes with furfuryl

Close inspection of the stacked chromatograms in Figure 2.15 shows that there were probably no more than mono-adducts present, since the peaks do not shift substantially from those of the stock solution. Furfural alcohol was allowed to react with a mixture of fullerenes extracted from soot for a day at room temperature. The solution was extracted using methanol, and the residual fullerenes were characterized by HPLC.

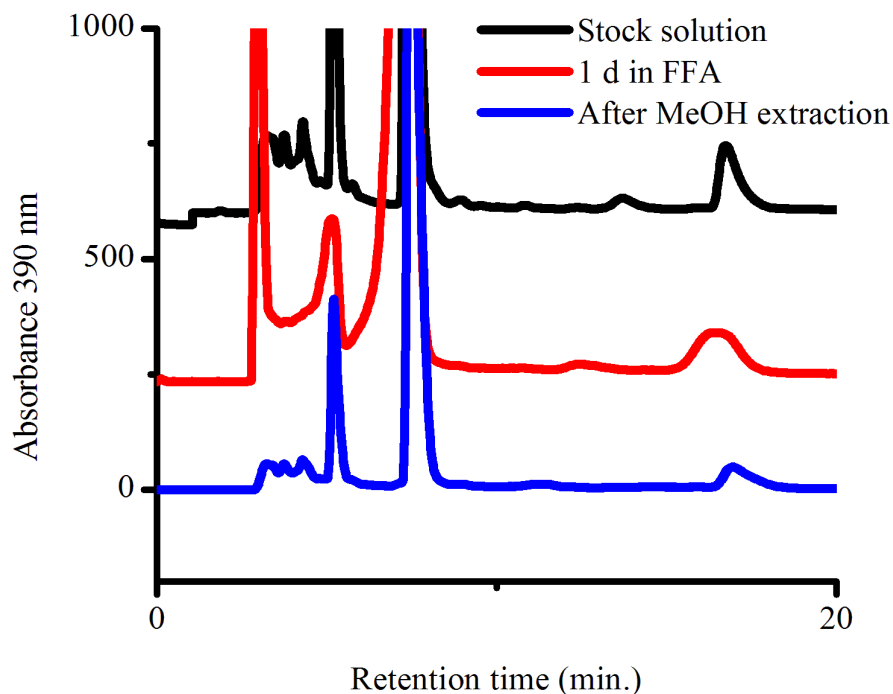
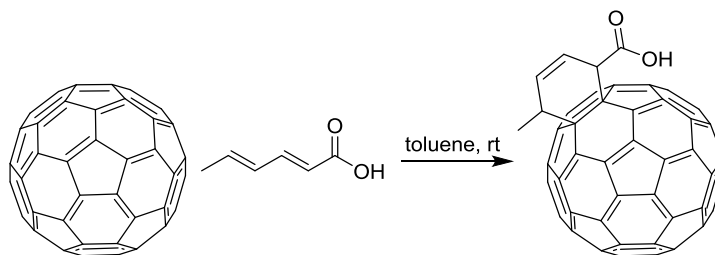


Figure 2.15. Stacked chromatograms showing the removal of mainly C_{60} by functionalization with furfuryl alcohol. HPLC: toluene 1 mL/min, pyrene functionalized silica.

The stacked chromatograms in Figure 2.15 show the removal of a significant amount of C_{60} from the mixture by methanol extraction after furfuryl alcohol functionalization, as indicated by the peak at 5.8 minutes. The peak for C_{70} remains nearly constant. This is probably due to the higher reactivity of C_{60} compared to other empty cage fullerenes. Due to this separation technique and the removal of most of the C_{60} , the relative area of the $Sc_3N@C_{80}$ peak doubled from that of the stock solution. The speed and efficiency of this reactive separation are very poor compared to the other dienes.

F. Functionalization with sorbic acid

The reaction of empty cage fullerenes with sorbic was unsuccessful. In this case, the diene is of poor reactivity due to the carboxylic acid moiety, as well as the less than ideal conformational freedom of the diene. Sorbic acid also has very limited solubility in toluene, which makes it a poor choice for reactions with fullerenes.

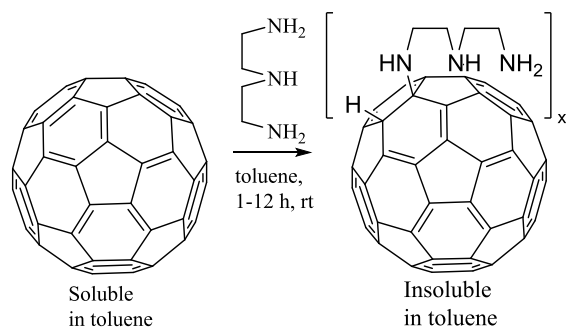


Scheme 2.6. Reaction of empty cage fullerenes with sorbic acid.

Nucleophilic Addition Reactions

G. Functionalization and separation using diethylenetriamine (DETA)

This type of reaction was considered based on the success of the work done by Stevenson et al. with amine functionalized silica gel.²⁹ Diethylenetriamine (DETA) is a readily available, inexpensive organic reagent. In this case nucleophilic substitution on empty cage fullerenes by the primary and secondary amine moieties decreases the solubility of the fullerene adducts in toluene. A second benefit of this approach is the trifunctionality of the reacting species. It should be possible to form polymeric and cross-linked networks from empty cage fullerene species and DETA.



Scheme 2.7. Reaction between empty cage fullerenes and DETA.

The mass spectrum of the solid products of C_{60} and DETA (Figure 2.16) shows a large number of adducts; most of the functionalized material precipitates from solution in toluene. The undecorated C_{60} (+H) peak is seen at m/z 721 Da. The other major peaks in the mass spectrum that occur at m/z 820, 921, and 1022 Da are mono-, bis- and tris-adducts after the loss of several protons in each case.

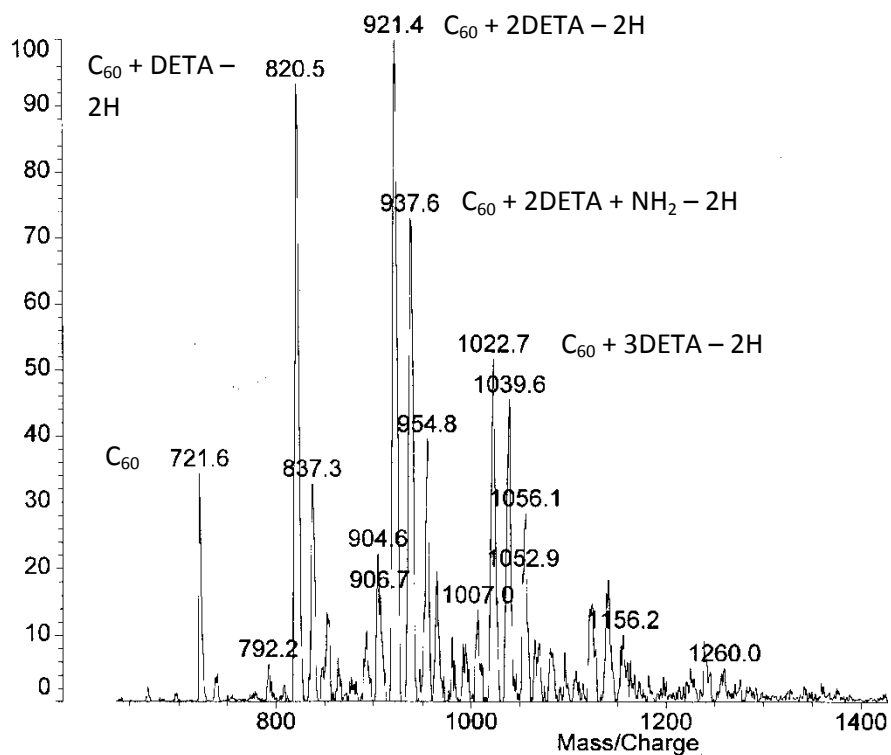


Figure 2.16. Mass spectrum of the crude reaction product of C_{60} and DETA.

The initial experiment for this reactant was performed in the same manner as that for cyclopentadiene. Portions of the fullerene extract stock solution were reacted with DETA in toluene at room temperature for 4 hours. After the reaction the solutions were separated on silica gel using toluene and analyzed by HPLC using the same conditions as the CP separations. Thus, while the DETA process is slower than separation by CP functionalization, it does contain a simpler chromatographic step.

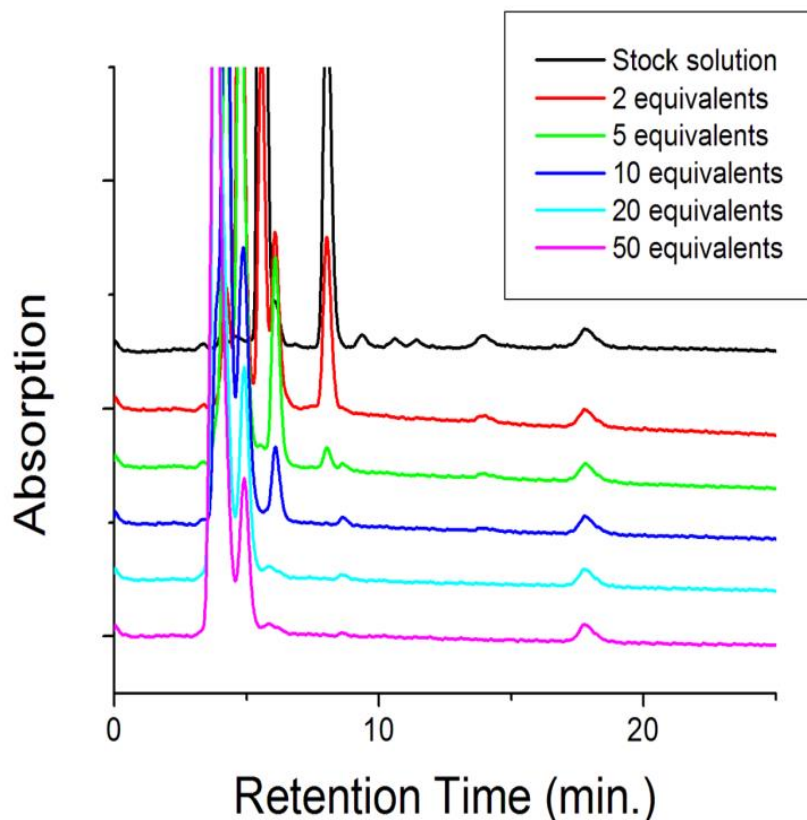


Figure 2.17. Stacked chromatographic plots showing the conversion of empty cage fullerenes, after reaction with DETA, to amine functionalized material that elutes shortly after the void volume (approximately 3 minutes). The extent of conversion increases as the number of equivalents of DETA increase. HPLC: pyrene functionalized silica, toluene 1 mL/min.

Figure 2.17 shows the conversion of empty cage fullerenes to functionalized materials. The reaction with DETA was slower than cyclopentadiene; therefore, more equivalents are required to functionalize all of the empty cage fullerenes in the stock solution in the same amount of time.

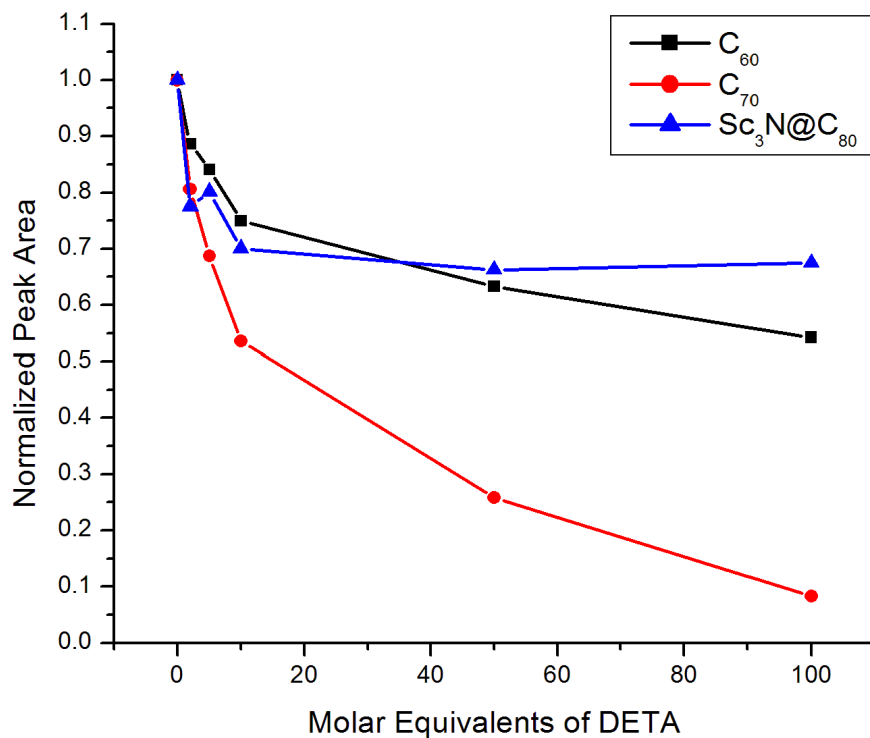


Figure 2.18. Plot of the chromatographic peak areas of C_{60} (black), C_{70} (red), and $Sc_3N@C_{80}$ (blue) as the molar equivalents of DETA in the reaction increase. The C_{60} and C_{70} peak areas decrease faster than the $Sc_3N@C_{80}$ peak.

Figure 2.18 shows the relative consumption of empty cages as the number of molar equivalents of DETA was increased. In the reaction with DETA the $Sc_3N@C_{80}$ peak loses area faster than in the experiment with CP. This indicates that the DETA functionalization process is less selective under these conditions.

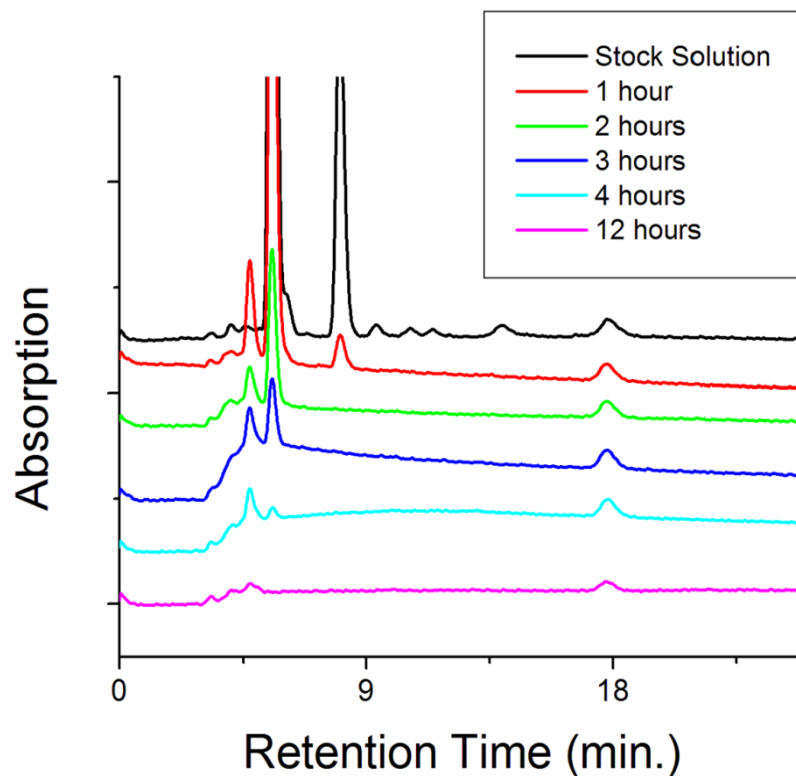


Figure 2.19. Stacked chromatograms showing the functionalization and removal (by precipitation) of empty cage fullerenes over time. The chromatogram for 12 hours of reaction time (violet) shows only small amounts of poly(aromatic hydrocarbon)s in addition to the $\text{Sc}_3\text{N@C}_{80}$ peak. HPLC: pyrene functionalized .silica, toluene 1.0 mL/min.

Figure 2.19 shows stacked chromatograms from a reaction time study completed using 20 molar equivalents of DETA. The DETA reaction takes longer, as much as half a day, but with the reduced solubility of the reacted empty cages, the resulting mixture of fullerenes is almost exclusively $\text{Sc}_3\text{N@C}_{80}$ as shown in Figures 2.18 and 2.19.

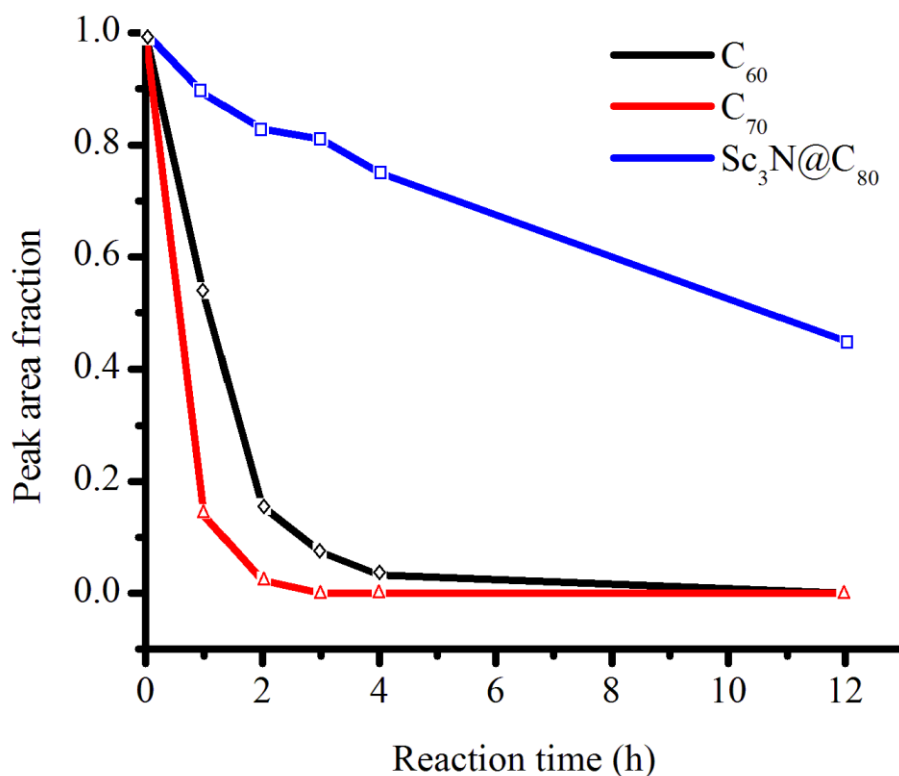


Figure 2.20. Plot of chromatographic peak area for C₆₀ (black), C₇₀ (red), and Sc₃N@C₈₀ (blue). The empty cage peaks disappeared quickly over time due to reaction with DETA while the Sc₃N@C₈₀ peak retained much of its area. An excess of DETA (10 molar equivalents) was used for this study.

Figure 2.20 shows the conversion and removal of C₆₀, C₇₀, and Sc₃N@C₈₀ over time. While this method removes the vast majority of empty cage species over time, the final concentration of Sc₃N@C₈₀ is less than half of that in the stock solution. Thus, while this method is very effective for the removal of fullerenes from solution, it is less selective than the method using CP.

H. Functionalization with dimsyl sodium

The reaction of empty cage fullerenes with dimsyl sodium was discovered during attempts to react imidazolium ionic liquids with C_{60} . In an effort to dissolve the ionic liquid and the fullerene in the same solution, a mixture of toluene and DMSO was employed. Sodium hydride was used to deprotonate the ionic liquid, and generate the carbene that would hopefully add to the fullerene cage. MALDI TOF mass spectrometry of the reaction mixture seen in Figure 2.21 did not show the anticipated imidazole adduct, but multiple adducts separated by 100 Da each.

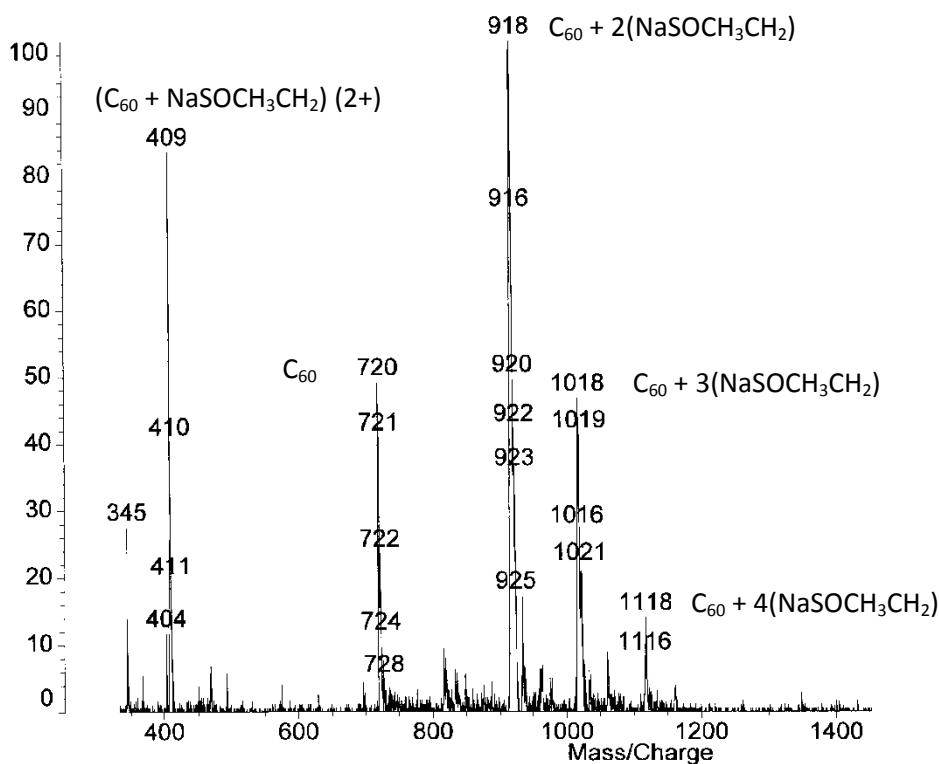
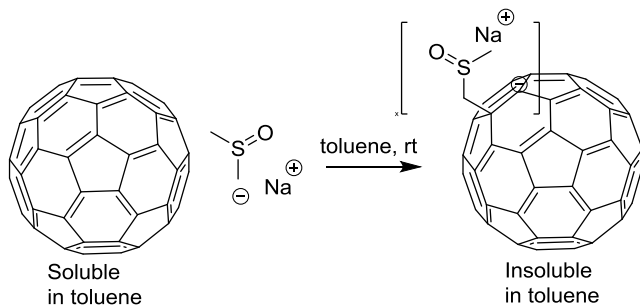


Figure 2.21. MALDI TOF spectrum of the crude product of the reaction of C_{60} and dimsyl sodium.

Perusal of the literature revealed that the products of sodium hydride addition to DMSO are the strong base dimethyl sodium, and hydrogen.⁴⁵⁻⁴⁷ Dimethyl sodium has a molecular weight of 100.13 Da. Thus it was speculated that in the same manner as the addition of butyllithium to C₆₀ to form the butylated fulleride anion lithium salt, dimethyl sodium was adding to C₆₀ to form a sulfoxide fulleride salt as shown in Scheme 2.8. The MALDI TOF mass spectrum of the reaction mixture of C₆₀ with an excess of dimethyl sodium in toluene is given in Figure 2.21. The major peaks correspond to the original C₆₀ at m/z 720 Da, the bis-adduct of dimethyl sodium (- 2H) at m/z 918 Da, the tris-adduct (- 2H) at m/z 1018, and the tetra-adduct (- 2H) at m/z 1118. The large peak at m/z 409 Da is probably the mono-adduct with a double negative charge (818 Da, 2⁻ charge, - 2H).



Scheme 2.8. Reaction of empty cage fullerenes with dimethyl sodium.

Further investigation of this phenomenon with a mixture of fullerenes showed that the dimethyl sodium anion preferentially reacts with empty fullerene cages over Sc₃N@C₈₀. It is also useful to note that the fulleride salts precipitate from solution. Thus a separation scheme was based on the reaction of dimethyl sodium with empty cage fullerenes in order to render a solution of mainly Sc₃N@C₈₀. This reaction was found to be very fast and effective compared to the CP and DETA separations. The stacked chromatograms in

Figure 2.22 show the removal of empty cage fullerenes within 30 minutes total time, and no chromatographic step is required.

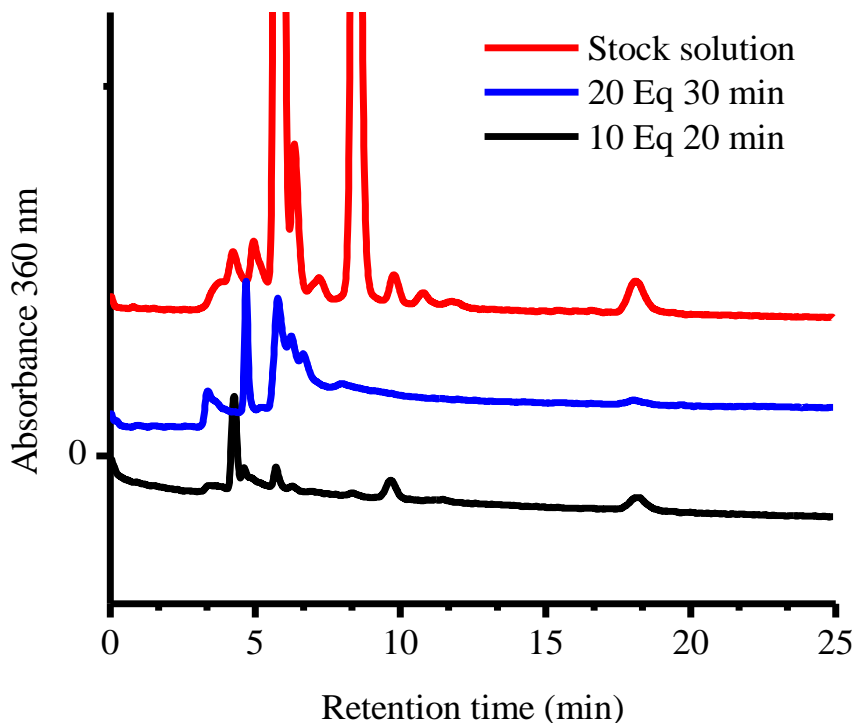


Figure 2.22. Stacked chromatograms showing the removal of fullerenes from solution after reacting with dimethyl sodium, precipitation and filtering. HPLC: pyrene functionalized silica, toluene 1.0 mL/min.

CONCLUSIONS

Separation of TNT EMF species from fullerene soot can be achieved by functionalization using small molecules that are inexpensive and readily available. Pre-extraction of empty cage fullerenes using mixtures of furan and methanol proved to be less effective than separation media such as Merrifield resin or amine functionalized silica gel. CP functionalization was fast and efficient, but required the use of column

chromatography. Consequently, functionalization with cyclopentadiene is slower and less effective than using Merrifield resin. The use of DETA, while slower than the CP method, was effective, and employed a simpler chromatographic separation. Functionalization with DETA compares well with amine-functionalized silica gel. The reaction is slower, but does not require the preparation of a separation media. Finally the reaction of empty cage fullerenes with dimethyl sodium and their subsequent removal by filtration proved to be fastest and most effective method for removal of empty cage fullerenes. This compares fairly well with purification by Lewis acids.^{30, 32-34, 48} The reaction times are similar and final purification is also straightforward.

EXPERIMENTAL

Instrumentation

MALDI-TOF Mass spectrometry was run using a Kratos PCKompact spectrometer. This instrument was calibrated with either C₆₀ or Sc₃N@C₈₀ known samples and all measurements are ± 1 Da. Spectra were generated in positive ion mode. HPLC analyses were performed using an Agilent 1100 HPLC with a UV-Vis diode array detector set at 360 nm. The column was a 4.6 x 150 mm pyrene functionalized silica with a 1.0 ml/min toluene mobile phase.

Extraction of Fullerene containing soot

Fullerene containing soot was procured from the Dorn research group at Virginia Tech and produced in a Kratchmer-Huffman type generator. The raw soot was placed in a cellulose thimble and extracted in a Soxhlet apparatus using toluene. The solvent was

then removed from the soot extract under reduced pressure, and the resulting residue was washed with acetone three times in order to remove poly(aromatic hydrocarbon)s. The residue was dried under reduced pressure and dissolved in toluene. Small aliquots of this solution were used in the following reactions.

Fullerene Pre-extraction with Furan/Methanol

Aliquots of fullerene-containing soot (ca. 100 mg) were weighed into a series of 12 vials. Furan was purified by passage through an alumina plug, and methanol was used as received. Solvent mixtures were made by combining furan and methanol in 10 percent volume increments from 0 to 100 % methanol. Then 10.0 mL of mixed solvent were added to each of the first 11 soot samples, and 10.0 mL of toluene was added to the last soot sample as a control. The mixtures were sonicated in an ultrasonic cleaning bath for 4 h before the insoluble fractions were separated by centrifugation. Afterwards, 4.0 mL aliquots of the solution phase were removed via volumetric pipette and placed in tare weighed sample vials. Solvent was removed via rotary evaporation and the mass of extract was measured. These samples were reconstituted with toluene (2.0 mL) and analyzed by HPLC.

Functionalization with Cyclopentadiene

Cyclopentadiene was cracked from the dimer by heating at reflux and then distilling at 45 °C. For each experiment a 1 mL aliquot of extract solution was added to a glass vial and the solvent was removed under reduced pressure. Since the majority of material in the extract residue is a mixture of C₆₀ and C₇₀ the molecular weight of the material was taken to be 780 Daltons as an average of the formula weights of the two

major constituents. The resulting residues were dissolved in 1.0 mL of toluene solution containing an appropriate molar amount of CP. Solutions were allowed to sit for 1 h. Toluene and CP were removed under reduced pressure, and the residues were dissolved or suspended in hexanes. The mixtures were separated on silica gel by eluting with hexanes first, followed by toluene. Solvent was removed from the toluene fractions and they were redissolved in the original volume of toluene for HPLC analysis. After HPLC purification, the Sc₃N@C₈₀ was identified by MALDI TOF MS: m/z 1109 Da (M⁺), m/z 1110 Da (M + H)⁺.

Recyclability and Recoverability

Fullerene soot extract (4.0 mg) was dissolved in toluene (2.0 mL) and reacted with cyclopentadiene (20 molar equivalents) for 1 h. Samples of the stock solution and the functionalized material solution were analyzed by HPLC using the same conditions as above. The solution was then subjected to the following conditions before being reconstituted and analyzed by HPLC: 65 °C @ 20 mm Hg, 65 °C @ 0.1 mm Hg, and 150 °C @ 0.01 mm Hg.

Functionalization with Anthracene

Anthracene (18.3 mg, 103 μmol) (as received from Alpha Aesar) was added to 4.0 mg of fullerene soot extract. The mixture was dissolved in 2.0 mL of toluene and maintained at room temperature for 2 days. During the reaction time, aliquots were taken for analysis using HPLC (pyrene stationary phase, toluene 1.0 mL/min). The resulting chromatograms were evaluated for peak areas corresponding to C₆₀, C₇₀, and Sc₃N@C₈₀.

Functionalization with Isoprene

Isoprene (1.0 mL, 10 mmol) (as received) was added to 4.0 mg of fullerene soot extract. The mixture was dissolved in 2.0 mL of toluene and maintained at room temperature for 3 days. During the reaction time, aliquots were taken for analysis using HPLC (pyrene stationary phase, toluene 1.0 mL/min). The resulting chromatograms were evaluated for peak areas corresponding to C₆₀, C₇₀, and Sc₃N@C₈₀.

Functionalization with Furfuryl Alcohol

Fullerene soot (4.0 mg) was dissolved in 4.0 mL of toluene. Furfuryl alcohol (0.10 mL, 1.2 mmol) was added to the solution. The resulting solution was stirred for 1 day at room temperature. Toluene was removed under reduced pressure, and the residue was extracted three times with methanol. HPLC analysis was performed before and after the methanol extraction (pyrene stationary phase, toluene, 1.0 mL/min).

Functionalization with Sorbic Acid

Sorbic acid (0.11 g, 0.98 mmol) was suspended in a solution of fullerene extract (4.0 mg) dissolved in 5.0 mL of toluene. The suspension was stirred for 1 day and then filtered to remove the suspended acid. The resulting solution was analyzed by HPLC (pyrene stationary phase, toluene, 1.0 mL/min).

Functionalization with DETA

The fullerene stock solution used for the CP functionalization studies was also used for the DETA studies. Aliquots (1 mL) of the stock solution were taken and the

solvent was removed under pressure. The residues were reconstituted with 1 mL of solution containing an appropriate amount of DETA. After the appropriate amount of time had passed the solutions were passed through a plug of silica gel and washed with toluene. Solvent was removed from the samples under vacuum and they were reconstituted to their original volume with toluene for HPLC analysis. The crude reaction mixture was analyzed by MALDI TOF MS: m/z 722 Da ($C_{60} + 2H$)⁺, m/z 820 Da ($C_{60} + DETA - 2H$)⁺, m/z 920 Da ($C_{60} + 2DETA - 2H$)⁺, m/z 1022 Da ($C_{60} + 3DETA - 2H$)⁺.

Functionalization with Dimsyl Sodium

A 0.1M solution of dimsyl sodium was made by adding 0.04 g of 60 % sodium hydride to 10.0 mL of dimethyl sulfoxide which had been dried over molecular sieves. After there was no more gas evolved from the solution, 0.5 or 1.0 mL of the dimsyl sodium solution was added to a 5.0 mL solution of 4.0 mg of fullerene extract dissolved in toluene. The reaction mixture was allowed to stand for 20 to 30 min at room temperature. After the reaction time was completed, the mixture was poured through paper filter, and the solid material was washed with toluene. Solvent was removed from the resulting solution under reduced pressure, and the residue was dissolved in 1.0 mL of toluene before being characterized by HPLC (pyrene stationary phase, toluene 1.0 mL/min). The crude reaction mixture was characterized by MALDI TOF MS: m/z 720 Da (C_{60})⁺, m/z 409 Da ($C_{60} + NaSOCH_3CH_2 - 2H$)²⁺, m/z 918 Da ($C_{60} + 2NaSOCH_3CH_2 - 2H$)⁺, m/z 1018 Da ($C_{60} + 3NaSOCH_3CH_2 - 2H$)⁺, m/z 1118 Da ($C_{60} + 4NaSOCH_3CH_2 - 2H$)⁺.

References

1. Stevenson, S.; Rice, G.; Glass, T.; Harlch, K.; Cromer, F.; Jordan, M. R.; Craft, J.; Hadju, E.; Bible, R.; Olmstead, M. M.; Maltra, K.; Fisher, A. J.; Balch, A. L.; Dorn, H. C., *Nature* **1999**, *401*, 55-57.
2. Zhang, J.; Fatouros, P. P.; Shu, C.; Reid, J.; Owens, L. S.; Cai, T.; Gibson, H. W.; Long, G. L.; Corwin, F. D.; Chen, Z.-J.; Dorn, H. C., *Bioconjugate Chemistry* **2010**, *21*, 610-615.
3. Shu, C.; Corwin, F. D.; Zhang, J.; Chen, Z.; Reid, J. E.; Sun, M.; Xu, W.; Sim, J. H.; Wang, C.; Fatouros, P. P.; Esker, A. R.; Gibson, H. W.; Dorn, H. C., *Bioconjugate Chemistry* **2009**, *20*, 1186-1193.
4. Shu, C.-Y.; Ma, X.-Y.; Zhang, J.-F.; Corwin, F. D.; Sim, J. H.; Zhang, E.-Y.; Dorn, H. C.; Gibson, H. W.; Fatouros, P. P.; Wang, C.-R.; Fang, X.-H., *Bioconjugate Chemistry* **2008**, *19*, 651-655.
5. Cui, R.; Li, J.; Huang, H.; Zhang, M.; Guo, X.; Chang, Y.; Li, M.; Dong, J.; Sun, B.; Xing, G., *Nano Research* **2014**, Ahead of Print.
6. Kong, K. V.; De Liao, L.; Goh, D.; Thakor, N. V.; Olivo, M., *Journal of Nanomedicine & Nanotechnology* **2014**, *5*, 1000223/1-1000223/11.
7. Shu, C.-Y.; Wang, C.-R., *RSC Drug Discovery Series* **2012**, *15*, 261-284.
8. Zhang, J.; Stevenson, S.; Dorn, H. C., *Accounts of Chemical Research* **2013**, *46*, 1548-1557.
9. Zhang, J.; Ye, Y.; Chen, Y.; Pregot, C.; Li, T.; Balasubramaniam, S.; Hobart, D. B.; Zhang, Y.; Wi, S.; Davis, R. M.; Madsen, L. A.; Morris, J. R.; LaConte, S. M.; Yee, G. T.; Dorn, H. C., *Journal of the American Chemical Society* **2014**, *136*, 2630-2636.
10. Ingber, D. E.; Korin, N.; Kanapathipillai, M.; Uzun, O.; Papa, A.-L. Nanotherapeutics for drug targeting. 2013-US44709 2013185032, 20130607., 2013.
11. Ingber, D. E.; Roberts, K. Self-assembling peptides forming nanostructures and their use in drug delivery. 2013-US46821 2014014613, 20130620., 2014.
12. Burriss, D. L.; Atwood, D. A., *Rare Earth Elements* **2012**, 495-499.
13. Karthik, K.; Barg, M.; Khandai, M.; Chakravarthi, I. K.; Kamal, P. D., *Inventi Impact: NDDS* **2012**, 17-22.

14. Djordjevic, A.; Injac, R.; Jovic, D.; Mrdjanovic, J.; Seke, M., *Advanced Carbon Materials and Technology* **2014**, 193-271.
15. Guan, M.; Qin, T.; Ge, J.; Zhen, M.; Xu, W.; Chen, D.; Li, S.; Wang, C.; Su, H.; Shu, C., *Journal of Materials Chemistry B: Materials for Biology and Medicine* **2015**, *3*, 776-783.
16. Hu, Z.; Li, J.; Huang, Y.; Chen, L.; Li, Z., *RSC Advances* **2015**, *5*, 654-664.
17. Huang, Y.-Y.; Sharma, S. K.; Yin, R.; Agrawal, T.; Chiang, L. Y.; Hamblin, M. R., *Journal of Biomedical Nanotechnology* **2014**, *10*, 1918-1936.
18. Jiang, G.; Yin, F.; Duan, J.; Li, G., *Journal of Materials Science: Materials in Medicine* **2015**, *26*, 1-7.
19. Yin, R.; Wang, M.; Huang, Y.-Y.; Landi, G.; Vecchio, D.; Chiang, L. Y.; Hamblin, M. R., *Free Radical Biology & Medicine* **2015**, *79*, 14-27.
20. Yumita, N.; Iwase, Y.; Watanabe, T.; Nishi, K.; Kuwahara, H.; Shigeyama, M.; Sadamoto, K.; Ikeda, T.; Umemura, S.-I., *Anticancer Research* **2014**, *34*, 6481-6487.
21. Shu, C.; Xu, W.; Slebodnick, C.; Champion, H.; Fu, W.; Reid, J. E.; Azurmendi, H.; Wang, C.; Harich, K.; Dorn, H. C.; Gibson, H. W., *Organic Letters* **2009**, *11*, 1753-1756.
22. Dorn, H. C.; Fatouros, P. P., *Nanoscience and Nanotechnology Letters* **2010**, *2*, 65-72.
23. Li, Y., *Endohedral Fullerenes* **2014**, 417-431.
24. Ross, R. B.; Cardona, C. M.; Swain, F. B.; Guldi, D. M.; Sankaranarayanan, S. G.; Van Keuren, E.; Holloway, B. C.; Drees, M., *Advanced Functional Materials* **2009**, *19*, 2332-2337.
25. Wodo, O.; Roehling, J. D.; Moule, A. J.; Ganapathysubramanian, B., *Energy & Environmental Science* **2013**, *6*, 3060-3070.
26. Gibson, H. W.; Dorn, H. C.; Ge, Z.; Cai, T. Methods for purification of trimetallic nitride endohedral metallofullerenes and related fullerene derivatives. 2005-US22386 2006002341, 20050623., 2006.
27. Klute, R. C.; Dorn, H. C.; McNair, H. M., *J. Chromatogr. Sci.* **1992**, *30*, 438-42.
28. Ge, Z.; Duchamp, J. C.; Cai, T.; Gibson, H. W.; Dorn, H. C., *Journal of the American Chemical Society* **2005**, *127*, 16292-16298.

29. Olmstead, M. M.; De Bettencourt-Dias, A.; Duchamp, J. C.; Stevenson, S.; Marciu, D.; Dorn, H. C.; Balch, A. L., *Angewandte Chemie, International Edition* **2001**, *40*, 1223-1225.
30. Stevenson, S.; Rottinger, K. A., *Inorganic Chemistry* **2013**, *52*, 9606-9612.
31. Akiyama, K.; Hamano, T.; Nakanishi, Y.; Takeuchi, E.; Noda, S.; Wang, Z.; Kubuki, S.; Shinohara, H., *Journal of the American Chemical Society* **2012**, *134*, 9762-9767.
32. Edelmann, F. T., *Coordination Chemistry Reviews* **2015**, *284*, 124-205.
33. Stevenson, S.; Rose, C. B.; Robson, A. A.; Heaps, D. T.; Buchanan, J. P., *Fullerenes, Nanotubes, and Carbon Nanostructures* **2014**, *22*, 182-189.
34. Stevenson, S.; Rottinger, K. A.; Field, J. S., *Dalton Transactions* **2014**, *43*, 7435-7441.
35. Hirsch, A.; Brettreich, M., *Fullerenes: Chemistry and Reactions*. Wiley - VCH: Weinheim, 2005.
36. Ge, Z.; Duchamp, J. C.; Cai, T.; Gibson, H. W.; Dorn, H. C., *Journal of the American Chemical Society* **2005**, *127*, 16292-8.
37. Qureshi, Z. S.; Deshmukh, K. M.; Bhanage, B. M., *Sonochemistry: Theory, Reactions, Syntheses, and Applications* **2010**, 157-187.
38. Li, L.; Cai, Z.; Shen, B.; Xin, Z.; Ling, H., *Chemical Engineering & Technology* **2011**, *34*, 1468-1472.
39. Ranjbar-Karimi, R.; Loghmani-Khouzani, H., *Journal of the Iranian Chemical Society* **2011**, *8*, 223-230.
40. Badri, G. E.; El-Baih, F. E. M.; Al-Hazimi, H. M., *Asian Journal of Chemistry* **2013**, *25*, 5006-5012.
41. Anacleto, J. F.; Quilliam, M. A., *Analytical Chemistry* **1993**, *65*, 2236-42.
42. Pang, L. S. K.; Wilson, M. A., *Journal of Physical Chemistry* **1993**, *97*, 6761-3.
43. Hildebrand, A.; Blume, R., *Praxis der Naturwissenschaften, Chemie* **1997**, *46*, 24-27.
44. Mamo, M. A.; Freitas, F. S.; Forbes, R. P.; Black, R. S.; Nogueira, A. F.; van Otterlo, W. A. L.; Coville, N. J., *Fullerenes, Nanotubes, and Carbon Nanostructures* **2013**, *21*, 198-212.

45. Fokin, A. A.; Kushko, A. O.; Kirij, A. V.; Yurchenko, A. G.; Schleyer, P. v. R., *Journal of Organic Chemistry* **2000**, *65*, 2984-2995.
46. Nair, S. K.; Samuel, R.; Asokan, C. V., *Synthesis* **2001**, 573-576.
47. Samuel, R.; Nair, S. K.; Asokan, C. V., *Synlett* **2000**, 1804-1806.
48. Akiyama, K.; Hamano, T.; Nakanishi, Y.; Takeuchi, E.; Noda, S.; Wang, Z.; Kubuki, S.; Shinohara, H., *Journal of the American Chemical Society* **2012**, *134*, 9762-7.

Chapter Three

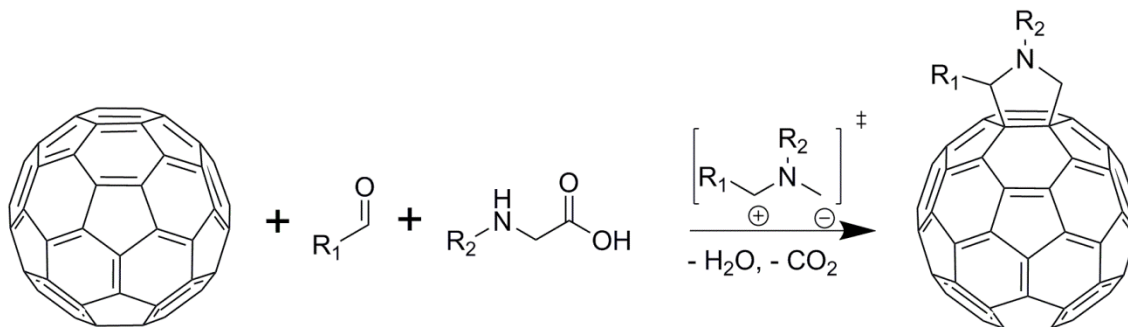
Prato Functionalization of Fullerenes

Abstract

The Prato reaction of an azomethine ylide with C₆₀ fullerene was used to synthesize several derivatives of the parent fullerene. Four different alcohol functionalized compounds as well as an ester were isolated. The propiolate ester was used in an attempted synthesis of a fullerene diad, which was unsuccessful. Cyclic voltammetry measurements were made using some of the alcohol adducts, and the tris-adduct of this group was used to construct and test a photovoltaic devices.

Introduction

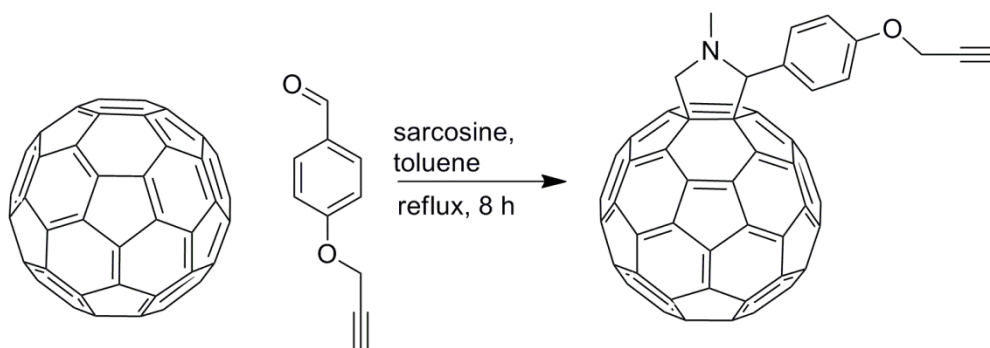
The Prato reaction is a 1,3-dipolar cycloaddition reaction that can be used to functionalize fullerenes.¹⁻² In this chapter the reaction is used to generate a number of adduct species from C₆₀. The reaction is begun by the combination of an amino acid and an aldehyde to form a Schiff base. Subsequent loss of water and carbon dioxide generates an azomethine ylide as the reactive intermediate. This species reacts with fullerenes at either a 6,6- or 5,6-junction to form a pyrrolidino product. For adducts with C₆₀ fullerene, the addition happens across the 6,6-bond junction. For adducts to TNT EMF species, the initial addition is across the 5,6-bond, giving the kinetic product. Thermal equilibration of the kinetic product eventually leads to the thermodynamic product with addition across a 6,6-bond.³⁻⁴



Scheme 3.1. Generic Prato reaction with N-functionalized glycine and an aldehyde.

Reaction with alkyne functionalized benzaldehyde

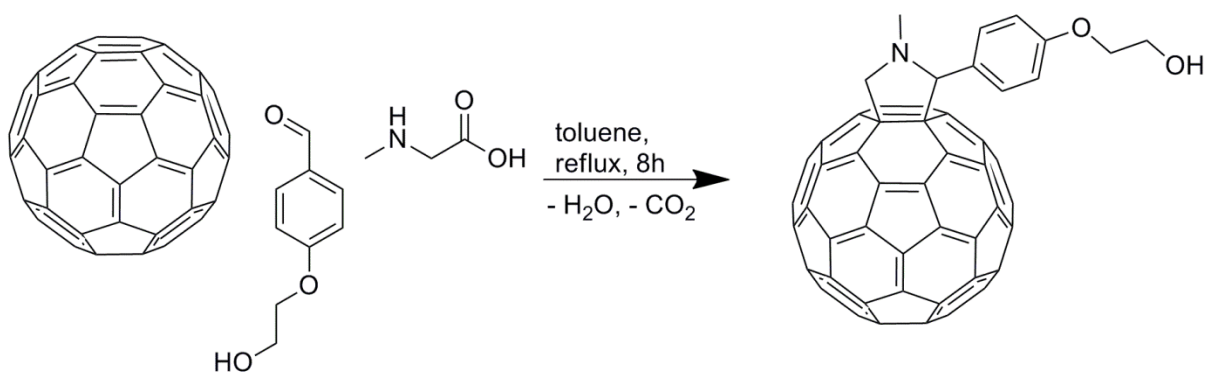
This was the first reaction attempted using the Prato fullerene scheme. The alkynyl benzaldehyde was synthesized via a Williamson ether synthesis reaction. The reason for attempting this reaction was to provide an alkyne functionalized fullerene that could be used in later “click” reactions. This scheme was intended to provide fullerene functionalized polymers and other useful and interesting materials through this seemingly facile reaction method. It was determined by HPLC analysis of the reaction mixture that the reaction was unsuccessful. The azomethine ylide that is produced by the reaction of the aldehyde and amino acid is not only reactive with the fullerene species, but is also quite reactive with alkyne moieties as well.⁵ Hence it is easy to surmise why this reaction failed to produce any functionalized material.



Scheme 3.2. Reaction of C_{60} with 4-(prop-2-yn-1-yloxy)benzaldehyde

Prato reaction with 4-(2'-hydroxyethoxy)benzaldehyde

Since the reactions to produce alkyne adducts of C_{60} seemed to be difficult, it was decided to attempt the Prato reaction with an alcohol functionalized benzaldehyde and subsequently convert it to an alkyne derivative. The aldehyde was synthesized from 4-hydroxybenzaldehyde and 2-bromoethanol via a Williamson ether synthesis. This functionalized benzaldehyde was then reacted with methyl glycine and C_{60} as shown in Scheme 3.3. Previous reactions with unprotected phenols or alkynes had failed to yield products due to deprotonation. The alcoholic moiety did not suffer from this liability.



Scheme 3.3. Prato reaction of C_{60} with sarcosine and 4-(2'-hydroxyethoxy)benzaldehyde.

The reaction mixture was characterized by HPLC (Figure 3.1). The adduct peak appears after the parent C_{60} peak due to its reduced solubility in toluene. After purification on silica gel, the mono-adduct was characterized by HPLC (Figure 3.2). The second chromatogram indicates a small amount of residual C_{60} seen as the peak at 12 minutes as well as a residual solvent peak at 7 minutes.

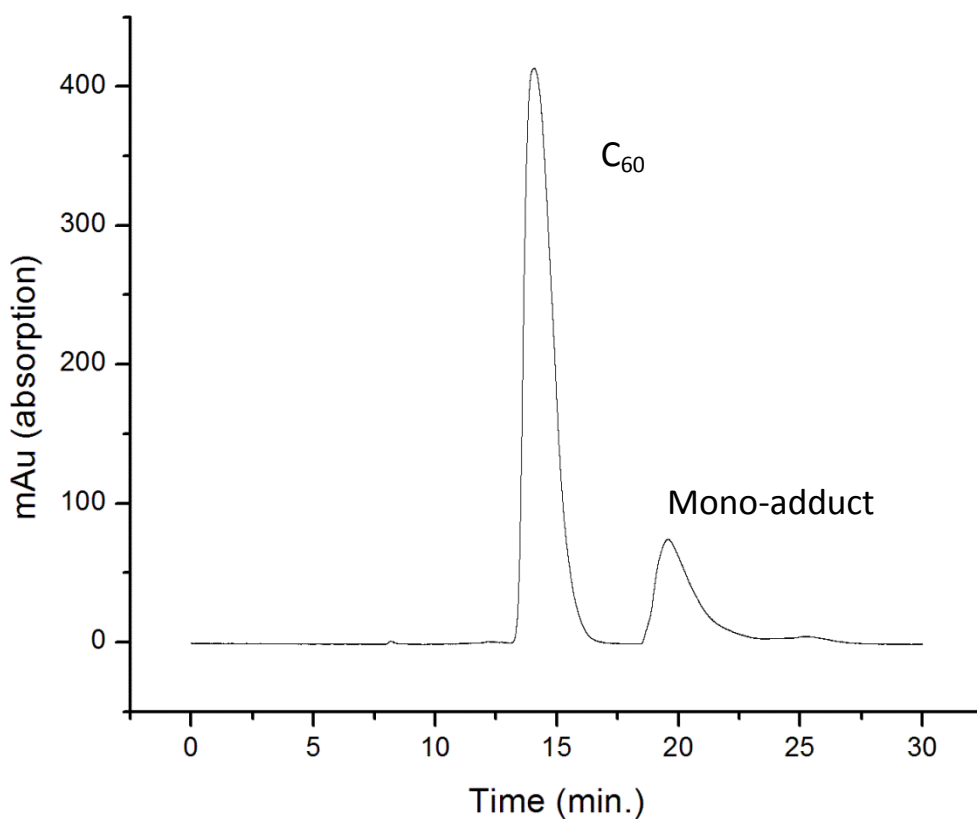


Figure 3.1. HPLC trace of the reaction mixture of sarcosine and 4-(2'-hydroxyethoxy)benzaldehyde and C_{60} . The C_{60} peak is at 14.9 minutes and the adduct peak is at 20 minutes (PYE functionalized silica 0.5 mL/min toluene).

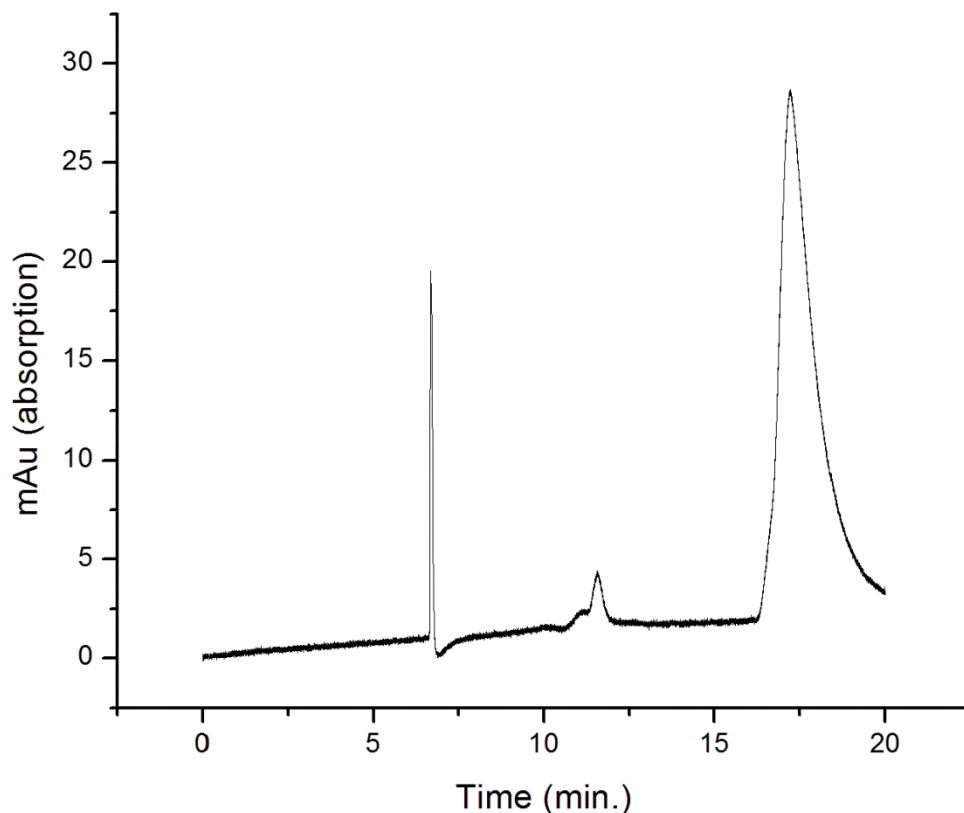


Figure 3.2. HPLC trace of the purified reaction product of 4-(2'-hydroxyethoxy)benzaldehyde and sarcosine with C_{60} . Residual C_{60} is seen at 12 minutes, the product at 18 minutes, and residual solvent at 7 minutes (PYE functionalized silica, 0.5 mL/min toluene).

The proton NMR spectrum (Figure 3.3) indicates the formation of the intended product. The solubility of the Prato adducts synthesized in this chapter, particularly the hydroxyl functionalized species, was found to be very poor. Consequently obtaining NMR spectra for these species was very difficult. Signal intensity for 1H NMR experiments suffered significantly due to the low concentrations. Low solubility, coupled with the lack of protons on the fullerene cage which would enhance ^{13}C signal strength, the relatively high molecular weight, and lack of

symmetry of these products makes obtaining ^{13}C NMR an extremely difficult proposition. Consequently, the addition products in this chapter were only characterized by ^1H NMR.

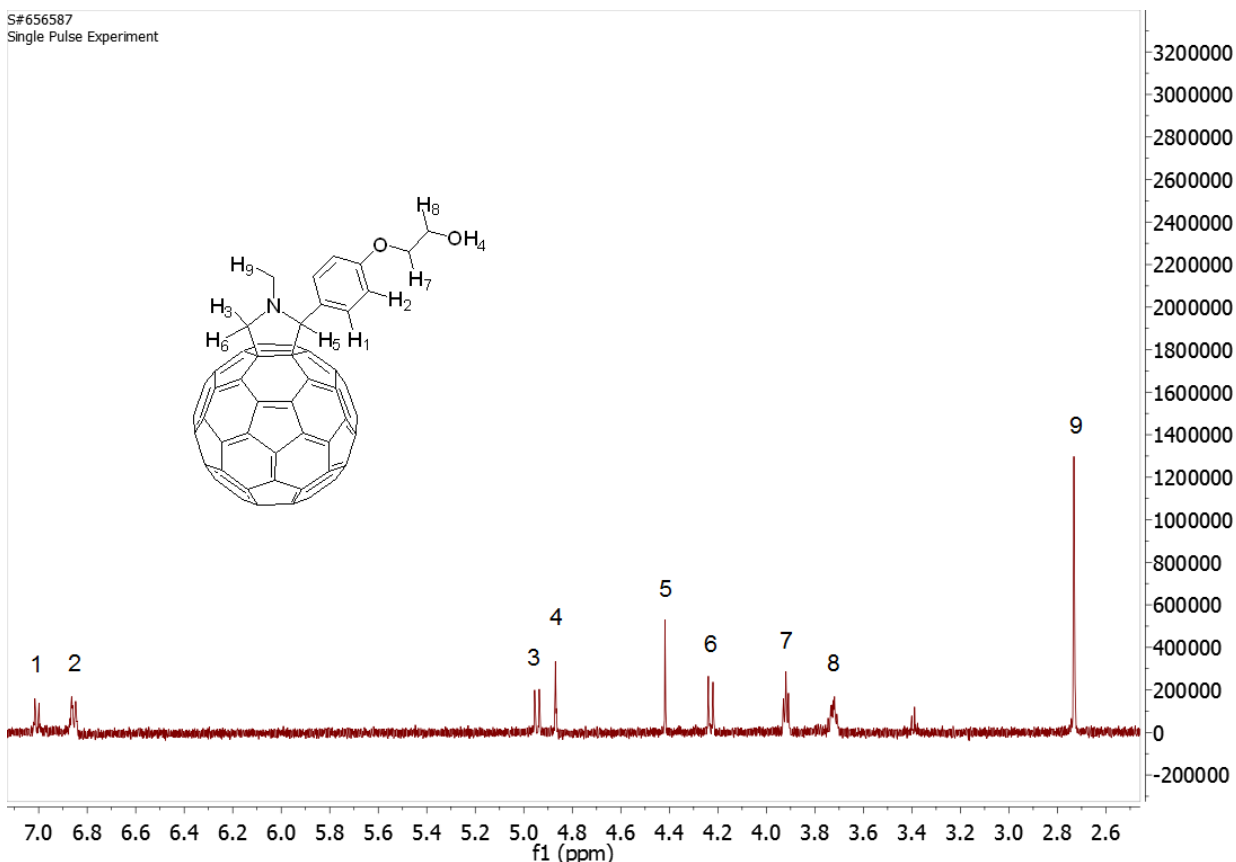


Figure 3.3. ^1H NMR spectrum for the purified product of the reaction of 4-(2'-hydroxyethoxy)benzaldehyde, sarcosine and C_{60} (CDCl_3 500 MHz).

The major peak in the mass spectrum ($m/z = 913$ Da) is that of the mono-adduct. The prevalence of this peak in the mass spectrum also indicates that the product is reasonably stable as it does not seem to fragment in the spectrometer. The major liability in running this reaction is the stability of the starting aldehyde. After purification, it degrades quickly, even if stored in the freezer. There are other possibilities as well of forming a vinyl ether from the adduct by dehydration. This may be why the acid catalyzed esterification of this product failed in later steps.

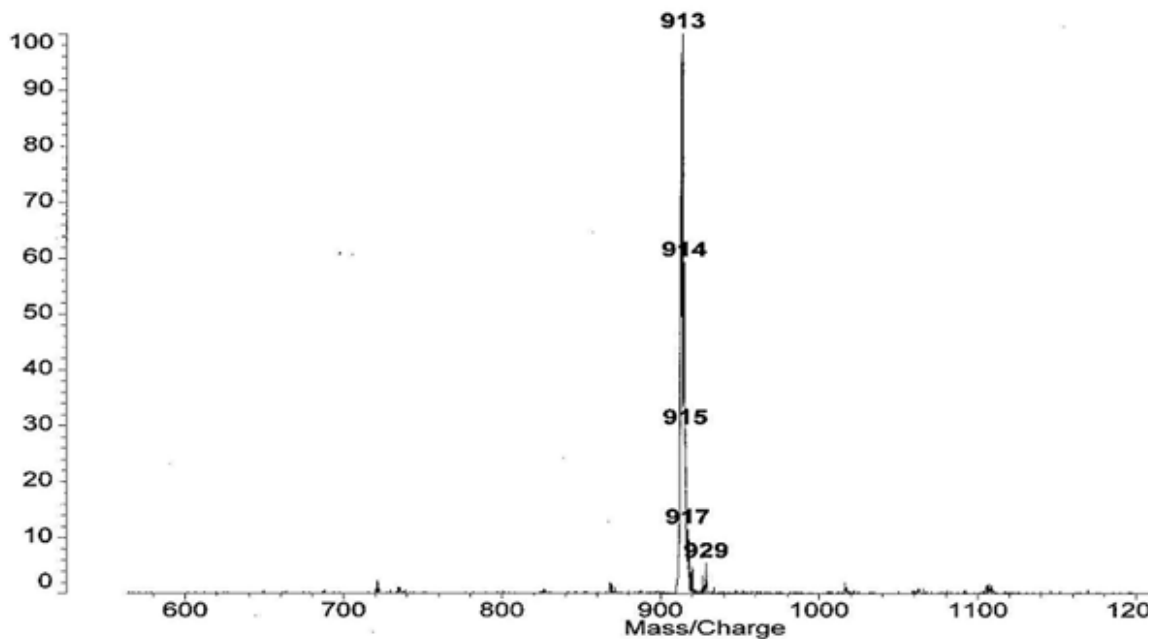
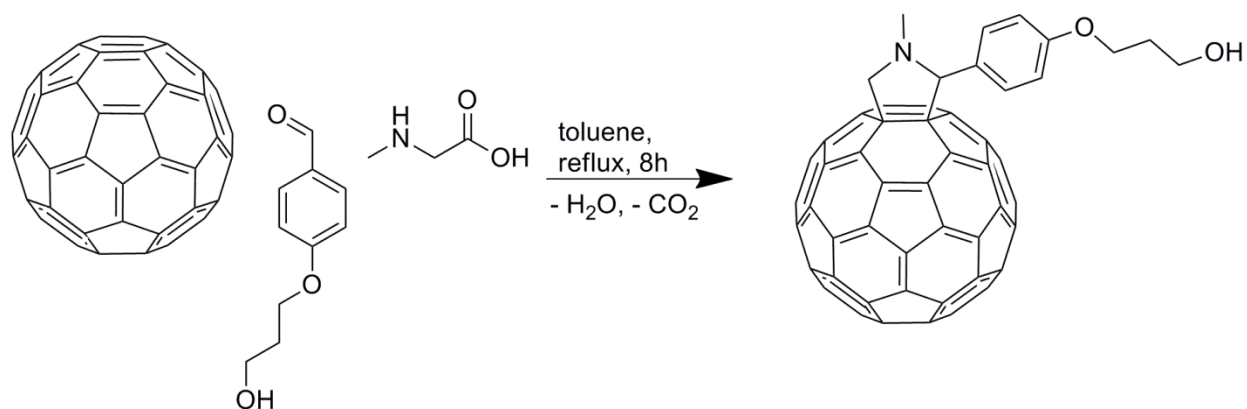


Figure 3.4. MALDI TOF MS for the isolated product of the reaction of 4-(2'-hydroxyethoxy)benzaldehyde, sarcosine and C_{60} ($M^+ = m/z$ 913 Da for $C_{71}H_{15}NO_2$).

Prato reaction with 4-(3'-hydroxypropoxy)benzaldehyde

The synthesis of the propanol functionalized benzaldehyde via Williamson ether synthesis was completed in order to provide a fullerene adduct species that is more stable than the ethanol functionalized product previously discussed. Reactions with the ethanol functionalized fullerene were difficult due to elimination and subsequent formation of the labile vinyl ether. The propanol functionalized ether was much more stable, and its adducts with C_{60} were more easily synthesized (Scheme 3.4).



Scheme 3.4. Prato reaction of C₆₀ with sarcosine and 4-(3'-hydroxypropoxy)benzaldehyde.

The two chromatograms (Figures 3.5 and 3.6) below show the reaction mixture, and the purified mono-adduct. The C₆₀ starting material elutes at 11.8 minutes and the mono-adduct elutes at 17.2 minutes. Separation of the reaction mixture was accomplished on silica gel, eluting first with toluene and then a mixture of toluene and ethyl acetate.

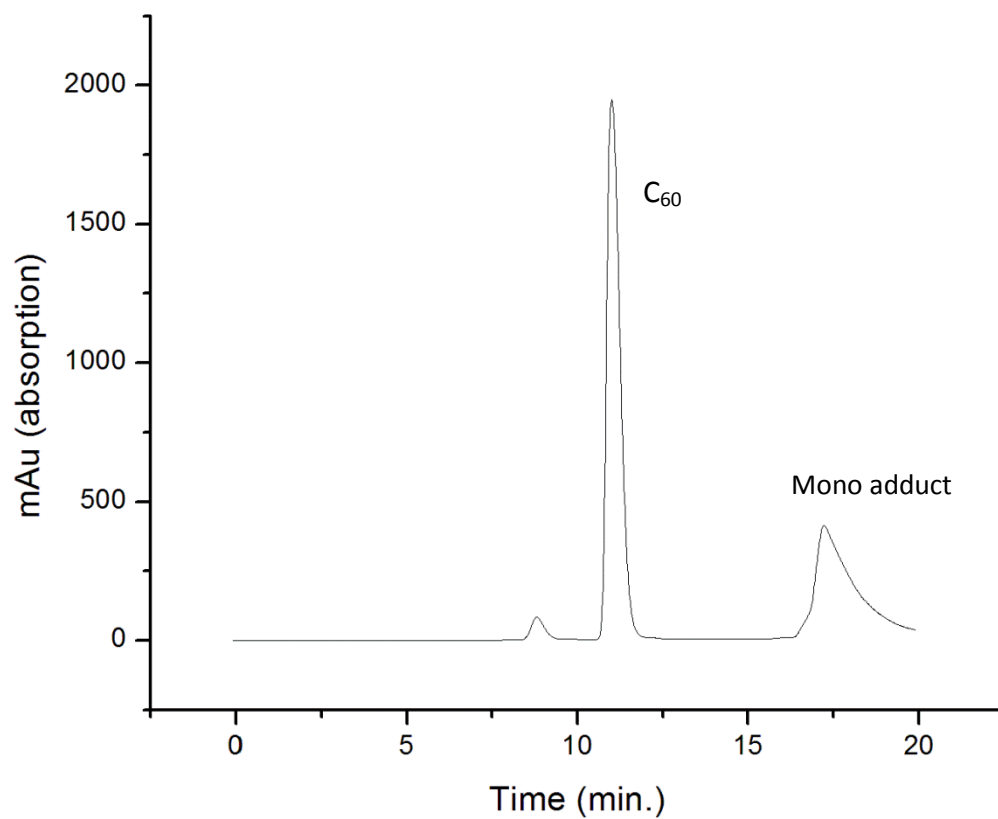


Figure 3.5. HPLC trace of the reaction mixture from the reaction of 4-(3'-hydroxypropoxy)benzaldehyde, sarcosine and C₆₀. The peak for C₆₀ is seen at 12 minutes, and the adduct peak is at 17.5 minutes (PYE functionalized silica, 0.5 mL/min toluene).

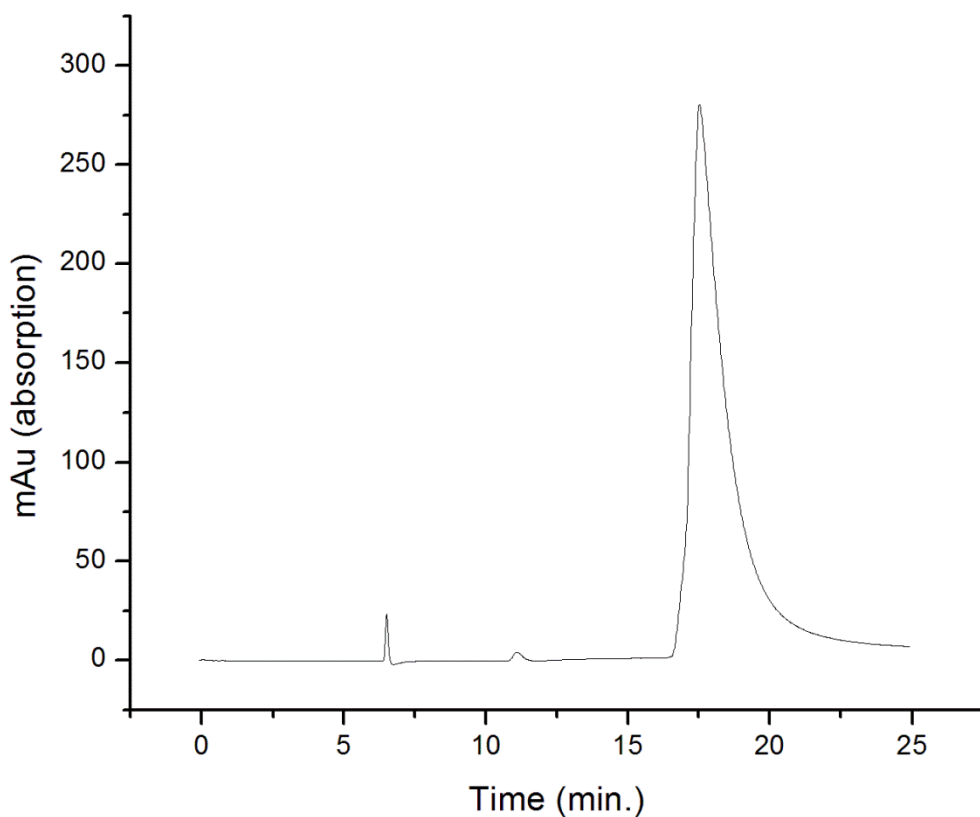


Figure 3.6. HPLC trace of the purified product of the reaction of 4-(3'-hydroxypropoxy)benzaldehyde, sarcosine and C₆₀ (PYE functionalized silica 0.5 mL/min toluene).

The ¹H NMR spectrum shown below (Figure 3.7) indicates the formation of the product. Interestingly, the protons H₁ as illustrated in Figure 3.7 do not appear in the spectrum. The H₁ signal may have shifted into the chloroform signal at 7.26 ppm.

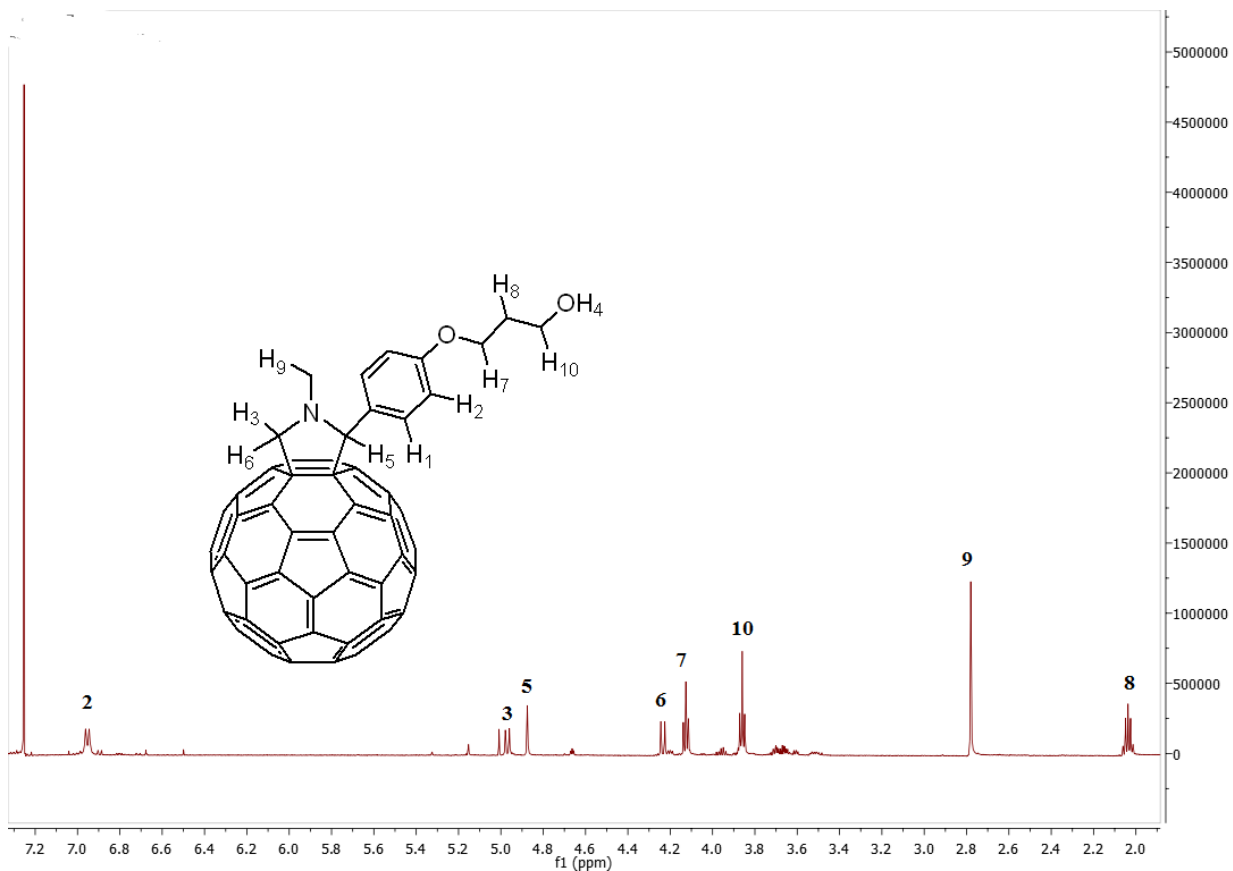


Figure 3.7. ¹H NMR spectrum of the product of the reaction of 4-(3'-hydroxypropoxy)benzaldehyde, sarcosine and C₆₀ (CDCl₃, 500 MHz).

The MALDI TOF MS (Figure 3.8) contains major peaks for both the mono-adduct at m/z 927 Da and C₆₀ at m/z 720 Da. It is not unusual to observe the unfunctionalized C₆₀ parent fullerene in the MALDI TOF spectrum due to degradation of the adducts in the spectrometer.

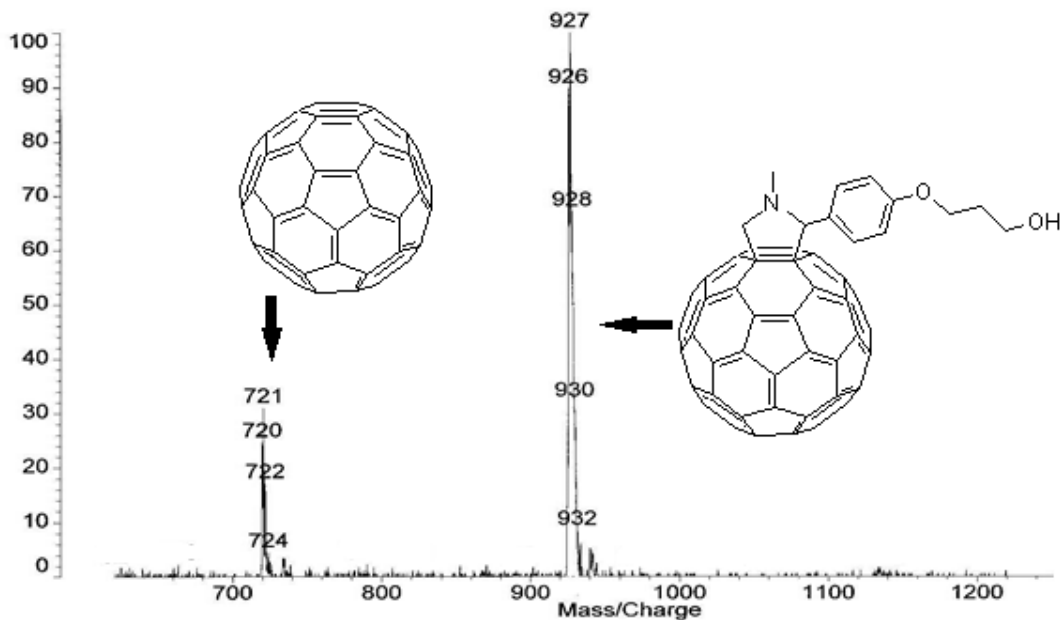


Figure 3.8. MALDI TOF MS of the product of the reaction of 4-(3'-hydroxypropoxy)benzaldehyde, sarcosine and C_{60} . $M^+ = m/z$ 927 Da ($C_{72}H_{17}NO_2$).

Subsequent reactions allowed for the isolation of not only the mono-adduct, but the bis- and tris-adducts as well. These materials were submitted to Hunter Champion in the Dorn research group for electrochemical analysis. The cyclic voltammograms given below (Figure 3.9) show the shift of the reversible reduction peaks to more negative values. This quality is important in the construction of organic photovoltaic devices. Fullerenes, and specifically functionalized fullerenes, are employed to cause charge separation from a photoexcited conductive polymer in the photovoltaic device. The more negative the reduction potential, the larger the energy gap will be between the functionalized fullerene and the corresponding electrode, providing a larger voltage for the cell. As the number of Prato additions to the C_{60} fullerene increase, the reduction potential becomes more and more negative.

Analysis of the bis- and tris-adducts of C_{60} with 4-(3'-hydroxypropoxy)benzaldehyde

In addition to the mono-addition product of the previous reaction, bis- and tris-adducts were also produced and isolated. These adducts were characterized by HPLC, and in the case of the tris-adduct MALDI TOF MS. Due to the number of isomers predicted for both products, NMR spectra were not obtained. The different isomers present in the bis- and tris-adduct samples are also expected to have slightly different reduction potentials. This is seen in the broadening of the reduction and oxidation peaks of those two families of adducts compared to those of the single mono-adduct.

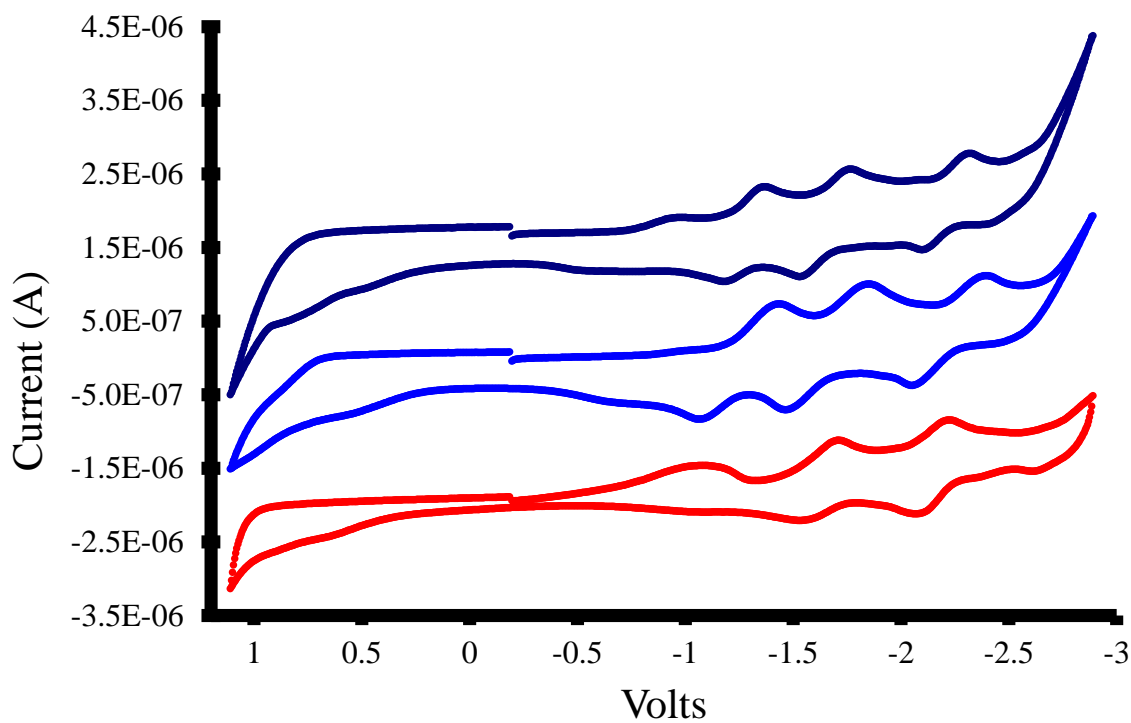


Figure 3.9. Cyclic voltammogram traces for mono- (dark blue), bis- (light blue) and tris-tris-3-(4'-(1''-methylpyrrolidin-2''-yl)phenoxy)propan-1-ol adducts of C₆₀ (red).

Table 3.1. Reduction half potentials for C₆₀, mono-, bis-, and tris-3-(4'-(1''-methylpyrrolidin-2''-yl)phenoxy)propan-1-ol adducts of C₆₀. Scan rate 250 mV/sec, Ag/AgCl reference electrode. All values are relative to ferrocene/ferrocinium couple.

	E ^{Red 1} _{1/2} (V)	E ^{Red 2} _{1/2} (V)	E ^{Red 3} _{1/2} (V)
Pristine C ₆₀	-1.10	-1.57	-2.07
Mono	-1.26	-1.64	-2.21
Bis	-1.25	-1.64	-2.33
Tris	-1.62	-1.14	Not Measured

A bulk heterojunction photovoltaic device was constructed from the tris-3-(4'-(1''-methylpyrrolidin-2''-yl)phenoxy)propan-1-ol adduct of C₆₀ as an electron acceptor and poly(3-hexylthiophene) (P3HT) as the donor and light absorber. The cell was characterized using an AM 1.5 light source. The current and voltage responses of the device, before and after annealing are plotted in Figure 3.19. The annealed device was held at 110 °C for one hour and then slowly cooled to room temperature. By heating the bulk heterojunction mixture of the fullerene and P3HT, the morphology of the heterojunction layer was changed, leading to more continuous domains for both the fullerene and P3HT. This usually has the effect of increasing the current-producing characteristics of the photovoltaic device. In the device produced, annealing increased the short circuit current by a factor of three. The open circuit voltage (extrapolated to zero current) was not affected as it remained close to 0.2 Volts.

AM 1.5 Light Source

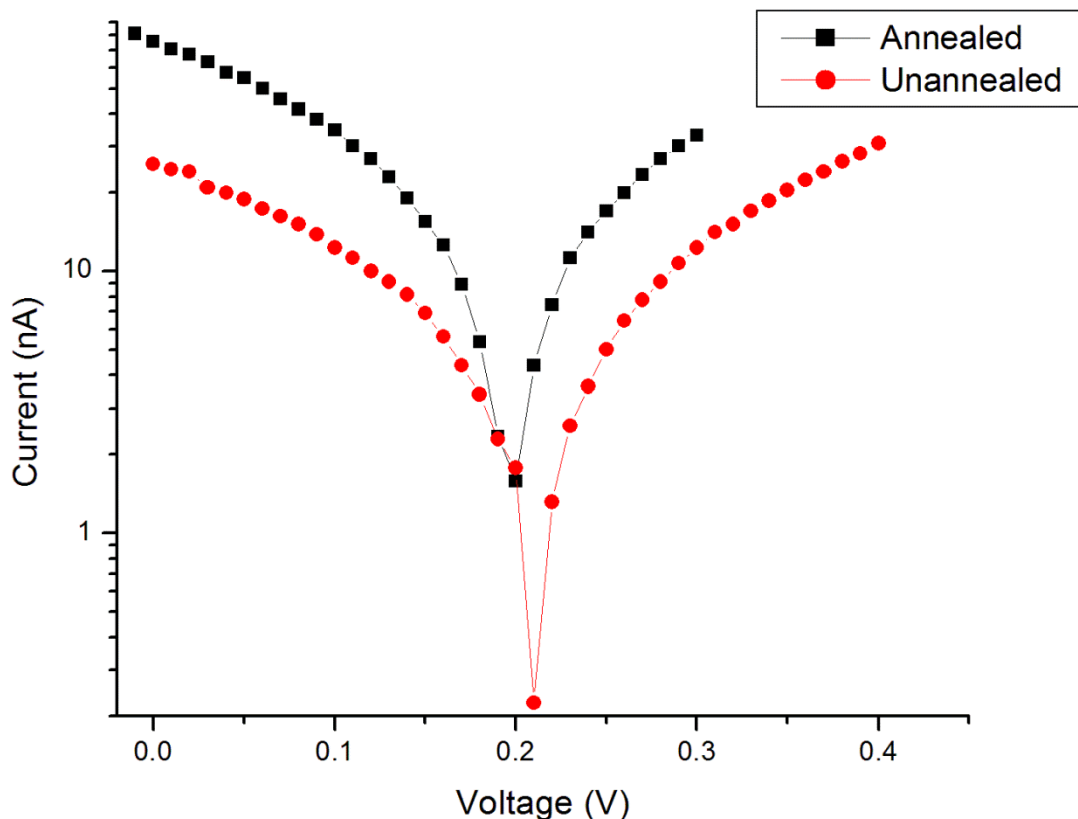


Figure 3.10. Current/voltage plot for a photovoltaic device constructed from tris-3-(4'-(1''-methylpyrrolidin-2''-yl)phenoxy)propan-1-ol adduct of C₆₀ and P3HT, illuminated with AM 1.5 light before and after annealing the device at 110 °C.

The fill factor (FF) is the ratio of the maximum power output of the photovoltaic cell compared to the product of the open circuit voltage and the short circuit current. The fill factor is defined below in Equation 3.1. The higher the value of the fill factor, the more closely the photovoltaic device mimics the behavior of a photo diode, and thus it is used as an indication of the efficiency of the device. The fill factors for the original and annealed device are given in Table 3.2.

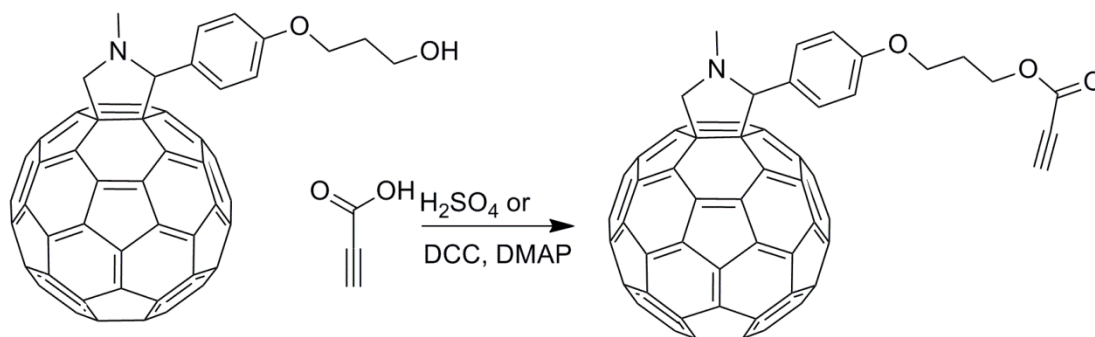
$$FF = \frac{V_{MP} \times I_{MP}}{V_{OC} \times I_{SC}} \quad (\text{Equation 3.1})$$

Table 3.2. Characteristics of the two photovoltaic cells made with the tris-adduct of C₆₀ under AM 1.5 conditions.

Light Source		V _{oc} (V)	J _{sc} (nA/cm ²)	Fill Factor
AM 1.5	Original	0.205	25.7	0.24
	Annealed	0.195	75.9	0.23

Synthesis of Propiolate Ester of 3-(4'-(1''-methylpyrrolidin-2''-yl)phenoxy)propan-1-ol - Functionalized C₆₀

The synthesis of the propiolate ester of 3-(4'-(1''-methylpyrrolidin-2''-yl)phenoxy)propan-1-ol functionalized C₆₀ was accomplished using dicyclohexyl carbodiimide (DCC) coupling as seen in Scheme 3.5. The esterification reaction was attempted using an acid catalyzed approach, but it did not succeed.



Scheme 3.6. Synthesis of propiolate ester from 3-(4'-(1''-methylpyrrolidin-2''-yl)phenoxy)propan-1-ol functionalized C₆₀.

The propiolate ester product was initially characterized by HPLC and then by ^1H NMR spectroscopy and MALDI TOF MS. The chromatogram shown below (Figure 3.11) indicates the formation of the product by the peak at 8.8 minutes retention time. The residual starting material peak is seen at 9.5 minutes and constitutes a small impurity which was removed upon purification on silica gel.

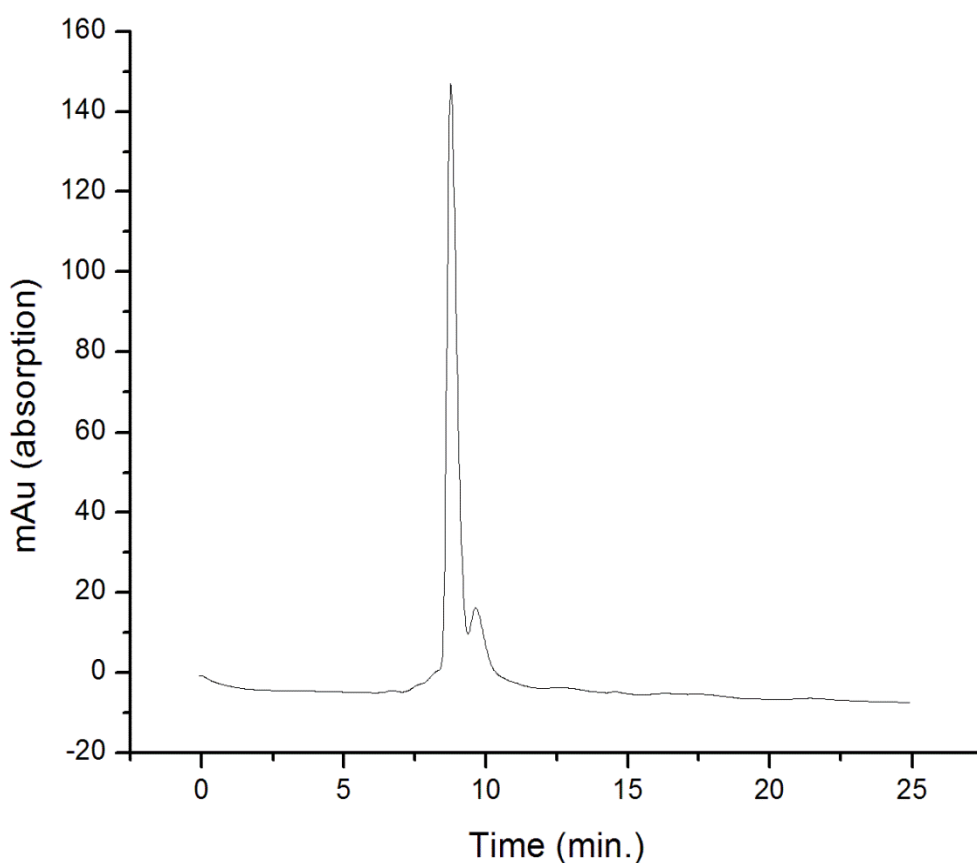


Figure 3.11. HPLC chromatogram of the propiolate product derived from 3-(4'-(1''-methylpyrrolidin-2''-yl)phenoxy)propan-1-ol Functionalized C_{60} . Pyrene functionalized silica, toluene 0.5 mL/min.

The alkyne proton appears at 2.86 ppm in the NMR spectrum below in Figure 3.12. The peaks in the baseline between 3.4 and 3.9 ppm, and between 2.3 and 2.5 ppm are dicyclohexyl urea, a byproduct of the DCC coupling reaction. The mass spectrum (Figure 3.13) shows the expected M^+ peak at m/z 979 Da.

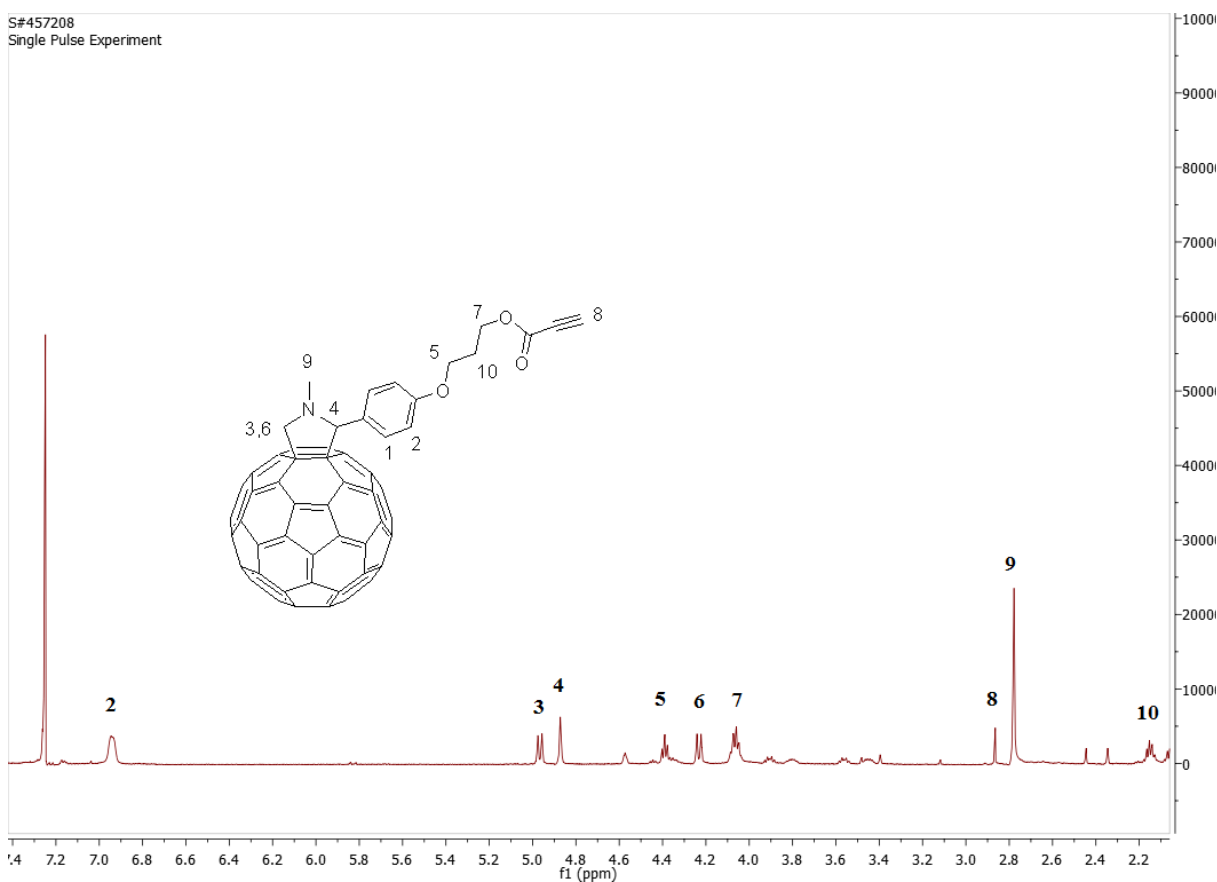


Figure 3.12. ^1H NMR spectra showing the propiolate ester of 3-(4'-(1''-methylpyrrolidin-2''-yl)phenoxy)propan-1-ol Functionalized C₆₀. The presence of the alkynyl proton at 2.86 ppm indicates the product. (CDCl_3 , 500 MHz).

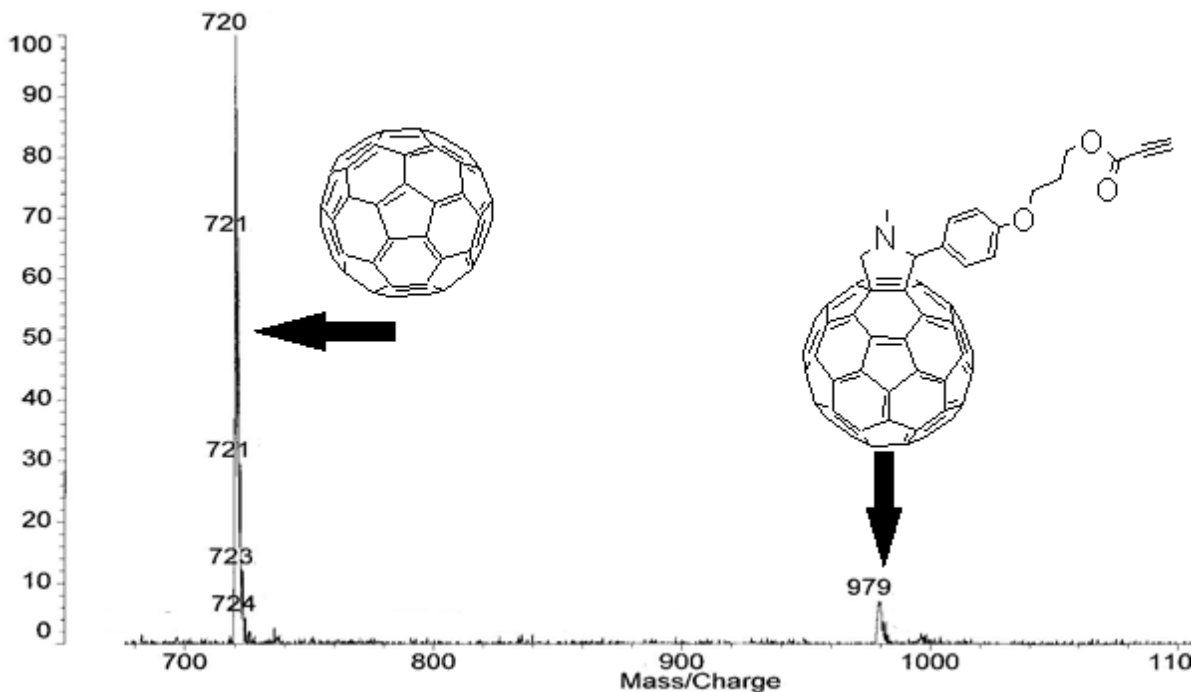
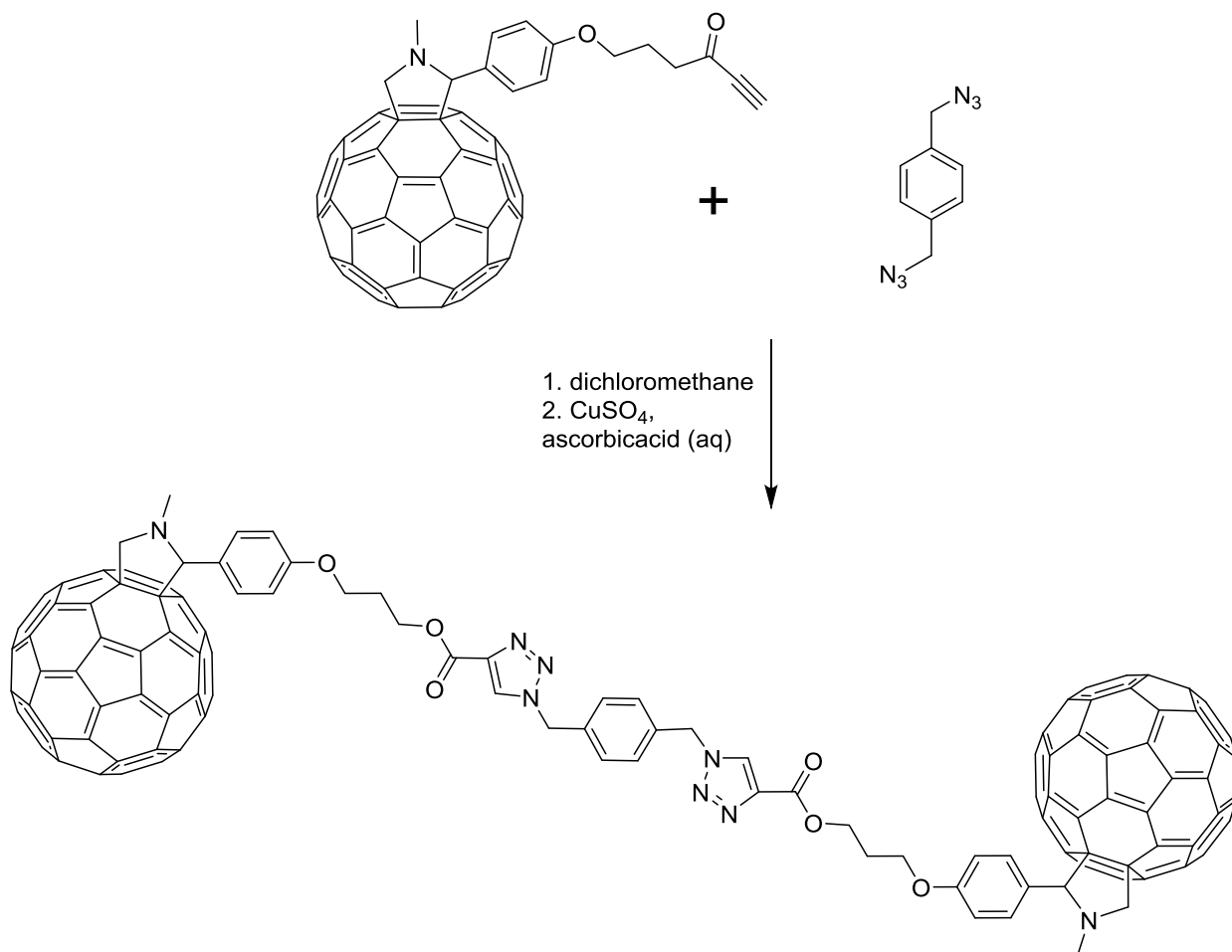


Figure 3.13. MALDI TOF MS of the C₆₀ propiolate ester product. M⁺ = m/z 979 Da for C₂₇H₁₇NO₃.

C₆₀ Diad synthesis

The synthesis of a diad or dimer of functionalized C₆₀ was attempted via a click reaction with 1,4-bis(azidomethyl)benzene. This reaction was attempted several times and under different conditions. The desired product was not formed. The HPLC trace (Figure 3.14) of the starting material is the same as that of the reaction mixture (Figure 3.15).



Scheme 3.7. Click reaction using 1,4-bis(azidomethyl)benzene and 3-(4'-(1''-methylpyrrolidin-2''-yl)phenoxy)propyl propiolate functionalized C₆₀.

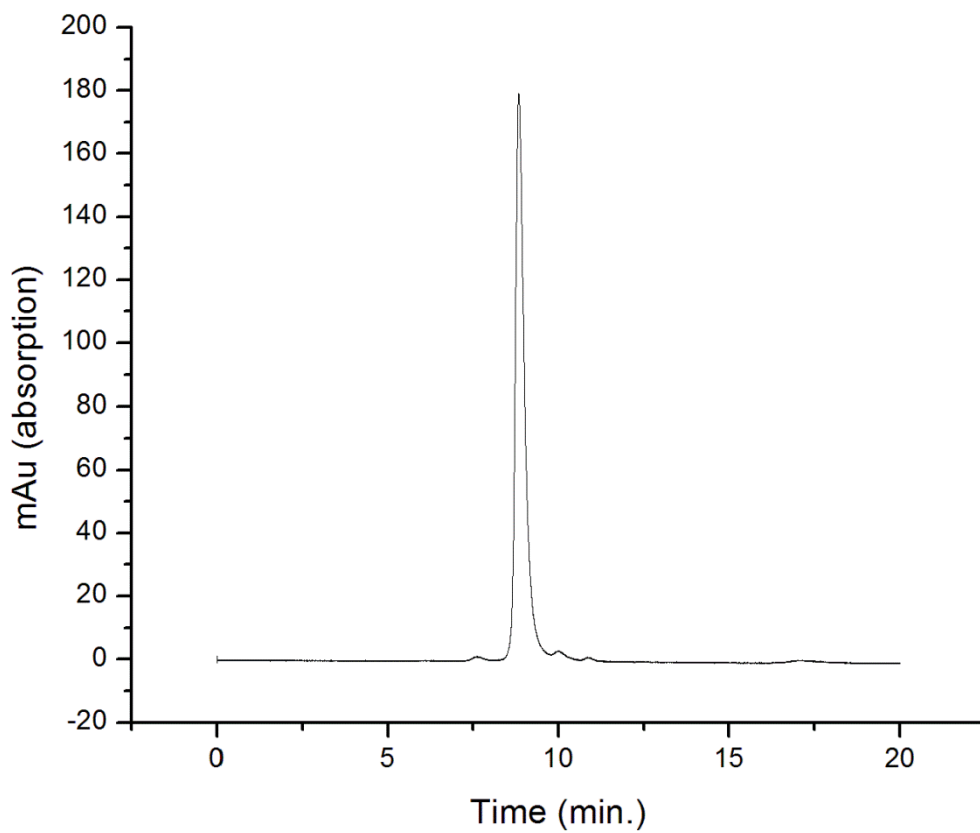


Figure 3.14. HPLC chromatogram of C₆₀ propiolate ester (PYE functionalized silica, toluene 0.5 mL/min).

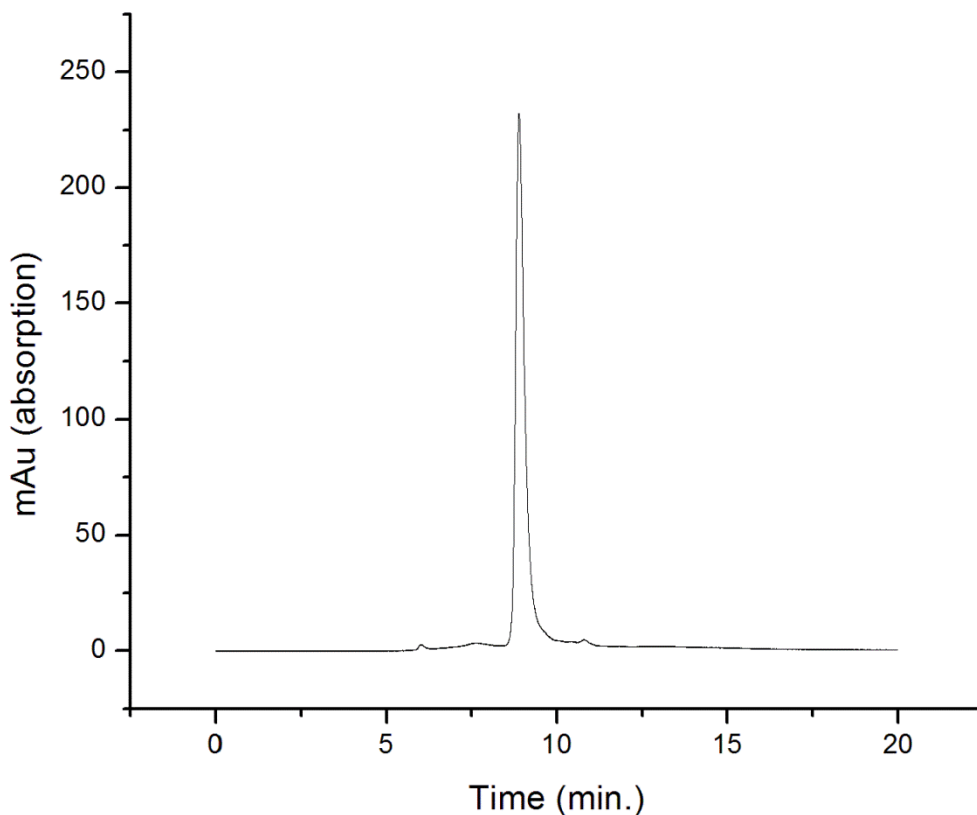


Figure 3.15. HPLC chromatogram for the click reaction mixture of C₆₀ propiolate and 1,4-bis(azidomethyl)benzene (PYE functionalized silica, toluene 0.5 mL/min.).

Conclusions

Several functional adducts of fullerene C₆₀ were synthesized using the Prato reaction. An alkyne functionalized C₆₀ was produced by DCC coupling of 3-(4'-(1''-methylpyrrolidin-2''-yl)phenoxy)propyl propiolate functionalized C₆₀ and propiolic acid. The alkyne functionalized C₆₀ species was employed in attempted “click” type reactions with 1,4-bis(azidomethyl)benzene, but these reactions were unsuccessful. Some of the alcohol functionalized C₆₀ adducts were also evaluated by cyclic voltammetry, and one was used to construct a photovoltaic device. The

device was functional, and while it was not very efficient, the measured open circuit voltage was higher than similar devices made from unfunctionalized C₆₀ due to the increased negative reduction potential provided by the fullerene tris-adduct. Annealing of the photovoltaic device improved its current producing abilities.

Experimental

Instrumentation

MALDI-TOF Mass spectrometry was run using a Kratos PCKompact spectrometer. Spectra were generated in positive ion mode. The matrix used for MALDI TOF MS was 9-nitroanthracene. The matrix and samples were cast on the target from toluene solutions. HPLC analyses were performed using an Agilent 1100 HPLC with a UV-Vis diode array detector set at 360 nm. The column was a 4.6 x 150 mm pyrene functionalized silica with a 1.0 ml/min toluene mobile phase. ¹H and ¹³C NMR spectra were obtained using a Bruker Avance 500 MHz (¹H) spectrometer. HPLC separations were accomplished using an Agilent 1100 series HPLC with a UV-Vis diode array detector. Separations were monitored for absorbance at 360 nm. Cyclic voltammogram measurements were taken using a CHI600A Electrochemical Analyzer. The working electrode was glassy carbon. A platinum wire was used as the counter electrode, and the reference electrode was Ag/AgCl. The supporting electrolyte was tetrabutylammonium tetrafluoroborate (0.1 M) dissolved in 1,2-dichlorobenzene. The scan rate was 250 mV/sec, and potential values were reported relative to the ferrocene/ferrocenium couple. The photovoltaic device was constructed by spin coating a layer of PEDT/PSS (Baytron PH) onto an indium tin oxide coated glass slide at 1.4k RPM. A solution of P3HT and fullerene tris-adduct (both dissolved in 1,2-dichlorobenzene at 15 mg/ml) was added next, spinning at 1k RPM. Aluminum was deposited on top of the heterojunction layer using chemical vapor deposition, with a source

to substrate height of 12.5 cm and a pressure of 5 μ torr. The resulting device was characterized for its current/potential properties under AM 1.5 light, before and after annealing at 110 $^{\circ}$ C.

Reaction of C₆₀ with Sarcosine and 4-(2'-hydroxyethoxy)benzaldehyde

C₆₀ (0.05137 g, 71.34 μ mol), 4-(2'-hydroxyethoxy)benzaldehyde (0.02082 g, 125.3 μ mol) and sarcosine (0.00625 g, 70.2 μ mol) of were dissolved in toluene. A few milliliters of chloroform were added to the aldehyde. The solution was heated at reflux and stirred overnight. The reaction mixture was separated on silica gel, toluene first to elute unreacted C₆₀ and then with 15:1 toluene and EA to elute the product. ¹H NMR (500 MHz, acetone-d₆) δ 7.05 (d, J = 8 Hz, 2H), 6.90 (d, J = 8 Hz, 2H), 4.98 (d, J = 9 Hz, 1H), 4.91 (s, 2H), 4.46 (s, 1H), 4.27 (d, J = 9 Hz, 1H), 3.96 (t, J = 5.0 Hz, 2H), 3.76 (t, J = 5 Hz, 2H), 2.77 (s, 3H). MALDI TOF MS: m/z 913 Da = M⁺, m/z 914 Da (M + H)⁺, m/z 915 Da (M + 2H)⁺, calcd. for M = C₇₁H₁₅NO₂ = m/z 913 Da.

Reaction of 4-(3'-hydroxypropoxy)benzaldehyde with Sarcosine and C₆₀

Fullerene C₆₀ (102.43 mg, 1432.3 μ mol), 4-(3'-hydroxypropoxy)benzaldehyde (33.57 mg, 186.3 μ mol), and sarcosine (26.56 mg, 298.1 μ mol) were added to a round bottom flask. The contents of the flask were dissolved in 50.0 mL toluene and heated at reflux overnight. The reaction solution was separated on silica gel with toluene, and 5% EA in toluene to yield the starting fullerene and mono-adduct, respectively. ¹H NMR (500 MHz, CDCl₃) δ 6.96 (d, J = 8 Hz, 2H), 4.98 (d, J = 9 Hz, 1H), 4.88 (s, 1H), 4.24 (d, J = 9 Hz, 1H), 4.13 (t, J = 6 Hz, 2H), 3.87 (t, J = 6 Hz, 2H), 2.79 (s, 3H), 2.04 (p, J = 6 Hz 2H). MALDI TOF MS: m/z = 720 Da = (C₆₀)⁺, m/z = 721 Da = (C₆₀+H)⁺, m/z = 722 Da = (C₆₀ + 2H)⁺, m/z = 927 Da = M⁺, m/z = 928 Da = (M + H)⁺, calcd. for M = C₇₂H₁₇NO₂ = m/z 927 Da.

Synthesis of Propiolate Ester of 3-(4'-(1''-methylpyrrolidin-2''-yl)phenoxy)propan-1-ol Functionalized C₆₀

2-(4'-(1''-Methylpyrrolidin-2''-yl)phenoxy)ethan-1-ol functionalized C₆₀ (5.65 mg, 6.18 μmol), 2.37 mg (33.8 μmol) of propiolic acid, and 1.26 mg (10.3 μmol) of DMAP were dissolved in dry THF. DCC (11.95 mg, 57.91 μmol) was dissolved in 5.0 mL of dry THF. The fullerene solution was cooled in an ice bath. The DCC solution was slowly added to the fullerene solution over about 5 min. The reaction mixture was stirred overnight under nitrogen and the THF was evaporated under blowing nitrogen. The crude reaction residue was redissolved in toluene and analyzed via HPLC. The residue was then separated on silica gel with toluene. ¹H NMR (500 MHz, CDCl₃) δ 6.94 (d, *J* = 6 Hz, 2H), 4.97 (d, *J* = 9 Hz, 2H), 4.87 (s, 1H), 4.39 (t, *J* = 6 Hz, 2H), 4.23 (d, *J* = 9 Hz, 1H), 4.06 (t, *J* = 6 Hz, 2H), 2.86 (s, 1H), 2.78 (s, 3H), 2.15 (p, *J* = 6 Hz, 2H). MALDI TOF MS: *m/z* = 720 Da = (C₆₀)⁺, *m/z* = 721 Da = (C₆₀ + H)⁺, *m/z* = 979 Da = M⁺, calcd. for M = (C₇₅H₁₇NO₃) = *m/z* 979 Da.

Synthesis of C₆₀ diad

Alkyne functionalized fullerene (30.15 mg, 31.24 μmol) was added to a round bottom flask. A solution of 1,4-bis(azidomethyl)benzene (0.5 ml of a 2.98 mg/ml solution in dichloromethane, 7.90 μmol) was added to the round bottom flask. The contents of the flask were dissolved in 10.0 ml of dichloromethane. Copper sulfate (0.01 g, 62.65 μmol) and ascorbic acid (0.01 g, 56.78 μmol) were dissolved in 5.0 ml of water. The aqueous solution was mixed with the organic solution in the round bottom flask with vigorous stirring overnight. The layers were separated and the organic layer was washed once with 5.0 ml of water. Characterization was made by HPLC which determined no product was formed.

References

1. Cox, C. T., Jr.; Cooper, M. M., *Journal of Chemical Education* **2006**, 83, 99-100.
2. Wei, X.-W.; Avent, A. G.; Boltalina, O. V.; Street, J. M.; Taylor, R., *Journal of the Chemical Society, Perkin Transactions 2* **2002**, 47-52.
3. Cai, T.; Ge, Z.; Iezzi, E. B.; Glass, T. E.; Harich, K.; Gibson, H. W.; Dorn, H. C., *Chemical Communications* **2005**, 3594-3596.
4. Cai, T.; Xu, L.; Gibson, H. W.; Dorn, H. C., *Abstracts, 57th Southeast/61st Southwest Joint Regional Meeting of the American Chemical Society, Memphis, TN, United States, November 1-4* **2005**, NOV04-177.
5. Mochulskaya, N. N.; Andreiko, A. A.; Charushin, V. N.; Shulgin, B. V.; Raikov, D. V.; Solomonov, V. I., *Mendeleev Communications* **2001**, 19-21.

Chapter Four

Bingel Functionalization of Fullerenes

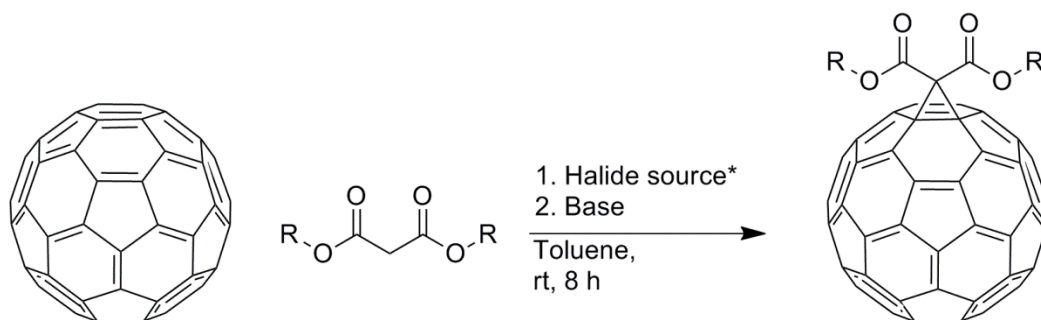
Abstract

The Bingel cyclopropanation reaction was used to functionalize C₆₀ fullerene. One particular malonate, Meldrum's acid, was used to prepare both mono- and bis-adducts of fullerene C₆₀. The Meldrum's acid adducts of C₆₀ were then thermally degraded to produce C₆₀ ketene. The fullerene ketene was then used to synthesize a C₆₀ dimer, and polymeric products.

Introduction

The Bingel reaction of fullerenes has historically been accomplished with malonate esters and empty cage fullerenes. Generally, a halogenated malonate diester, and base are used to effect the reaction.¹ A modified version of these conditions employs a malonate, a halogen source, such as iodine or carbon tetrabromide, and a base. The mechanism of the reaction requires the deprotonation of the malonate, and subsequent attack of the carbanion on the fullerene cage to produce the fullerene anion. Intramolecular elimination then occurs as the fullerene anion displaces the halide leaving group to form a cyclopropyl moiety. When the functionalization reaction is used to treat C₆₀ the addition occurs across a 6,6-double bond on the fullerene cage between two five-membered rings. Bingel reaction conditions can also be employed with other activated species such as ketones and monoesters, particularly those already possessing a good leaving group at the position α to the carbonyl. Cyclopropyl adducts have also been generated from reactions of fullerenes and diazo compounds.²⁻³ In this case, the diazo moiety acts as a 1,3-dipole, and initially adds to the fullerene cage as it acts as a 1,3-dipolarophile. Under thermal or ultraviolet excitation, dinitrogen is extruded from the initial pyrazole adduct ring to form either a

cyclopropyl adduct or a ring opened adduct. This type of reaction was originally discovered and exploited by Wudl's group.³⁻⁵ For some time Bingel type reactions were considered to be inaccessible for use on endohedral metallofullerenes, but that was proven incorrect by Echegoyen et al.⁶ The Bingel reaction run in this work was the functionalization of fullerenes using Meldrum's acid.⁷ Meldrum's acid is a cyclic malonate diester, that once installed can lead to some very interesting chemistry. Upon heating to 150⁰ C, the Meldrum's acid moiety releases acetone and carbon dioxide to form a ketene moiety. The ketene functional group is very versatile, and can be used to generate esters, amides, lactones, and cyclobutanedione moieties. By adding the Meldrum's acid moiety to a fullerene cage, new and interesting functionality can be invoked. This includes the dimerization of fullerene ketenes, and polymerization of fullerene bis-ketenes.



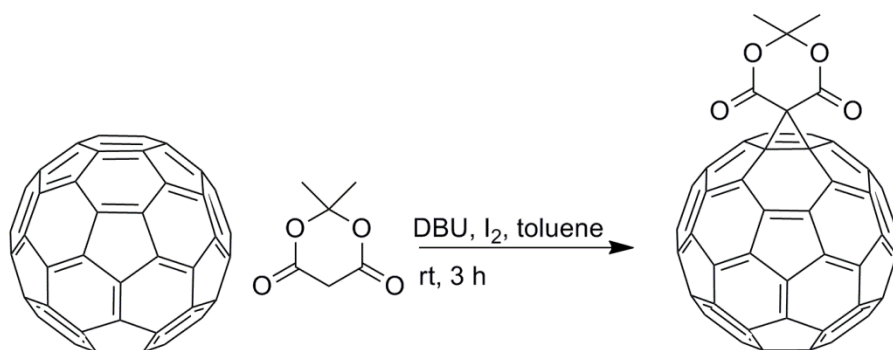
Scheme 4.1. Generic Bingel reaction employing a malonate, base (DBU or NaH) and a halide source (I_2 or CBr_4).

Results and Discussion

Synthesis of C_{60} meldrum's acid adduct

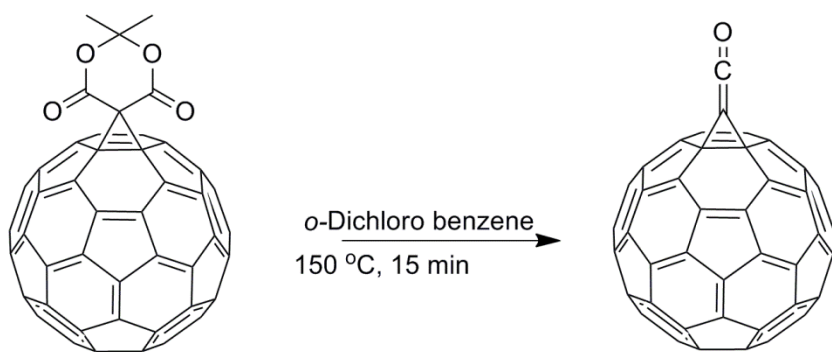
Meldrum's acid is a cyclic malonate. Its mono-adduct of C_{60} has been previously prepared and characterized by a group in China as seen in Scheme 4.1.⁷ The original synthesis

used iodine as a halogen source, and 1,8-diazabicyclo[5.4.0]undec-7-ene (DBU) as the base. A comparable reaction should be possible with CBr_4 as the halogen source as well.



Scheme 4.2. Reaction of C_{60} with Meldrum's acid, iodine, and DBU.

Syntheses of the Meldrum's acid adducts of fullerenes are interesting due to the possibility of producing a reactive ketene species. It has already been mentioned that the hydrolysis products of malonate adducts of fullerenes, i. e., malonic acids, can easily decarboxylate, and the Meldrum's acid adduct is a special case that will undergo this type of reaction by thermolysis. Upon heating to temperatures above $150\text{ }^{\circ}\text{C}$, the Meldrum's acid moiety releases acetone as well as CO_2 to produce a fullerene ketene (Scheme 4.3).⁸⁻¹² The ketene moiety is a very reactive intermediate that will react with itself as well as other functional groups.



Scheme 4.3. Degradation of the Meldrum's acid adduct of C_{60} to form C_{60} ketene.

The MALDI TOF mass spectrum shown below (Figure 4.1) also indicates production of the ketene in the mass spectrometer. The parent Meldrum's acid mono-adduct peak is not seen in the spectrum; however, the photolysis products generated by the laser are detected. The major peaks besides the C_{60} parent fullerene are $C_{60} + C$ from decarbonylation of the ketene at m/z 733 Da; $C_{60} + 2C$ from the loss of oxygen from the ketene at m/z 744 Da, and the ketene ($C_{60} + C + C + O$) at m/z 760 Da.

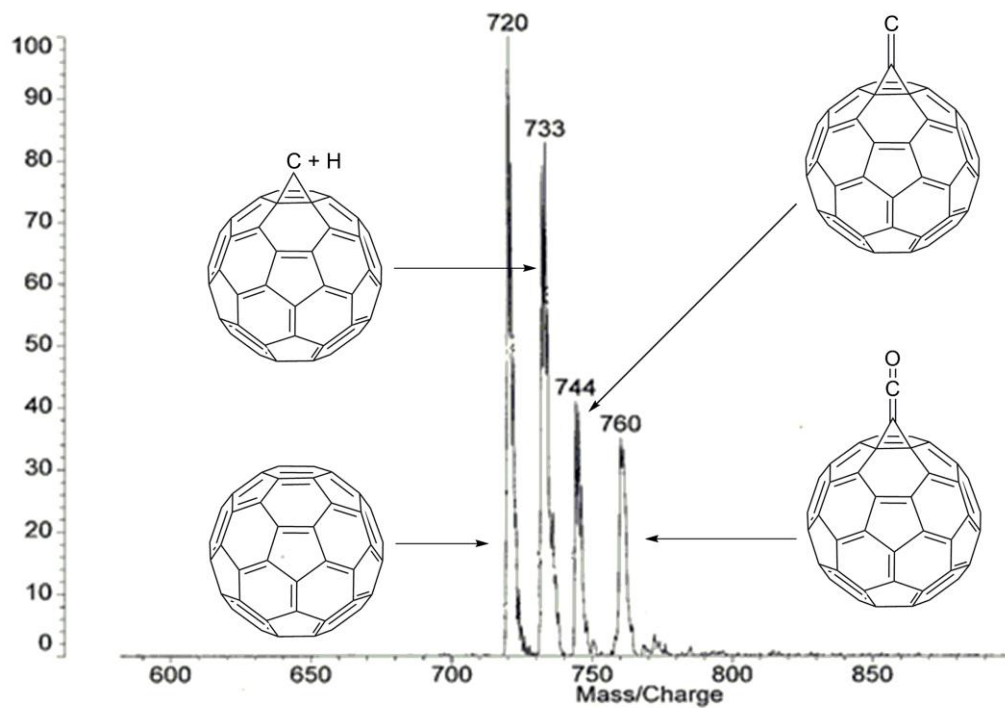
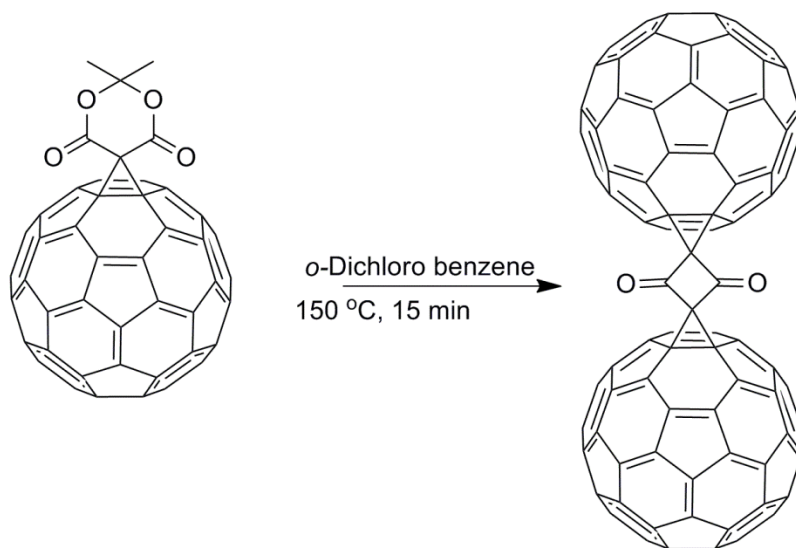


Figure 4.1. MALDI TOF MS of the mono-adduct of Meldrum's acid and C_{60} indicating the degradation products of the adduct and the presence of C_{60} ketene.

Synthesis of C_{60} dimer from Meldrum's acid mono adduct

Heating the Meldrum's acid mono-adduct without a second reactive compound causes rapid dimerization of the ketene intermediate. Instead of the lactone product expected from the dimerization of ketene itself, steric hindrance directs the formation of the butanedione product seen in Scheme 4.4.



Scheme 4.4. Synthesis of C_{60} dimer from C_{60} Meldrum's acid mono adduct.

The mono-adduct of Meldrum's acid and C_{60} was heated in dichlorobenzene until it boiled ($178\text{ }^{\circ}\text{C}$) and then cooled. The original solution was a dark peach color which quickly turned brown. The reaction was stopped after 15 minutes when no further noticeable change in color could be detected. The reaction mixture was analyzed by HPLC (Figure 4.2). Residual mono-adduct was observed as the peak at 6.0 minutes, and the parent C_{60} appeared at 10.8 minutes. The dimer peak was detected at 26.9 minutes; the longer retention time for the dimer was expected due to the presence of the two fullerene moieties. The reaction mixture was separated on silica gel and further characterization of the dimer was completed by ^{13}C NMR and MALDI TOF MS. This is a new and unpublished compound.

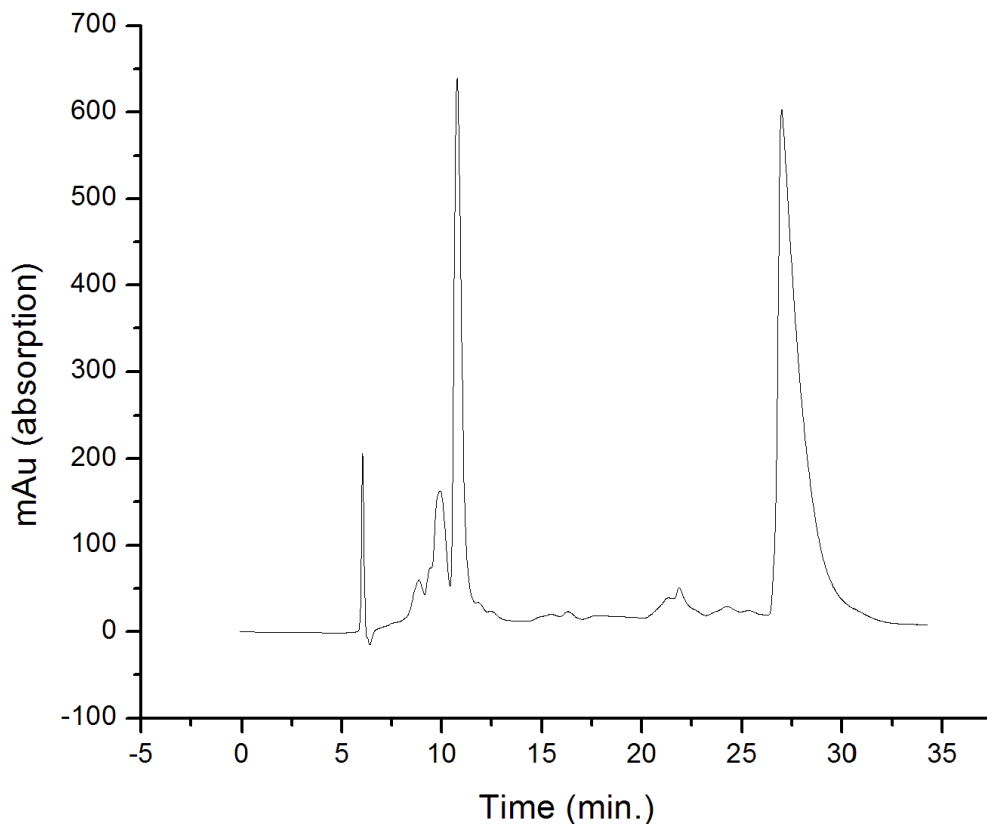


Figure 4.2. HPLC chromatogram showing the major dimer product from thermal decomposition of C₆₀ Meldrum's acid adduct at 26.9 minutes. The other major peak at 10.8 minutes is residual starting material.

The MALDI TOF mass spectrum for the dimer (Figure 4.5) contains a peak for the M-H⁺ at m/z 1519 Da. The other peaks near the dimer mass are at m/z 1494 and 1490 Da, respectively. These correspond to losses of carbon and oxygen from the strained cyclobutanedione ring. Other masses include the collection of peaks near m/z 720 Da that are accounted for by losing one fullerene from the dimer. The peak at m/z 910 Da may show a reaction between the methanofullerene generated by the MALDI laser and the matrix itself. The matrix in this case was nitroanthracene and the peak at m/z 910 Da corresponds to the addition of anthracene to C₆₁.

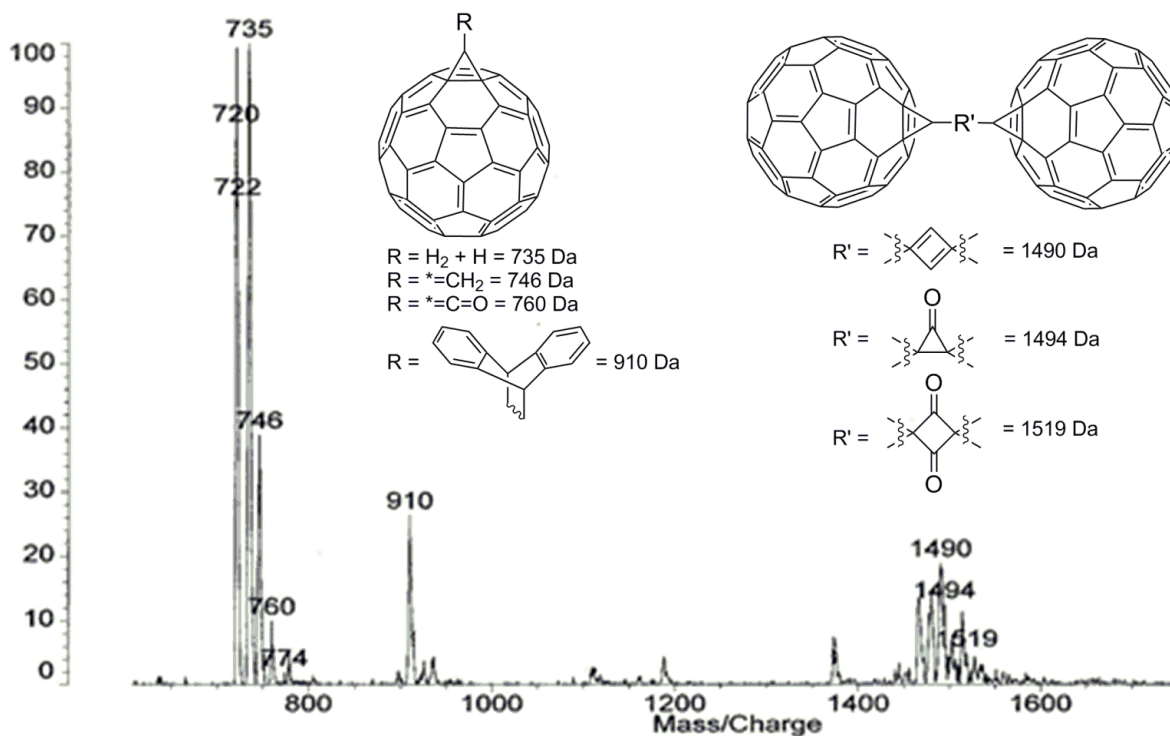


Figure 4.3. MALDI TOF MS for the C₆₀ dimer product showing several degradation products as well as the dimer at m/z 1519 Da (M-1)⁺.

The ¹³C NMR spectrum of the dimer (Figure 4.4.) contains 30 peaks in the fullerene region. This can be accounted for by the C_{2v} symmetry of the product. On initial inspection, the product seems like it should have C₄ type symmetry, but the cyclobutanedione ring is very strained and is consequently probably not planar. Other peaks for the bridgehead carbons, and the carbonyl carbons are also seen in the spectrum. No ¹H NMR spectrum was taken since the product is devoid of protons. Due to the lack of hydrogen substituents in this molecule, and its substantial molecular weight, it was difficult to measure the ¹³C NMR of this molecule. Consequently, the sample had to be run at the highest possible concentration, with a large number of scans in order to develop a suitable spectrum. Small amounts of impurities are seen in

the spectrum, including: dimethyl sulfoxide ($\delta = 40.76$ ppm), acetone ($\delta = 30.92, 207.07$ ppm), and grease ($\delta = 1.04, 29.76$ ppm).

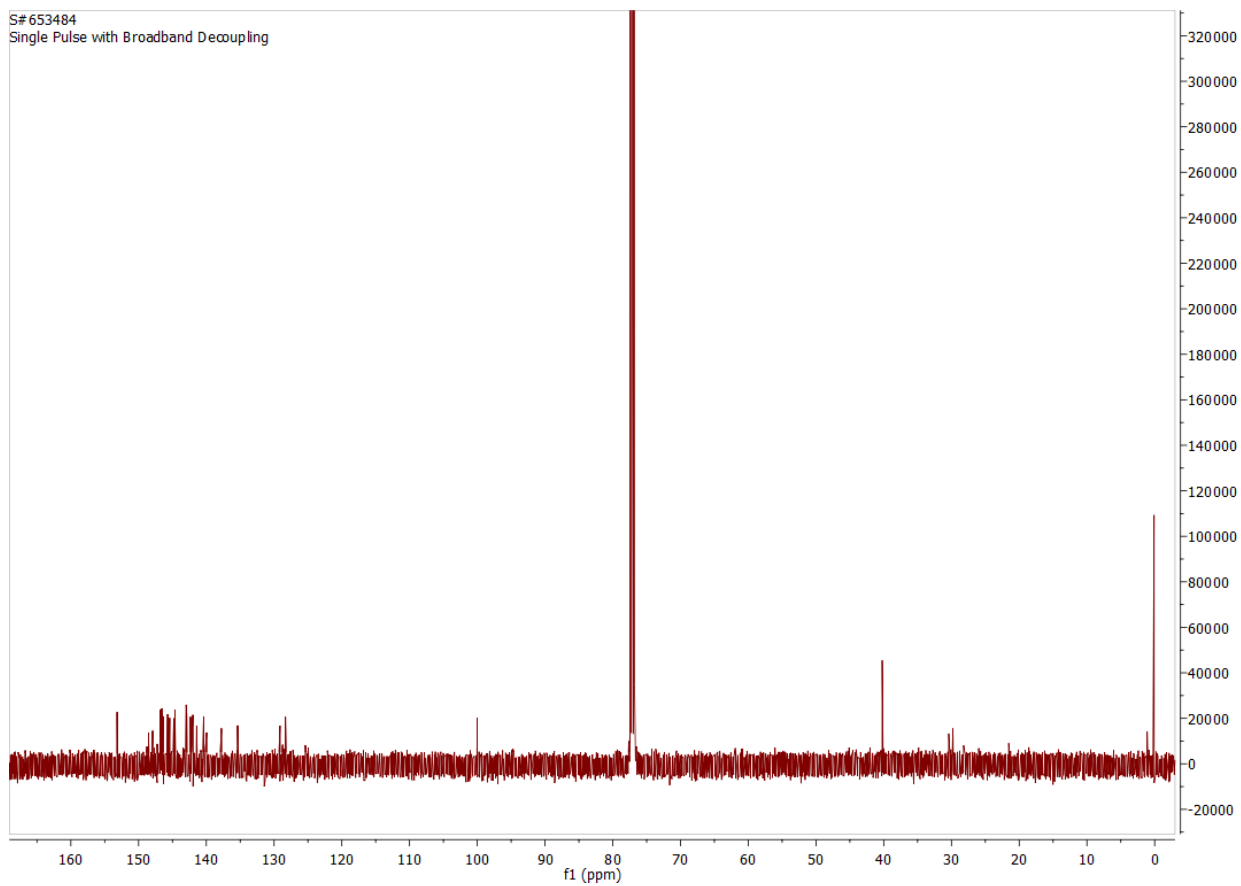
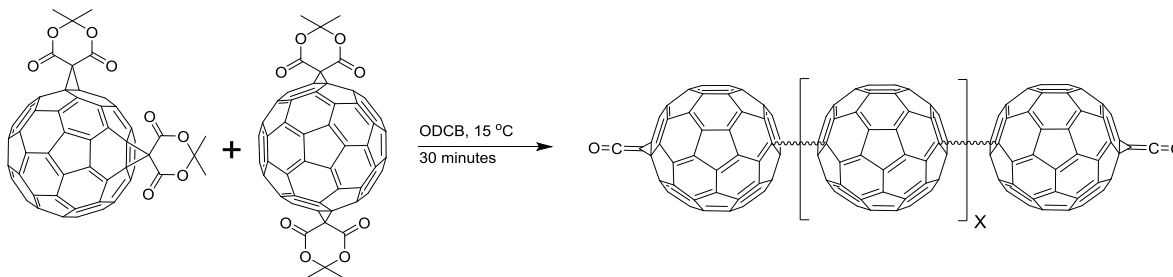


Figure 4.4. ¹³C NMR spectrum for the dimer synthesized from C₆₀ Meldrum's acid mono-adduct.

Synthesis of Meldrum's acid polymer from bis-adduct

The bis-adduct of Meldrum's acid was heated in boiling dichlorobenzene (178 °C) to afford oligomeric polyfullerene derivatives. Scheme 4.5 shows both the axially and orthogonally functionalized derivative. The oligomeric polyfullerene was comprised of a random series of

axial and orthogonal linkages. The hexamer product is indicated in the MALDI TOF MS (Figure 4.5).



Scheme 4.5. Polymerization of C₆₀ Meldrum's acid bis-adduct from thermal production of the bis-ketene with up to six repeat units. The linker moiety is cyclobutanedione in the fullerene repeat units.

The polyfullerenes were generated by a step growth method, and consequently, without high conversion to the cyclobutanedione, low degrees of polymerization are expected. If the solution was heated for an extended period of time, the longer oligomers began to precipitate from solution. Thus a short reaction time of 30 minutes was ideal for this reaction. TLC separation using a 10 cm long plate showed no less than 13 distinct spots (chloroform, silica). The MALDI TOF mass spectrum (Figure 4.5) reinforces the assertion that oligomeric species were produced. The groups of peaks are spread approximately 720 Da from each other indicating a C₆₀ repeat unit. The group of peaks centered on m/z 4651 Da indicates a hexamer is present. Due to fragmentation in the instrument and the labile nature of the cyclobutanedione linking moiety (as illustrated by the C₆₀ dimer MALDI TOF MS Figure 4.3) it is not unreasonable to expect that larger oligomers may be present.

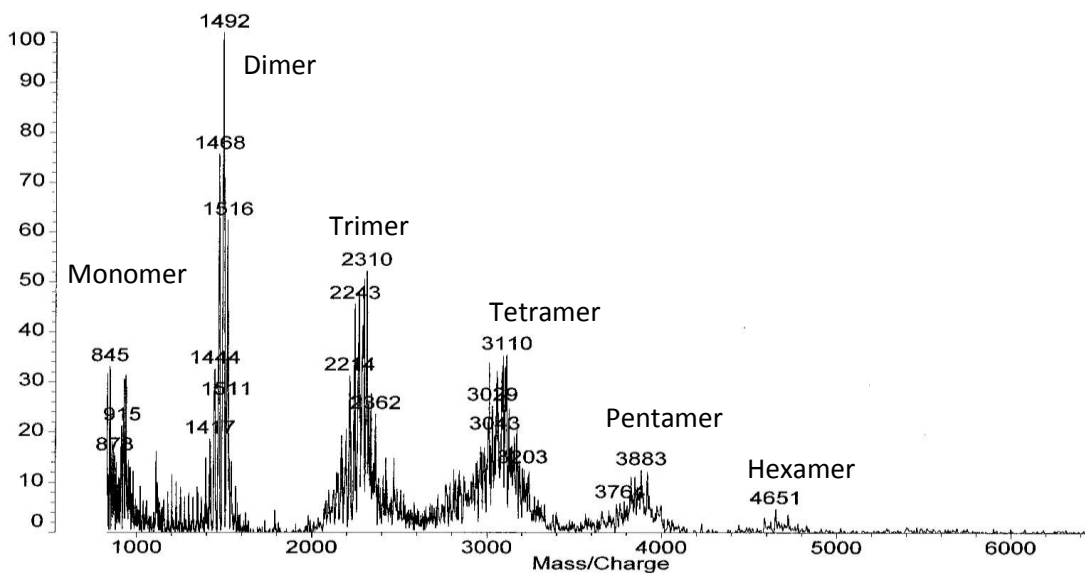


Figure 4.5. MALDI TOF MS of the fullerene polymer made from the C₆₀ Meldrum's acid bis-adduct showing up to six repeat units.

Conclusions

Several functionalized fullerene species were synthesized using either traditional or modified Bingel methods. The mono- and bis-addition to both C₆₀ were accomplished. The mono- and bis-adducts with Meldrum's acid and C₆₀ were successfully used to generate a fullerene dimer, and oligomeric polyfullerenes.

EXPERIMENTAL

Instruments

MALDI-TOF Mass spectrometry was run using a Kratos PCKompact spectrometer. Spectra were generated in positive ion mode. HPLC analyses were performed using an Agilent 1100 HPLC with a UV-Vis diode array detector set at 360 nm. The column was a 4.6 x 150 mm pyrene functionalized silica with a 1.0 ml/min toluene mobile phase. ¹H and ¹³C NMR were obtained using a Bruker Avance 500 MHz (¹H) spectrometer.

Synthesis of Meldrums acid

Dry acetone (100.0 ml 1.36 mol), malonic acid (10.12 g 97.25 mmol) and acetic anhydride (20.1 g 197 mmol) were added to an Erlenmeyer flask and cooled in an ice bath. A catalytic amount of sulfuric acid (0.50 g 5.1 mmol) was added slowly and the reaction mixture was allowed to stir in the ice bath overnight. The reaction mixture was moved to the freezer for 3 h, and finally, the solid product was removed by filtration. The product (7.12 g 52 %), a white solid, was analyzed by ^1H NMR and compared to the literature spectrum (mp 94.1 – 95.2 °C, lit. mp 94 - 95 °C).⁷ ^1H NMR (500 MHz, CDCl_3) δ 3.63 (s, 2H), 1.79 (s, 6H).

Synthesis of C_{60} Meldrum's acid mono-adduct

C_{60} (99.22 mg 138.2 μmol), iodine (68.43 mg 449.5 μmol), and Meldrum's acid (60.78 mg 421.7 μmol) were dissolved in toluene (approximately 100 mL) and placed under an N_2 blanket. DBU (107.40 mg 423.15 μmol) was added to the solution and it was stirred overnight at room temperature. The resulting solution was separated on silica gel (50 g) with toluene, yielding 45.37 mg of dark brown solid (38 %). ^1H NMR (500 MHz, CDCl_3) δ 2.19 (s). MALDI TOF MS: m/z 720 Da (C_{60}), m/z 733 Da ($\text{C}_{60} + \text{CH}$), m/z 744 Da ($\text{C}_{60} + \text{C}=\text{C}$), m/z 760 Da ($\text{C}_{60} + \text{C}=\text{C}=\text{O}$).

Synthesis of C_{60} Meldrum's acid dimer

C_{60} Meldrum's acid adduct (10.0 mg 12 μmol) was placed in a small round bottom flask. *ortho*-dichlorobenzene (1.0 mL) was added to the flask to dissolve the fulleroid. The resulting solution was stirred and heated at reflux overnight. The crude mixture was analyzed by HPLC and MS. The solution was purified by HPLC. ^{13}C NMR (126 MHz, CDCl_3) δ 153.08, 148.44, 147.84, 146.67, 146.49, 146.43, 146.31, 145.62, 145.48, 145.46, 145.33, 144.72, 144.68, 144.54,

144.41, 143.01, 142.88, 142.80, 142.33, 142.31, 142.26, 142.20, 141.90, 141.34, 140.31, 139.88, 137.69, 135.30, 129.04, 128.23, 99.92; dimethyl sulfoxide ($\delta = 40.76$ ppm), acetone ($\delta = 30.92$, 207.07 ppm), and grease ($\delta = 1.04$, 29.76 ppm) were also detected. MALDI TOF MS: m/z 760 Da (C_{60}), m/z 735 Da ($C_{60} + CH_2 + H$), m/z 746 Da ($C_{60} + C=CH_2$), m/z 760 Da ($C_{60} + C=C=O$), m/z 910 Da ($C_{60} + \text{anthracene}$), m/z 1490 Da ($M - 2O$), m/z 1494 Da ($M - C=O$), m/z 1519 Da ($M - 1$), $M = C_{124}O_2$.

Synthesis of Meldrum's acid polymer from bis-adduct

C_{60} bisadduct (9.2 mg 9.1 μmol) was placed in a small Erlenmeyer flask with N_2 purge. Approximately 2 ml of dichlorobenzene was added. The flask was heated over a heat gun with N_2 purge for 15 min. The resulting solution was characterized by MALDI TOF: m/z 1492 Da (dimer), m/z 2310 Da (trimer), m/z 3110 Da (tetramer), m/z 3883 Da (pentamer), m/z 4651 Da (hexamer).

References

1. Bingel, C., *Chemische Berichte* **1993**, *126*, 1957-9.
2. Suzuki, T.; Li, Q.; Khemani, K. C.; Wudl, F., *Journal of the American Chemical Society* **1992**, *114*, 7301-2.
3. Suzuki, T.; Li, Q.; Khemani, K. C.; Wudl, F.; Almarsson, O., *Science (Washington, DC, United States)* **1991**, *254*, 1186-8.
4. Wudl, F., *Accounts of Chemical Research* **1992**, *25*, 157-61.
5. Wudl, F.; Hirsch, A.; Khemani, K. C.; Suzuki, T.; Allemand, P. M.; Koch, A.; Eckert, H.; Srdanov, G.; Webb, H. M., *ACS Symposium Series* **1992**, *481*, 161-75.
6. Pinzon, J. R.; Zuo, T.; Echegoyen, L., *Chemistry - A European Journal* **2010**, *16*, 4864-4869, S4864/1-S4864/15.
7. Jiang, H.; Zhang, J.-M.; Du, W.-Q.; Zhu, S.-Z., *Chinese Journal of Chemistry* **2007**, *25*, 86-89.
8. Kim, J.; Kang, E.-H.; Choi, T.-L., *ACS Macro Letters* **2012**, *1*, 1090-1093.

9. Knapp, J. M.; Zhu, J. S.; Wood, A. B.; Kurth, M. J., *ACS Combinatorial Science* **2012**, *14*, 85-88.
10. Postikova, S.; Tite, T.; Levacher, V.; Briere, J.-F., *Advanced Synthesis & Catalysis* **2013**, *355*, 2513-2517.
11. Steinbacher, A.; Roeding, S.; Brixner, T.; Nuernberger, P., *Physical Chemistry Chemical Physics* **2014**, *16*, 7290-7298.
12. Wolffs, M.; Kade, M. J.; Hawker, C. J., *Chemical Communications (Cambridge, United Kingdom)* **2011**, *47*, 10572-10574.

Chapter Five

Introduction to Isothermal Titration Microcalorimetry

Instrument

Isothermal titration microcalorimetry (ITC) is a powerful tool that can be used for a wide range of analyses, including the determination of binding constants, critical micelle concentrations, and acid/base titrations.¹ The interactive behavior of molecules in solution is of great interest in many different areas of scientific research including chemistry, physics, and biology.² ITC titrations have traditionally been used to determine binding constants between molecules in solution;³⁻⁴ however, the technique can be used to determine several other solution based parameters. Titrations are only limited to changes that provide an enthalpic response.⁵ In this way, ITC can also be used for traditional acid/base titrations, and even the determination of critical micelle concentrations of surfactants.⁶ Since nearly all chemical and physical changes in solution involve a change in enthalpy, ITC is an almost universal titration system.⁷ Binding constants in solution are determined by fitting the gathered isothermal data with a Weisman isotherm model.⁸ The ability to determine binding constants by measuring and tracking the changes in enthalpy caused by the interaction also has advantages over other types of binding titration. Binding constants can be calculated using other spectroscopic methods, such as ¹H NMR or UV-Vis. These types of titrations require several measurements, and depend on changes in the spectrum in order to effectively measure a binding constant. If there is no measurable spectroscopic change, these methods cannot be used. This is again in contrast to the use of ITC which measures the nearly ever present change in enthalpy that accompanies most physical and chemical changes in solution. The change in heat measured during a titration can also be compared to that measured by differential scanning calorimetry.⁹ In fact, ITC

measurements can further elucidate polymeric behaviors in solution. Titrations of block copolymers can characterize their aggregation properties.¹⁰ The original systems studied extensively by the use of ITC were biopolymers such as DNA. Thermodynamic properties of biological systems are very important, particularly in terms of drug and chemical interactions with living systems.^{2, 11}

Two cell design

The ITC instrument generally employs two liquid cells. The measurement cell houses the titration. A reference cell is used to normalize the amount of energy entering or leaving the cell according to the different solvents used for various titrations.⁶ Since different solvents have different specific heat capacities, the reference cell and thermal calibration are used to ensure that peak areas accurately represent the energy change in the cell. In the Microcal MCS ITC instrument, the two cells are mounted back to back, separated by a thermocouple pile. A very small difference in temperature is maintained between the two cells so that there is a small voltage signal present from the thermocouple.¹² As the titration occurs in the measurement cell, a feedback system varies the amount of current supplied to the cell heater in order to maintain the voltage signal from the thermocouple. In this way the amount of heat added or withheld from the measurement cell can be quantified if one knows the heat capacity of the cell and its contents and the resistance of the heater circuit.

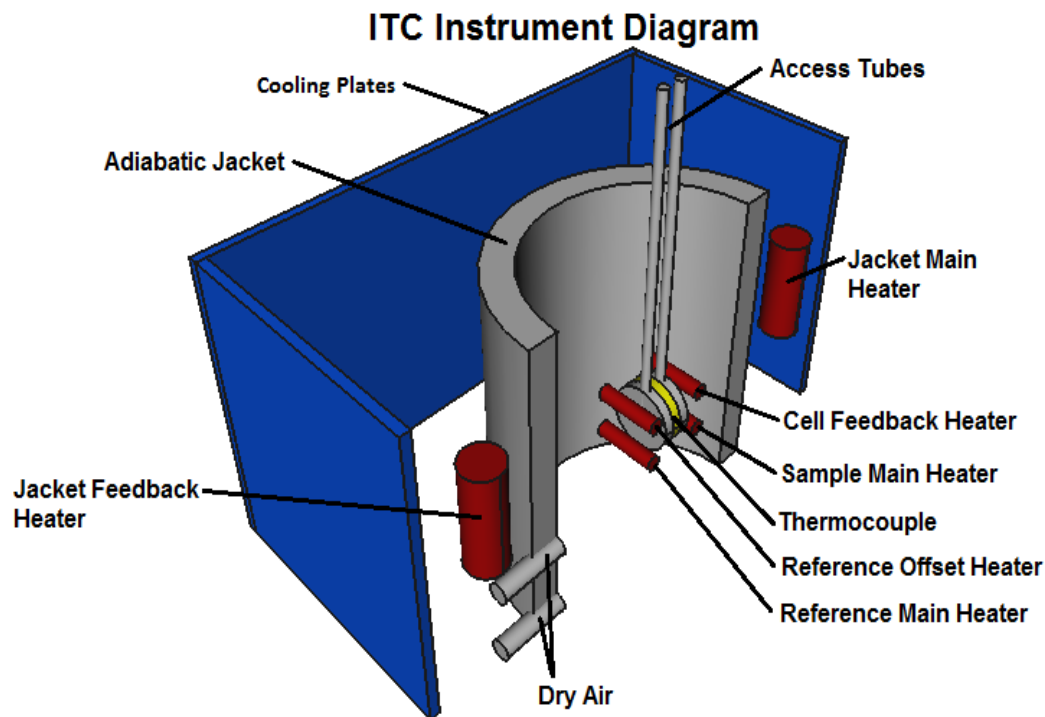


Figure 5.1. Cutaway drawing and diagram of the inside of the Microcal MCS ITC instrument.

The sample cell operates under constant volume conditions, ejecting excess solution into the access tube as titrant is added.¹³ Since the difference in temperature and heating only occur in the sample and reference cells, only the change in energy that occurs inside the sample cell is measured by the instrument. During the titration, excess solution is pushed into the access tube for the coin shaped cell. Thus changes in concentration of solution in the cell must be accounted for in the calculations used to fit the enthalpogram data. A constant volume is required for the physical model which also requires constant temperature and pressure to ensure adiabatic conditions.¹⁴

The heat flow into and out of the cell is calibrated using a series of timed pulse experiments. A linear response factor is calculated to relate the change in the cell heater current

to the heat added to the cell. This response factor depends on the heat capacity of the cell and its contents. Consequently the factor changes significantly when the titration solvent is changed from water to an organic liquid. The response factor does not change linearly with the specific heat capacity, but does seem to scale with the volumetric heat capacity. This is illustrated in Figure 5.3 at the end of the chapter.

Cells increase in temperature slowly

During the titration, the two cells are very slowly heated such that a small amount of current is used to maintain the rate of heating. This amount of current is used as the baseline for the titration and the current peaks generated. The level of feedback current can be controlled and is set using the reference offset parameter in the software. If the interaction being measured is exothermic, the feedback current peaks will be negative in direction. Since the current cannot be measured below a value of zero, the baseline, or reference offset must be set high enough so that the peak amplitude does not extend below zero current. If the interaction being measured is endothermic, the peak direction will be positive. It generally is not a problem to have positive peaks, but if their amplitude is higher than the allowable feedback current, the peak height and consequently peak area could be erroneous. Thus the cell feedback baseline, as set by the reference offset, creates a working window or thermal headspace for the titration to occur. The titration parameters must therefore be set for each new titration so that the measurements can be accurate. The reference offset is set as a percentage out of 100. Low levels of reference offset can be used for dilute titrations wherein high binding constants are expected. For lower binding constant titrations or those in which high concentrations need to be used, the low gain system may be used to further extend the thermal headspace.

Adiabatic cooling jacket

Since the measurement and reference cells in the instrument slowly heat up during a titration, there is also a system in place to make sure the cells do not overheat, and slow the heating effect. An adiabatic cooling jacket is placed around the two cells. The cooling jacket is fed circulating water from a temperature regulating unit outside the titration head unit. The temperature bath is regulated by the control software. There are also heaters placed inside the cooling jacket to more carefully control the temperature and the heat flow from the cells to the jacket. The jacket is thus kept at a lower temperature than the cells.

Titration Model

Calculations based on isothermal titration data require the use of a constant volume adiabatic cell. As injections are made into the measurement cell, a mixture of the original cell solution and the previously injected titrant is ejected into the access tube. Construction of the instrument is such that only heat released or absorbed inside the cell is measured, and thus constant volume, temperature, and pressure conditions are maintained. A cut away diagram of the cell is shown below. The volumes V_0 and ΔV are taken to represent the cell volume and the injected or ejected volume respectively. Changes in concentration for both titration components are calculated for each injection, and assume thorough mixing of the previous injection, and that no new titrant is ejected during the injection.¹⁴ The changes in heat associated with dilution and or dissociation of salts are measured and subtracted from the measurement data set after completing a background titration of titrant into blank solvent. The same solvent is used in both the syringe and cell to avoid solvent mixing. Generally, low concentrations of both the components in the titration are used in order to minimize any changes in solution volume that might accompany their interaction.^{12, 14}

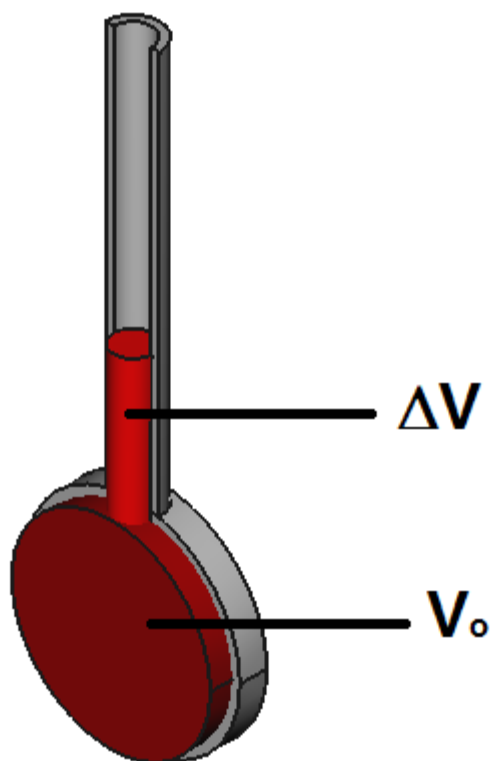


Figure 5.2. Cutaway drawing of the ITC titration cell including the working volume V_o and the volume ejected (ΔV), after every injection of titrant.

The quantities V_o and ΔV are used with the initial concentrations of the cell solution (M_t^o) to calculate the concentration of the cell species after any injection (M_t). The relationship between these quantities is given below as Equation 5.1; it is based on the average of the initial and final concentrations.

$$M_t = M_t^o \left[\frac{1 - \left(\frac{\Delta V}{2V_o} \right)}{1 + \left(\frac{\Delta V}{2V_o} \right)} \right] \quad (\text{Equation 5.1})$$

The concentration of titrant molecule in the cell after any given injection is calculated using the Equation 5.2. It is a running average of the total amount injected during the titration and the ejected volume. The concentration of the cell species in the cell is described by Equation 5.2, and is also a running average accounting for the loss of ejected solution.

$$X_t = X_t^o \left[1 - \left(\frac{\Delta V}{2V_o} \right) \right] \quad (\text{Equation 5.2})$$

When describing the binding constant for a simple binding model with one set of sites, Equation 5.3 reflects the concentration of the binding constituents instead of their activities. Consequently, binding coefficients are reported in units of M^{-1} instead of the expected unitless quantity. In the equations, K is the binding constant. The variable n is the number of sites or the binding stoichiometry. The variables M_t , and $[M]$ are the overall and free concentration of the cell species. X_t and $[X]$ are the overall and free concentrations of the titrant solution. Finally, θ is the fraction of available sites that are bound. The equations defining K (Equation 5.3), X_t (Equation 5.4), and M_t (Equation 5.4) are combined by substituting for $[X]$ in Equation 5.3 and multiplying to form the quadratic equation (Equation 5.5) that describes the fractional saturation of binding sites during the titration.

$$K = \frac{\theta}{(1 - \theta)[X]} \quad (\text{Equation 5.3})$$

$$X_t = [X] + n\theta M_t \quad (\text{Equation 5.4})$$

$$\theta^2 - \theta \left[1 + \left(\frac{X_t}{nM_t} \right) + \left(\frac{1}{nKM_t} \right) \right] + \left(\frac{X_t}{nM_t} \right) = 0 \quad (\text{Equation 5.5})$$

The total heat that is either released or absorbed after each injection is the quantity measured during an ITC experiment. If a simple binding model is used that employs a single set of binding sites, the assumption is made that measured change in heat accounts for the change in enthalpy due to the binding of the two components. Equation 5.6 relates the total heat to the change in enthalpy.

$$Q = n\theta M_t \Delta H V_o \quad (\text{Equation 5.6})$$

Thus, by solving the quadratic Equation 5.5 and substituting the values into the Equation 5.6 for the measured heat, Equation 5.7 is generated. Equation 5.7 allows for the calculation of heat energy for any single injection during the titration using appropriate values of K, n, and ΔH . These are the fitting parameters for the single set of sites model. During the titration, the titrant interacts with the cell species until all of the molecules in the cell are bound. The ratio of titrant to cell molecules ranges from an excess of cell species at the beginning of the titration, to an excess of titrant at the end of the titration. After a titration is run, and all of the injection energies are analyzed, integrated and plotted in an enthalpogram; the data are fit using the three fitting parameters using standard Marquardt methods to give the best values for the binding constant, enthalpy change, and stoichiometry.¹⁴

$$Q = \frac{nM_t \Delta H V_o}{2} \left[1 + \frac{X_t}{nM_t} + \frac{1}{nKM_t} - \sqrt{\left(1 + \frac{X_t}{nM_t} + \frac{1}{nKM_t} \right)^2 - \frac{4X_t}{nM_t}} \right] \quad (\text{Equation 5.7})$$

For a model with two sets of independent sites, Equation 5.1 and Equation 5.2 are used to define the concentrations of both components in the measurement cell. Equation 5.8 and Equation 5.9 describe the independent association constants according to the equilibrium concentrations of the titrant and cell species. Solving for θ_1 and θ_2 and combining the equations provides Equation 5.10 and Equation 5.11 relating the titrant concentration to the binding fraction θ , and the association constants K_1 and K_2 .

$$K_1 = \frac{\theta_1}{(1 - \theta_1)[X]} \quad (\text{Equation 5.8})$$

$$K_2 = \frac{\theta_2}{(1 - \theta_2)[X]} \quad (\text{Equation 5.9})$$

$$X_t = [X] + nM_t(n_1\theta_1 + n_2\theta_2) \quad (\text{Equation 5.10})$$

$$X_t = [X] + \frac{n_1M_1[X]K_1}{1 + [X]K_1} + \frac{n_2M_2[X]K_2}{1 + [X]K_2} \quad (\text{Equation 5.11})$$

Reducing and canceling the variables in the Equations 5.10 and 5.11 produce a cubic equation. The coefficients for the later terms of the cubic equation are defined as the variables p, q, and r, as shown in Equation 5.12, Equation 5.13 and Equation 5.14. These equations are solved for the variable X numerically using Origin software by Newton's Method with the fitting

parameters n_1 , n_2 , K_1 , and K_2 . The values for θ_1 , and θ_2 are solved using the equations in the previous section.¹⁴

$$p = \frac{1}{K_1} + \frac{1}{K_2} + (n_1 + n_2)M_t - X_t \quad (\text{Equation 5.12})$$

$$q = \left(\frac{n_1}{K_1} + \frac{n_2}{K_2}\right)M_t - \left(\frac{1}{K_1} + \frac{1}{K_2}\right)X_t + \frac{1}{K_1K_2} \quad (\text{Equation 5.13})$$

$$r = -\frac{X_t}{K_1K_2} \quad (\text{Equation 5.14})$$

As in the single set of sites model, the heat absorbed or released during each injection is defined in terms of the constituent concentrations, stoichiometry, completion, and change in enthalpy values. This is described in Equation 5.15 below. In Equation 5.16, the heat exchanged for each injection in a titration is quantified. By using the fitting parameters described in the single set of sites model, a calculated enthalpogram curve can be compared to the measured data and the curve can then be fit to the data using iterative techniques.

$$Q = M_t V_o (n_1 \theta_1 \Delta H_1 + n_2 \theta_2 \Delta H_2) \quad (\text{Equation 5.15})$$

$$\Delta Q(i) = Q(i) + \frac{dV_i}{V_o} \left[\frac{Q(i) + Q(i-1)}{2} \right] - Q(i-1) \quad (\text{Equation 5.16})$$

Titration

Several types of titrations can be accomplished using ITC. The standard type of titration is to determine binding constants between complimentary molecules in solution. The true advantage of a thermal titration is that any reaction or interaction that is accompanied by a change in enthalpy can be measured. ITC can thus be used to titrate acids and bases, and even determine parameters like critical micelle concentrations. In both of these cases, the enthalpic change due to the addition of one component can be tracked and used to determine the parameter of interest. Parameters such as heats of dilution and solvation can also be measured. This type of information tends to be very valuable when evaluating possible drug effects in complicated biological systems. Even though the exact nature of interaction cannot be determined using ITC, the thermal parameters as well as the activity of the model applied to the system can be evaluated.

Diagram of peak and parameters

There are several parameters available within the control software for the MCS ITC that can be used to produce consistent measurable peak energies. During a titration, several injections of the titrant solution are made into either a blank solvent, or a second component solution. As the injections are made, the temperature difference between the cells is monitored through the use of a thermocouple pile placed between the cells. The thermocouple voltage is measured and maintained through the use of a feedback controlled heater in the titration cell. If the injection produces an exothermic interaction, the amount of heat in the cell increases, and the feedback current to the titration cell heater is decreased, resulting in a downward pointing peak or trough in the baseline. If the injection produces an endothermic interaction, the feedback current is increased, and the result is a peak in the baseline. In either case, the peak size must be controlled

so that valid measurements can be made for the current and consequent peak area. In the case of endothermic interactions, with positive peaks, this is less important and only requires that the highest current value is smaller than what can be achieved by the instrument. In the case of exothermic interactions with negative peaks, the control parameters are very important. A thermal headspace between the baseline current value, and zero current to the cell heater is created according to the reference offset parameter. While it would seem that in this case the best results could be obtained by using the maximum thermal headspace, this is not the case. Using an excessively large reference offset tends to cause noise in the baseline as well as rapid heating of the titration cell. In these situations the cell temperature can increase more than 1 °C during a titration. For a single titration this may be acceptable; however, if several titrations are to be completed in a day, the machine will be outside the appropriate temperature range quickly. The volume and duration or rate of injection can also be changed in order to minimize the thermal headspace necessary. Smaller volumes delivered at a slower rate will decrease the peak amplitude. The time between injections is another parameter in the titration scheme. The length of time necessary for an injection to occur and the system to return to equilibrium varies from one system to the next. This parameter depends on the maximum energy of an injection, as well as the heat capacity of the system. The time between injections should be long enough that the system returns to equilibrium, but not so long that the titration takes longer than necessary. There are two reasons for not over-allotting time between injections. The MCS ITC has a maximum number of data points that it will collect. The longer the time between injections, the more data points will be used. There is also the issue of diffusion from the syringe tip within the sample cell. The faster the titration is run, the smaller the effect of this diffusion. Finally there is a division of data collecting regimes during each injection. The parameters involved with this

are t_1 , and t_2 , as well as t_{switch} . The t_1 and t_2 parameters set the data point recording frequency. The t_{switch} parameter sets the point during the injection cycle that the frequency parameter is changed. It is therefore useful to have a high frequency of data collection during the first part of the peak collection period in order to more accurately measure the peak area. After the majority of the peak has been recorded, the data collection frequency can be reduced in order to produce a more stable baseline for the next peak. These parameters when optimized can lead to significantly improved peak shapes. There is also the added ability to reduce the number of data points consumed during the second time period, and thereby conserve the finite amount of data points available.

Types of titrations

Historically, the ITC instrument was devised to determine the binding characteristics of ligands and biological macromolecules in aqueous solutions. The instrument is still widely used for this purpose, but the near universality of the measurement scheme has extended its use into many diverse fields. Since nearly all reactions or interactions are accompanied by an exchange of heat in the system, ITC can be used to investigate many different types of systems. Interactions between macromolecules can be explored, as well as some drug interactions with biological macromolecules. The method has been exceedingly useful in elucidating the properties of small molecule binding, such as our host/guest systems. Small molecule systems are even more convenient due to the fact that they probably correspond more truly to the simple models that are used for curve fitting. Acid and base titrations can be made using the ITC system. The MCS ITC is limited, due to its cell construction, from using strong mineral acids; however, some of the new instruments from TA instruments are designed for the use of strong acids and have a gold lined cell. Determinations of other phenomena that involve thermal

changes can also be made. Critical micelle concentrations can be determined using ITC. In this case a solution that is more concentrated than the CMC is titrated into blank solvent. As the titrant is diluted, all micelles dissociate until the CMC is reached. This is seen as a sigmoid shaped shift in the integrated enthalpogram.

Calibrations

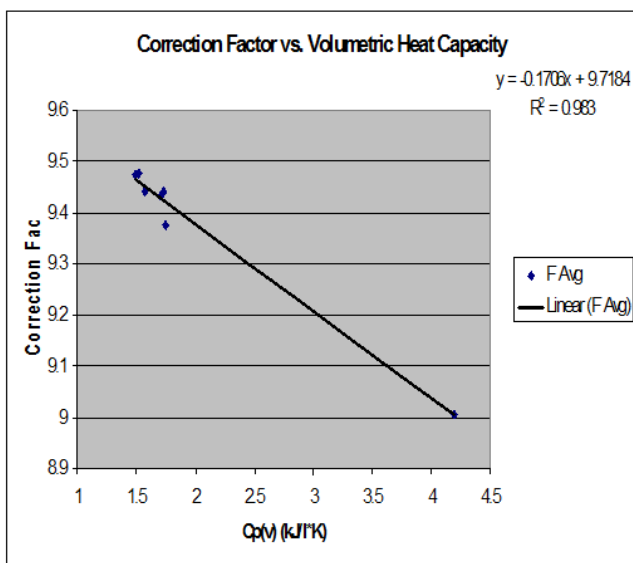


Figure 5.3. Plot of the ITC scaling factor vs. the volumetric heat capacity of the solvent used to calibrate the instrument.

Calibrations of the instrument are carried out through a timed pulse experiment. Specific amounts of heat energy are generated from pulses to the calibrated heaters around the cells. The response of the feedback heaters is then recorded. By integrating the enthalpogram the energy and response can be related by a calibration factor. This factor is related to the volumetric heat capacity of the solvent used in the measurement and reference cells. A plot of the calibration factor against the volumetric heat capacity is shown above in Figure 5.3. The timed pulse sequence plot is shown below in Figure 5.4. In this experiment, calibrated resistance heaters are

used to add heat at a specific rate to the titration cells. The feedback current required to maintain the cell temperature at a steady rate is recorded. In this way, the input heat is calculated over time, and the feedback response can be calibrated by the use of a multiplied coefficient.

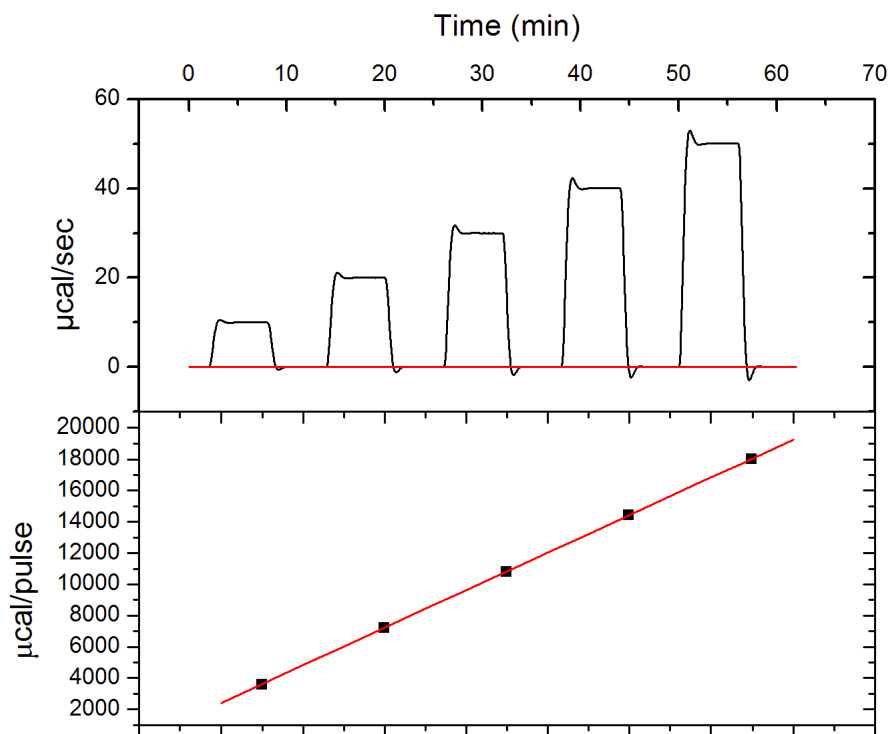


Figure 5.4. Enthalpogram of a timed pulse experiment showing 5 pulses of different heating rates, and the linear plot of their integrated energies. Different heating rates are used in order to determine the linearity of the response coefficient over the heating range of the instrument.

Conclusions

ITC is a flexible and powerful method for the elucidation of chemical interactions in solution. Nearly all chemical changes are accompanied by some transfer of heat which can be

measured using ITC. The method is used to describe several types of interaction including acids and bases, aggregation and complexation, dilution, and even enzyme kinetics. In addition to calculating the association constant for binding systems, ITC also provides the change in enthalpy due to binding. The change in enthalpy and association constant can be used to determine other physical constants for the system such as the change in entropy and the Gibbs free energy. This wealth of information is simply unavailable from other single analytical methods. ITC is hindered somewhat by its lack of specificity and consequently may not adequately elucidate complex systems; however, the models available for fitting the resulting data work well with simpler models.

References

1. Schmidtchen, F. P., *Supramolecular Chemistry: From Molecules to Nanomaterials* **2012**, *2*, 275-296.
2. Falconer, R. J.; Penkova, A.; Jelesarov, I.; Collins, B. M., *Journal of Molecular Recognition* **2010**, *23*, 395-413.
3. Wilcox, D. E., *Inorganica Chimica Acta* **2008**, *361*, 857-867.
4. Bouchemal, K.; Mazzaferro, S., *Drug Discovery Today* **2012**, *17*, 623-629.
5. Dan, F.; Hamed, M. H.; Grolier, J. P. E., *Journal of Thermal Analysis and Calorimetry* **2006**, *85*, 531-540.
6. Blandamer, M. J.; Cullis, P. M.; Engberts, J. B. F. N., *Journal of the Chemical Society, Faraday Transactions* **1998**, *94*, 2261-2267.
7. Cliff, M. J.; Ladbury, J. E., *Journal of Molecular Recognition* **2003**, *16*, 383-391.
8. Freyer, M. W.; Lewis, E. A., *Methods in Cell Biology* **2008**, *84*, 79-113.
9. Jelesarov, I.; Bosshard, H. R., *Journal of Molecular Recognition* **1999**, *12*, 3-18.
10. Cliff, M. J.; Gutierrez, A.; Ladbury, J. E., *Journal of Molecular Recognition* **2004**, *17*, 513-523.
11. Falconer, R. J.; Collins, B. M., *Journal of Molecular Recognition* **2011**, *24*, 1-16.
12. *Microcal Inc. Micro Calorimetry System User's Manual*. Microcal Inc. : 1993; p 127.
13. Lightbody, B., *Innovations in Pharmaceutical Technology* **2008**, *26*, 14, 16-17.

14. ITC Data Analysis in Origin (TM). Microcal Inc. : 1993; p 73.

Chapter Six

Complexation Behavior of Bisimidazolium Salts

Abstract

Several bisimidazolium salts were examined to determine their binding characteristics with crown ether, and cryptand hosts. Crown ether and cryptand binding systems were explored in acetone solution. The type of linker between the two imidazolium moieties was varied from C₂ to C₄ alkyl chains as well as a 1,4-disubstituted phenyl and 1,4-xylyl. Binding interactions were found for most systems, with the highest binding constants coming from the phenyl linked bisimidazolium guest and the cryptand hosts.

Introduction

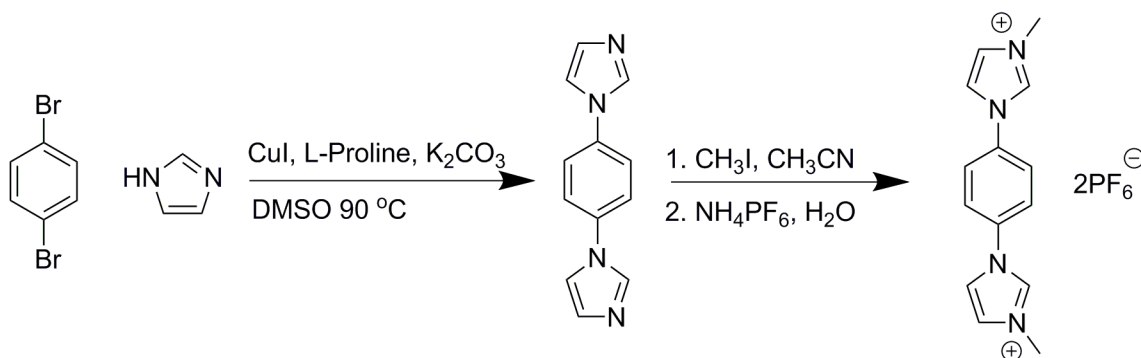
Imidazolium salts tend to fall into the category of ionic liquids (salts with melting point < 100 °C), and thus have very interesting physical and chemical properties. Ionic liquids have been proposed for uses as reaction solvents,¹ liquid crystals,² and even high temperature lubricants.³ In the Gibson lab, we have explored the use of imidazolium based ionic liquids for the production of ion conductive materials for use in electrically actuated devices.⁴⁻⁶ When deprotonated, the imidazolium moiety forms a stable N-heterocyclic carbene.⁷⁻¹³ These carbenes have been used for a wide variety of metal binding systems. As ligands for several metals, bisimidazolium molecules have been used to form complexes with Cu, Hg, Ag, Pd, Se, Pt, Cd, and Fe.^{7-11, 13-16} The proposed uses for these complexes are usually catalytic in nature, the most famous of which are the Grubbs catalysts for metathetic reactions.¹⁷⁻²¹ Bisimidazolium salts have been synthesized for a number of reasons and applications. These bidentate ligands have also been used for the formation of metal organic frameworks (MOFs).²² Biological applications

of bisimidazolium salts include the formation of water channels in their crystal lattice,²³ and the recognition of nucleotides in solution.²⁴ The behavior of bisimidazolium salts and their binding with several different anions in solution has also been explored.²⁵⁻³⁰ The biscations have even been used as aids in ESI MS determinations so that negatively charged analytes can be detected in positive mode.³¹ Finally, bisimidazolium species have been characterized in terms of their binding with macrocyclic hosts in solution, including cyclodextrins,^{15, 32-33} cucurbiturils,³⁴⁻³⁷ crown ethers,³⁷ and calixarenes.³⁸⁻⁴⁰

Traditionally, host-guest work in the Gibson group has focused on the use of dibenzylammonium, diquat, or paraquat type guests. Host species have mostly been crown ethers or crown ether derivatives. Paraquats are very electron poor, and consequently, they are very good guest species for electron rich hosts, such as crown ethers and their cryptands. However, they easily undergo multiple reductions in the presence of even the mildest reducing agents. Most bases will destroy paraquat even under mild conditions. Unfortunately, paraquat species are also highly toxic.⁴¹⁻⁴⁴ Imidazolium salts are much less toxic⁴⁵⁻⁴⁹ in comparison to paraquat salts. This may be due to their lower reactivity toward bases, and their preferential deprotonation to neutral carbenes instead of the radical cations generated by paraquat. Therefore, it would be advantageous to use imidazolium moieties instead of paraquats for host/guest systems, particularly those that may encounter biological processes.

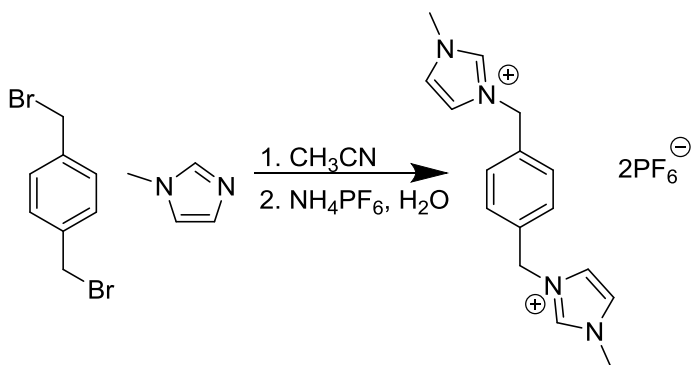
In the current work, five different bisimidazolium guest species were synthesized and their binding behaviors with different host molecules were explored. All guests were titrated with dibenzo-24-crown-8 as a model host, and the two with the highest binding constants were titrated with several more hosts including dibenzo-30-crown-10, a dibenzo-30-crown-10 cryptand and α -, β -, and γ -cyclodextrins.

Scheme 6.1 shows the synthetic method employed for the production of the *p*-phenylene bisimidazolium (PPBI) guest (**G1**). The first step is a modified Ullmann reaction, and the second step is methylation of the bisimidazole.



Scheme 6.1. Synthesis of **G1**: *p*-phenylenebis(3-methylimidazol-1-ium) 2 PF₆ salt via a three step process.

Scheme 6.2 shows the method for production of the *p*-xylyl bisimidazolium guest (**G2**). After diquaternization of N-methylimidazole with *p*-xylylene dibromide the counter ions were exchanged to give the PF₆ salt.



Scheme 6.2. Synthesis of **G2** *p*-phenylenebis(3-methylimidazol-1-ium) 2 PF_6^- guest via a two-step process.

In the case of these two guests, the halide salts were used in titrations with cyclodextrins in water, and the PF_6^- salts were used in titrations with crown ethers or the crown ether-based cryptand in acetone. The other three alkyl bisimidazolium guests were synthesized from the appropriate alkylene dihalide and either N-methyl- or N-butyl-imidazole. They were then converted to their respective PF_6^- salts for titration with dibenzo-24-crown-8 in acetone.

Results and Discussion

Guest G3 with dibenzo-24-crown 8

The titration of dibenzo-24-crown-8 (DB24C8) with 1,4-bis(3-butyl-imidazol-1-yl)butane (PF₆)₂ was run using the low gain system of the ITC. The enthalpogram is shown in Figure 6.2. The dilution energies from a background titration were subtracted from the measured values. The data were fit using the one set of sites model in the Microcal MCS ITC software using Origin. This model is described in Chapter 5. The association constant for the fit curve is $1.7 \pm 0.65 \text{ M}^{-1}$. This value is very low with respect to the values measured well by this instrument. A useful parameter c is defined as the product of the association constant and the cell concentration. The value of c generally describes the shape of the enthalpogram according to the thermodynamic model. High values of c ($c > 50$) represent enthalpograms with a distinct sigmoidal shape. The sigmoidal shape allows the curve fitting to more accurately determine the stoichiometry (n) and the enthalpy. Low values of c ($c < 10$) represent enthalpograms that have a simple curved shape with no sigmoidal inflection. To properly fit these data, the stoichiometry of the binding system must be separately determined, as it is not well represented by the sigmoid inflection.⁵⁰ This titration has a low c value due to the low association constant, and consequently, the stoichiometry must be imposed for curve fitting. A stoichiometric ratio of 1:1 was imposed for this system. The enthalpy of binding (ΔH°) was measured to be -2.80 ± 0.88 kcal/mol. The Gibbs free energy change (ΔG°) was calculated to be -314 ± 120 cal/mol from the equation $\Delta G^\circ = -RT \text{Ln}K_a$. The change in entropy (ΔS°) was calculated to be -8.32 ± 0.36 cal/mol K from the equation $\Delta G^\circ = \Delta H^\circ - T\Delta S^\circ$. This system has one of the lowest binding constants ever measured with this instrument.

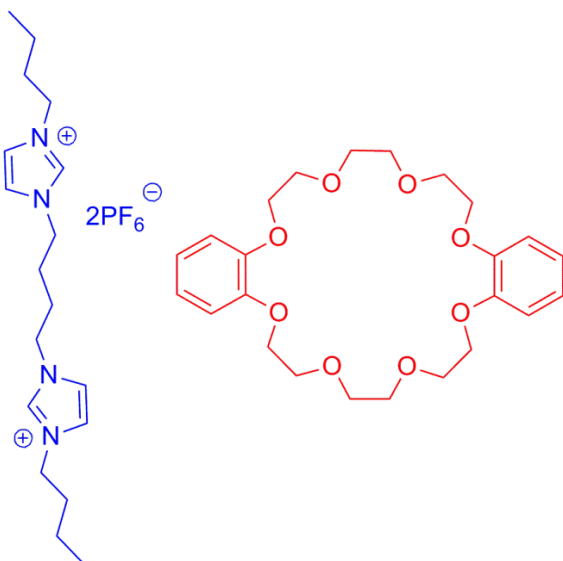


Figure 6.1. Chemical structures of the butylene bisimidazolium $G3(PF_6)_2$ and dibenzo-24-crown 8.

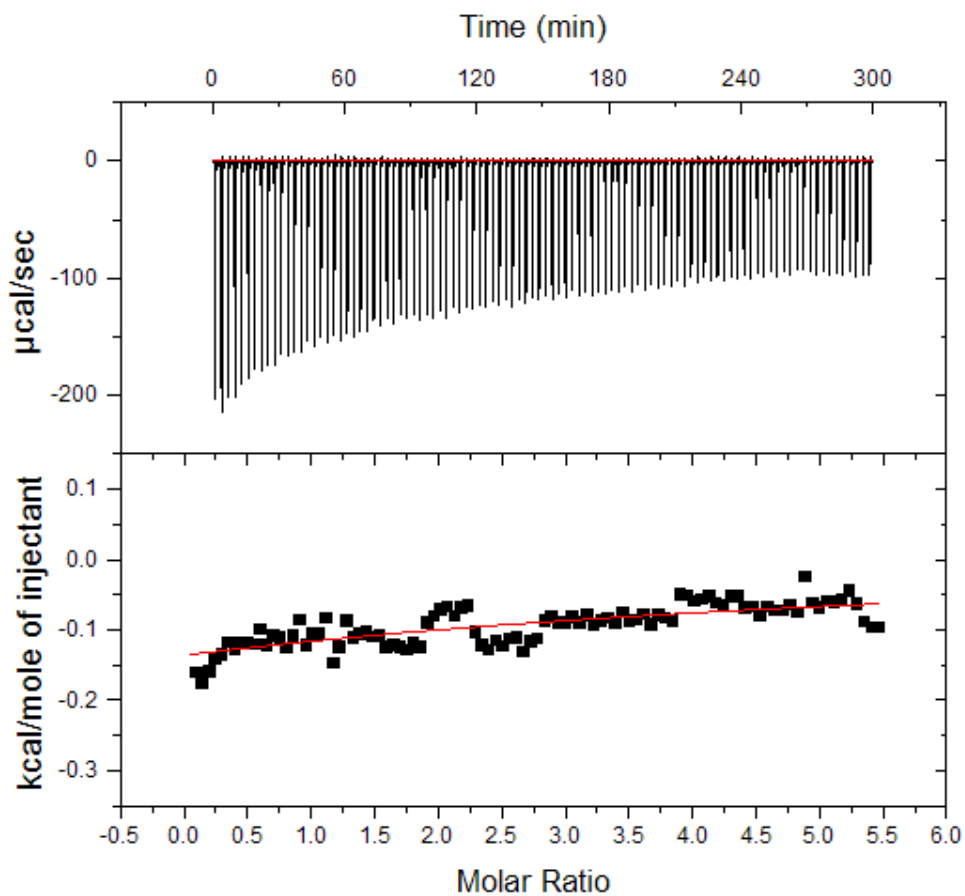


Figure 6.2. Enthalpogram for the binding of $\text{G3}(\text{PF}_6)_2$ (806.5 mM) and dibenzo-24-crown-8 (30.2 mM) in acetone at 25 °C.

Guest G4 with dibenzo-24-crown 8

The second system evaluated by ITC employed a guest with a propylene center linker and butyl chains attached to the imidazolium moieties, **G4(PF₆)₂**, shown in Figure 6.3. This system was evaluated using the low gain titration system, because the low *c* value, due to the low association constant, would yield an unfittable isotherm at lower concentrations. The fitting isotherm for the system is given below. The association constant for this titration was calculated to be $4.31 \pm 0.81 \text{ M}^{-1}$. ΔH° as measured to be $-2.35 \pm 0.30 \text{ kcal/mol}$. ΔG° was calculated to be $-865 \pm 160 \text{ cal/mol}$, and the ΔS° was calculated as $-4.98 \pm 0.17 \text{ cal/mol K}$. Again in this system the stoichiometry was artificially set at 1:1.

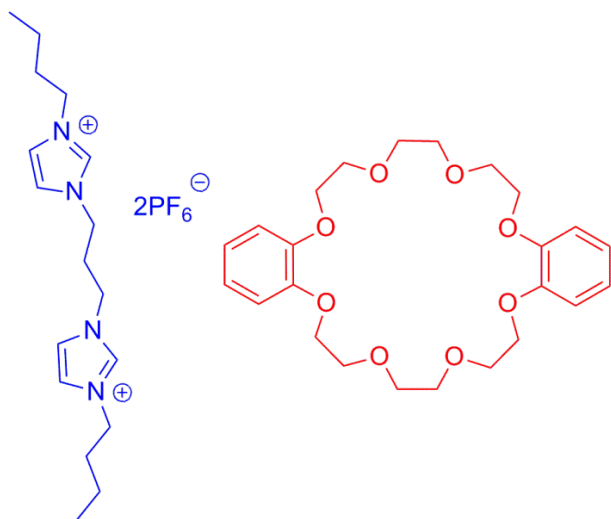


Figure 6.3. Chemical structures of propylene linked bisimidazolium **G4(PF₆)₂** and dibenzo-24-crown-8.

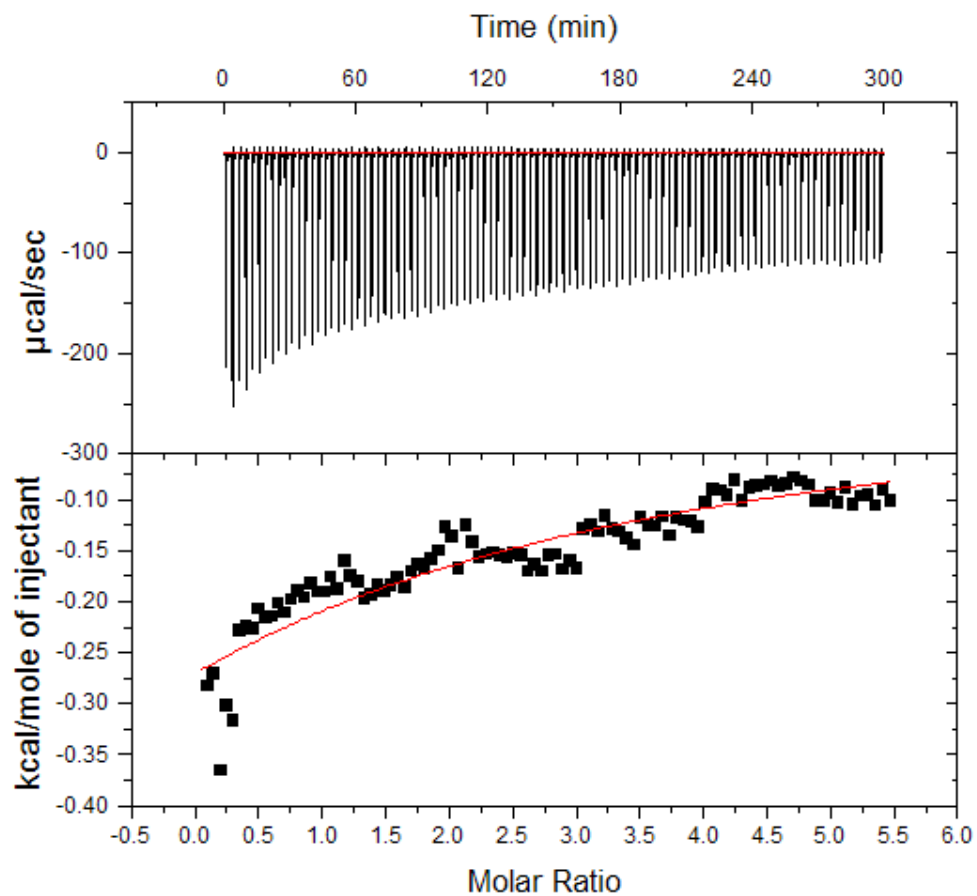


Figure 6.4. Enthalpogram for propylene linked bisimidazolium $\mathbf{G4(PF_6)_2}$ (802.4 mM) and dibenzo-24-crown-8 (30.2 mM) in acetone at 25 °C.

Guest G5 with dibenzo-24-crown 8

The last titration was done with the ethylene linked species with methyl terminal moieties $G5(PF_6)_2$. This system displayed the highest association constant of all of the alkylene linked bisimidazolium guests. The titration isotherm shown below was fit using a single set of sites model. The calculated association constant was $27.1 \pm 2.7 M^{-1}$. While this is an order of magnitude greater than the two previous guests, it is still comparatively low for the ITC. ΔH° was measured to be -2.67 ± 0.14 kcal/mol. ΔG° was calculated to be -1.95 ± 0.19 kcal/mol, and ΔS° was calculated to be -2.40 ± 0.45 cal/mol K.

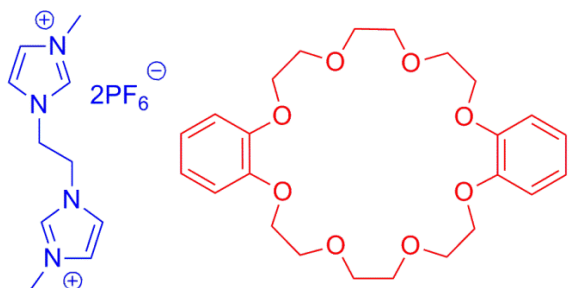


Figure 6.5. Chemical structures of ethylene linked bisimidazolium $G5(PF_6)_2$ and dibenzo-24-crown-8.

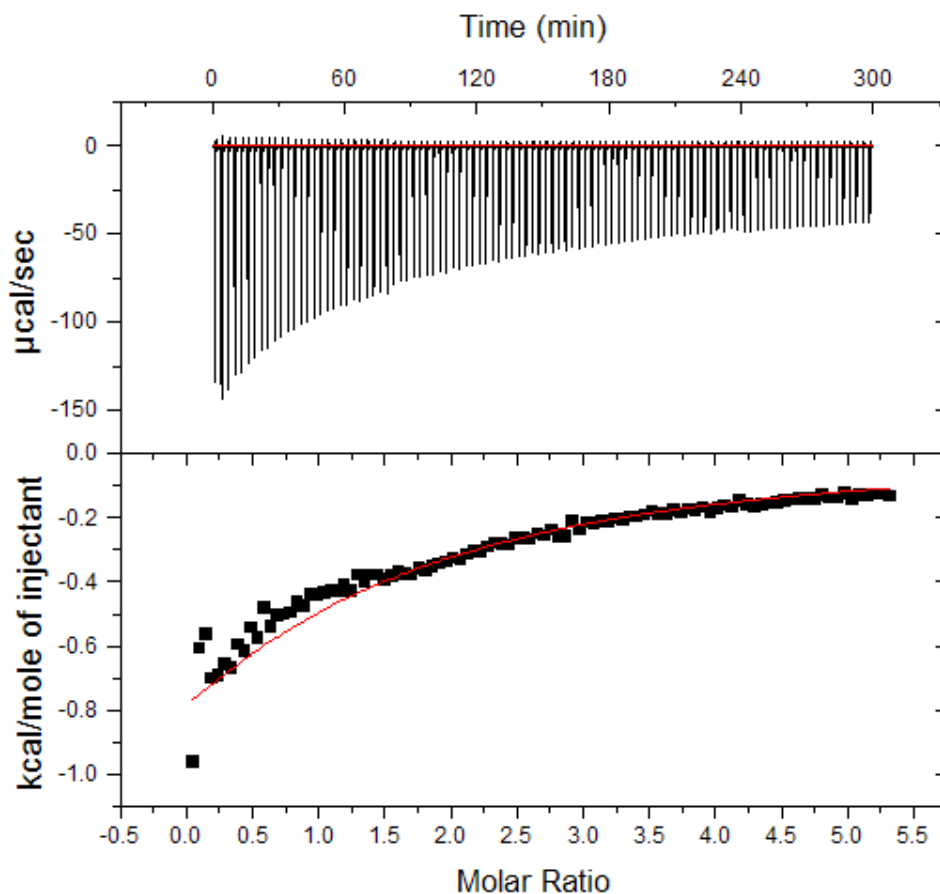


Figure 6.6. Enthalpogram for the binding of ethylene linked bisimidazolium **G5** (PF_6)₂ (393.7 mM) and dibenzo-24-crown-8 (15.2 mM) in acetone at 25 °C.

These three titrations, though they reveal very low binding affinities, do illustrate some interesting trends. As the length of the central linker between the imidazolium moieties decreases, the association constant increases. Thus, from these three titrations, the need to optimize the size and type of the linker between the imidazolium groups can be seen. The enthalpy of binding for all of these systems is very similar, but as the alkylene length increases, the change in entropy for binding becomes more negative, thus decreasing the K_a value.

Guest G1(PF_6)₂ with DB24C8

The titration of DB24C8 with **G1(PF₆)₂** revealed a significant increase in binding constant over the entire group of alkylene linked bisimidazolium guests. This guest is conjugated along nearly its entire length, and consequently is a brown crystalline solid as either the iodide or PF₆ salt. The association constant calculated from the isotherm given below was $166 \pm 67 \text{ M}^{-1}$. With the higher association constant for this titration, the high gain system in the instrument was used. ΔH° was measured by peak area to be $-3.43 \pm 0.46 \text{ kcal/mol}$. ΔG° and ΔS° were calculated as $-3.03 \pm 1.2 \text{ kcal/mol}$, and $-1.36 \pm 0.33 \text{ cal/mol K}$, respectively.

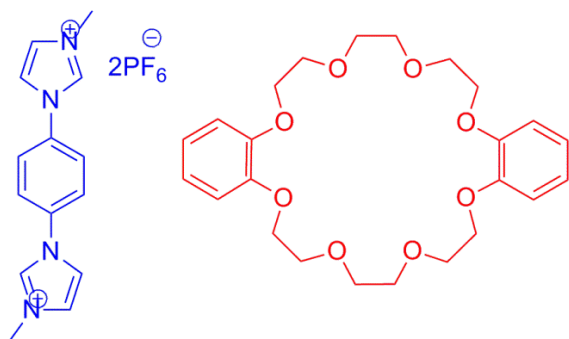


Figure 6.7. Chemical structures of phenylene bisimidazolium **G1(PF₆)₂** and dibenzo-24 crown-8.

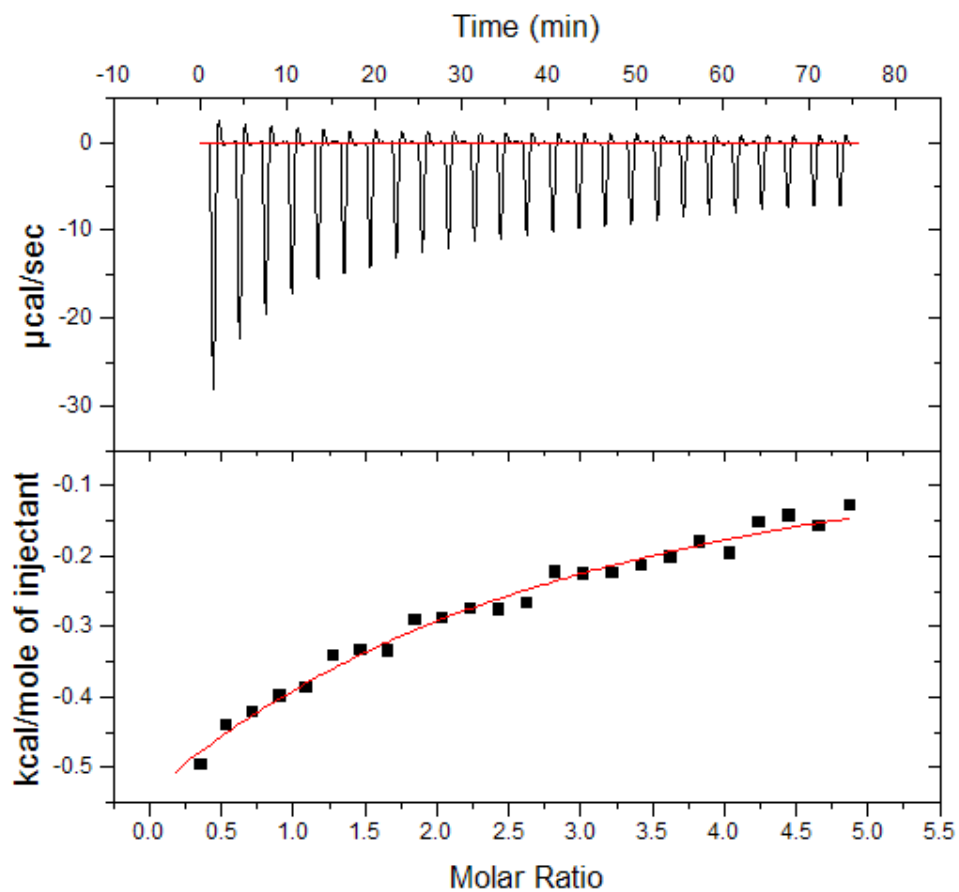


Figure 6.8. Enthalpogram for phenylene bisimidazolium **G1(PF₆)₂** (25.96 mM) and dibenzo-24-crown 8 (1.09 mM) in acetone at 25 °C.

Guest $G1(PF_6)_2$ with DB30C10

The titration of DB30C10 with $G1(PF_6)_2$ was also run in acetone. The association constant with the larger host increased slightly from the DB24C8 titration. The calculated association constant from the isotherm shown below was $171 \pm 100 \text{ M}^{-1}$. ΔH° was -2.8 ± 0.63 kcal/mol. ΔG° was -3.04 ± 1.8 kcal/mol, and ΔS° was -0.82 ± 0.40 cal/mol K. In both this and the previous titration, the lower c value necessitated the artificial selection of binding stoichiometry. The curves were initially fit without imposing the stoichiometric ratio, and the fit curves indicated a 1:1 stoichiometric ratio.

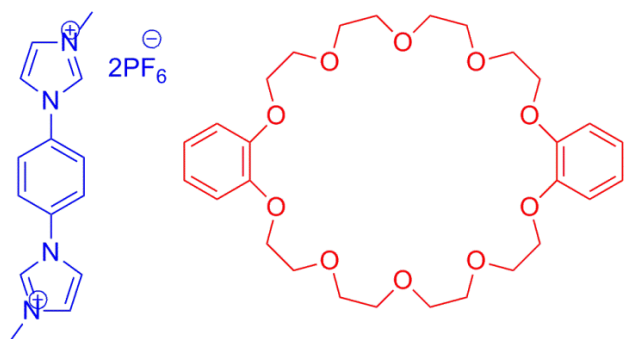


Figure 6.9. Chemical structures of phenylene bisimidazolium $G1(PF_6)_2$ and dibenzo-30-crown 10.

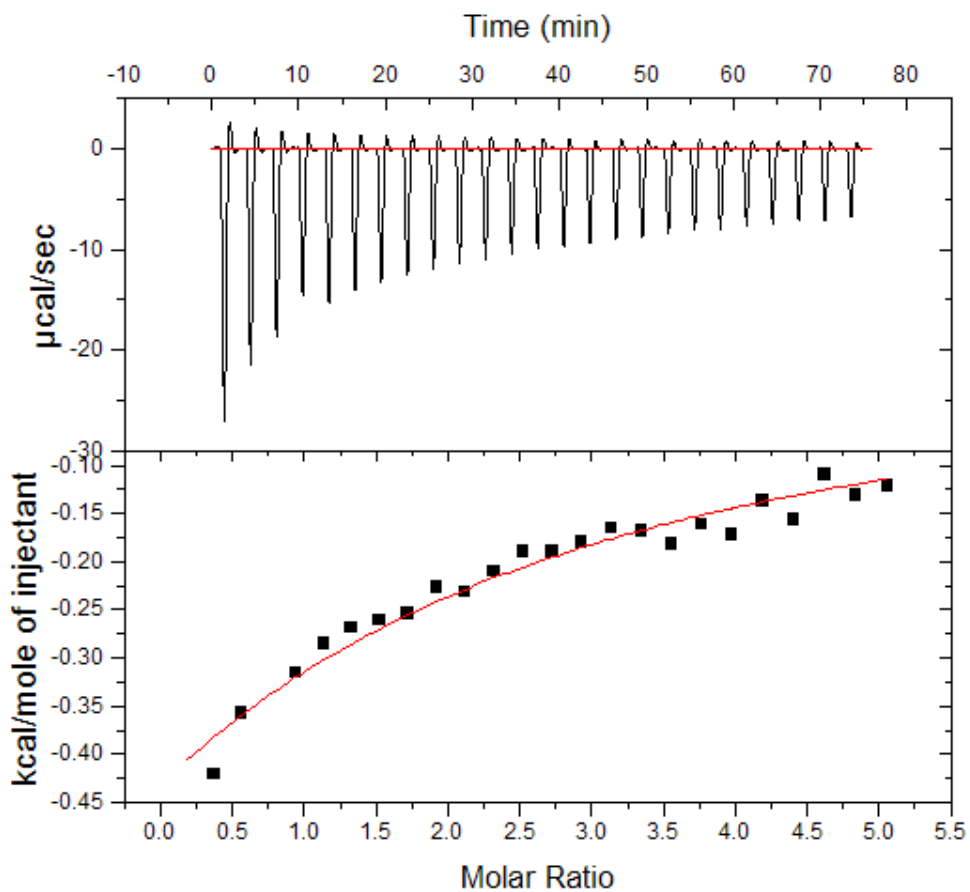


Figure 6.10. Enthalpogram for the binding of phenylene bisimidazolium $G1(PF_6)_2$ (25.96 mM) and dibenzo-30-crown-10 (1.05 mM) in acetone at 25 °C.

Guest $M1(PF_6)_2$ with DB30C10 based cryptand:

The titration of the DB30C10 based cryptand with $G1(PF_6)_2$ indicated a much higher association constant. The sigmoidal curve of the titration isotherm indicates a high c titration and the association constant was calculated to be $3.42 \pm .08 \times 10^4 M^{-1}$. ΔH° was measured as $-11.8 \pm .06$ kcal/mol. ΔG° and ΔS° were calculated to be $-6.18 \pm .01$ kcal/mol, and -18.7 ± 0.29 cal/mol K, respectively. This is very impressive binding behavior for a bisimidazolium guest. Previous titrations with alkylene linked bis imidazolium species revealed binding constants on the order of $10^2 M^{-1}$ or less.

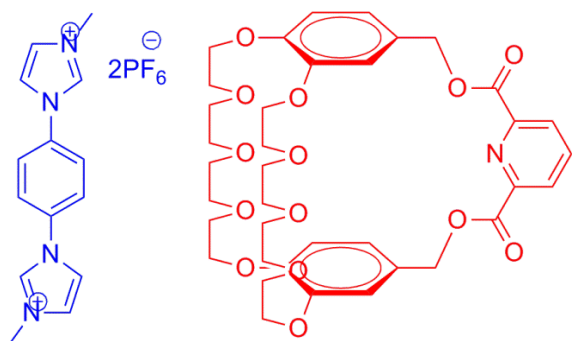


Figure 6.11. Chemical structures of phenylene bisimidazolium $G1(PF_6)_2$ and dibenzo-30-crown-10 based cryptand.

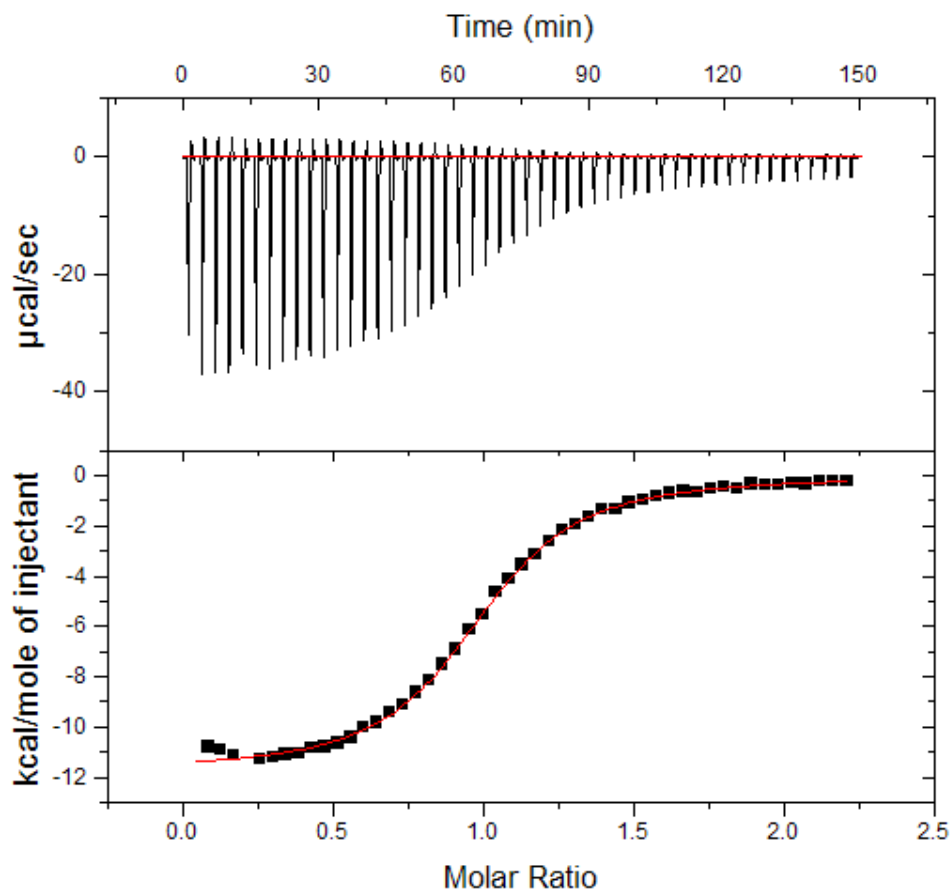


Figure 6.12. Enthalpogram for the binding of phenylene bisimidazolium **G1(PF₆)₂** (27.46 mM) and dibenzo-30-crown-10 based cryptand (0.978 mM) in acetone at 25 °C.

Guest G2(PF₆)₂ with DB24C8:

The binding of the xylyl centered bisimidazolium salt was initially anticipated to be greater than that of the *p*-phenylene centered guest due to the methylene protons present in the former guest and the possible resultant “hydrogen bonding” of these protons. This, however, was not the case. In the titration of the xylylene guest with DB24C8 the binding constant was not measurable at the concentration used for the titration. The integrated isotherm shown below has no recognizable shape and is close enough to a straight line to be considered unsuitable for

model fitting. There may be binding in this system, but it would need to be explored at much higher concentrations.

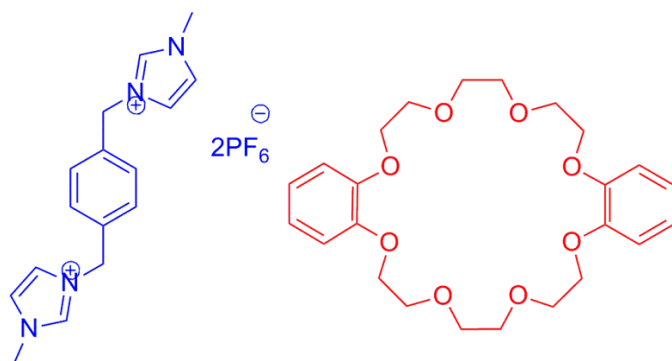


Figure 6.13. Chemical structures of xylene bisimidazolium guest G2(PF₆)₂ and dibenzo-24-crown-8.

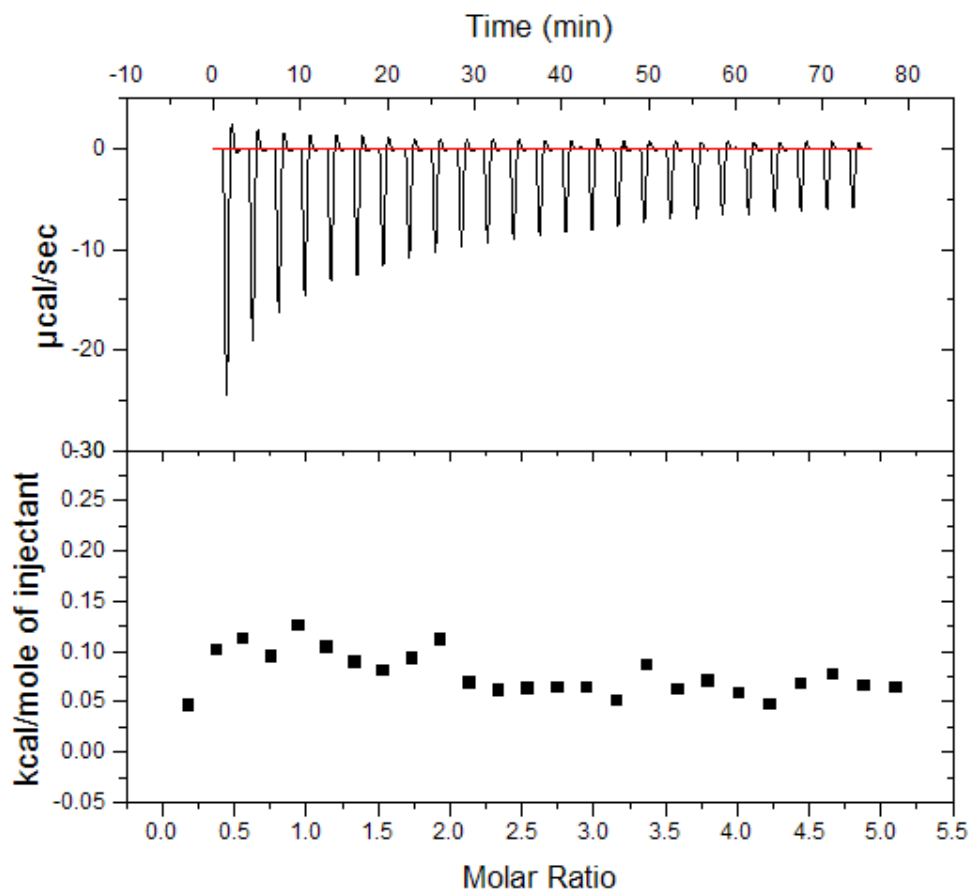


Figure 6.14. Enthalpogram for the interaction of xylene bisimidazolium guest $\text{G2}(\text{PF}_6)_2$ (27.19 mM) and dibenzo-24-crown-8 (1.09 mM) in acetone at 25 °.

Guest $G2(PF_6)_2$ with DB30C10:

The binding between the xylylene guest $G2(PF_6)_2$ and DB30C10 shows a very interesting isotherm. After integration and subtraction of the background titration, the integrated isotherm shows a positive, endothermic interaction between the xylyl guest and DB30C10. The calculated association constant for this system is $768 \pm 290 \text{ M}^{-1}$. $\Delta H^\circ = +377 \pm 65 \text{ cal/mol}$, $\Delta G^\circ = -3.93 \pm 0.23 \text{ kcal/mol}$, and $\Delta S^\circ = -14.5 \pm 4.3 \text{ cal/mol K}$. The inverted shape of the curve and the small energies measured indicate that these titration data may not adequately describe the binding system.

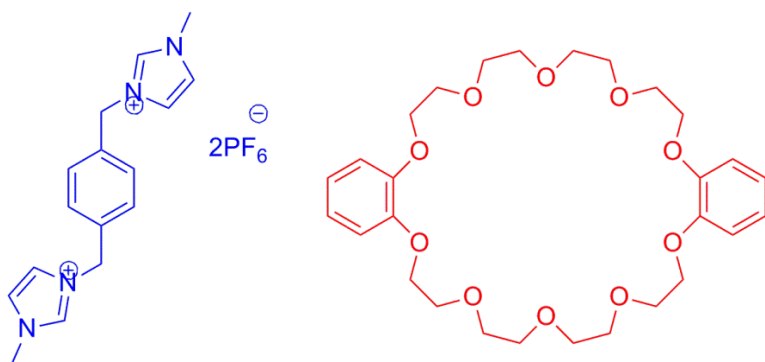


Figure 6.15. Chemical structures of xylylene bisimidazolium guest $G2(PF_6)_2$ and dibenzo-30-crown-10.

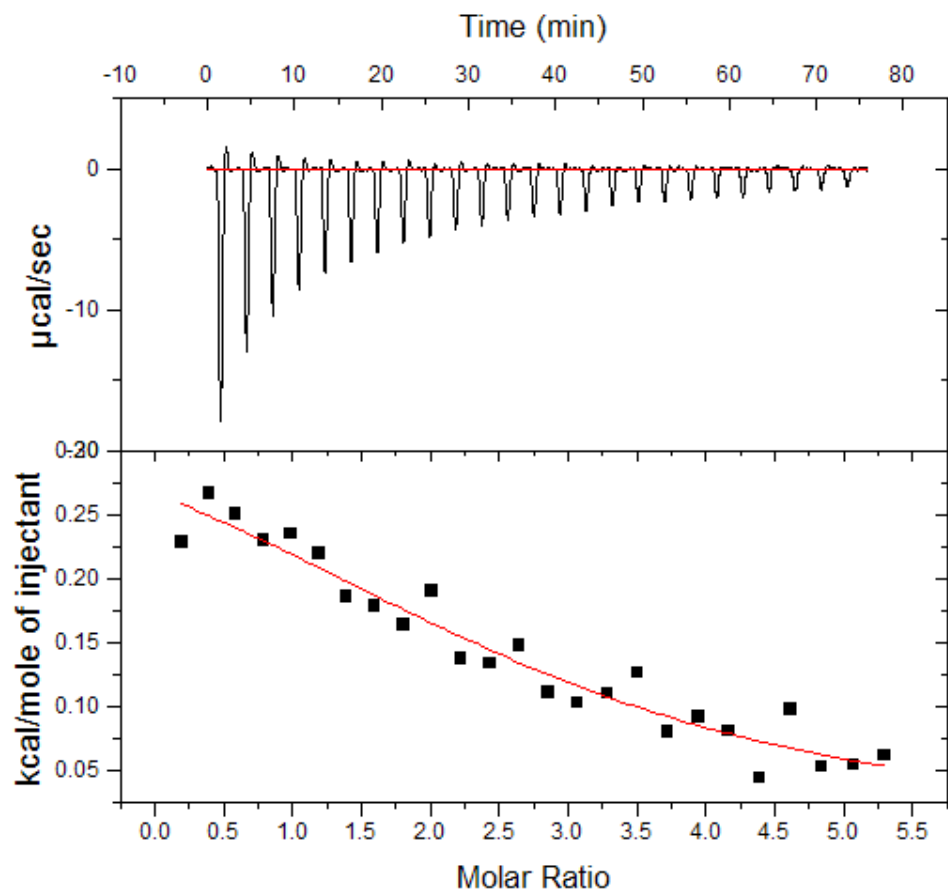


Figure 6.16. Enthalpogram for the binding of the xylylene bisimidazolium guest $\text{G2}(\text{PF}_6)_2$ (27.19 mM) and dibenzo-30-crown-10 (1.05 mM) in acetone at 25 °C.

Guest $G2(PF_6)_2$ with DB30C10-based cryptand:

The titration of the xylene guest $G2(PF_6)_2$ with the DB30C10-based cryptand did yield convincing binding behavior. The titration was fit using a one set of sites model. The association constant calculated from the integrated isotherm was $937 \pm 59 M^{-1}$. $\Delta H^\circ = -8.03 \pm 1.0$ kcal/mol, $\Delta G^\circ = -4.05 \pm 0.04$ kcal/mol, and $\Delta S^\circ = -13.3 \pm 0.73$ cal/mol K. This system has a relatively low association constant compared to other guests with the DB30C10 cryptand.

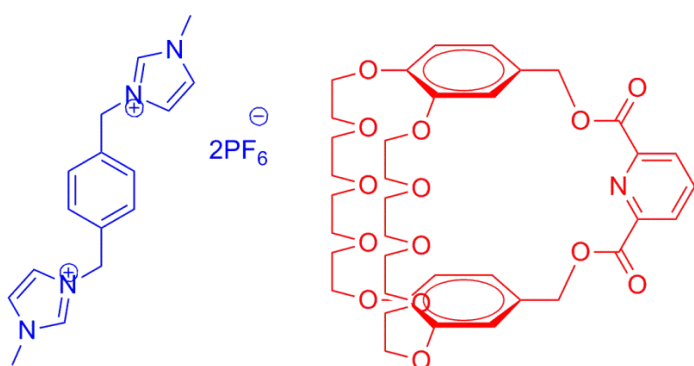


Figure 6.17. Chemical structures of xylene bisimidazolium guest $G2(PF_6)_2$ and dibenzo-30-crown-10-based cryptand.

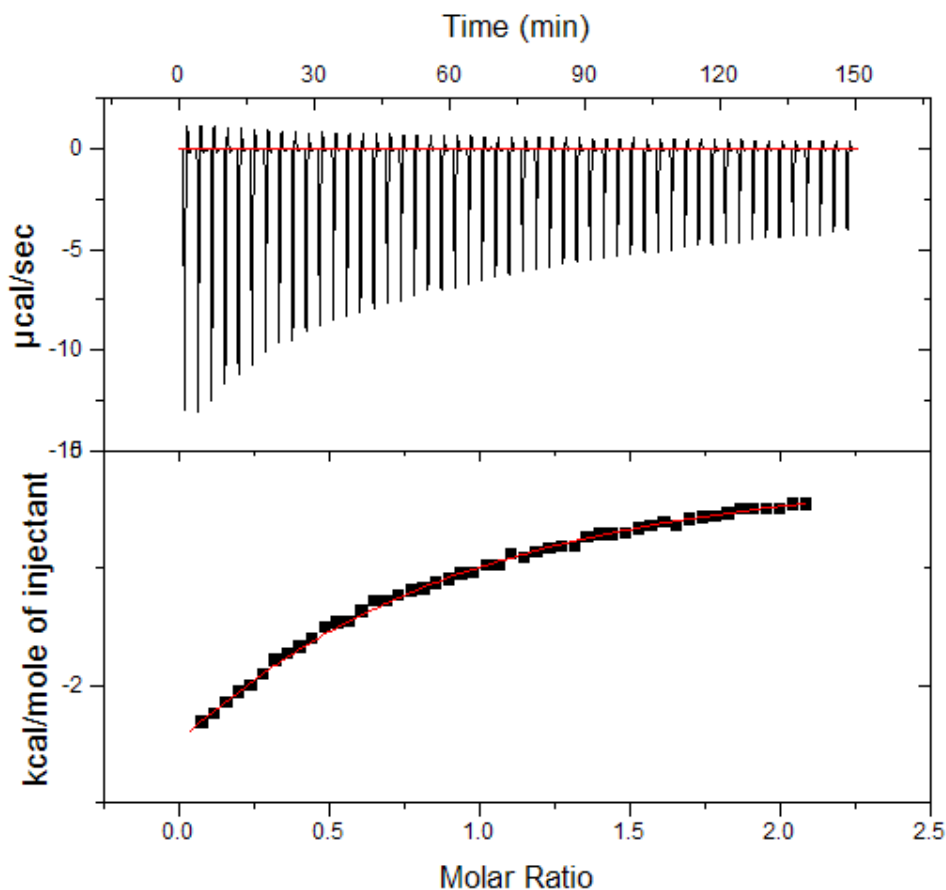


Figure 6.18. Enthalpogram for the binding of the xylylene bisimidazolium guest **G2(PF₆)₂** (26.35 mM) with dibenzo-30-crown-10 cryptand (0.977 mM) in acetone at 25 °C.

Conclusions

Bisimidazolium salts bind in solution with crown ether and cryptand host species. The alkylene linked bisimidazolium species have very small association constants with DB24C8 in acetonitrile. The xylene linked guest was a better guest for crown ether hosts, but was not as good at binding with the cryptand as was expected. The phenylene linked compound was by far the best guest for all hosts, particularly the cryptand.

Experimental

Chemicals and instruments

All chemicals were used as received from vendors. NMR spectra were gathered using a Bruker Avance 400 MHz spectrometer. ITC titrations were completed using a Micrical MCS ITC titrator. Titration data were analyzed using Origin software.

Synthesis of alkylene linked bisimidazolium salts:

Alkylene linked bisimidazolium salts were synthesized as reported in our previous work.⁴

Synthesis of *p*-phenylene bisimidazole:

Dibromobenzene (0.23 g, 0.97 mmol), 0.15 g (2.2 mmol) of imidazole, 0.03 g (0.2 mmol) of copper(1) iodide, 0.04 g (0.3 mmol) of L-proline, and 0.42 g (3.0 mmol) of potassium carbonate were dissolved in 20.0 mL of dimethyl sulfoxide. The resulting solution was heated at 90 °C and stirred under nitrogen for 18 hours. The solution was taken up in dichloromethane and extracted five times with water. The dichloromethane solution was passed through Celite® and solvent was removed via rotary evaporation. The resulting residue was passed through a silica column to give pure product, 0.13 g (28 %), mp 207.2 – 209.1 °C. ¹H NMR (400 MHz, CD₃CN) δ 8.06 – 7.98 (m, 2H), 7.67 (s, 4H), 7.53 (t, J = 1 Hz, 2H), 7.07 – 6.98 (m, 2H). ¹³C NMR (101 MHz, CD₃CN) δ 205.1, 135.4, 130.2, 122.0, 117.7. Lit. mp 208 – 210 °C.⁵¹

Synthesis of *p*-phenylene bisimidazolium salt G1:

Phenylene bisimidazole (0.13 g, 0.06 mmol) and 0.12 g (0.08 mmol) of methyl iodide were dissolved in acetonitrile and heated under reflux for one day. The solid product was removed via filtration and dissolved in water. A concentrated aqueous solution of ammonium hexafluorophosphate was added. The resulting bisimidazolium hexafluorophosphate salt that precipitated was removed by filtration and recrystallized three times from water to yield a pure

product 0.10 g (32 %), mp 256 °C. ¹H NMR (400 MHz, CD₃CN) δ 8.9 (s, 2H), 7.8 (s, 4H), 7.8 (d, J = 1 Hz, 2H), 7.6 (d, J = 1 Hz, 2H), 4.0 (s, 6H). ¹³C NMR (101 MHz, CD₃CN) δ 135.6, 124.7, 124.5, 121.7, 117.3, 36.4. The ¹H NMR compared well to the literature report.⁵¹

Synthesis of *p*-xylylene bisimidazolium salt G2:

□□□-Dibromo-*p*-xylene (1.5 g, 5.7 mmol) was dissolved in acetonitrile with 1.0 g (12 mmol) of methyl imidazole. The resulting solution was heated under reflux for one day. The solid product was removed by filtration and dissolved in water. An aqueous solution of ammonium hexafluorophosphate was added to the solution and the resulting bisimidazolium hexafluorophosphate salt was removed via filtration. The solid product was recrystallized three times from water, 1.16 g (50 %), mp 224.3 – 226.1 °C. ¹H NMR (400 MHz, D₂O) δ 8.61 (s, 2H), 7.31 (s, 4H), 7.29 (s, 4H), 5.26 (s, 4H), 3.73 (s, 6H). ¹³C NMR (101 MHz, D₂O) δ 136.1, 134.5, 129.2, 123.8, 122.2, 52.2, 35.7. Lit. mp 225 – 228 °C.¹³

ITC titrations:

ITC titrations were generally run by placing a low concentration solution of the host molecule in the titration cell, and a high concentration solution of the guest molecule in the titration syringe. Solutions for both titrant and titrand were made using HPLC grade acetone as received. Titrations with cyclodextrin hosts were run in HPLC grade water as received. Titrations were run at 25 °C using a Microcal MCS titrator with MCS Observer software. Thermal data were integrated and titration curves were fit using Origin software.

References

1. D'Anna, F.; Ferrante, F.; Noto, R., *Chemistry--A European Journal* **2009**, *15*, 13059-13068, S13059/1-S13059/8.

2. Li, X.; Bruce, D. W.; Shreeve, J. n. M., *Journal of Materials Chemistry* **2009**, *19*, 8232-8238.
3. Zeng, Z.; Phillips, B. S.; Xiao, J.-C.; Shreeve, J. n. M., *Chemistry of Materials* **2008**, *20*, 2719-2726.
4. Lee, M.; Niu, Z.; Schoonover, D. V.; Slebodnick, C.; Gibson, H. W., *Tetrahedron* **2010**, *66*, 7077-7082.
5. Aitken, B. S.; Lee, M.; Hunley, M. T.; Gibson, H. W.; Wagener, K. B., *Macromolecules (Washington, DC, United States)* **2010**, *43*, 1699-1701.
6. Zheng, L.; Chen, F.; Xie, M.; Han, H.; Dai, Q.; Zhang, Y.; Song, C., *Reactive & Functional Polymers* **2007**, *67*, 19-24.
7. Baker, M. V.; Brown, D. H.; Haque, R. A.; Skelton, B. W.; White, A. H., *Journal of Inclusion Phenomena and Macrocyclic Chemistry* **2009**, *65*, 97-109.
8. Liu, Q.-X.; Chen, A.-H.; Zhao, X.-J.; Zang, Y.; Wu, X.-M.; Wang, X.-G.; Guo, J.-H., *CrystEngComm* **2011**, *13*, 293-305.
9. Mercks, L.; Neels, A.; Stoeckli-Evans, H.; Albrecht, M., *Dalton Transactions* **2009**, 7168-7178.
10. Rit, A.; Pape, T.; Hahn, F. E., *Journal of the American Chemical Society* **2010**, *132*, 4572-4573.
11. Rit, A.; Pape, T.; Hepp, A.; Hahn, F. E., *Organometallics* **2011**, *30*, 334-347.
12. Scherg, T.; Schneider, S. K.; Frey, G. D.; Schwarz, J.; Herdtweck, E.; Herrmann, W. A., *Synlett* **2006**, 2894-2907.
13. Willans, C. E.; Anderson, K. M.; Paterson, M. J.; Junk, P. C.; Barbour, L. J.; Steed, J. W., *European Journal of Inorganic Chemistry* **2009**, 2835-2843.
14. Schneider, S. K.; Schwarz, J.; Frey, G. D.; Herdtweck, E.; Herrmann, W. A., *Journal of Organometallic Chemistry* **2007**, *692*, 4560-4568.
15. Liu, F.; Chen, W.; You, X., *Journal of Solid State Chemistry* **2002**, *169*, 199-207.
16. Liu, D.; Li, D., *Applied Organometallic Chemistry* **2003**, *17*, 811-812.
17. Chen, S.-W.; Zhang, Z.-C.; Zhai, N.-N.; Zhong, C.-M.; Lee, S.-g., *Tetrahedron* **2015**, *71*, 648-653.
18. Lummiss, J. A. M.; Botti, A. G. G.; Fogg, D. E., *Catalysis Science & Technology* **2014**, *4*, 4210-4218.
19. Masoud, S. M.; Mailyan, A. K.; Dorcet, V.; Roisnel, T.; Dixneuf, P. H.; Bruneau, C.; Osipov, S. N., *Organometallics* **2015**, Ahead of Print.

20. Meng, F.; McGrath, K. P.; Hoveyda, A. H., *Nature (London, United Kingdom)* **2014**, *513*, 367-374.
21. Sauer, D. F.; Bocola, M.; Broglia, C.; Arlt, M.; Zhu, L.-L.; Brocker, M.; Schwaneberg, U.; Okuda, J., *Chemistry - An Asian Journal* **2015**, *10*, 177-182.
22. Gong, H.-Y.; Rambo, B. M.; Cho, W.; Lynch, V. M.; Oh, M.; Sessler, J. L., *Chemical Communications (Cambridge, United Kingdom)* **2011**, *47*, 5973-5975.
23. Kohmoto, S.; Okuyama, S.; Nakai, T.; Takahashi, M.; Kishikawa, K.; Masu, H.; Azumaya, I., *Journal of Molecular Structure* **2011**, *998*, 192-197.
24. Kim, H. N.; Moon, J. H.; Kim, S. K.; Kwon, J. Y.; Jang, Y. J.; Lee, J. Y.; Yoon, J., *Journal of Organic Chemistry* **2011**, *76*, 3805-3811.
25. Sato, K.; Okabe, Y.; Onitake, T.; Yamaguchi, M.; Arai, S.; Yamagishi, T., *Supramolecular Chemistry* **2011**, *23*, 249-251.
26. Alcalde, E.; Dinares, I.; Ibanez, A.; Mesquida, N., *Chemical Communications (Cambridge, United Kingdom)* **2011**, *47*, 3266-3268.
27. Ganesan, K.; Alias, Y.; Ng, S. W., *Acta Crystallographica, Section C: Crystal Structure Communications* **2008**, *C64*, o478-o480.
28. Ganesan, K.; Alias, Y., *International Journal of Molecular Sciences* **2008**, *9*, 1207-1213.
29. Walter, S. M.; Kniep, F.; Herdtweck, E.; Huber, S. M., *Angewandte Chemie, International Edition* **2011**, *50*, 7187-7191, S7187/1-S7187/31.
30. Walter, S. M.; Kniep, F.; Rout, L.; Schmidtchen, F. P.; Herdtweck, E.; Huber, S. M., *Journal of the American Chemical Society* **2012**, *134*, 8507-8512.
31. Remsburg, J. W.; Soukup-Hein, R. J.; Crank, J. A.; Breitbach, Z. S.; Payagala, T.; Armstrong, D. W., *Journal of the American Society for Mass Spectrometry* **2008**, *19*, 261-269.
32. Subramaniam, P.; Mohamad, S.; Alias, Y., *International Journal of Molecular Sciences* **2010**, *11*, 3675-3685.
33. Cabildo, P.; Sanz, D.; Claramunt, R. M.; Bourne, S. A.; Alkorta, I.; Elguero, J., *Tetrahedron* **1999**, *55*, 2327-2340.
34. Jiao, D.; Biedermann, F.; Scherman, O. A., *Organic Letters* **2011**, *13*, 3044-3047.
35. Samsam, S.; Leclercq, L.; Schmitzer, A. R., *Journal of Physical Chemistry B* **2009**, *113*, 9493-9498.
36. Wang, R.; Yuan, L.; Macartney, D. H., *Chemical Communications (Cambridge, United Kingdom)* **2006**, 2908-2910.

37. Noujeim, N.; Jouvelet, B.; Schmitzer, A. R., *Journal of Physical Chemistry B* **2009**, *113*, 16159-16168.
38. Leclercq, L.; Noujeim, N.; Schmitzer, A. R., *Crystal Growth & Design* **2009**, *9*, 4784-4792.
39. Ling, I.; Alias, Y.; Sobolev, A. N.; Byrne, L. T.; Raston, C. L., *CrystEngComm* **2011**, *13*, 787-793.
40. Ling, I.; Alias, Y.; Sobolev, A. N.; Raston, C. L., *Crystal Growth & Design* **2009**, *9*, 4497-4503.
41. Awadalla, E. A., *Experimental and Toxicologic Pathology* **2012**, *64*, 431-434.
42. Brent, J.; Schaeffer, T. H., *Journal of Occupational and Environmental Medicine* **2011**, *53*, 1332-1336.
43. Goldman, S. M.; Kamel, F.; Ross, G. W.; Bhudhikanok, G. S.; Hoppin, J. A.; Korell, M.; Marras, C.; Meng, C.; Umbach, D. M.; Kasten, M.; Chade, A. R.; Comyns, K.; Richards, M. B.; Sandler, D. P.; Blair, A.; Langston, J. W.; Tanner, C. M., *Movement Disorders* **2012**, *27*, 1652-1658.
44. Kobayashi, S.; Kuwata, K.; Sugimoto, T.; Igarashi, K.; Osaki, M.; Okada, F.; Fujii, J.; Bannai, S.; Sato, H., *Free Radical Biology & Medicine* **2012**, *53*, 2197-2203.
45. Galluzzi, M.; Zhang, S.; Mohamadi, S.; Vakurov, A.; Podesta, A.; Nelson, A., *Langmuir* **2013**, *29*, 6573-6581.
46. Pan, W.; Qi, Y.; Wang, R.; Han, Z.; Zhang, D.; Zhan, J., *Chemosphere* **2013**, *91*, 157-164.
47. Pereiro, A. B.; Araujo, J. M. M.; Martinho, S.; Alves, F.; Nunes, S.; Matias, A.; Duarte, C. M. M.; Rebelo, L. P. N.; Marrucho, I. M., *ACS Sustainable Chemistry & Engineering* **2013**, *1*, 427-439.
48. Radosevic, K.; Cvjetko, M.; Kopjar, N.; Novak, R.; Dumic, J.; Sreck, V. G., *Ecotoxicology and Environmental Safety* **2013**, *92*, 112-118.
49. Ventura, S. P. M.; Goncalves, A. M. M.; Sintra, T.; Pereira, J. L.; Goncalves, F.; Coutinho, J. A. P., *Ecotoxicology* **2013**, *22*, 1-12.
50. Freyer, M. W.; Lewis, E. A., *Methods in Cell Biology* **2008**, *84*, 79-113.
51. Tronnier, A.; Strassner, T., *Dalton Transactions* **2013**, *42*, 9847-9851.

Chapter Seven

Isothermal Titration Calorimetric (ITC) Analysis of Polymeric Materials

Abstract

Isothermal titration calorimetric (ITC) analyses were used to determine the binding characteristics of several polymeric guest species with either small molecule or polymeric hosts. One system was used to generate a three armed star shaped polymer, and a second was used to demonstrate the effect of changing the polymer chain on the binding constant. Finally, a series of paraquat terminated polystyrene guests was titrated with a small molecule host to determine the effects of increasing molecular weight on the association constant.

Introduction

The intersection between supramolecular chemistry and polymer chemistry provokes thoughts of new materials with interesting and useful physical characteristics. Supramolecular polymer chemistry is responsible for the mechanics of DNA and other biological systems, yet it has few industrial uses at this point in time. One might envision supramolecular polymers made by non-covalently linked monomer units, multi-armed and branched polymers held together by non-covalent interactions, and even self-healing materials that reform from previously separated binding sites. Supramolecular polymers may have optimized processing properties due to reversibility of their non-covalent binding. As we progress toward some of these systems, we need to have a good understanding of how non-covalent supramolecular polymers behave. One very important parameter is the effective association constant for a host and guest pair at the end of a polymer chain, as well as the enthalpic and entropic parameters of the interaction. The work

described in this chapter revolves around the question of how the size of a polymer affects the binding characteristics of a host or guest moiety that is attached to it.

The effective binding constant for a host-guest system is an important parameter in the field of non-covalently linked polymeric systems. If different materials and architectures are to be achieved, the binding characteristics of the host/guest system must be well known and easily predicted. In the case of supramolecular polymers made from host and guest monomer units, the length of polymer chains produced depend on the binding efficiency of the monomer units. If an isodesmic model is assumed, wherein each binding constant along the chain is equal, then the length of the polymer chain can be calculated based upon the association constant, and the concentration of monomers present in solution. In the melt phase or in bulk, the concentration of host and guest moieties is high, and predictably, the polymer chain length will be very high as well. This is predicted from the Carothers equation based upon the relationship of the percentage of converted monomer to the degree of polymerization. As the binding constant is increased, the conversion and length of the polymer chain also increase (Figure 7.1).¹

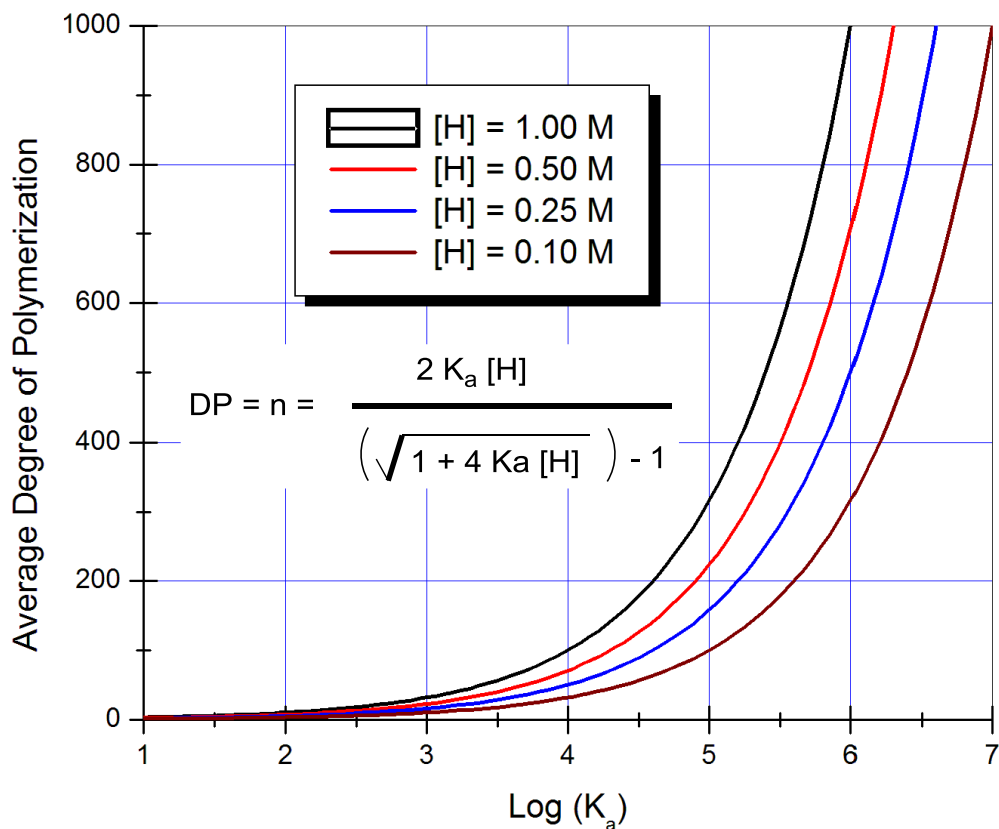
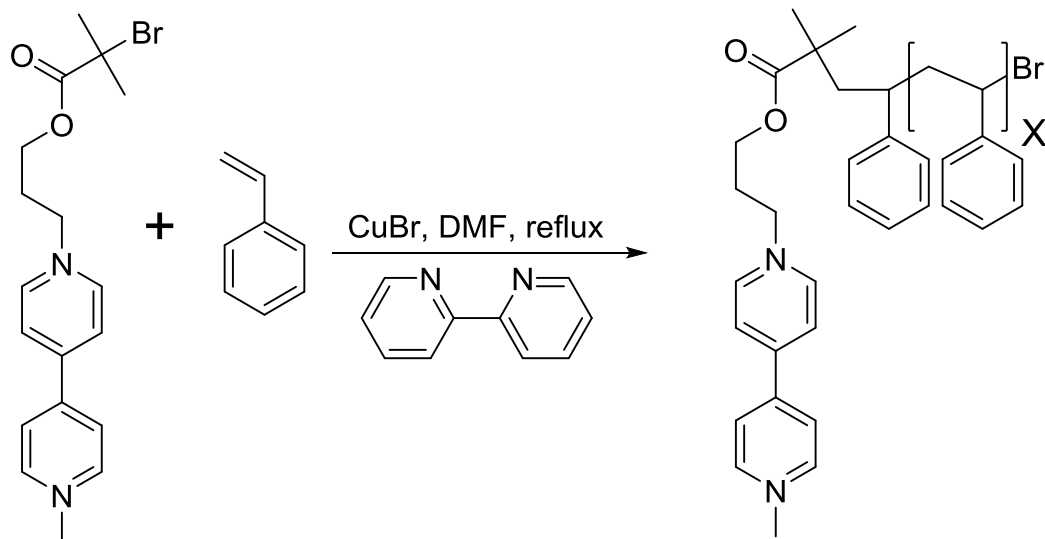


Figure 7.1. Plot of the predicted degree of polymerization versus the association constant between host and guest chain ends, and the concentration of the chain ends [H] in an AB monomer system.

Paraquat Terminated Polystyrene Synthesis and Characterization

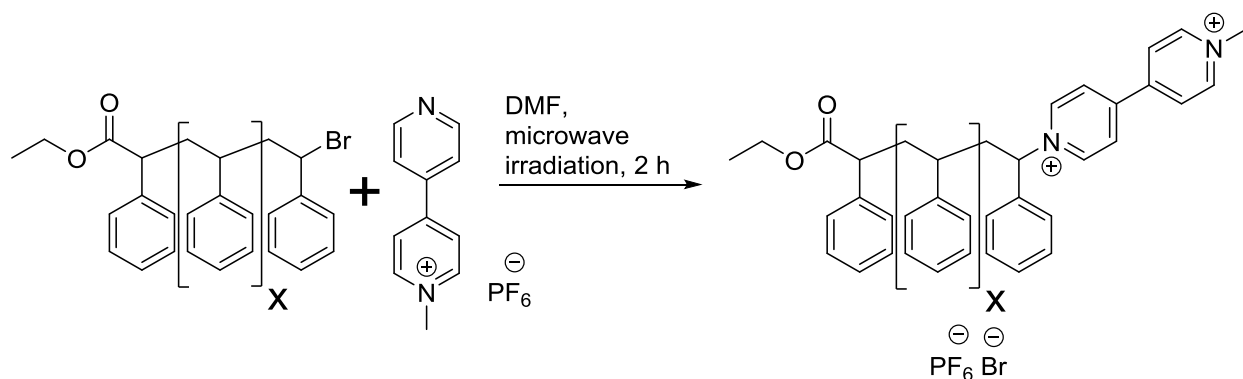
A set of four paraquat terminated polystyrene samples was synthesized by Dr. Minjae Lee.² These samples were characterized by Size Exclusion Chromatography (SEC), as well as Isothermal Titration Calorimetry (ITC). The results of those titrations are discussed later in this chapter. Several other methods were attempted to synthesize more samples having higher molecular weight styrene moieties. These methods were generally unsuccessful in producing suitable samples for titration.

Synthesis of polystyrene terminated with paraquat using an atom transfer radical polymerization (ATRP) reaction was attempted. Some liabilities of this method include the need for an amount of polar solvent to dissolve the paraquat initiator, and the need for a ligand to dissolve the copper halide used as a catalyst. This reaction was done repeatedly by Dr. Minjae Lee. Dr. Lee found that DMF was a good solvent additive to aid in solubility; however, the breakdown of that solvent to produce dimethyl amine at high temperature requires the use of very pure DMF (Scheme 7.1). Outside of Dr. Lee's efforts this reaction was very seldom successful. The samples that were provided by him showed an unexpectedly high PDI value, and so the samples were generally disregarded.



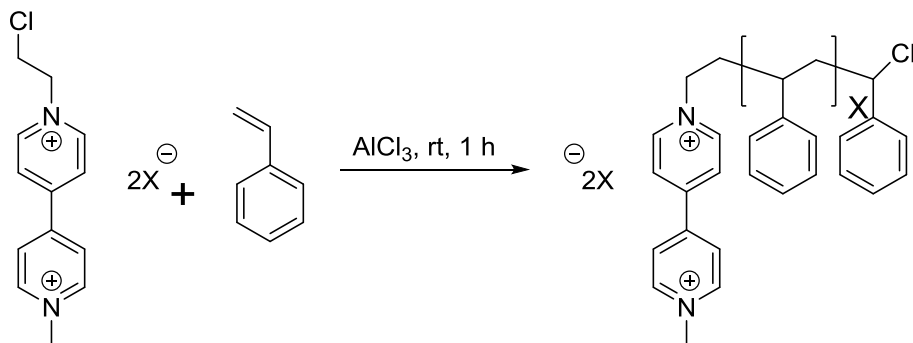
Scheme 7.1. Synthesis of paraquat terminated polystyrene via ATRP method.

Synthesis of paraquat terminated polystyrenes from preformed ATRP polymers was also attempted. In Scheme 7.2, preformed, halide terminated polystyrene was reacted with methyl halfquat. The quaternization reaction with the terminal halide would then provide the final guest functionalized polymer. This reaction was attempted several times using microwave irradiation in a solution of DMF. NMR analysis and anecdotal evidence suggest that the preliminary reactions were successful. Unfortunately, this method was never used to generate more samples for titration. The advantages of this scheme lie in the fact that the preformed polymer can be synthesized under highly controllable conditions, and then characterized before the addition of the paraquat end group. The drawback to this method is that there is no guarantee of quantitative end group functionalization, and the separation of unfunctionalized materials would perhaps be problematic.



Scheme 7.2 Synthesis of paraquat terminated polystyrene from preformed, halide terminated polystyrene and 1-methyl-[4,4'-bipyridin]-1-ium hexafluorophosphate using microwave irradiation.

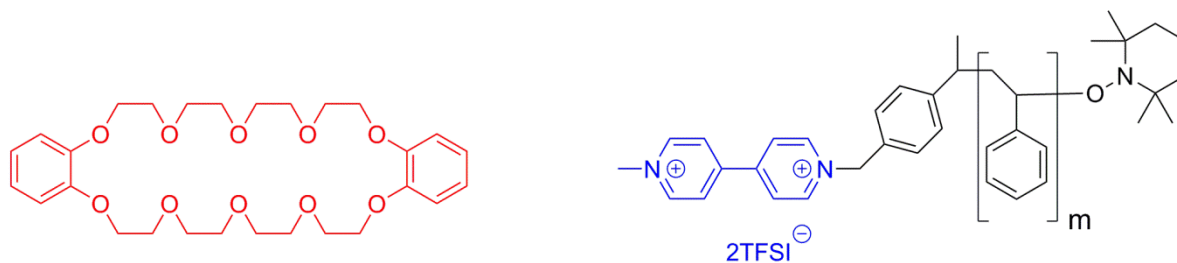
Finally, a cationic synthesis of paraquat terminated polystyrene was attempted as diagramed in Figure 7.3. In this case, a chloride functionalized paraquat and a Lewis acid (aluminum chloride) were used to form a cationic species. The cationic polymerization of styrene is very fast and is consequently difficult to control. Several attempts were made using this system, but none was successful. The use of quaternary ammonium salts is suggested in some cationic polymerizations as a means of controlling the molecular weight and distribution.³⁻¹¹ In retrospect, the type of paraquat initiator and even its counterion are important in this kind of reaction. The use of PF₆ anions should be avoided as they tend to terminate the growing polymer chain.¹²



Scheme 7.3. Cationic polymerization of polystyrene using chlorinated paraquat as an initiator in conjunction with AlCl_3 .

Titration of Paraquat Terminated Polystyrene with Dibenzo-30-crown 10

Initially, titrations were run using the paraquat terminated polystyrene from Dr. Minjae Lee¹³ with dibenzo-30-crown-10 as host molecule as seen in Scheme 7.4. Unfortunately, these systems did not show appreciable binding. This was not surprising considering the results Moody et al. who found no binding between dimethyl paraquat and dibenzo-30-crown 10.¹⁴

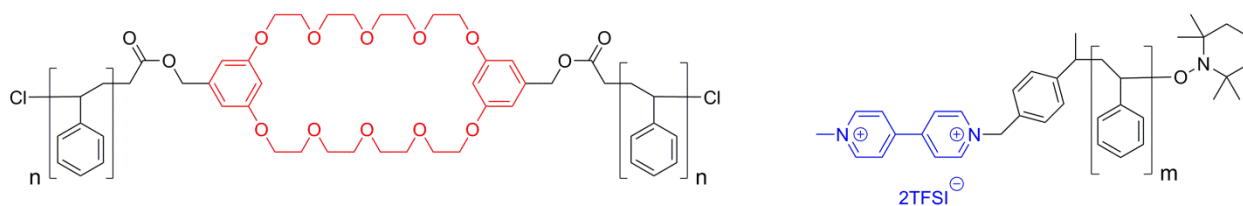


Scheme 7.4. Chemical structures of dibenzo-30-crown 10 and paraquat terminated polystyrene.

Titrations with Crown Centered Polystyrene and Paraquat Terminated Polystyrene

The titration of paraquat terminated polystyrene (SEC: $M_n=31.5$ kDa, PDI=1.07) with a crown-centered polystyrene (SEC: $M_n = 13.5$ kDa PDI = 1.25) showed interesting binding

characteristics.¹³ A well-shaped enthalpogram was generated with this system. The association constant was calculated to be $4.38 \pm 0.33 \times 10^3 \text{ M}^{-1}$ with a ΔH° value of $-11.7 \pm 0.31 \text{ kcal/mol}$. The ΔG° value was then calculated as $-4.96 \pm 0.37 \text{ kcal/mol}$, and the ΔS° value was calculated to be $-22.6 \pm 1.1 \text{ cal/mol K}$. These results were reported by Minjae Lee and illustrated the formation of a three armed star polymer topology.^{2,15} As a point of reference bis(*meta*-phenylene)-32-crown-10 complexes paraquat with $K_a = 1.9 (\pm 0.7) \times 10^3$ in a 3:1 mixture of chloroform and acetonitrile according to Zhu et al.¹⁶



Scheme 7.5. Chemical structures for both bis(*meta*-phenylene)-32-crown-10 centered polystyrene, and paraquat terminated polystyrene.

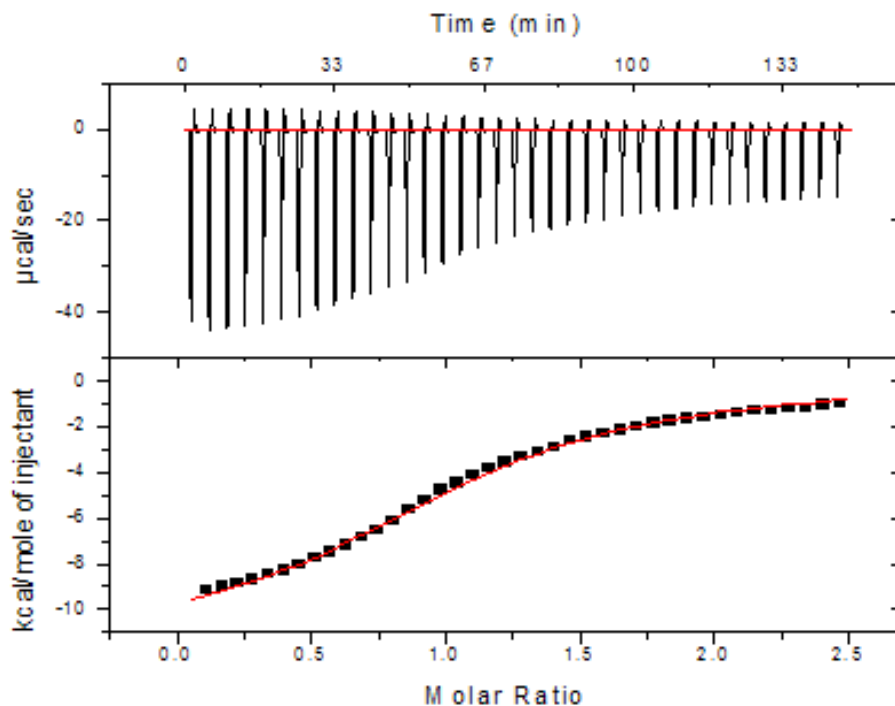
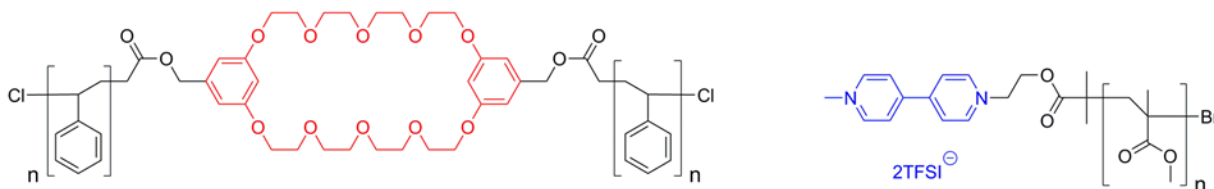


Figure 7.2. Enthalpogram for the binding titration of bis(*meta* phenylene)-32-crown 10 centered polystyrene and paraquat terminated polystyrene in acetone at 25 °C. Reprinted (adapted) with permission from Lee, M.; Schoonover, D.; Gibson, H. W., *Polymer Preprints (American Chemical Society, Division of Polymer Chemistry)* **2008**, *49*, 107-108. Copyright 2009 American Chemical Society.

Titration with Crown Centered Polystyrene and Paraquat Terminated Poly (methyl methacrylate)

Titration of the same crown-centered polystyrene with a sample of paraquat terminated poly(methyl methacrylate) (SEC: $M_n = 40.7$ kDa, PDI = 1.33), shown in Scheme 7.6, also gave an interesting result.¹³ In this case, the association constant decreased significantly compared to the titration with paraquat terminated polystyrene. This may have been due to complexation of the PMMA polymer with the paraquat guest. It may also have been due to poor mixing between the polymer phases. The association constant decreased to $363 \pm 12 \text{ M}^{-1}$. The ΔH° value was $-2.35 \pm 05 \text{ kcal/mol}$, and the stoichiometry was artificially set to be 1:1. The calculated value for

ΔG° was -3.49 ± 0.12 kcal/mol, and the value for ΔS° was 3.54 ± 0.32 cal/mol K. The positive value of the change in entropy is a strong indication of a complexation interaction between the paraquat and the poly(methyl methacrylate), resulting in aggregation of the PMMA.



Scheme 7.6. Chemical structures for for both bis(*meta*-phenylene)-32-crown-10 centered polystyrene, and paraquat terminated poly(methyl methacrylate).

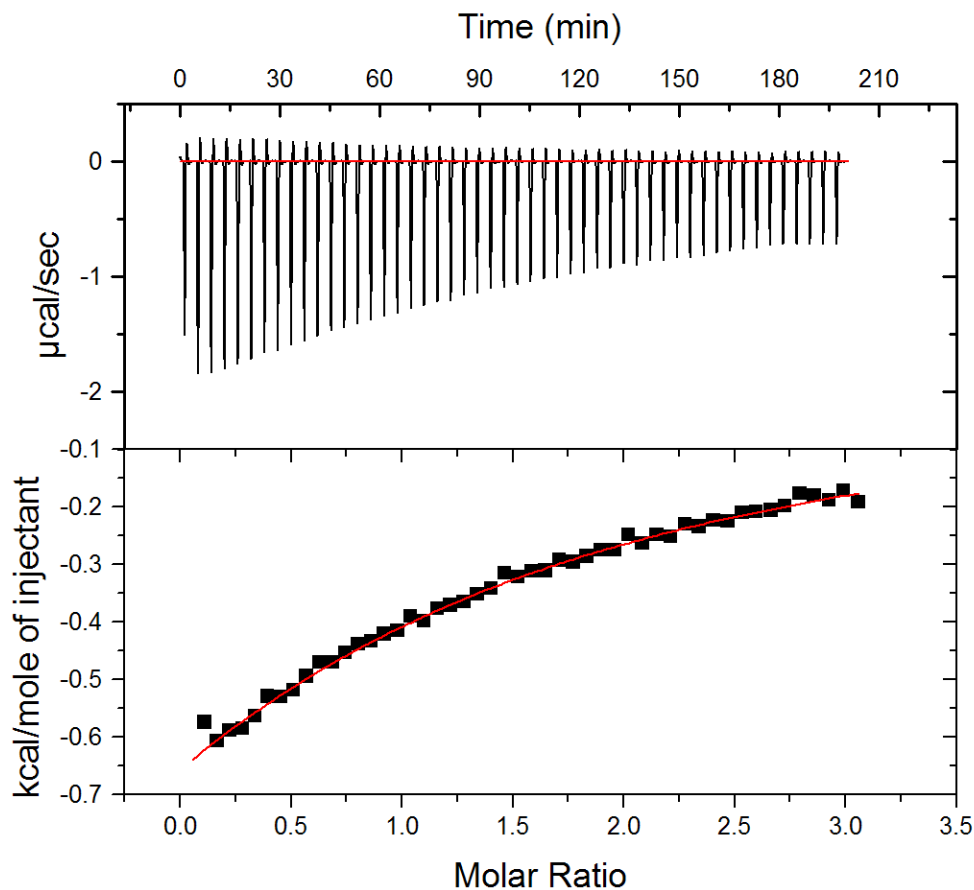
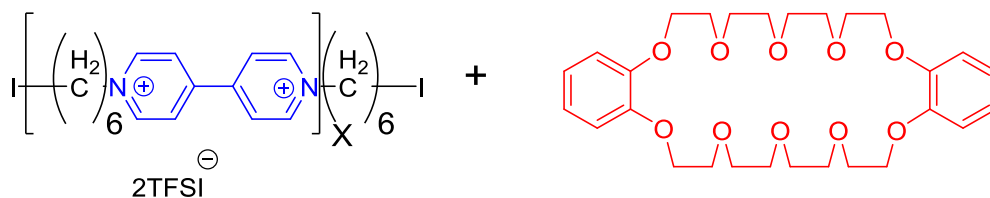


Figure 7.3. Enthalpogram for the ITC titration of bis meta phenylene-32-crown 10 with paraquat terminated poly(methyl methacrylate), in acetone at 25 °C.

Titration of Dibenzo-30-crown 10 with Polyviologen

A titration was run using a polyviologen (M_n 12 kDa from ^1H NMR end group analysis¹⁷) and dibenzo-30 crown-10 as the guest and host, respectively (Scheme 7.7). A mixture of chloroform and acetonitrile was used to dissolve the two components. The host was used in the syringe solution and the polymeric guest was placed in the cell. The curve fitting is based on the ratio of crown ether host to the monomer unit of the guest in the polymer. Since the c value of this titration was rather low, the stoichiometry was artificially set at 1:1, based on the repeat unit, before fitting. The binding constant for this system was calculated to be $48 \pm 3.0 \text{ M}^{-1}$. The

change in enthalpy was -3.50 ± 0.14 kcal/mol. The change in Gibbs free energy was -2.29 ± 0.14 kcal/mol, and the change in entropy was -4.04 ± 0.36 cal/mol K.



Scheme 7.7. Chemical structures for polyviologen and dibenzo-30-crown 10.

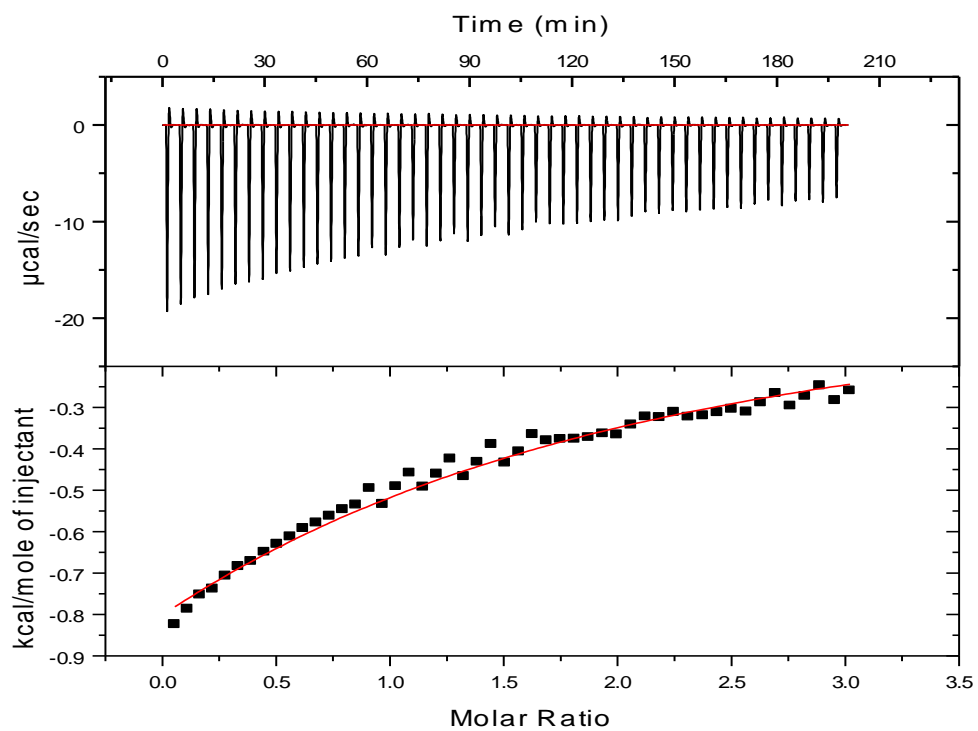
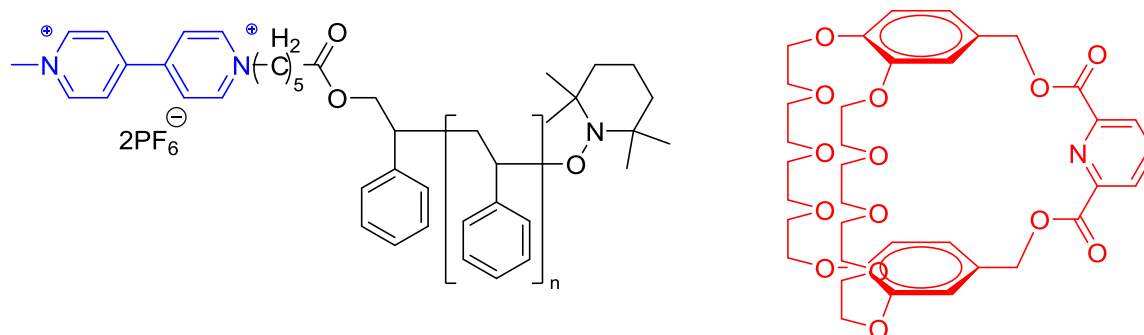


Figure 7.4. Enthalpogram for the titration of polyviologen with dibenzo-30-crown 10 in acetone at 25 °C

Titration with Paraquat Terminated Polystyrene and Dibenzo-30 crown-10 Cryptand

Titration of the paraquat terminated polystyrenes with the dibenzo-30-crown-10-based cryptand, as seen in Scheme 7.6, showed much more interesting results using samples from Dr. Minjae Lee of the structures shown in Scheme 7.8.² The first thing that was notable was the magnitude of the association constants calculated for these titrations (Table 7.1). In the first three titrations, with the lowest molecular weight polymers, the calculated association values were larger than 10^6 M^{-1} . This is approximately an order of magnitude larger than the association constant calculated for dimethyl paraquat with the same host.¹⁸ The difference in the titrations can be attributed to solvent effects. Due to solubility limitations, the original titration for monomeric paraquat and the dibenzo-30-crown-10 cryptand was run in acetone. For the polymeric guest titrations, the polystyrene provided enough solubility that the titrations could be run in a much less polar solvent. Consequently, the polymeric guest titrations were run in chloroform. The solvent change was in fact necessary due to the very limited solubility of polystyrene in acetone. The first three titrations generated very similar results for the three smallest polymeric guests. Only the fourth and final sample in this series showed a change in the association constant.



Scheme 7.8. Chemical structures of paraquat terminated polystyrene and dibenzo-30-crown-10 based cryptand.

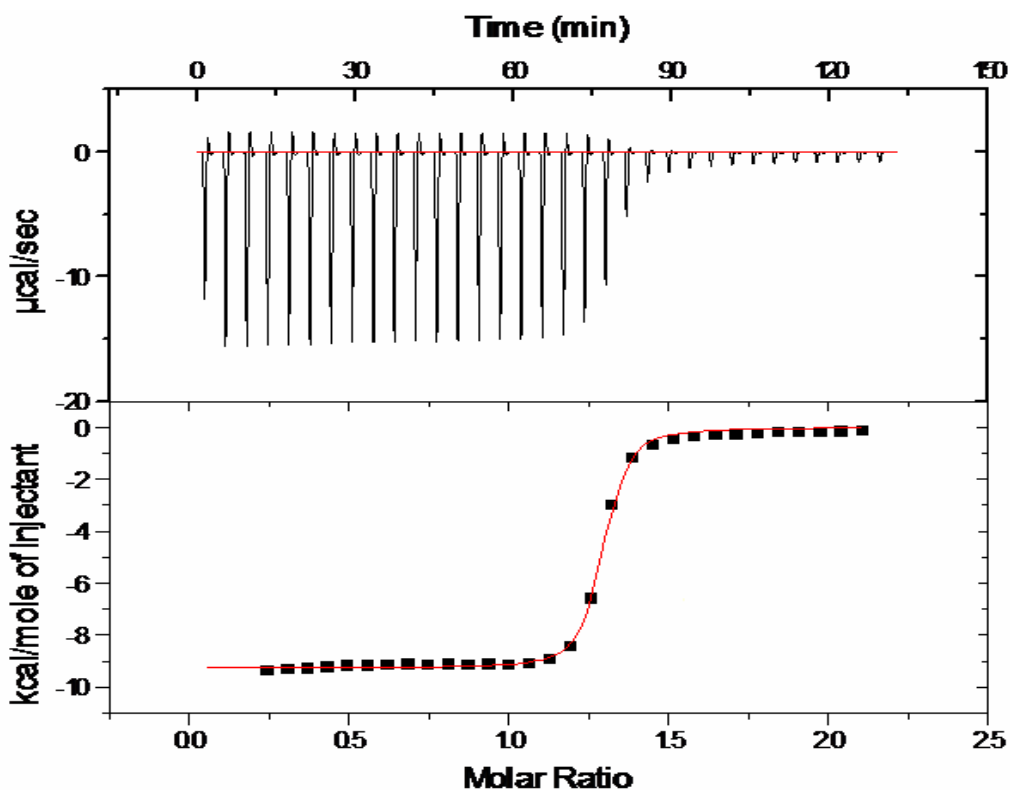


Figure 7.5. Enthalpogram for the ITC titration of paraquat terminated polystyrene with dibenzo-30-crown-10 based cryptand in chloroform at 25 °C.

Another interesting aspect of these titrations was the ability to determine the number average molecular weight of the polymer by measuring the stoichiometry of the titration. At the equivalence point of the titration, all of the guest chain ends should have been consumed by the host titrant. Assuming then that there is a guest species on only one chain end, and that the binding of host and guest is 1:1, the number of polymer chains and consequently the number average molecular weight can be calculated. The number average molecular weight (M_n) values determined by ITC titration generally agree with the SEC results.

Table 7.1. Binding parameters for the titration of paraquat terminated polystyrene with dibenzo-30-crown-10 based cryptand in chloroform at 25 °C.

M_n^a (kDa)	M_n^b (kDa)	$K_a / 10^4$ (M^{-1})	ΔH° (kcal/mol)	ΔG° (kcal/mol)	ΔS° (cal/mol K)
3.1	3.1	150 ± 1	-8.73 ± 0.12	-8.42 ± 0.56	-1.04 ± 0.17
7.5	5.9	210 ± 3	-9.13 ± 0.08	-8.62 ± 0.61	-1.71 ± 0.36
20	17	186 ± 2	-9.25 ± 0.04	-8.55 ± 0.72	-2.35 ± 0.26
31	37	16.6 ± 0.7	-9.23 ± 0.04	-7.12 ± 0.52	-7.05 ± 0.88

^a Determined by SEC. ^b Determined by ITC titration

A plot of the association constants and changes in Gibbs free energies is shown in Figure 7.6. The general trend is that as the molecular weight of the polymer increases, the effective association constant decreases.

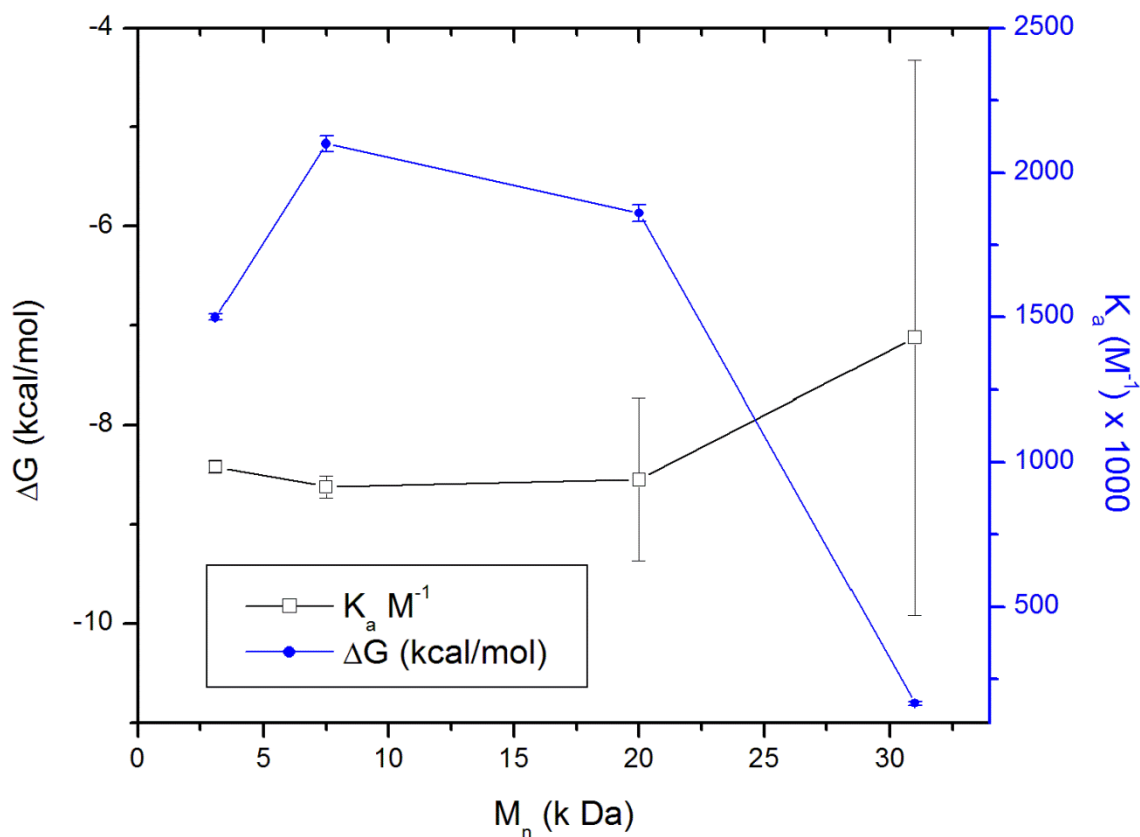


Figure 7.6. Stacked plot of the association constants (blue) and change in Gibbs free energy (red) for the titrations of paraquat terminated polystyrene and dibenzo-30-crown-10 based cryptand.

Take out “two series of”.. K scale is mislabeled; it indicates K values of 0.5 to 2 M⁻¹. It should read K / 1000. Also the line for free energy is not red, but black!

A plot of the changes in enthalpy and changes in entropy for the different titrations is shown in Figure 7.7. The plot shows a marginal decrease in the change in enthalpy accompanied by an increasingly negative change in entropy as the molecular weight of the polystyrene increases. This increasingly negative entropy as molecular weight increases is reasonable due to the effects of chain folding in the polymer and immediate availability of the paraquat chain end. As the polymer length increases, the availability of a non-occluded binding site decreases.¹⁹

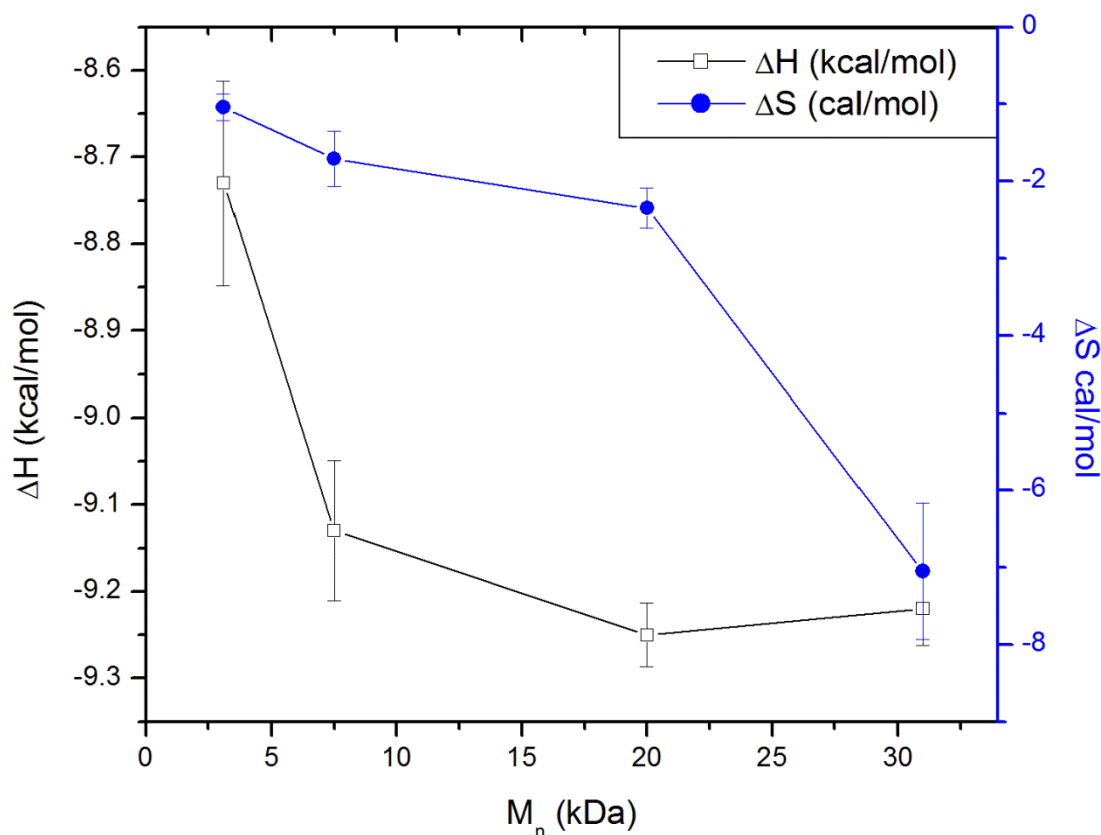


Figure 7.7. Stacked plot of the changes in enthalpy (red) and changes in entropy (blue) for titrations involving paraquat terminated polystyrene and dibenzo-30-crown-10 based cryptand.

Conclusions

Guest functionalized polymeric species were characterized to determine their binding properties with small molecule and polymeric host moieties. A three arm star shaped polymer was generated from both paraquat terminated polystyrene and paraquat terminated poly(methyl methacrylate) with crown centered polystyrene. The identity of the polymer chain played a significant role in the magnitude of the association constant measured for the two systems. The paraquat terminated poly(methyl methacrylate) guest had an association constant an order of magnitude lower than the paraquat terminated polystyrene, using the same host. The effective association constant for a guest at the end of a polymer chain with a small molecule host decreases at sufficiently high molecular weight. This decrease may be attributed to a number of causes including steric effects and possible aggregation into micellar structures..

Experimental

All titrations were run in chloroform. Standard solutions were made in class A volumetric glassware and allowed to dissolve until clear. All titrations were run at 25 °C with the host cryptand in the cell and the paraquat polymer in the syringe. Fitting was accomplished with a one set of sites model.

Cryptand samples for the first series of polymer paraquat titrations were provided by Dr. Adam Pederson.¹⁸ Paraquat terminated polystyrene samples,² paraquat terminated poly(methyl methacrylate),² polyviologen,¹⁷ and BPP32C10 centered polystyrene,² were provided by Dr. Minjae Lee and were used as received. Dibenzo-30-crown 10 was used as received from commercial sources.

References

1. Sijbesma, R. P.; Beijer, F. H.; Brunsveld, L.; Folmer, B. J. B.; Hirschberg, J. H. K. K.; Lange, R. F. M.; Lowe, J. K. L.; Meijer, E. W., *Science (Washington, D. C.)* **1997**, *278*, 1601-1604.
2. Lee, M.; Schoonover, D. V.; Gies, A. P.; Hercules, D. M.; Gibson, H. W., *Macromolecules (Washington, DC, United States)* **2009**, *42*, 6483-6494.
3. Hasebe, T.; Kamigaito, M.; Sawamoto, M., *Macromolecules* **1996**, *29*, 6100-6103.
4. Higashimura, T.; Ishihama, Y.; Sawamoto, M., *Macromolecules* **1993**, *26*, 744-51.
5. Higashimura, T.; Sawamoto, M.; Kojima, K.; Ishihama, Y., *Yuki Gosei Kagaku Kenkyusho Koenshu* **1991**, *5*, 11-23.
6. Ishihama, Y.; Sawamoto, M.; Higashimura, T., *Polymer Bulletin (Berlin)* **1990**, *24*, 201-6.
7. Ishihama, Y.; Sawamoto, M.; Higashimura, T., *Polymer Bulletin (Berlin)* **1990**, *23*, 361-6.
8. Kostyuk, S. V.; Dubovik, A. Y.; Shiman, D. I.; Gaponik, L. V.; Mardykin, V. P.; Kaputskii, F. N.; Antipin, L. M., *Dokl. Nats. Akad. Nauk Belarusi* **2004**, *48*, 62-64.
9. Li, Y.; Liang, H.; Lu, J.; Deng, Y., *Gongneng Gaofenzi Xuebao* **1997**, *10*, 542-547.
10. Lin, C. H.; Xiang, J. S.; Matyjaszewski, K., *Macromolecules* **1993**, *26*, 2785-90.
11. Xiang, J. S.; Lin, C. H.; Matyjaszewski, K., *Polymer Preprints*, **1992**, *33*, 154-5.
12. Gupta, M. K.; Singh, R. P., *Journal of Applied Polymer Science* **2009**, *112*, 3707-3713.
13. Lee, M.; Schoonover, D.; Gibson, H. W., *Polymer Preprints (American Chemical Society, Division of Polymer Chemistry)* **2008**, *49*, 107-108.
14. Moody, G. J.; Owusu, R. K.; Thomas, J. D. R., *Analyst (Cambridge, United Kingdom)* **1987**, *112*, 121-7.
15. Gibson, H. W.; Huang, F.; Ge, Z.; Wang, H.; Pederson, A. M. P.; Lee, M.; Rouser, M.; Schoonover, D., *Polymer Preprints (American Chemical Society, Division of Polymer Chemistry)* **2008**, *49*, 1030-1031.
16. Zhu, K.; Li, S.; Wang, F.; Huang, F., *Journal of Organic Chemistry* **2009**, *74*, 1322-1328.
17. Lee, M.; Choi, U. H.; Colby, R. H.; Gibson, H. W., *Macromolecular Chemistry and Physics* **2014**, Ahead of Print.
18. Pederson, A. M. P.; Ward, E. M.; Schoonover, D. V.; Sledobnick, C.; Gibson, H. W., *Journal of Organic Chemistry* **2008**, *73*, 9094-9101.

19. Coumans, R. G. E.; Elemans, J. A. A. W.; Nolte, R. J. M.; Rowan, A. E., *Proceedings of the National Academy of Sciences of the United States of America* **2006**, *103*, 19647-19651.

Chapter Eight

Synthesis of Imidazolium-Based Ion Conductive Polymers

Abstract

Imidazolium-containing monomers and polymers were synthesized and characterized for their physical and ionic conductivity properties. Isomerically pure norbornene carboxylic acid was synthesized and functionalized with different imidazolium-containing tail groups to form monomers. The four monomers were polymerized under ROMP conditions to provide four ionically conductive polymers. The measured conductivities of the monomers were on the order of 10^{-4} Siemens per centimeter (S/cm) and the conductivities of the polymers were on the order of 10^{-5} S/cm. The conductivities of the monomers compare well with other imidazolium ionic liquid monomers, and the conductivities for the polymers are similar to those found for acrylate and methacrylate polyimidazolium materials produced by our group.

Introduction

Recently there has been considerable interest in the area of ionically conductive polymers.¹⁻⁴ In contrast to electronically conductive materials, ion conducting materials move charge by the transport of ions instead of electrons. These systems may be analogous to solutions of electrolytes.⁵ The focus of the present work has been the synthesis of monomers and polymers that show ion conductivity by the movement of anionic counterions of polymer-bound imidazolium cations.⁶ Imidazolium cationic species were selected for this work due to their physical and electronic properties. Many imidazolium salts fall into the category known as ionic liquids. Ionic liquids generally have melting temperatures below 100 °C; a subset of room temperature ionic liquids have melting points below 25 °C.⁴

The purpose of this work is to generate materials that can be used as electrochemical actuators. This is achieved through an interesting combination of chemistry, physics, and mechanics. The ideal material contains an ionic component whose ions are made to move within the material using an electrical potential.⁷ In the case of this work, it was decided to use a tethered imidazolium cation.⁸ Two electrodes are placed on either side of the material, and when an electrical potential is generated between them, the resulting field transports the “free” anions toward cathode. If the geometry of the system is correct, this electrical transport of mass will lead to strain and thus deform the polymer in the direction away from the counterion movement.

In this work, the mobility of ions through material is of great importance. High ionic conductivity is most easily achieved in a liquid phase that allows free or much less hindered movement of ions in an applied direct current (DC) electric field.⁹ Consequently it was a useful idea to begin this work using a liquid salt that would show high ionic mobility in its liquid phase. In addition to being liquids at low temperatures, imidazolium salts are less toxic than some other organic cations such as paraquat.¹⁰⁻¹⁸ The main type of reaction that occurs with imidazolium salts is reversible deprotonation with base to form a stable carbene. Conversely, paraquat salts are very easily reduced under basic conditions, usually irreversibly.

In previous work, our group and collaborators found that there is a general correspondence of the glass transition temperature of a monomer or polymer with its ionic conductivity.^{3, 19-21} In most cases, samples that have lower glass transition temperatures (T_g) show higher ionic conductivity (α_{DC}) when evaluated using differential scanning calorimetry (DSC) and dielectric spectroscopy, respectively. This trend may be due to several conditions met in the monomeric and polymeric materials. From a mechanical standpoint, the lower the viscosity of the conducting phase, the lower the barrier to mass transport. Materials with low T_g

characteristics are liquids, and behave as such during conductivity testing. From a chemical standpoint, the structure of the monomers and resulting polymers is also important. Popular moieties include ethyleneoxy chains of varying lengths.²¹⁻²² The inclusion of these structural units is well thought out. Ethyleneoxy polymers often have very low glass transition temperatures, and at low molecular weights are liquids at room temperature. The ethyleneoxy moieties stabilize the imidazolium cation, and encourage the separation and transport of the counterion away from it. Finally, the ethyleneoxy moieties have a high dipole moment. This more highly polar medium stabilizes the charged species and allows for their separation, yielding more of the free ions necessary for charge transport.

The previous work in this area from our group was completed by Dr. Minjae Lee and Dr. Anuj Mittal.¹⁹⁻²⁴ Their work focused on the synthesis of acrylate and methacrylate esters that carried an imidazolium salt with differing chain lengths between the salt and vinyl monomer. A large problem was discovered with these systems in that they very easily autopolymerize. Ideally these materials would have been used to form well controlled and defined polymeric materials, so that their physical properties could be predicted and tuned to specific applications, but their tendency to autopolymerize ruled out that possibility. After this discovery, it was determined that Ring Opening Metathesis Polymerization (ROMP) could be a viable alternative to the use of vinyl and or acrylate monomers in the production of well-defined ion-containing polymers.²⁵⁻²⁹

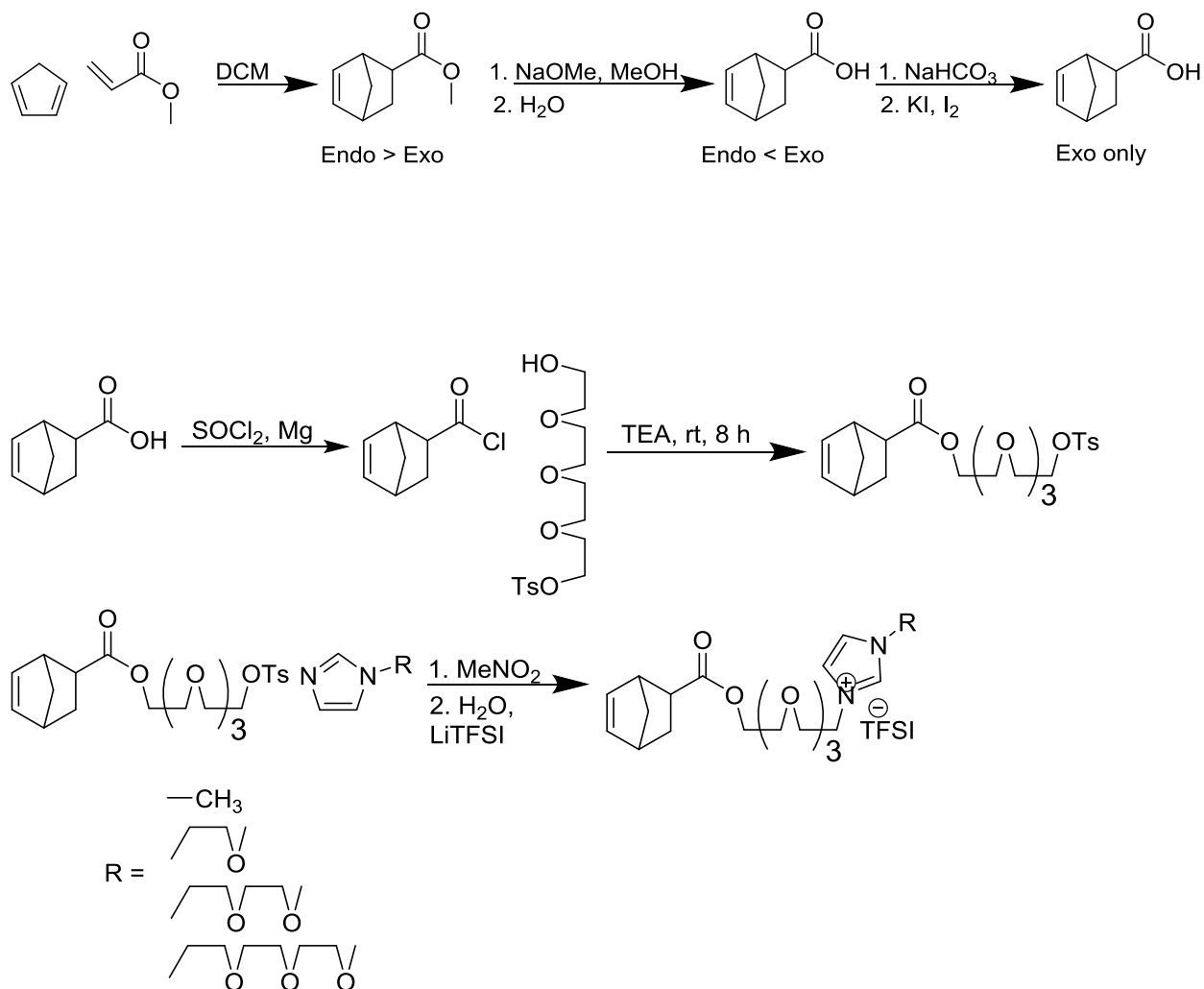
The ion-containing polymers produced during the previous work all had very low glass transition temperatures, and consequently were all liquids at room temperature. This would be problematic for the construction of electromechanical actuators. Bending actuators require rigidity and a solid form; the modulus of the material is important. Ideally the actuator material

would be tough and creasible as a film. Consequently, an ion conducting material for this application must have predictable and advantageous mechanical properties. Since the homopolymers are liquids, it was decided to prepare ABA triblock copolymers to generate the type of materials required. With controlled polymerizations, polymers with predictable morphologies can be produced. In this case, the ideal morphology would be a bicontinuous microphase-separated polymer, one phase for mechanical integrity and the other for ionic conduction. Consequently, a “living” ROMP polymerization is ideal for the production of such materials. The sequential addition of monomers can lead to the synthesis of multi-block copolymers.²⁹⁻³⁰ The tetra(ethyleneoxy) linker was selected in an effort to keep the glass transition temperature of the polymers as low as possible, as well as provide stabilization and solvation to the imidazolium ions pendant on the polymer backbone. Previous work by other group members indicated that the tetra(ethyleneoxy) linker was a very good platform for the synthesis of imidazolium-functionalized monomers and polymers.^{22, 31-32} The terminal imidazolium moieties were selected to be either N'-methyl or N'-(ethyleneoxy) groups.

Synthesis

Norbornene functionalized monomers were synthesized through a multi-step process as depicted in Scheme 8.1. Methyl norbornenate was synthesized from methyl acrylate and freshly cracked cyclopentadiene. The majority of this product was the *endo* isomer. Consequently, this product was isomerized and hydrolyzed in a single process, according to the work by Kanao et al., to provide an *exo* isomer rich norbornene carboxylic acid.³³ The *exo* isomer is desirable for polymerizations as it has less steric hindrance and polymerizes more readily.^{30, 33} The *exo* isomer was isolated by selectively lactonizing the *endo* isomer in the presence of iodine. The *exo* acid was converted into the acid chloride, in the presence of magnesium in order to preserve the

alkene, and then esterified with tetra(ethylene glycol) monotosylate. This monomer precursor was then used to quaternize the appropriately functionalized imidazole. The end result was an isomerically pure monomer that could be used for ROMP polymerizations.



Scheme 8.1. Synthesis of ROMP monomers containing different end groups and *exo* norbornene functional groups

Results and discussion

After synthesis of the monomers, they were characterized by DSC to determine their glass transition temperatures. There is a tendency for monomers with low glass transition temperatures to also have high conductivity. The T_g values for the four monomers synthesized are shown in the Table 9.1 below. All the T_g values are low compared to similar acrylate²¹ and di-substituted norbornene monomers.³¹ This was a good indication that the conductivity value for these monomers would be high.

Table 8.1. T_g and conductivity values measured for ROMP monomers of different tail length as described in Scheme 8.1

Monomer	R	T_g (°C)	α_{DC} at 25 °C(S/cm)
RM 1	CH ₃	-55	2.80×10^{-4}
RM 2	(CH ₂ CH ₂ O) ₁ CH ₃	-66	2.07×10^{-4}
RM 3	(CH ₂ CH ₂ O) ₂ CH ₃	-69	4.39×10^{-4}
RM 4	(CH ₂ CH ₂ O) ₃ CH ₃	-56	2.79×10^{-4}

Sample: DVS_rm4a_062012
Size: 9.2000 mg
Method: Heat/Cool/Heat

DSC

File: F:\DSC data\DVS_rm4a_062012.001
Operator: Andy
Run Date: 20-Jun-2012 14:43
Instrument: DSC Q1000 V9.8 Build 296

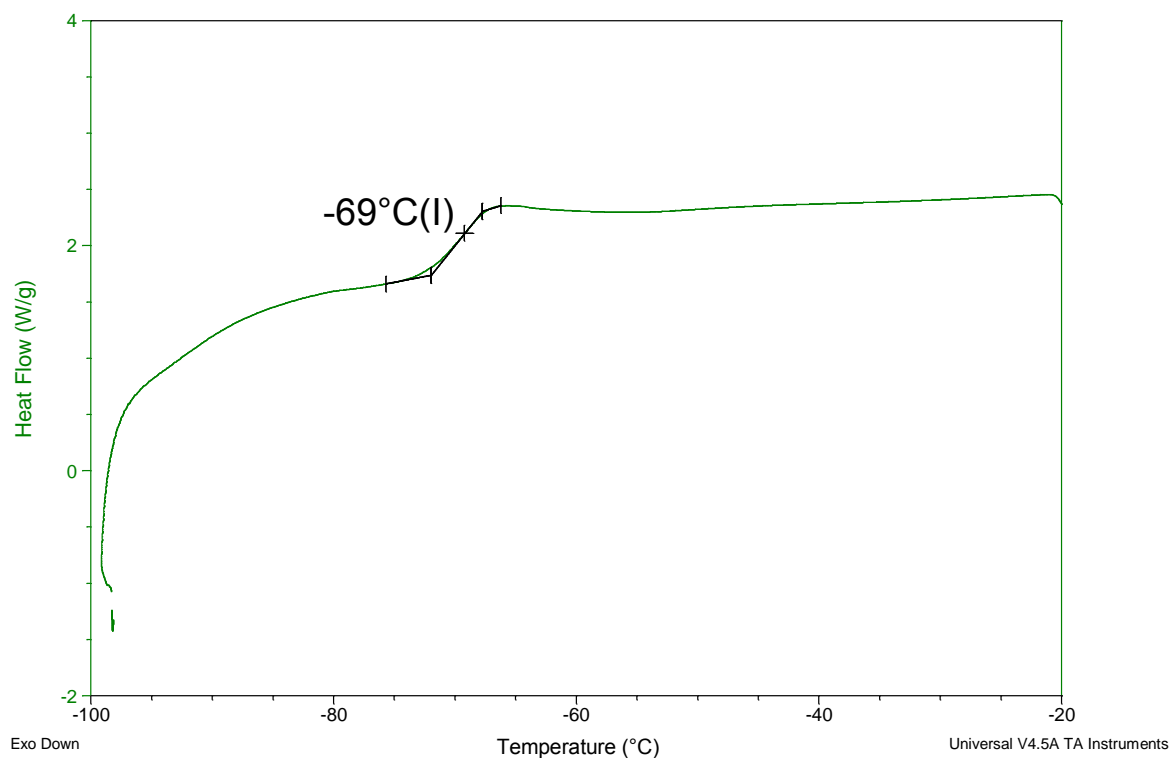


Figure 8.1. DSC trace for the monomer **RM4** with a T_g of -69 °C. All monomers had similarly low T_g values. Second heat cycle shown.

The ionic conductivities of the four different monomers were determined through dielectric spectroscopic measurements in the laboratory of Prof. Ralph Colby at Penn State University. Prior to this determination, samples were heated under vacuum to remove water and solvent contaminants. The ionic conductivity was then measured over a range of temperatures and frequencies. The log of the conductivity was plotted against the inverse of the temperature (**Figure 8.2**). Materials with desirable conductivities for the electro-mechanical actuator applications should have the highest conductivities possible. The monomers with the highest conductivities of the previous acrylates were slightly lower than 10^{-4} S/cm at room

temperature.^{19, 21-22} All the monomers synthesized for this work had conductivities higher than 10^{-4} S/cm at room temperature. The **RM3** sample had the highest room temperature conductivity. This corresponds well with the results obtained by Mr. Terry Price for similar difunctional imidazolium norbornene monomers.

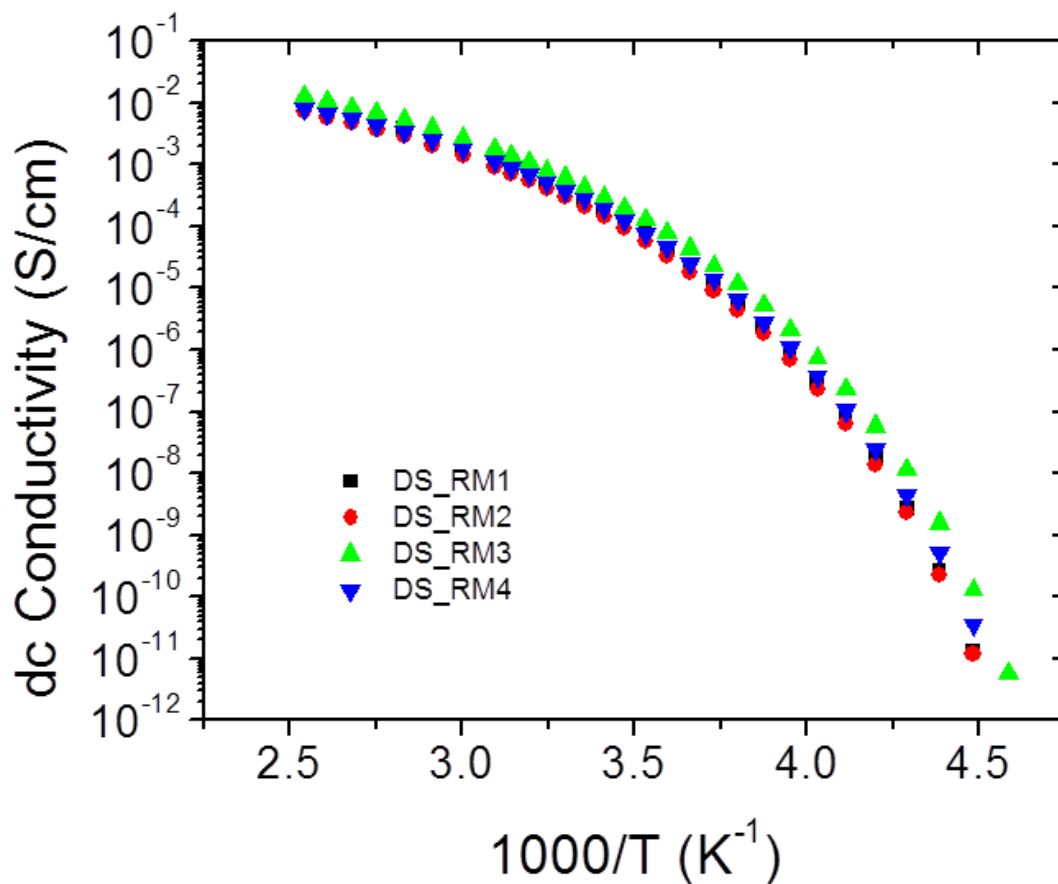


Figure 8.2. DC conductivity vs. inverse temperature for all four monomers.

Synthesis of polymers from the four monomers was accomplished using Grubbs first generation catalyst (GC1). The monomers were dissolved in dichloromethane, degassed, and the catalyst was added in dichloromethane solution. After polymerization, the reaction was quenched using either benzaldehyde or ethyl vinyl ether. All of the resulting polymers were liquids and were

isolated by washing repeatedly with dichloromethane. The polymers were characterized by DSC to determine their T_g values. It is noteworthy and unusual that the polymers had glass transition temperatures similar to their parent monomers. The polymers were also run through the GPC instrument to determine their molecular weight and distribution. Unfortunately as seen in the figure below, using 0.5 % LiBr in NMP as solvent the polymer samples eluted after the monomer samples. This indicates that the solvent system was inadequate and that these polyelectrolytes were interacting with the column material. Consequently, the number average molecular weights for the polymers were calculated from the $^1\text{H NMR}$ spectra of the samples.

Table 8.2. T_g , α_{DC} , and molecular weights of the four polymers shown in Scheme 9.2. $^1\text{H NMR}$ in CD_3CN , 400 MHz. M_n determined by comparison of imidazolium 2H peak and the benzyl end group peaks. Error in M_n values: $\pm 10\%$.

Polymer	R	T_g ($^{\circ}\text{C}$)	M_n (kDa)	α_{DC} @ 25 $^{\circ}\text{C}$ (S/cm)
RP 1	CH_3	-57	45	1.32×10^{-5}
RP 2	$(\text{CH}_2\text{CH}_2\text{O})_3\text{CH}_3$	-65	54	2.12×10^{-5}
RP 3	$(\text{CH}_2\text{CH}_2\text{O})_2\text{CH}_3$	-50	55	2.87×10^{-5}
RP 4	$\text{CH}_2\text{CH}_2\text{OCH}_3$	-56	63	3.05×10^{-5}

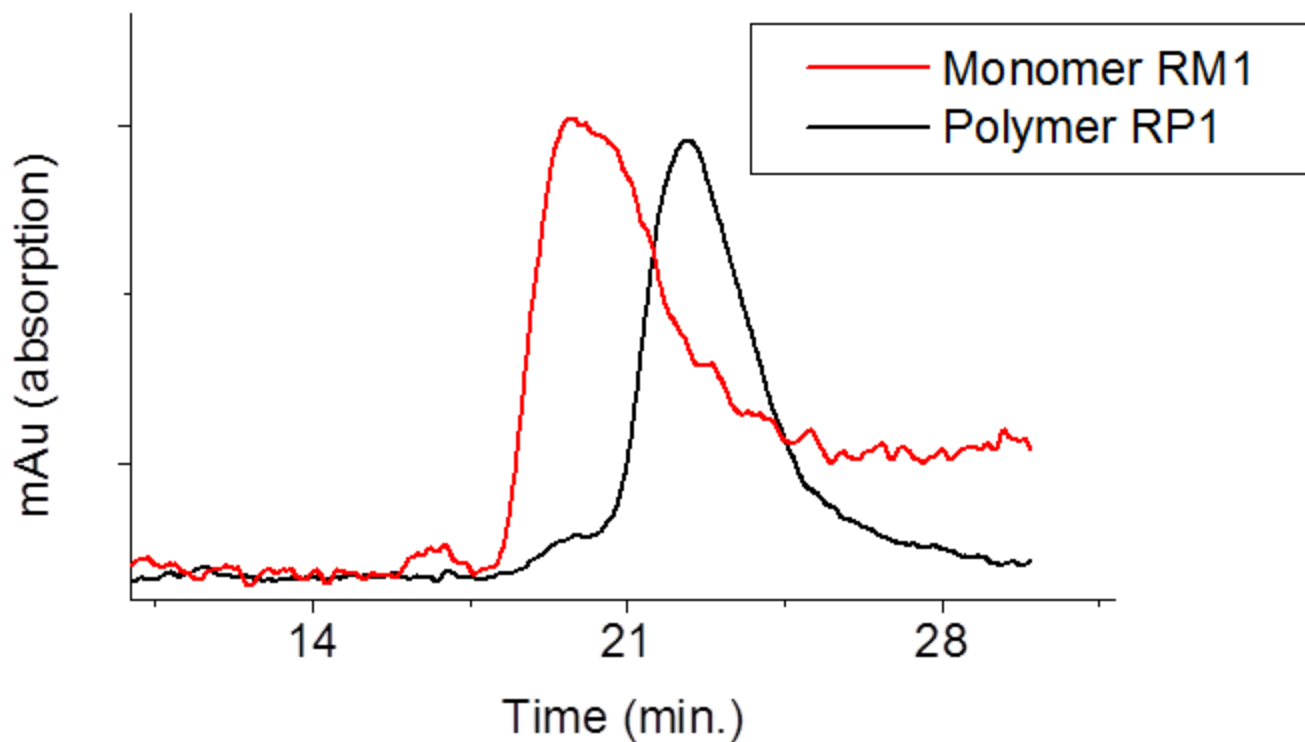


Figure 8.3 Stacked SEC chromatogram showing the relative retention times for monomer **RM1** and polymer **RP1**. The monomer shows less retention than the polymer, indicating that the SEC conditions are not suitable for the polymer.

The conductivity plot for the four samples is shown in Figure 8.4. The room temperature conductivity for all samples decreased from the values measured for the monomers. While all of the monomer samples had conductivities at room temperature near 1×10^{-4} S/cm, the conductivities for the polymer samples were between 1.29×10^{-5} S/cm and approximately 2.85×10^{-5} S/cm. Comparison of the conductivities of these materials to other materials made previously in the group by Dr. Minjae Lee, Dr. Anuj Mital, and Terry Price Jr. show agreement

in the order of magnitude, but while these materials may be good for ROMP polymers, they do not compare favorably to some of the previous acrylate materials.

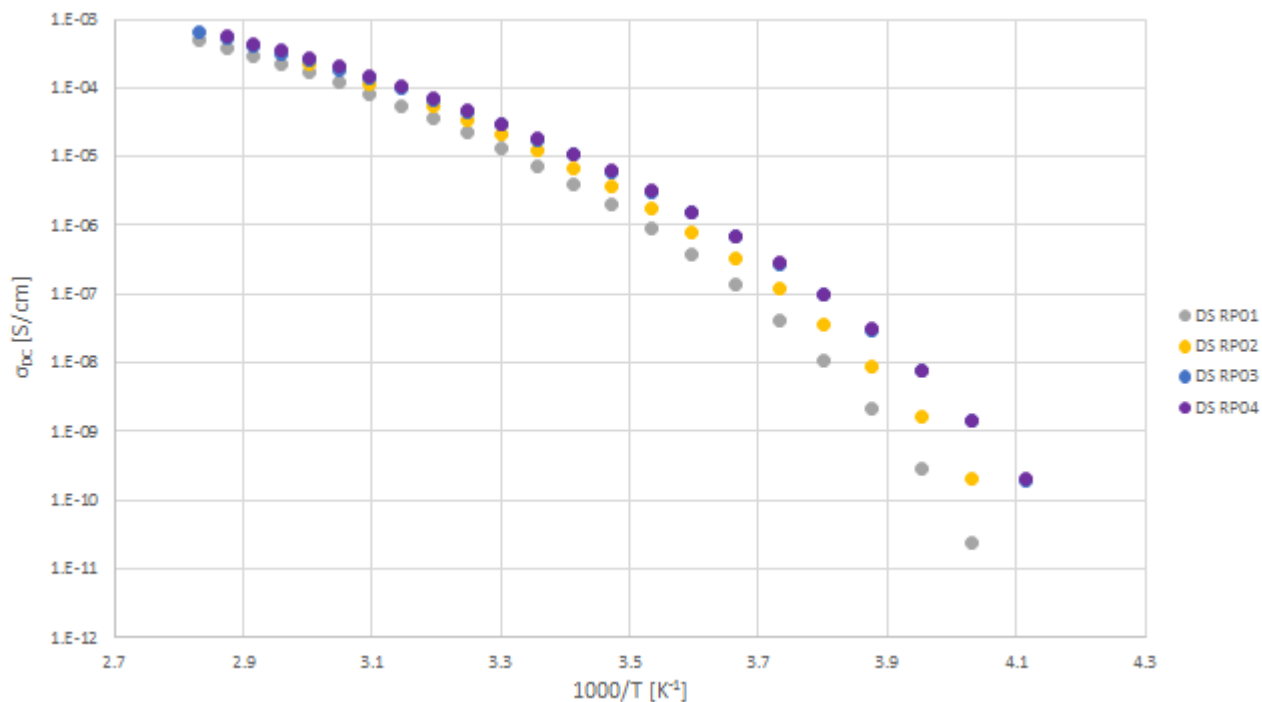


Figure 8.4. DC conductivity α_{DC} plotted against inverse temperature for the four ROMP polymers.

Conclusions

Four different norbornene monomers containing both ethyleneoxy and imidazolium moieties were synthesized and subjected to ROMP polymerization. The monomers and resulting polymers were found to have very low glass transition temperatures. The monomers were characterized by dielectric spectroscopy and determined to have suitably high ionic conductivity. The number average molecular weights of the polymers were calculated by ¹H NMR as the polymers were found to interact with the column material of the SEC. The conductivities of the polymers were similar to other norbornene-based polymers with two imiazolium moieties per repeat unit, but somewhat lower than similar acrylate-based polymers.

Experimental

Instruments

^1H and ^{13}C NMR were gathered using either a 500 MHz Bruker Avance or 400 MHz Varian Unity spectrometer. HRMS spectra were generated using an Agilent 6220 LCMS TOF with ESI in positive ion mode. Conductivity measurements were made using a Novocontrol GmbH Concept 40 dielectric relaxation spectrometer with a frequency range of 100 Hz to 100 MHz and an amplitude of 100 mV. Samples were allowed to flow between two polished brass electrodes (radius 15.0 mm) after being heated to 100 $^{\circ}\text{C}$ under vacuum in order to remove water and other volatile compounds. The electrodes were spaced 50 μm apart by silica spacers that left a space of 20 μm diameter as the active parallel plate capacitor. Conductivity data were collected at discrete temperatures going from high (above T_m) to low (below T_g) over the range of available frequencies. Glass transition temperatures were measured using a TA instruments Q2000 differential scanning calorimeter (DSC) heating and cooling at a rate of 5.0 $^{\circ}\text{C}/\text{min}$.

Chemicals

Chemicals used for preliminary synthesis were purchased in the highest purity grade available and used as received from the manufacturer. Compounds used in subsequent synthesis were purified and described below.

(1R,2S,4R)-bicyclo[2.2.1]hept-5-ene-2-carboxylic acid (M5):

Norbornene carboxylic methyl ester was synthesized from cyclopentadiene and methyl acrylate in dichloromethane. Cyclopentadiene (66 g, 1.0 mol) was cracked from the dimer by heating under reflux, and distilling the product under a temperature of 45 $^{\circ}\text{C}$. Methyl acrylate (86 g, 1.0 mol) was added to the cyclopentadiene. Dichloromethane (200 mL) was added to the solution.

The resulting solution was heated under reflux for 8 h. Dichloromethane and unreacted starting materials were removed under vacuum. The product (145 g, 95 % yield) was a light yellow oil. Methyl (1R,2S,4R)-bicyclo[2.2.1]hept-5-ene-2-carboxylate (50.01 g, 328.6 mmol) was isomerized to increase the *exo* isomer concentration by heating in a solution of 250 mL methanol and 20.12 g (372.6 mmol) of sodium methoxide under reflux. The ester was then slowly hydrolyzed at low temperature by the slow addition of water over 8 h. The slow hydrolysis coupled with the isomerization inverted the isomer mixture from ~80:20 *endo:exo* to ~20:80 *endo:exo*. At this point the two isomers were separated by iodo-lactonization. The acid isomers (45.34 g, 328.6 mmol) were dissolved in 250 mL of an aqueous solution of sodium carbonate (36.26 g, 342.1 mmol), and titrated with approximately 80 mL of an aqueous solution of iodine (20.0 g, 78.8 mmol) and potassium iodide (12.5 g, 75.3 mmol). After lactonization the *endo* isomer was extracted with diethyl ether. The remaining *exo* isomer was acidified and extracted from the aqueous solution with diethyl ether, 35.41 g (71%), mp 36.6–39.0 °C, lit. mp 37–41 °C.³⁴ ¹H NMR (500 MHz, CDCl₃) δ 6.13 (dd, J = 6, 3 Hz, 1H), 6.09 (dd, J = 6, 3 Hz, 1H), 3.14 (s, 1H), 2.97 (s, 1H), 2.30 (ddd, J = 9, 4, 3 Hz, 1H), 2.01 – 1.96 (m, 1H), 1.56 (d, J = 8 Hz, 1H), 1.42 (dd, J = 10, 8 Hz, 1H).

(1R,2S,4R)-2-(2'-(2''-(2'''-(Tosyloxy)ethoxy)ethoxy)ethoxy)ethyl bicyclo[2.2.1]hept-5-ene-2-carboxylate (6)

M5 (10.01 g, 72.45 mmol) was dissolved in approximately 50 mL of thionyl chloride with a small amount of dimethylformamide. Magnesium turnings (2.04 g, 83.9 mmol) were added to the solution. The mixture was stirred for 4 h at room temperature. Excess thionyl chloride was removed under vacuum and the resulting material was extracted with dry dichloromethane, and cooled in an ice bath. Tetra(ethylene glycol) monotosylate³⁵ (12.08 g, 34.67 mmol), and dry

pyridine (5.0 mL 62 mmol) were also dissolved in dry dichloromethane. The tetra(ethylene glycol) mono tosylate solution was added slowly over 30 min to the acid chloride solution. The resulting mixture was stirred at room temperature for 8 h before the product was isolated by aqueous workup. The product was isolated as a light brown liquid (13.97g, 86%). ^1H NMR (400 MHz, CDCl_3) δ 7.78 (d, $J = 8$ Hz, 1H), 7.68 – 7.61 (m, 1H), 7.33 (d, $J = 8$ Hz, 1H), 6.13 (dd, $J = 6, 3$ Hz, 1H), 6.09 (dd, $J = 6, 3$ Hz, 1H), 4.26 – 4.21 (m, 1H), 4.17 – 4.12 (m, 1H), 3.68 (dd, $J = 10, 5$ Hz, 2H), 3.62 (dd, $J = 3, 2$ Hz, 2H), 3.57 (d, $J = 2$ Hz, 2H), 3.15 (s, 1H), 2.96 (t, $J = 25$ Hz, 1H), 2.44 (s, 2H), 2.32 (dd, $J = 10, 4$ Hz, 1H), 2.24 (dd, $J = 10, 4$ Hz, 1H), 1.99 (dt, $J = 12, 4$ Hz, 1H), 1.94 – 1.87 (m, 1H), 1.51 (d, $J = 9$ Hz, 1H), 1.42 (d, $J = 10$ Hz, 1H), 1.34 (d, $J = 8$ Hz, 1H). HRMS: m/z 469.1841 Da = $(M + H)^+$, m/z = 486.2134 Da = $(M + \text{NH}_3)^+$, m/z = 491.1693 Da = $(M + \text{Na})^+$, calcd. for $M = \text{C}_{23}\text{H}_{32}\text{O}_8\text{S}$ m/z 469.1818 Da (Figure 9.5).

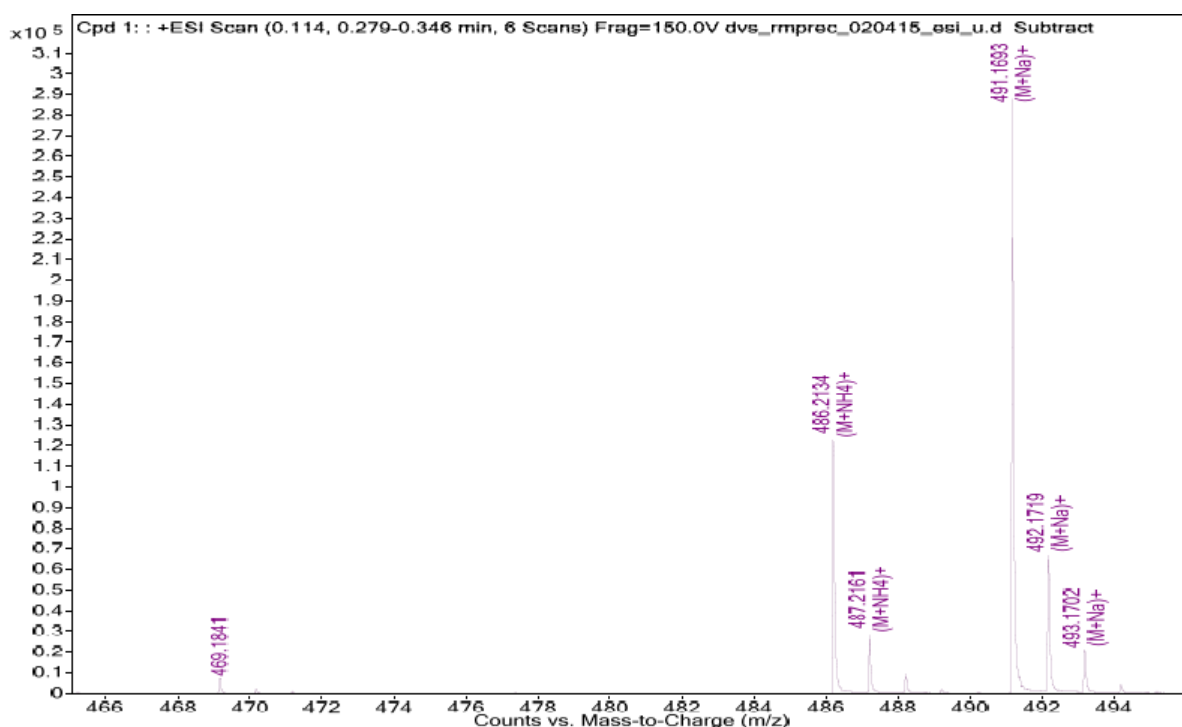


Figure 8.5. HRMS spectrum of (1R,2S,4R)-2-(2'-(2''-(2'''-(Tosyloxy)ethoxy)ethoxy)ethyl bicyclo[2.2.1]hept-5-ene-2-carboxylate (6) monomer precursor.

1-(2'-methoxyethyl)imidazole (M7)

Imidazole (1.36 g, 20 mmol) and sodium hydroxide (0.72 g, 18 mmol) were dissolved in approximately 25 mL of water. 2-Methoxyethyl *p*-toluenesulfonate (2.31 g, 10 mmol) was dissolved in approximately 25 mL of tetrahydrofuran. The two solutions were mixed together, and stirred at room temperature overnight. THF was removed under vacuum and the aqueous mixture was extracted three times with dichloromethane. The combined organic solution was washed twice with 5% aqueous sodium hydroxide. Dichloromethane was removed under vacuum. The resulting product was a yellow oil (1.08 g, 86 %). ¹H NMR (400 MHz, CDCl₃) δ 7.46 (s, 1H), 6.97 (s, 1H), 6.91 (s, 1H), 4.06 – 3.97 (t, J = 5 Hz, 2H), 3.59 – 3.51 (t, J = 6 Hz, 2H), 3.27 (s, 3H). The ¹H NMR spectrum was compared with the literature version.³⁶

1-(2'-(2"-methoxyethoxy)ethyl)imidazole (M8)

This compound was synthesized in the same manner as the one preceding, using the same molar scale. The product was a yellow oil (1.5 g 88 %). ¹H NMR (400 MHz, CDCl₃) δ 7.46 (s, 1H), 6.95 (s, 1H), 6.91 (s, 1H), 4.03 (t, J = 5 Hz, 2H), 3.69 – 3.61 (m, 2H), 3.52 – 3.46 (m, 1H), 3.45 – 3.39 (m, 1H), 3.28 (s, 3H). The ¹H NMR spectrum was compared with the literature version.²²

1-(2'-(2"- (2'''-methoxyethoxy)ethoxy)ethyl)imidazole (M9)

This compound was prepared in the same manner as the preceding two, using the same molar scale. The product was isolated as a yellow oil (1.78 g 83 %). ¹H NMR (400 MHz, CDCl₃) δ 7.48 (s, 1H), 6.96 (s, 1H), 6.93 (s, 1H), 4.04 (t, J = 5.2 Hz, 2H), 3.71 – 3.64 (t, 2H), 3.56 – 3.51 (m, 6H), 3.50 – 3.43 (m, 2H), 3.30 (s, 3H). The ¹H NMR spectrum was compared with the literature version.³⁷

1-(Bicyclo[2.2.1]hept-5'-en-2'-yl)-1''-oxo-2'',5'',8'',11''-tetraoxatridecan-13''-yl)-3-methylimidazolium TFSI (RM1):

M6 (2.34 g, 5 mmol) was added to a round bottom flask equipped with a stir bar. Imidazole (1.36 g, 20 mmol) was added to the flask, and the contents were dissolved in approximately 50 mL of nitromethane. The resulting solution was heated under reflux for 2 days. Nitromethane was removed under vacuum, and the residue was suspended in acetonitrile. The tosyl salt product was isolated using silica gel column chromatography, eluting first with acetonitrile, and then with a mixture of methanol, nitromethane, and 2M aqueous ammonium chloride (7:2:1). The resulting solution was distilled under vacuum to remove as much solvent as possible and the residue was dissolved in a minimum of water. Lithium TFSI salt (2.87 g, 10 mmol) was dissolved in water and added to the aqueous product. The monomer salt was then extracted with dichloromethane. The organic solution was washed three times with 10 % HCl, and dried over sodium sulfate. Finally dichloromethane was removed under vacuum. The resulting product was a brown oil (3.07 g 93 %). HRMS: m/z 379.2227 Da, calcd. for $C_{20}H_{31}N_2O_5$ m/z 379.2235 Da (Figure 9.6). DSC (5.0 °C/min): T_g -55 °C. 1H NMR (500 MHz, CD_3CN) δ 8.56 (s, 1H), 7.45 (t, $J = 2$ Hz, 1H), 7.35 (t, $J = 2$ Hz, 1H), 6.13 (dd, $J = 6, 3$ Hz, 1H), 6.09 (dd, $J = 6, 3$ Hz, 1H), 4.32 – 4.26 (m, 2H), 4.19 (d, $J = 4$ Hz, 2H), 3.86 (s, 4H), 3.84 – 3.77 (m, 2H), 3.66 (s, 2H), 3.64 – 3.56 (m, 10H), 2.93 (s, 1H), 2.25 – 2.16 (m, 2H), 1.92 – 1.84 (m, 1H), 1.49 (d, $J = 10$ Hz, 1H). ^{13}C NMR (101 MHz, CD_3CN) δ 175.63, 138.30, 137.20, 136.01, 123.75, 123.10, 121.49, 118.29, 70.13, 70.08, 69.98, 69.93, 68.75, 68.54, 63.63, 49.17, 46.48, 46.29, 42.86, 41.46, 36.12.

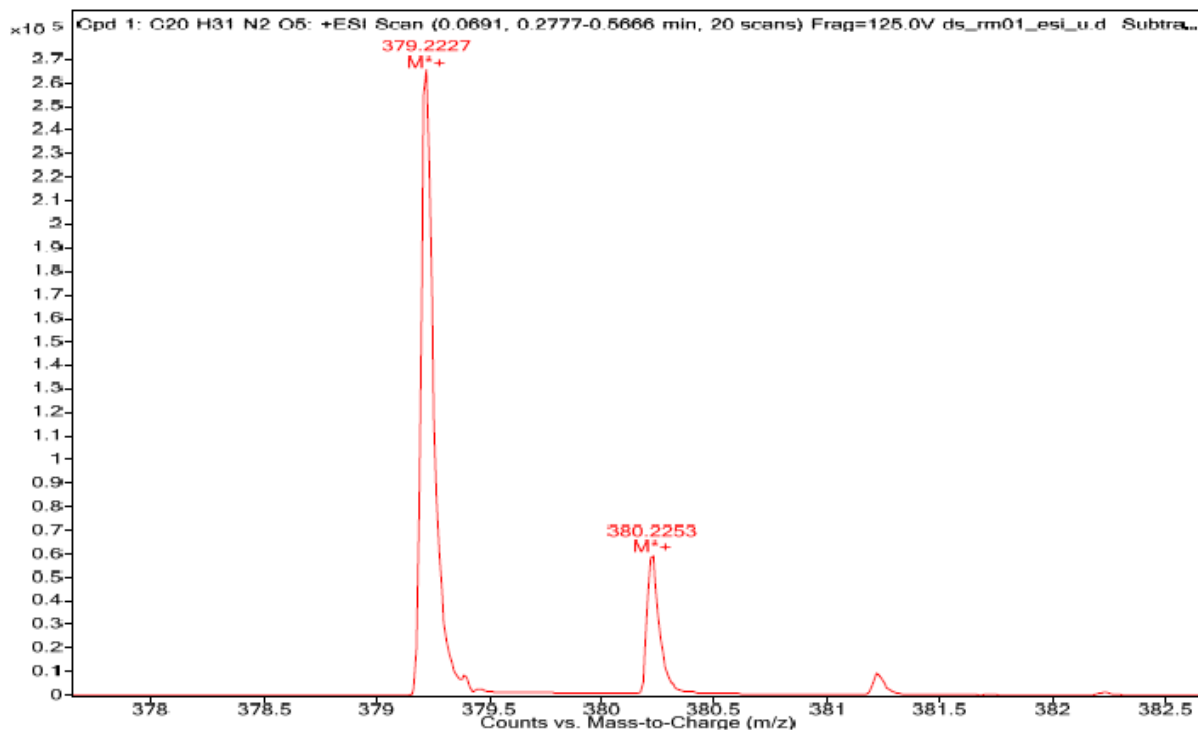


Figure 8.6. HRMS of monomer RM 01.

1-(Bicyclo[2.2.1]hept-5'-en-2'-yl)-1''-oxo-2'',5'',8'',11''-tetraoxatridecan-13''-yl)-3-(2''-methoxyethyl)imidazolium TFSI (RM2):

RM2 was synthesized in the same manner as **RM1** (2.96g, 84%); the final quaternization was accomplished using 1-(2'-methoxyethyl)imidazole. HRMS: m/z 423.2493 Da, calcd. for $C_{22}H_{35}N_2O_6$ m/z 432.2490 Da (Figure 9.7). DSC (5.0 °C/min): T_g -65 °C. 1H NMR (500 MHz, CD_3CN) δ 8.61 (s, 1H), 7.48 (s, 1 H), 7.47 (s, 1 H), 6.13 (dd, $J = 6, 3$ Hz, 1H), 6.09 (dd, $J = 6, 3$ Hz, 1H), 4.39 – 4.26 (m, 6H), 4.20 (d, $J = 4$ Hz, 2H), 3.88 – 3.50 (m, 16H), 3.34 (s, 6H), 3.02 (s, 2H), 2.93 (s, 2H), 2.21 (dd, $J = 8, 4$ Hz, 1H), 1.89 (d, $J = 12$ Hz, 1H), 1.49 (d, $J = 8$ Hz, 1H), 1.35 (dd, $J = 18, 8$ Hz, 2H), 1.23 (t, $J = 8$ Hz, 2H).

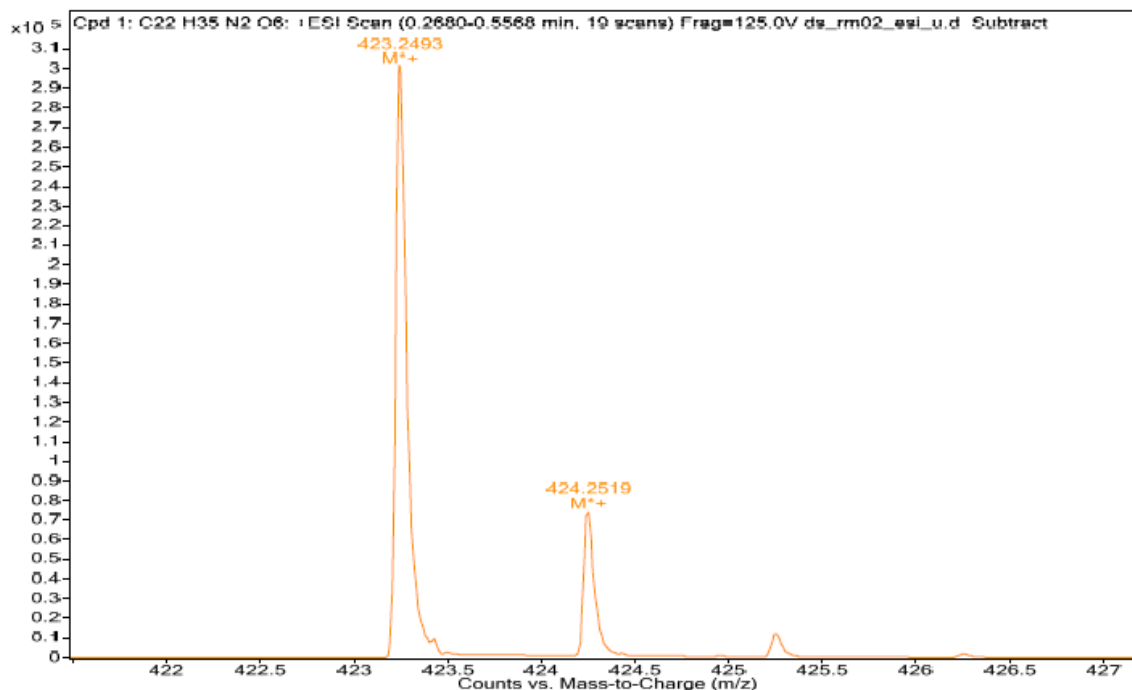


Figure 8.7. HRMS for monomer RM 02.

1-(Bicyclo[2.2.1]hept-5'-en-2'-yl)-1''-oxo-2'',5'',8'',11''-tetraoxatridecan-13''-yl)-3-(2''''-(2''''-methoxyethoxy)ethyl)imidazolium (RM3):

RM3 was synthesized in the same manner as **RM1** (2.92g, 79%); the final quaternization was accomplished using 1-(2'-(2''-ethoxyethyl)methoxy)imidazole. HRMS: m/z 467.2757 Da, calcd. for $C_{24}H_{38}N_2O_7$ m/z 467.2752 Da (Figure 9.8). DSC (5.0 °C/min): T_g -50 °C. 1H NMR (500 MHz, CD_3CN) δ 8.68 (s, 1H), 7.48 (d, $J = 5$ Hz, 2H), 6.13 (dd, $J = 6, 3$ Hz, 1H), 6.09 (dd, $J = 6, 3$ Hz, 1H), 4.36 – 4.28 (m, 4H), 4.20 (dd, $J = 8, 4$ Hz, 2H), 3.86 – 3.79 (m, 4H), 3.70 – 3.47 (m, 18H), 3.32 (s, 3H), 3.02 (s, 1H), 2.93 (s, 1H), 1.49 (d, $J = 8$ Hz, 1H), 1.40 – 1.31 (m, 2H), 1.23 (t, $J = 8$ Hz, 1H).

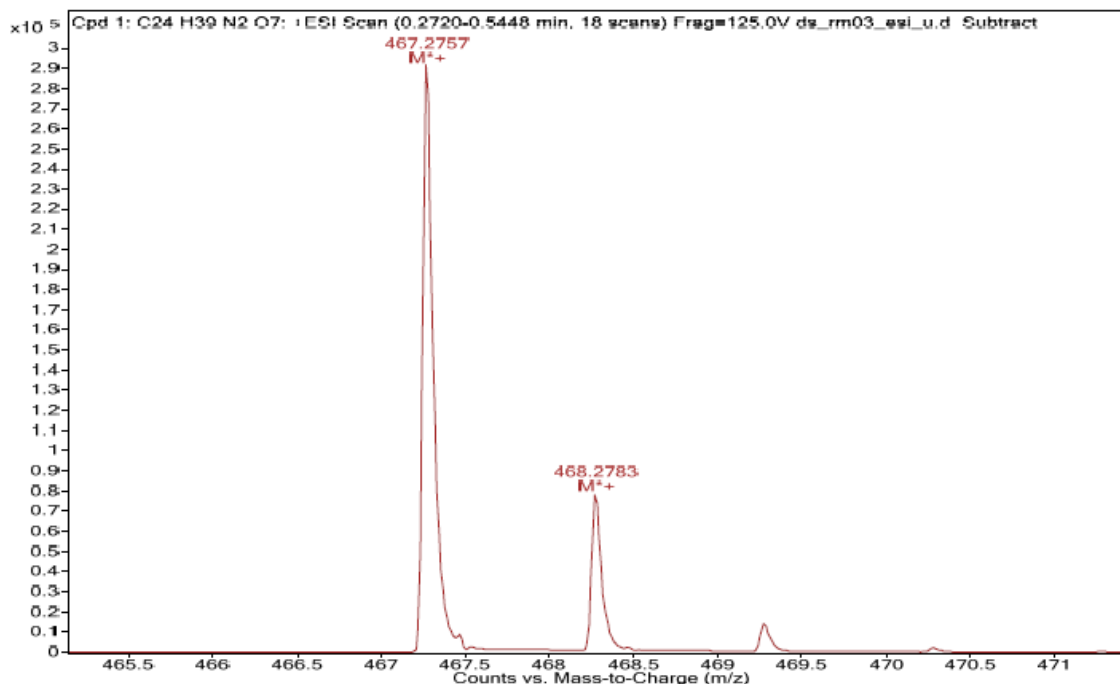


Figure 8.8. HRMS for monomer RM 03.

1-(Bicyclo[2.2.1]hept-5'-en-2'-yl)-1''-oxo-2''',5'',8'',11''-tetraoxatridecan-13''-yl)-3-(2''''-(2''''''-methoxyethoxy)ethoxy)ethyl)imidazolium TFSI (RM4):

RM4 was synthesized and purified in the same manner as **RM1** (2.81g, 71%); the final quaternization was run using 1-(2'- (2''-(2'''-methoxyethoxy)ethoxy)ethyl)imidazole. HRMS: m/z 511.3011 Da, calcd. for C₂₆H₄₃N₂O₈ m/z 511.3014 Da (Figure 9.9). DSC (5.0 °C/min): T_g -56 °C. ¹H NMR (400 MHz, CD₃CN) δ 8.67 (s, 1H), 7.47 (dq, J = 4, 2 Hz, 2H), 6.13 (dd, J = 6, 3 Hz, 1H), 6.09 (dd, J = 6, 3 Hz, 1H), 4.31 (d, J = 5 Hz, 5H), 4.19 (dd, J = 8, 3 Hz, 2H), 3.84 – 3.79 (m, 2H), 3.68 – 3.63 (m, 2H), 3.63 – 3.53 (m, 18H), 3.49 (dd, J = 7, 6 Hz, 3H), 3.31 (s, 4H), 3.01 (s, 1H), 2.92 (s, 1H), 2.26 – 2.14 (m, 1H), 1.87 (dd, J = 10, 6 Hz, 1H), 1.48 (d, J = 8 Hz, 1H), 1.39 – 1.28 (m, 2H).

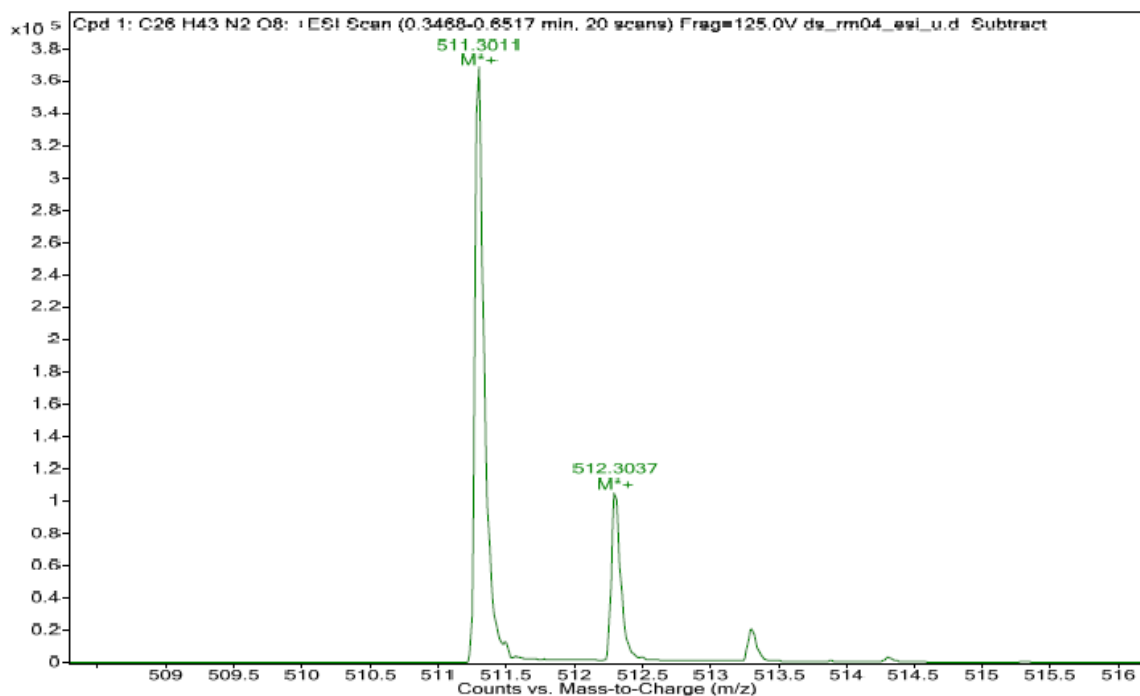


Figure 8.9. HRMS for monomer RM 04.

Polymer RP1 from monomer RM1

Monomer **RM1** (1.0985 g, 1.667 mmol) was dissolved in dry dichloromethane (2.0 mL). Grubbs' first generation catalyst (18.5 mg, 21.9 μ mol) was dissolved in 2.0 mL of dry dichloromethane. The catalyst solution was added quickly to the monomer solution and the resulting solution was allowed to stir for 3 h at room temperature. After stirring the solution separated into two phases. Ethyl vinyl ether (1.0 mL, 10 mmol) was added to quench the reaction. The two phases were separated, and the resulting polymer was washed five times with dichloromethane. Residual solvents and ethyl vinyl ether were removed under vacuum. The polymer product was a dark brown viscous liquid (0.90 g, 82 %). The glass transition temperature was measured by DSC (5.0 $^{\circ}$ C/min) as -57° C. 1 H NMR (400 MHz, acetone- d_6) δ 9.00 (s, 1H), 7.75 (s, 1H), 7.67 (s, 1H), 5.42 (s, 2H), 4.64 – 4.41 (m, 2H), 4.33 – 4.09 (m, 3H),

4.06 (s, 3H), 3.98 – 3.86 (m, 2H), 3.60 (s, 8H), 2.64 (d, J = 61.8 Hz, 1H), 2.04 (dt, J = 4.4, 2.2 Hz, 1H), 1.95 – 1.84 (m, 1H), 1.75 – 1.57 (m, 1H), 1.22 (s, 1H). ¹³C NMR (101 MHz, acetone-d₆) δ 175.04, 137.00, 124.86, 123.47, 123.20, 121.67, 118.47, 70.22, 70.14, 70.08, 70.04, 68.82, 68.47, 63.11, 54.06, 49.60, 47.54, 42.14, 40.99, 35.81. The number average molecular weight (M_n) as measured by ¹H NMR was 45 kDa (comparing the benzyl aromatic peaks to the imidazolium proton peak). Theoretical M_n = 50 kDa.

Polymer RP2 from monomer RM2

Monomer **RM2** was polymerized using the same procedure as **RM1**. The monomer (1.1054 g 1.57 mmol) was polymerized with 18.6 mg (22.6 μmol) of Grubbs first generation catalyst in dry dichloromethane over 3 h. The polymerization was terminated by the addition of ethyl vinyl ether. The resulting polymer phase separated from the solvent and was washed 5x with dichloromethane, and the residual solvent and ethyl vinyl ether were removed under vacuum. The isolated product was a dark brown viscous liquid (0.93 g, 84 %). The glass transition temperature (-65 °C) was measured by DSC. ¹H NMR (400 MHz, acetone-d₆) δ 9.02 (s, 1H), 7.76 (s, 1H), 7.72 (s, 1H), 5.44 (d, J = 8 Hz, 1H), 5.26 (d, J = 8 Hz, 0H), 4.65 – 4.42 (m, 4H), 4.25 – 4.09 (m, 3H), 3.98 – 3.87 (m, 2H), 3.85 – 3.75 (m, 2H), 3.72 – 3.52 (m, 8H), 3.34 (s, 2H), 2.72 (s, 1H), 2.56 (s, 0H), 2.01 (s, 0H), 1.91 (s, 0H), 1.73 – 1.57 (m, 1H), 1.23 (q, J = 11, 10 Hz, 1H). ¹³C NMR (101 MHz, Acetone-d₆) δ 175.07, 136.82, 123.03, 122.72, 121.68, 118.48, 70.26, 70.23, 70.16, 70.15 – 70.14 (m), 70.07, 69.87, 68.82, 68.75, 68.49, 63.11, 58.07, 49.66, 49.61, 49.26, 47.59, 42.16, 41.00, 36.00. The number average molecular weight as calculated by ¹H NMR was 54 kDa. Theoretical M_n = 49 kDa.

Polymer RP3 from monomer RM3

The same general procedure used for the previous polymers was employed for the synthesis of **RP4**. Monomer (1.0923 g, 1.46 mmol) was dissolved in dichloromethane. Initiator GC1, 18.1 mg (22.0 μmol), was also dissolved in dichloromethane. The initiator solution was added to the monomer solution and the reaction mixture was stirred for 3 h. Ethyl vinyl ether was added to the reaction to terminate the polymerization process. The polymer phase separated from the solvent, and was washed five times with dichloromethane. Residual solvent and ethyl vinyl ether were removed under vacuum. The product was a viscous liquid, lighter brown than the previous sample 0.8 g (73 %). The glass transition temperature was $-50\text{ }^{\circ}\text{C}$ (DSC). ^1H NMR (400 MHz, Acetone- d_6) δ 9.04 (s, 1H), 7.76 (s, 1H), 7.74 (s, 1H), 5.39 (s, 1H), 5.27 (s, 0H), 4.58 – 4.47 (m, 5H), 4.24 – 4.10 (m, 3H), 3.91 (dd, $J = 12, 5\text{ Hz}$, 4H), 3.70 – 3.54 (m, 16H), 3.52 – 3.44 (m, 2H), 3.28 (s, 3H), 2.87 (s, 2H), 2.72 (s, 1H), 2.63 – 2.52 (m, 2H), 2.01 (s, 1H), 1.91 (s, 1H), 1.63 (s, 1H), 1.19 (s, 1H). ^{13}C NMR (101 MHz, acetone- d_6) δ 175.07, 136.91, 122.92, 122.79, 121.67, 118.48, 115.28, 71.52, 70.26, 70.23, 70.16, 70.13, 70.08, 69.92, 68.82, 68.51, 68.46, 63.13, 57.94, 49.66, 47.58, 42.19, 40.99, 36.02. The number average molecular weight was calculated from the ^1H NMR in the same manner as the previous samples, and determined to be 55 kDa. Theoretical $M_n = 50\text{ kDa}$.

Polymer RP4 from monomer RM4

Polymer **RP4** was synthesized using the same method as the previous polymers. Monomer **RM4**, 1.1142 g (1.40 mmol), was dissolved in dichloromethane. Initiator GC1, 17.8 mg (21.6 μmol), was also dissolved in dichloromethane. The initiator was quickly added to the monomer and the resulting solution was stirred at room temperature for 3 h. Ethyl vinyl ether was added to quench the reaction. **RP4** did not phase separate well from dichloromethane and consequently was washed with a solution of dichloromethane and chloroform five times. Residual solvent and

ethyl vinyl ether were removed under vacuum. The polymer product was a viscous oil of a slightly lighter brown color than the previous sample, 0.67 g (60 %). The glass transition temperature was determined by DSC as 56 °C. ¹H NMR (400 MHz, acetone-d₆) δ 9.04 (s, 1H), 7.77 (s, 2H), 7.75 (s, 1H), 5.46 (s, 1H), 5.23 (s, 1H), 4.53 (s, 4H), 4.23 – 4.11 (m, 4H), 3.97 – 3.87 (m, 6H), 3.65 (dd, J = 6, 3 Hz, 12H), 3.61 – 3.55 (m, 19H), 3.49 (dd, J = 6, 3 Hz, 3H), 3.29 (s, 3H), 2.73 (s, 1H), 2.57 (s, 2H), 2.02 (s, 0H), 1.92 (s, 1H), 1.74 – 1.61 (m, 2H), 1.28 – 1.17 (m, 2H). ¹³C NMR (101 MHz, acetone-d₆) δ 175.04, 136.91, 124.88, 122.93, 122.84, 121.69, 118.49, 71.69, 70.24, 70.17, 70.14, 70.08, 70.02, 70.00, 68.82, 68.55, 68.46, 63.12, 57.90, 49.62, 49.26, 47.61, 42.19, 41.01, 36.04. The molecular weight was calculated from the ¹H NMR spectrum as previously: 63 kDa. Theoretical M_n = 51 kDa.

References

1. Ohno, H.; Yoshizawa-Fujita, M., *Electrochemical Aspects of Ionic Liquids (2nd Edition)* **2011**, 419-431.
2. Armand, M. B.; Bruce, P. G.; Forsyth, M.; Scrosati, B.; Wieczorek, W., *Energy Materials* **2011**, 1-31.
3. Green, M. D.; Long, T. E., *Polymer Reviews (Philadelphia, PA, United States)* **2009**, *49*, 291-314.
4. Singh, V. V.; Nigam, A. K.; Batra, A.; Boopathi, M.; Singh, B.; Vijayaraghavan, R., *International Journal of Electrochemistry* **2012**, 165683, 19 pp.
5. Meziane, R.; Bonnet, J.-P.; Courty, M.; Djellab, K.; Armand, M., *Electrochimica Acta* **2011**, *57*, 14-19.
6. Shaplov, A. S.; Vlasov, P. S.; Armand, M.; Lozinskaya, E. I.; Ponkratov, D. O.; Malyshkina, I. A.; Vidal, F.; Okatova, O. V.; Pavlov, G. M.; Wandrey, C.; Godovikov, I. A.; Vygodskii, Y. S., *Polymer Chemistry* **2011**, *2*, 2609-2618.
7. Zook, L. A.; Leddy, J., *Analytical Chemistry* **1996**, *68*, 3793-3796.
8. Gibson, H. W.; Lee, M.; Choi, U. H.; Colby, R. H.; Salsa-de la Cruz, D.; Winey, K. I.; Aitken, B.; Wagener, K. B.; Schoonover, D.; Niu, Z., *Polymer Preprints (American Chemical Society, Division of Polymer Chemistry)* **2010**, *51*, 179.
9. Hanabusa, K., *Electrochemical Aspects of Ionic Liquids (2nd Edition)* **2011**, 395-401.

10. Awadalla, E. A., *Experimental and Toxicologic Pathology* **2012**, *64*, 431-434.
11. Goldman, S. M.; Kamel, F.; Ross, G. W.; Bhudhikanok, G. S.; Hoppin, J. A.; Korell, M.; Marras, C.; Meng, C.; Umbach, D. M.; Kasten, M.; Chade, A. R.; Comyns, K.; Richards, M. B.; Sandler, D. P.; Blair, A.; Langston, J. W.; Tanner, C. M., *Movement Disorders* **2012**, *27*, 1652-1658.
12. Brent, J.; Schaeffer, T. H., *Journal of Occupational and Environmental Medicine* **2011**, *53*, 1332-1336.
13. Kobayashi, S.; Kuwata, K.; Sugimoto, T.; Igarashi, K.; Osaki, M.; Okada, F.; Fujii, J.; Bannai, S.; Sato, H., *Free Radical Biology & Medicine* **2012**, *53*, 2197-2203.
14. Galluzzi, M.; Zhang, S.; Mohamadi, S.; Vakurov, A.; Podesta, A.; Nelson, A., *Langmuir* **2013**, *29*, 6573-6581.
15. Radosevic, K.; Cvjetko, M.; Kopjar, N.; Novak, R.; Dumic, J.; Sreck, V. G., *Ecotoxicology and Environmental Safety* **2013**, *92*, 112-118.
16. Ventura, S. P. M.; Goncalves, A. M. M.; Sintra, T.; Pereira, J. L.; Goncalves, F.; Coutinho, J. A. P., *Ecotoxicology* **2013**, *22*, 1-12.
17. Ventura, S. P. M.; Gurbisz, M.; Ghavre, M.; Ferreira, F. M. M.; Goncalves, F.; Beadham, I.; Quilty, B.; Coutinho, J. A. P.; Gathergood, N., *ACS Sustainable Chemistry & Engineering* **2013**, *1*, 393-402.
18. Pereiro, A. B.; Araujo, J. M. M.; Martinho, S.; Alves, F.; Nunes, S.; Matias, A.; Duarte, C. M. M.; Rebelo, L. P. N.; Marrucho, I. M., *ACS Sustainable Chemistry & Engineering* **2013**, *1*, 427-439.
19. Mittal, A.; Gibson, H. W.; Lee, M.; Choi, U. H.; Colby, R. H.; Salas-de la Cruz, D.; Winey, K. I., *Polymer Preprints (American Chemical Society, Division of Polymer Chemistry)* **2011**, *52*, No pp given.
20. Lee, M.; Choi, U. H.; Salas-de la Cruz, D.; Mittal, A.; Winey, K. I.; Colby, R. H.; Gibson, H. W., *Advanced Functional Materials* **2011**, *21*, 708-717.
21. Lee, M.; Choi, U. H.; Colby, R.; Gibson, H. W., *Polymer Preprints (American Chemical Society, Division of Polymer Chemistry)* **2009**, *50*, 624-625.
22. Lee, M.; Choi, U. H.; Colby, R. H.; Gibson, H. W., *Chemistry of Materials* **2010**, *22*, 5814-5822.
23. Lee, M.; Niu, Z.; Slebodnick, C.; Gibson, H. W., *Journal of Physical Chemistry B* **2010**, *114*, 7312-7319.
24. Aitken, B. S.; Lee, M.; Hunley, M. T.; Gibson, H. W.; Wagener, K. B., *Macromolecules (Washington, DC, United States)* **2010**, *43*, 1699-1701.
25. Boyd, T. J.; Schrock, R. R., *Macromolecules* **1999**, *32*, 6608-6618.

26. Santiago, A. A.; Vargas, J.; Cruz-Gomez, J.; Tlenkopatchev, M. A.; Gavino, R.; Lopez-Gonzalez, M.; Riande, E., *Polymer* **2011**, *52*, 4208-4220.
27. Santiago, A. A.; Vargas, J.; Cruz-Morales, J. A.; Tlenkopatchev, M. A.; Gavino, R.; Malkanduev, Y. A.; Sivov, N. A., *Open Journal of Organic Polymer Materials* **2014**, *4*, 84-91, 9 pp.
28. Suga, T.; Sakata, M.; Aoki, K.; Nishide, H., *ACS Macro Letters* **2014**, *3*, 703-707.
29. Wiesenauer, E. F.; Nguyen, P. T.; Newell, B. S.; Bailey, T. S.; Noble, R. D.; Gin, D. L., *Soft Matter* **2013**, *9*, 7923-7927.
30. Pollino, J. M.; Stubbs, L. P.; Weck, M., *Macromolecules* **2003**, *36*, 2230-2234.
31. Price, T. L., Jr.; Choi, U. H.; Wang, D.; Arunachalam, M.; Schoonover, D. V.; Zhang, M.; Colby, R. H.; Heflin, J. R.; Moore, R. B.; Gibson, H. W., *Abstracts of Papers, 245th ACS National Meeting & Exposition, New Orleans, LA, United States, April 7-11, 2013* **2013**, PMSE-575.
32. Gibson, H. W.; Lee, M.; Choi, U. H.; Colby, R. H.; Salas-de la Cruz, D.; Winey, K. I.; Aitken, B.; Wagener, K. B.; Schoonover, D.; Niu, Z., *Polymer Preprints (American Chemical Society, Division of Polymer Chemistry)* **2010**, *51*, 274-275.
33. Kanao, M.; Otake, A.; Tsuchiya, K.; Ogino, K., *International Journal of Organic Chemistry* **2012**, *2*, 26-30.
34. Krapcho, A. P.; Dundulis, E. A., *Journal of Organic Chemistry* **1980**, *45*, 3236-45.
35. Park, K. D.; Liu, R.; Kohn, H., *Chemistry & Biology (Cambridge, MA, United States)* **2009**, *16*, 763-772.
36. Lazaro, G.; Iglesias, M.; Fernandez-Alvarez, F. J.; Sanz Miguel, P. J.; Perez-Torrente, J. J.; Oro, L. A., *ChemCatChem* **2013**, *5*, 1133-1141.
37. Yang, Z.-Z.; He, L.-N., *Beilstein Journal of Organic Chemistry* **2014**, *10*, 1959-1966, 8 pp.

Chapter 9

Removal of Tosyl Chloride from Solution Using Cellulosic Materials

Abstract

Tosyl chloride was used as an excess reagent in the tosylation of several hydroxide containing substrates. The excess reagent was removed by reacting it with the hydroxyl moieties on cellulosic materials before filtration. This method of purification is quick and easily achieved.

Introduction



Scheme 9.1. Method for removal of TsCl from reaction solutions using cellulose and organic base.

Tosylation of hydroxyl-functionalized substrates with tosyl chloride is a popular method of preparing substrates for nucleophilic substitution.¹ There are several reasons that tosylation is preferable to analogous halogenation reactions. Beyond simply avoiding the use of halogenated substrates, tosylation facilitates purification by adding significant molecular weight to the product (155 Daltons). Tosylation is a simple and fast reaction compatible with several types of hydroxyl-functionalized substrates. Traditionally, the reaction is run in solution with a weak base such as pyridine or triethylamine. A popular method in our lab is tosylation using solid potassium carbonate and no solvent as described by Kazemi et al.² Tosyl chloride is usually used in excess compared to the hydroxyl-containing substrate, particularly if the substrate is

precious. Thus, the resulting reaction mixtures contain excess tosyl chloride, which must be removed during purification. Most methods of removal of tosyl chloride have some kind of drawback. Tosyl chloride is soluble in hexanes; thus, it can be extracted by washing with hexanes, but this method is limited to products that are immiscible with hexanes. Chromatography is widely used, but it is slow and costly in terms of materials and time. Tosyl chloride can also be removed by its reaction with primary or secondary amines.² In this case the tosyl amides must be removed from solution. Finally tosyl chloride can be removed from solution by its reaction with a second excess hydroxyl source in the presence of a base. The second alcohol is tosylated and then removed from the solution. This last method is simple and straightforward; however, it may require the use of a strong base, such as potassium hydroxide. Thus, it is unsuitable for use with substrates that are sensitive to strong bases. This last method of removal was interesting to us as it demonstrated that tosyl chloride could be reacted to completion using a second removable hydroxyl source.

An early paper shows that tosyl chloride will react with cellulose under mild conditions in the presence of a base.³ There are many papers dealing with the tosylation of cellulose in solution. Tosylated cellulose has been used to generate many different substituted cellulose polymers.⁴⁻⁷ Similar to other reactions of cellulose, the tosylation reaction is never entirely complete, and a concern of those working with such derivatives is the degree of substitution that can be achieved.⁸ There are also reactions such as the nitration of cellulose which occur on the undissolved cellulose substrate.^{3,9} Tosylation can also be accomplished on undissolved cellulose, and thus the excess reagent from tosylation reactions can be immobilized and subsequently removed from solution. Therefore, we undertook this work to determine if tosyl chloride could be removed from reaction mixtures by reaction with an insoluble cellulose support and then

mechanically removed by filtration. Initial experiments demonstrated that tosyl chloride easily reacts with untreated filter paper under proper conditions. Subsequent experiments determined that multiple sources of cellulose were useful in this method. And finally a series of different hydroxyl-functionalized substrates, both alcohols and phenols, were tosylated and purified using this method.

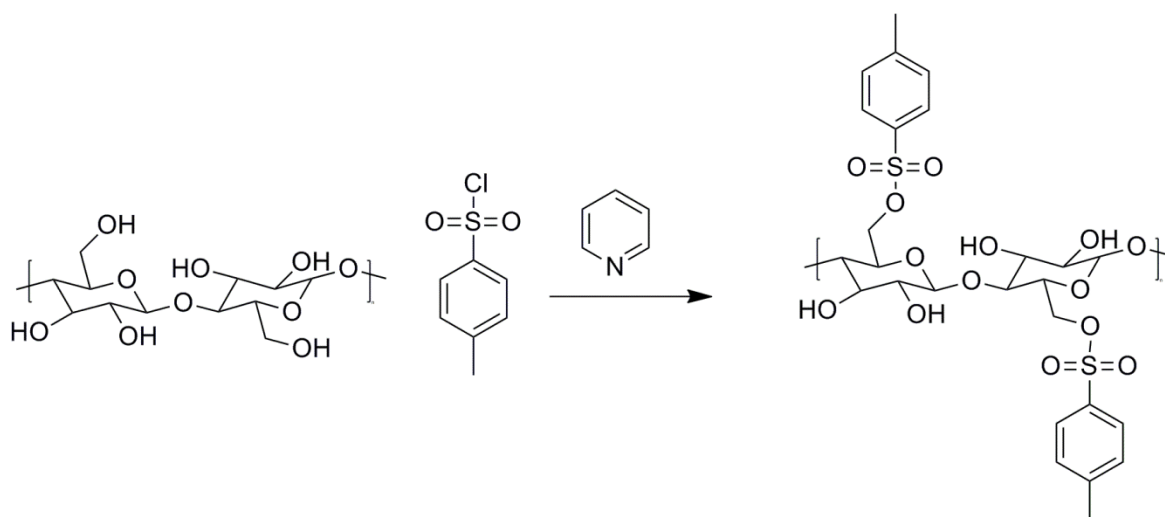
Results and Discussion

A. Effect of Stoichiometry of Cellulose and Pyridine

The preliminary experiments for this work hinged upon finding the proper conditions for removal of tosyl chloride from solution using cellulose and a weak base. Pyridine was chosen as the base due to its nearly ubiquitous use in tosylation reactions. The cellulose source was standard qualitative grade laboratory filter paper, which is universally available in the wet chemistry lab. A stock solution of tosyl chloride was made in dichloromethane (100 mM). Anthracene was added to the tosyl chloride solution as an internal standard (10 mM). Aliquots of the stock solution were treated with variable amounts of pyridine and cellulose. The initial experiments were done with filter paper cut into small pieces. In an effort to hasten the purification reaction, the aliquots were placed in an ultrasonic cleaning bath for one hour. Ultrasonic radiation has been shown to facilitate the interaction of solutions and solid surfaces.¹⁰⁻

¹¹ After sonication, the samples were washed with aqueous hydrochloric acid and characterized by ¹H NMR. The amount of tosyl chloride was determined by comparison to the amount of anthracene. The results of these experiments are shown in Table 9.1 and Table 9.2. Table 9.1 shows that the amount of pyridine used in the tosyl chloride removal process is important. It has been shown in previous papers that there should be a large excess of pyridine present during tosylation reactions. Here we show that more than 5 and preferably 10 equivalents of pyridine,

compared to tosyl chloride, are required for the complete reaction. In Table 9.1 an excess of pyridine was used and the cellulose component was varied to determine its importance. In all of the solutions, tosyl chloride was almost completely removed. The cellulose polymer chain which is comprised of anhydroglucose units contains six hydroxyl moieties per repeat unit. The two primary hydroxyl moieties are the more reactive, but the secondary moieties are also reactive under these conditions. These initial experiments show that with a proper excess of pyridine present, as little as 320 grams of cellulose per mole of tosyl chloride will completely remove the tosyl chloride from solution. Figure 9.1 shows a stacked ^1H NMR spectrum from before and after the reaction with pyridine and cellulose.



Scheme 9.2. Reaction of TsCl with cellulose in the presence of pyridine. Primary hydroxyl moieties are more reactive, but secondary hydroxyls also react.

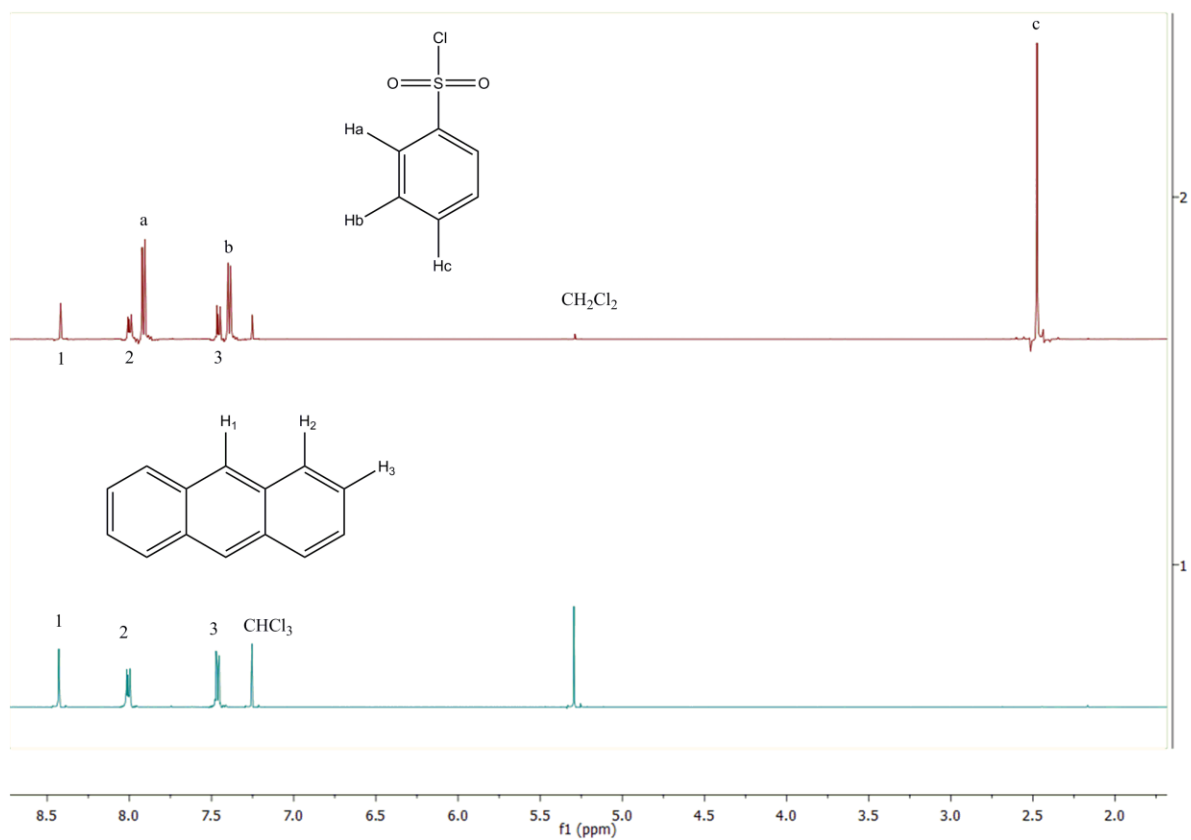


Figure 9.1. Stacked ¹H NMR plot showing a mixture (1:10) of anthracene and tosyl chloride (top red spectrum) and the nearly complete removal of tosyl chloride from anthracene (bottom blue spectrum) after sonication with pyridine and cellulose (filter paper). ¹H NMR CDCl₃ 500 MHz

Table 9.1. Primary hydroxyl content effect on tosyl chloride removal. Equivalents are based upon the anhydroglucose repeat unit. Initial tosyl chloride and anthracene concentrations 100 and 10 mM respectively.

Eq. 1 ^o OH in cellulose	Eq. pyridine	Residual TsCl (mol %)
2	21	Trace (0.19 %)
5.2	21	Trace (0.12 %)
10	21	Trace (0.16 %)
21	21	Trace (0.12 %)

Table 9.2. Pyridine content effect on removal of tosyl chloride from solution. Hydroxyl equivalents are based on anhydroglucose repeat unit. Initial tosyl chloride and anthracene concentrations 100 and 10 mM respectively.

Eq. 1 ^o OH in cellulose	Eq. pyridine	Residual TsCl (mol %)
13	2.2	41 %
13	4.5	4.3 %
13	9	Trace (0.16 %)
13	13	Trace (0.16 %)

In a second set of experiments, the different types of cellulose were tested to determine what materials were best suited for the purification method. In this study, only two equivalents

of pyridine were used so that the relative amount of tosyl chloride removed from solution could more easily be determined. Four different sources of cellulosic material were tested, including filter paper, semi-crystalline cellulose powder, cotton and starch. Solutions were shaken with the cellulosic material for eight hours, and then washed with aqueous hydrochloric acid before being characterized by ^1H NMR. The results of these experiments are given in Table 9.3. The amount of tosyl chloride removed with filter paper was 37 %. This was followed by starch (41%) and then cellulose powder (30%). We initially predicted that the cellulose powder would give the best results, but this was not the case. This is probably due to the semi-crystalline nature of the powdered cellulose. Finally, with nearly no change in the tosyl chloride concentration after purification (4% removal), cotton fibers seem to be unusable for this purpose. Again the high level of crystallinity in the cellulose cotton fibers is probably the cause of this ineffectiveness. The low cost of the first three materials makes them ideal for this application, and the measured amount of tosyl chloride removed by each is similar. Filter paper was primarily used in this work due to its availability and low cost. Cellulose powder is a bit less effective at removing tosyl chloride, and may not be on hand in most laboratories. Starch (food grade corn starch) was measured to have the highest uptake of tosyl chloride, and is probably the least expensive alternative; however, it tends to form a gel like substance and stick to glassware during filtering.

Table 9.3. Tosyl chloride removal by different types of cellulosic materials. Initial tosyl chloride and anthracene concentrations 100 and 10 mM respectively.

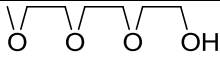
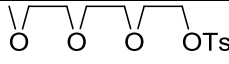
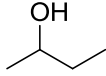
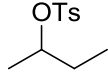
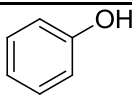
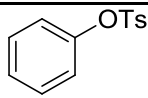
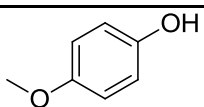
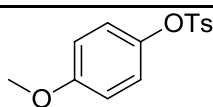
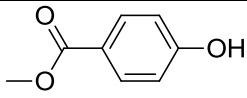
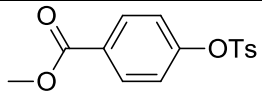
Cellulose source	Base	Residual tosyl chloride
Filter paper	Pyridine (2.2 Eq)	63%
Cellulose powder	Pyridine (2.2 Eq)	70%
Starch	Pyridine (2.2 Eq)	59%
Cotton	Pyridine (2.2 Eq)	96%

B. Application to Tosylation Reactions

Finally, a series of tosylation reactions were run, and the resulting reaction mixtures were purified using the sonication method. Both primary and secondary alcohols were used, as well as a number of phenols. Originally the tosylation employed grinding the alcohol or phenol with 1.5 equivalents of tosyl chloride in the presence of potassium carbonate. For secondary alcohols, potassium hydroxide was also added. This method was published by Kazemi et al.² and it is fast and efficient. A similar method for phenols, published by Xu et al.,¹² employed microwave irradiation. This method was less successful for us, but we found that the use of a hot mortar and pestle caused the reaction to proceed nicely. After tosylation the reaction mixtures were treated with pyridine and filter paper, and then sonicated for one hour. After aqueous acid workup, the compounds were characterized by ¹H NMR to determine their identity and purity. The results of both studies are given below in Table 4. Eventually though, all tosylations were done in a solution of dichloromethane with an excess of pyridine. This allowed the simple addition of filter paper and sonication to precede the aqueous workup steps and streamline the process. This

method is also more widely applicable than the grinding method as it does not depend on the melting of a mixture of alcohol and tosyl chloride.

Table 9.4. Alcoholic and phenolic materials tosylated by different methods and purified using pyridine and cellulose for the removal of tosyl chloride.

Starting Material	Product	Yield (%)	TsCl Visible in ^1H NMR?
		89	No
		87	No
		90	No
		85	No
		86	No

CONCLUSIONS

Treatment of tosylation reaction mixtures with pyridine and cellulose, in the form of filter paper, is a gentle and efficient method for the removal of excess tosyl chloride. The method can be accelerated by the use of sonication.

EXPERIMENTAL

Instrumentation

^1H NMR analysis was performed using a Bruker Avance 500 MHz instrument. Sonication of samples was accomplished using a Fisher Scientific ultrasonic cleaning bath model FS60 with an output of 100 W and a frequency of 42 kHz.

General procedure for tosyl chloride removal studies (Tables 1 and 2)

A 0.100 M solution of tosyl chloride and 0.01 M anthracene concentration (as an internal standard) was made in dichloromethane. To a 10.0 mL aliquot was added the required amount of pyridine, and cellulose (filter paper or other source). The mixture was shaken or stirred for 3 h depending on the type of cellulose; cotton containing samples could not be stirred and were thus shaken in a mechanical devise. After the reactions were complete, the mixtures were filtered to remove the cellulosic material. The dichloromethane solutions were then washed with 10 % aqueous hydrochloric acid, dried over sodium sulfate, and decanted. Solvent was removed from the filtrate by rotary evaporation. The composition of the residue was examined by ^1H NMR in CDCl_3 . The amount of tosyl chloride present in the residue was evaluated by comparing the integrated peak area for the doublet at 7.90 ppm to the area of the anthracene double of doublets at 7.99 ppm.

General procedure for the tosylation of alcohols

Pyridine (4.0 mL, 50 mmol) was added to a test tube with 2 mmol of alcohol and 3 mmol or more of tosyl chloride. The mixture was dissolved in 2.0 mL of dichloromethane and allowed to sit for 3 h at room temperature. Filter paper (0.32 g, two 5.5 cm circles) was added to the

solutions along with 8.0 mL of dichloromethane. The mixture was sonicated for 1 h. The solution was decanted into a separatory funnel and the filter paper and test tube were rinsed with a further 10 mL of dichloromethane. The resulting solution was washed 4 times with 10.0 mL of 10 % aqueous hydrochloric acid. The solution was dried over sodium sulfate and the solvent was removed by rotary evaporation in a tare weighed vial.

Tosylation of tri(ethylene glycol) monomethyl ether

Triethylene glycol monomethyl ether (0.34 g, 2.0 mmol) was added to a test tube along with 0.87 g (4.6 mmol) of tosyl chloride and dissolved in 2.0 mL of dichloromethane. Pyridine (4.0 mL, 50 mmol) was added to the solution, which immediately turned deep yellow. After swirling for 2 min, the solution was allowed to sit at room temperature for 3 h. Filter paper, 3.2 g (20 mmol of total hydroxyl groups), and a further 8.0 mL of dichloromethane were added. The solution was sonicated for 1 h until the color faded. The organic solution was washed 4 times with 10.0 mL of 10 % aqueous hydrochloric acid. The organic phase was dried over sodium sulfate, and the dichloromethane was removed via rotovap. The product was a yellow oil, 0.57 g (90 %), which was characterized by NMR. ^1H NMR (400 MHz, CDCl_3) δ 7.8 (d, $J = 8$ Hz, 2H), 7.3 (d, $J = 8$ Hz, 2H), 4.2 – 4.1 (t, 2H), 3.7 – 3.7 (t, 2H), 3.6 – 3.6 (m, 6H), 3.6 – 3.5 (t, 2H), 3.4 (s, 3H), 2.4 (s, 3H). ^{13}C NMR (101 MHz, CDCl_3) δ 144.73, 132.98, 129.76, 127.93, 71.86, 70.70, 70.52, 70.50, 69.19, 68.63, 58.98, 21.59 . NMR spectra compared favorably with those in the literature.¹³

Tosylation of 2-butanol

2-Butanol (0.18 g, 2.4 mmol), tosyl chloride (0.91 g 4.8 mmol) and pyridine (4.0 mL, 50 mmol) were placed in a test tube and dissolved in 2.0 mL of dichloromethane. The resulting solution was swirled for 2 min and allowed to stand at room temperature for 3 h. Two circles of filter

paper (0.32 g, 20 mmol primary hydroxyl content) were torn into strips and added to the solution. The resulting mixture was sonicated for 1 h. The organic solution was decanted and then washed 4 times with 10.0 mL of 10 % aqueous hydrochloric acid. Dichloromethane was removed under reduced pressure. The product, 0.48 g (87 %), was a light yellow oil and was characterized by NMR. ^1H NMR (400 MHz, CDCl_3) δ 7.79 (d, $J = 8$ Hz, 2H), 7.33 (d, $J = 8$ Hz, 2H), 4.57 (m, 1H), 2.44 (s, 3H), 1.62 (m, 2H), 1.25 (t, $J = 6$ Hz, 3H), 0.91 – 0.69 (t, 1H). ^{13}C NMR (101 MHz, CDCl_3) δ 144.35, 134.55, 129.64, 127.62, 81.74, 29.42, 21.56, 20.24, 9.24. NMR spectra compared favorably with those in the literature.¹⁴

Tosylation of phenol

Phenol (0.20 g, 2.1 mmol), tosyl chloride (0.73 g, 3.8 mmol) and 4.0 mL (50 mmol) of pyridine were dissolved in 2.0 mL of dichloromethane in a test tube. The resulting solution was swirled for 2 min and allowed to sit at room temperature for 3 hours. Two circles of filter paper (0.32 g, 20 mmol of total hydroxyl groups) and 8.0 mL of dichloromethane were added to the solution and the mixture was sonicated for 1 h. The resulting mixture was filtered, and the filtrate was washed 4 times with 10.0 ml of 10 % aqueous hydrochloric acid. Dichloromethane was removed by rotary evaporation. The product, 0.46 g (90 %), mp 92.5-93.8 $^{\circ}\text{C}$ (lit. 93-94 $^{\circ}\text{C}$)¹⁵ was characterized by NMR. NMR (400 MHz, CDCl_3) δ 7.70 (d, $J = 8$ Hz, 2H), 7.34 – 7.14 (m, 5H), 6.98 (d, $J = 8$ Hz, 2H), 2.44 (s, 3H). ^{13}C NMR (101 MHz, CDCl_3) δ 149.62, 145.28, 132.39, 129.69, 129.55, 128.48, 122.35, 115.24, 21.68. NMR spectra compared favorably with those in the literature.¹⁶

Tosylation of methyl *p*-hydroxybenzoate

Methyl *p*-hydroxybenzoate (0.30 g, 2.0 mmol) was dissolved in dichloromethane (2.0 mL). Pyridine (4.0 mL, 50 mmol) and tosyl chloride (0.87 g, 3.8 mmol) were added. The

resulting solution was held at room temperature for 3 h. Filter paper (0.32 g, 24 mmol based on primary hydroxyl content) was added to the solution along with a further 8.0 mL of dichloromethane. The mixture was placed in an ultrasonic cleaning bath for 1 h, and filtered to remove cellulosic material. The filtrate was washed 4 times with 10.0 mL of 10 % hydrochloric acid. Dichloromethane was removed by rotary evaporation and the resulting solid, 0.53 g (86%), mp 87.6-88.5 °C (lit. 88-89 °C)¹⁷ was characterized by ¹H NMR. ¹H NMR (400 MHz, CDCl₃) δ 7.98 (d, J = 8 Hz, 2H), 7.70 (d, J = 8 Hz, 2H), 7.32 (d, J = 8 Hz, 2H), 7.06 (d, J = 8 Hz, 2H), 3.90 (s, 3H), 2.45 (s, 3H). ¹³C NMR (101 MHz, CDCl₃) δ 165.96, 159.57, 152.93, 145.67, 131.26, 129.84, 128.46, 122.30, 52.31, 21.70 . NMR spectra compared favorably with those in the literature.¹⁷

Tosylation of *p*-methoxyphenol

Pyridine (2.0 mL, 25 mmol), 0.27 g (2.2 mmol) of *p*-methoxyphenol, and 0.70 g (3.7 mmol) of tosyl chloride were added to a test tube. The mixture dissolved in 2.0 mL of dichloromethane and swirled for 2 min. The solution was allowed to sit a room temperature for 3 h. Cellulose (0.32 g, 20 mmol of total hydroxyl groups) was added to the solution along with a further 8.0 mL of dichlormethane, and the mixture was placed in an ultrasonic cleaning bath for 1 h. The solution was filtered and washed four times with 10.0 mL of 10 % aqueous hydrochloric acid. The solution was dried over sodium sulfate. The solvent was removed under reduced pressure, and the solid product, 0.52 g (85 %), mp 70.1-71.0 °C (lit. 70-71 °C)¹⁸ was characterized by NMR. ¹H NMR (400 MHz, CDCl₃) δ 7.68 (d, J = 8. Hz, 2H), 7.30 (d, J = 8 Hz, 2H), 6.88 (d, J = 9 Hz, 2H), 6.76 (d, J = 9 Hz, 2H), 3.76 (s, 3H), 2.44 (s, 3H). ¹³C NMR (101 MHz, CDCl₃) δ 158.14, 145.23, 143.03, 132.27, 129.67, 128.53, 123.32, 114.44, 55.75, 21.67. NMR spectra compared favorably with those from the literature.¹⁸

References

1. Morita, J.-I.; Nakatsuji, H.; Misaki, T.; Tanabe, Y., *Green Chemistry* **2005**, *7*, 711-715.
2. Kazemi, F.; Massah, A. R.; Javaherian, M., *Tetrahedron* **2007**, *63*, 5083-5087.
3. Low, W.; White, E. V., *Journal of the American Chemical Society* **1943**, *65*, 2430-2.
4. Bahrami, K.; Khodaei, M. M.; Abbasi, J., *Tetrahedron* **2012**, *68*, 5095-5101.
5. Elchinger, P.-H.; Montplaisir, D.; Zerrouki, R., *Carbohydrate Polymers* **2012**, *87*, 1886-1890.
6. Gericke, M.; Schaller, J.; Liebert, T.; Fardim, P.; Meister, F.; Heinze, T., *Carbohydrate Polymers* **2012**, *89*, 526-536.
7. Heinze, T.; Dicke, R.; Koschella, A.; Kull, A. H.; Klohr, E.-A.; Koch, W., *Macromolecular Chemistry and Physics* **2000**, *201*, 627-631.
8. Granstroem, M.; Kavakka, J.; King, A.; Majoinen, J.; Maekelae, V.; Helaja, J.; Hietala, S.; Virtanen, T.; Maunu, S.-L.; Argyropoulos, D. S.; Kilpelainen, I., *Cellulose (Dordrecht, Netherlands)* **2008**, *15*, 481-488.
9. Hueckel, W.; Honecker, O., *Justus Liebigs Annalen der Chemie* **1964**, *678*, 10-19.
10. Qureshi, Z. S.; Deshmukh, K. M.; Bhanage, B. M., *Sonochemistry: Theory, Reactions, Syntheses, and Applications* **2010**, 157-187.
11. Zhang, L.; Belova, V.; Wang, H.; Dong, W.; Mohwald, H., *Chemistry of Materials* **2014**, Ahead of Print.
12. Zhang, J.; Xu, X.-D.; Wu, D.-Q.; Zhang, X.-Z.; Zhuo, R.-X., *Carbohydrate Polymers* **2009**, *77*, 583-589.
13. Guo, Z.; Tong, W.-L.; Chan, M. C. W., *Chemical Communications (Cambridge, United Kingdom)* **2014**, *50*, 1711-1714.
14. Galynker, I.; Still, W. C., *Tetrahedron Letters* **1982**, *23*, 4461-4.
15. Jalalian, N.; Petersen, T. B.; Olofsson, B., *Chemistry - A European Journal* **2012**, *18*, 14140-14149, S14140/1-S14140/63.
16. Lakshman, M. K.; Singh, M. K.; Kumar, M.; Chamala, R. R.; Yedulla, V. R.; Wagner, D.; Leung, E.; Yang, L.; Matin, A.; Ahmad, S., *Beilstein Journal of Organic Chemistry* **2014**, *10*, 1919-1932, 14 pp.
17. Wilson, D. A.; Wilson, C. J.; Moldoveanu, C.; Resmerita, A.-M.; Corcoran, P.; Hoang, L. M.; Rosen, B. M.; Percec, V., *Journal of the American Chemical Society* **2010**, *132*, 1800-1801.

18. Veisi, H.; Atae, M.; Fatolahi, L.; Lotfi, S., *Letters in Organic Chemistry* **2013**, *10*, 111-117.

Chapter 10

Conclusions and Future Work

Conclusions

Part I:

Fullerenes are unique materials with a large complement of desirable properties. Trimetallic Nitride Templated Endohedral Metallo Fullerenes (TNT EMF) are of particular interest due to their possible magnetic and electronic properties. A representative of this family of fullerenes, $\text{Sc}_3\text{N@C}_{80}$, was isolated from other empty cage fullerenes by a series of different reactions with small molecules. This approach was generally compared to the use of reactive stationary phases such as cyclopentadiene functionalized Merrifield resin or amine functionalized silica gel. The state of the art for separation of EMF species is the use of Lewis acids to precipitate the fullerenes of interest. Small molecule functionalization with cyclopentadiene (CP) and diethylene triamine (DETA) compared well with the reactive stationary phase separations. Reaction with small molecules and subsequent separation was generally not as efficient as the reactive stationary phases, but there was no need to prepare the stationary phase, so the methods would be comparable. Functionalization and separation using dimethyl sodium was very fast and efficient. This method is comparable in terms of efficiency with the Lewis acid separation.

The Prato reaction, which employs an azomethyne ylide intermediate, is a powerful reaction for the functionalization of fullerenes. Several reactions of this type were used to functionalize C_{60} adding hydroxyl functional groups to the fullerene cage. The mono-adducts were used to synthesize alkynyl esters which were subsequently used in an attempted reaction to

produce a fullerene diad. A series of adducts were characterized by cyclic voltammetry. It was determined that as the number of adduct moieties increased, the more negative the first reduction potential of the resulting fullerenes were. This data was used to choose one of the adducts for use in producing a photovoltaic device. The photovoltaic device prepared had an open circuit voltage of approximately 200 mV under AM 1.5 light, and the short circuit current increased after the device had been annealed at 110 °C. This indicates desired morphological changes in the bulk heterojunction of the device.

The Bingel reaction is a second method often used to add functional groups to fullerenes. Following the literature precedent of adding Meldrum's acid malonate to C₆₀ several reactions were undertaken to exploit the Meldrum's acid functionality. Upon heating to temperatures above 150 °C, Meldrum's acid thermally degrades and loses a molecule of water and a molecule of acetone to form a ketene. The ketene moiety is very reactive and was used to form a dimer from the reaction of the C₆₀ mono-adduct of Meldrum's acid with itself. Bis-adducts of Meldrum's acid and C₆₀ were used to form oligomeric poly(fullerides) up to a degree of polymerization of 6, as shown by MALDI TOF MS.

Part II

Bisimidazolium salts were synthesized and titrated by ITC to determine their binding behavior with crown ether and cryptand hosts in solution. The alkylene linked bisimidazolium salts complexed very poorly with dibenzo-24-crown-8 in acetonitrile solution. The xylylene linked bisimidazolium guest had a much higher association constant for its interaction with dibenzo-24-crown-8, as well as dibenzo-30-crown-10, and the cryptand based on that crown ether. The highest association constants were measured for the phenylene linked bisimidazolium guest.

Polymeric guests were synthesized and titrated with ITC to determine their binding characteristics in solution with several types of hosts including small molecules and polymeric hosts. Paraquat functionalized polymers, including paraquat terminated polystyrene, paraquat terminated poly(methyl methacrylate), and a polyviologen, were titrated with small molecule and polymer functionalized hosts. Titration of the same host with both poly(methyl methacrylate) and polystyrene functionalized paraquat species illustrated the effect of the presence of a polar polymer chain as the association constant decreased significantly from the polystyrene to the poly(methyl methacrylate) titrations. Paraquat terminated polystyrene samples with different molecular weights were titrated with dibenzo-30-crown-10 based cryptand. These titrations, run in chloroform, showed the highest association constants measured for a binding system with a paraquat and that host. It was also observed that as the molecular weight of the polymer chain increased, the change in entropy due to binding also increased for the set of titrations.

Part III

Four different monomers and their subsequent homopolymers were synthesized that contained an imidazolium moiety in the repeat unit. These monomers were synthesized for controlled polymerization by ROMP. The monomers and polymers were characterized by their glass transition temperatures (T_g) and DC conductivities. The monomers showed very low glass transition temperatures, and high ionic conductivities. The polymers showed higher glass transition temperatures, and lower ionic conductivities compared to previous group work with acrylate and methacrylate polymers.

The tosylation reaction is an extremely useful reaction for the organic chemist. The ability to convert an alcohol or phenol moiety to a tosyl leaving group is necessary for many organic transformations. The removal of residual tosyl chloride from reaction mixtures can be

problematic. It was found that the residual starting material could be removed by reacting it with the hydroxyl groups on a cellulosic substrate. This secondary reaction can be accomplished simply by the addition of filter paper to the reaction mixture after the original substrate has reacted. The tosyl functionalized filter paper can then be removed mechanically and the base used in the reaction can be removed via aqueous washing to provide high the intended product in high yield and purity.

Future Work

Part 1

The work presented in Chapter 2, dealing with the purification of TNT EMF species should be extended to explore the reaction of dimethyl sodium with empty cage fullerenes. This reaction should provide similar materials to those available from the reaction of empty cage fullerenes with alkyl lithium or Grignard reagents. Methyl sulfoxide functionalized fullerenes are not otherwise known from this type of reaction.

The use of ketene functionalized fullerenes should also be explored further. Ketenes are very reactive intermediates, and can form products with many different functional groups including alcohols, carboxylic acids, amines, and alkenes. The reaction of these different moieties with fulleroid ketenes could potentially produce many new materials with interesting properties.

Part II

Further investigation should be made into the viability of systems that use bisimidazolium guests with crown ether type hosts. The association constants determined for the phenylene linked bisimidazolium salts with dibenzo-30-crown-10 based cryptand were

significant and show promise for future work with this type of guest. The synthesis of asymmetric species of this form will be important if it is to compete with guests such as paraquat.

The effects of polymer chain length on the apparent binding constant for a paraquat terminated polymer and either a small molecule or polymer functionalized host should be exhaustively explored. The set of titrations discussed in Chapter 7 of this work should be extended to higher molecular weight species, and possibly binding between host and guest terminated polymers of different lengths. This type of study would provide an invaluable model for the study of non-covalently linked polymeric systems that might provide materials with highly desirable properties.

Part III

The family of monomers and polymers synthesized in Chapter 8 should be extended to include monomers based off of the oxanorbornene carboxylic acid analogue to the norbornene carboxylic acid substrate. This basis for the ROMP monomer may provide materials with lower glass transition temperatures, and higher ionic conductivities. A secondary monomer should also be found and used to produce ABA triblock copolymers from the best imidazolium containing monomers to make ion conductive membranes for electroactive devices.

Appendix A

Size Exclusion Chromatography Instrumentation

Introduction

Instrumentation and the physical measurements made on chemical compounds used and synthesized in the laboratory are vitally important to the science of chemistry. Not only is the chemist's skill in synthesis important in the lab, but skill and ability to use instruments and interpret the data produced by those instruments is crucial to the dissemination of research in any field of chemistry. The Gibson Group at Virginia Tech has a very diverse set of interests, and consequently requires the use and maintenance of several unique instruments. In this chapter, the construction, calibration, and use of a Size Exclusion Chromatography (SEC) or Gel Permeation Chromatography (GPC) instrument is described

Gel permeation chromatography (GPC) or size exclusion chromatography (SEC) is a powerful method used for the measurement of the molecular weight characteristics of polymers. This instrument can measure both the average and range of molecular weights of soluble polymers, based upon their hydrodynamic volume in comparison to known standards. SEC is different from most chromatographic methods in that there should be no enthalpic interaction between the analyte molecules and the stationary phase of the column. Separation is accomplished by eluting molecules through a packed column containing small porous particles as a stationary phase. As the molecules elute through the column, those with a small enough hydrodynamic volume will spend some time occupying the pores in the stationary phase. In this way, smaller molecules are retained on the column for longer periods of time than larger molecules. For a given column or set of columns, the pore size average and distribution tend to dictate the ability to separate molecules of different molecular weight. If the pore size is

relatively small, only lower molecular weights will be resolved, and all molecules with a hydrodynamic volume larger than the pore size will elute together in the excluded zone. If the pore size is larger, molecules with higher molecular weights will be resolved. In this case small molecules will be poorly resolved because they are all smaller than the smallest pore size and thus totally permeate the column.¹ A schematic representation of SEC separation ranges is given in **Figure A.1** below.

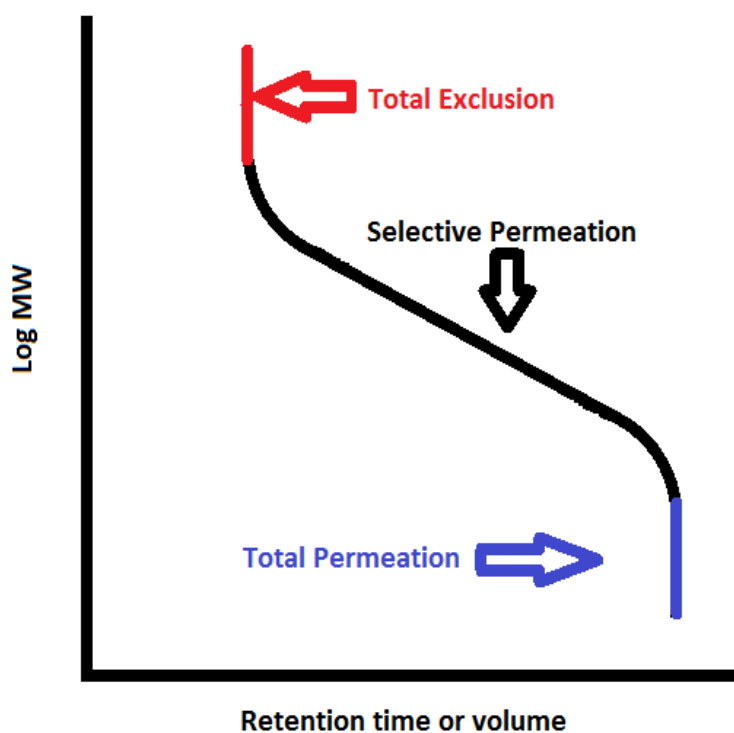


Figure A.1. Generic plot showing the exclusion and permeation limits of SEC columns.

For this reason, sets of multiple columns are usually used in order to separate a larger range of molecular weights. The Styragel type columns, manufactured by Waters Co., use several

columns with differing pore sizes.² Some columns manufactured by Polymer Labs use a mixture of particles with different pore sizes.³ Both of these types of columns have been used in the Gibson lab. The instrument used in the Gibson Group lab was constructed from several different components. A general schematic of the instrument is shown in **Figure A.2**. Two HPLC type pumps were used to provide solvent for an autosampler, column set, and a UV-Vis detector. The components were made by Waters, Hitachi, HP, and Polymer Labs.

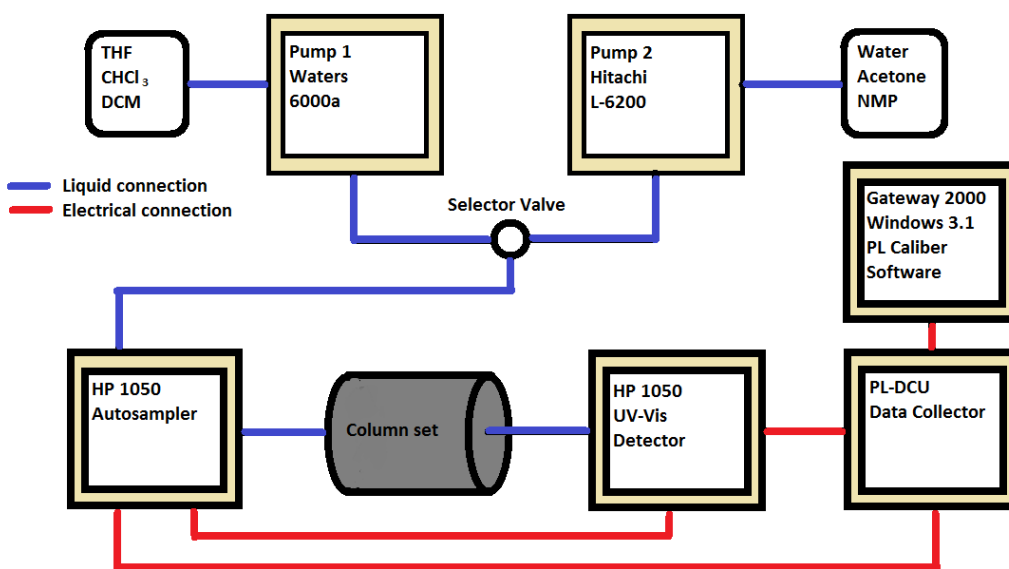


Figure A.2. Component schematic of the Gibson lab SEC instrument including liquid and electric connections.

Pumps

Two solvent pumps were used in the instrument. The first pump was a Hitachi L-6200 single solvent pump. This pump is digitally controlled, and uses two pistons in series to pump solvent. This design requires only two check valves, but since the pistons must move at different speeds, cam timing is important. This pump was fitted with a solvent selector valve to enable the choice between three solvents. N-Methylpyrrolidone (NMP) was the initial solvent selected for this

pump as it tends to work better with more viscous solvents, like NMP. Water and acetone were also selected to make the transition between NMP and other solvents easier. The second pump was a Waters 6000a pump. This pump came equipped with a solvent selector valve capable of handling three solvents. Chloroform and tetrahydrofuran (THF) were initially selected for this pump. Dichloromethane was later added. The selection of different solvents greatly extends the usefulness of this instrument. Different types of polymers require different solvents for analysis. By including several options, different column sets can be used, and the instrument can be used to analyze more samples. A six-way injection valve was used as a high pressure selector valve for the two pumps. The single output from the selector valve was connected to the autosampler.

Autosampler

An HP 1050 series autosampler was used to introduce samples into the system. Beyond the advantages of sample sequencing, the use of an autosampler increases the accuracy and precision of the instrument in general. Samples are measured and injected mechanically, and, therefore, sample size is very consistent.⁴ The autosampler is also used to trigger the collection of chromatographic data. While using a standard sample loop may reduce the need for automatic injections, automatic triggering of both the detector and the data collector increases the accuracy of retention times, and since SEC calibration depends on retention time, automatic triggering is nearly requisite. In SEC separations run with this instrument, a small amount of a small molecule (toluene) was added to all samples to measure the average flow rate of the separation. Toluene elutes in the totally permeated volume, and will not interfere with the detection of larger polymers and oligomers. The toluene peak is then labeled as a flow marker. The PL Caliber software then corrects for any variation in retention times caused by changes in the flow rate. The variation in the flow marker retention times across multiple sample runs was generally less

than one percent after the installation of the autosampler. The autosampler was also connected to the UV-Vis detector and rebalances the detector before and after every run, providing a consistent starting point for all chromatograms.

Detector

The detector used in this instrument was an HP 1050 multiple wavelength detector. The original short path (0.3 mm) flow cell was exchanged for a modified Hitachi flow cell with a longer path length (5.0 mm). This exchange increased the sensitivity of the instrument such that smaller samples could be analyzed. The detector was fit with a deuterium lamp as a UV source, and was capable of monitoring up to two different wavelengths during a chromatogram. The spectral range of the detector was 190 to 600 nm.⁵ For most separations, the wavelength monitored was 254 nm.

Software

The software and control program is Polymer Laboratories (PL) Caliber version 6.0 run in a Windows 3.1 operating system. The software, along with the PL Caliber data acquisition module, converts the detector signal into usable calibration and measurement data. The software communicates with the data collector, which is connected electronically to the detector and the autosampler. Once a series of samples is programmed into the software, as well as the autosampler, the instrument can run autonomously. The autosampler controls sample injection and rebalancing the detector. The Caliber software communicates with the data collector which is also triggered by the autosampler. Once a set of columns has been standardized using a mixture of different molecular weight polystyrene species, unknown polymer samples are separated using the same conditions, and the calibration data are used by the software to calculate the unknown samples' molecular weights and distributions.⁶

Calibration

The instrument in the Gibson lab separates and analyzes polymers based solely on their hydrodynamic volume as compared to standardized polystyrene. Without a universal method such as light scattering, viscometry, or osmotic pressure, a set of columns must be calibrated before any useful data can be generated from them. Calibration in this case comes from the separation of two mixtures of different polystyrene standards, and the plotting of the resulting data to generate a calibration curve relating molecular weight to retention time. The mixtures used are from the EasiCal kit and contain polystyrenes with molecular weights ranging from 580 to 377,400 Daltons (M_n). This is therefore the practical molecular weight range of the instrument, if the column set is capable of separation. Two samples are separated, and each contains 5 different molecular weight polymers. A general representation of the stacked chromatograms is shown below in **Figure A.3**. The first five peaks in each trace are different narrow molecular weight polystyrene bands. The last overlapping peak is the toluene flow marker peak. Toluene was added to all samples for calibration and the measurement of unknowns. As a small molecule with a molecular weight outside the calibration range, toluene is retained on the column longer than polymer and most oligomer analytes. The retention time of toluene is used as a flow marker for the generated chromatograms. Unknown samples are spiked with toluene, and the retention time is compared with that measured during calibration. A flow rate correction factor is then calculated based on the difference in retention times for toluene. This scalar factor is then applied to the entire unknown chromatogram so as to reduce the error associated with variable flow rates. This is very important due to the fact that calibration of this system, and all subsequent measurements are based on an analyte's retention characteristics. Using a flow marker peak can also help diagnose pump failures. With electronic triggering for

data recording, and consistent conditions, it is not unusual for the difference in flow marker retention times to be less than 0.1 % when compared to the calibration standard. All calibration curves were fit using a third order polynomial. The line equations are shown in the plot figures.

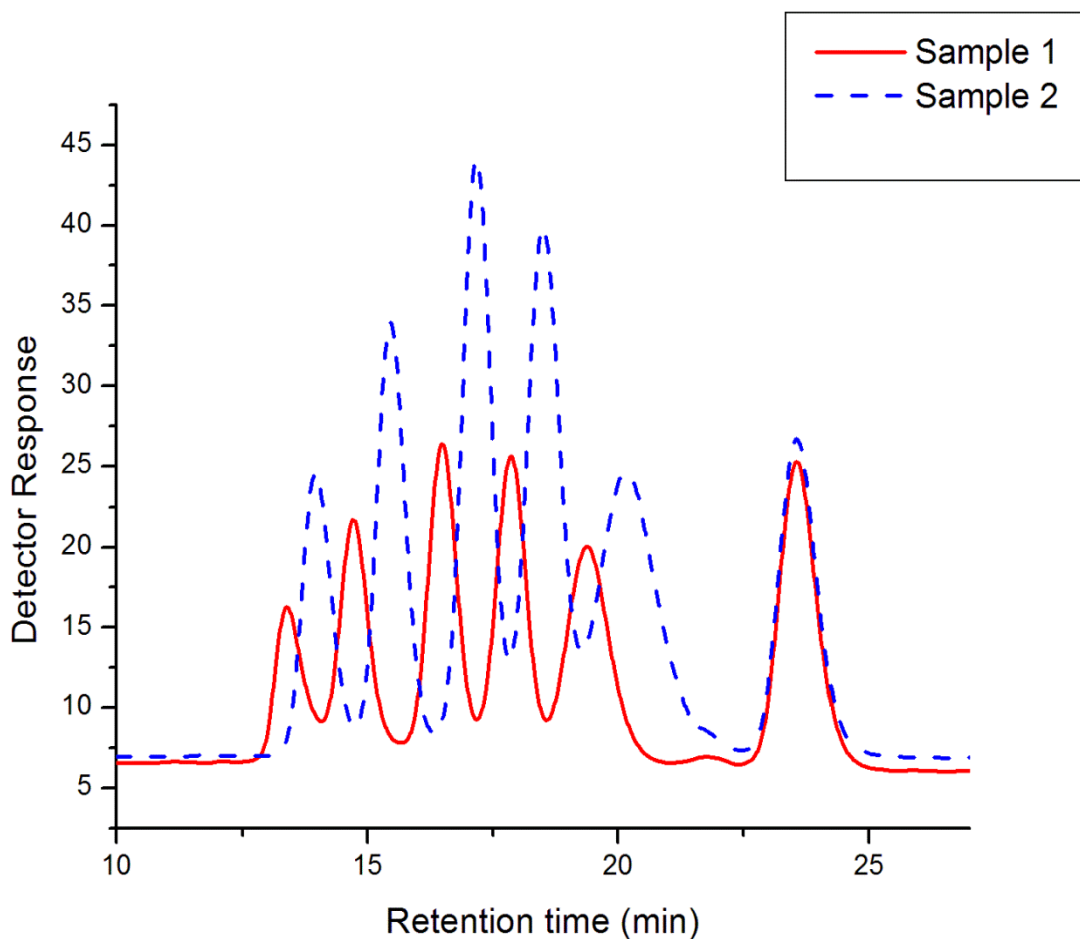


Figure A.3. Superimposed calibration chromatograms with toluene flow marker peak.

Eight sets of size exclusion columns were evaluated, and if possible, calibrated for use with the instrument. The column types and system conditions are described in the next sections.

Set 01: PolymerLabs Mixed-C columns with 5 micron particle size.

This column set was used with a chloroform mobile phase. The detected wavelength was 254 nm, and the flow rate was 1 mL/min. This set of columns separated well. The calibration chromatograms are shown below in **Figure A.4**. This set of columns uses a mixed bed of particles with a wide distribution of pore sizes. It is a two-column set and separates fairly well and fairly quickly. The molecular weight range for this column set is up to 2×10^6 Da per Agilent³ and thus it easily exceeds the limits of the calibration standards.

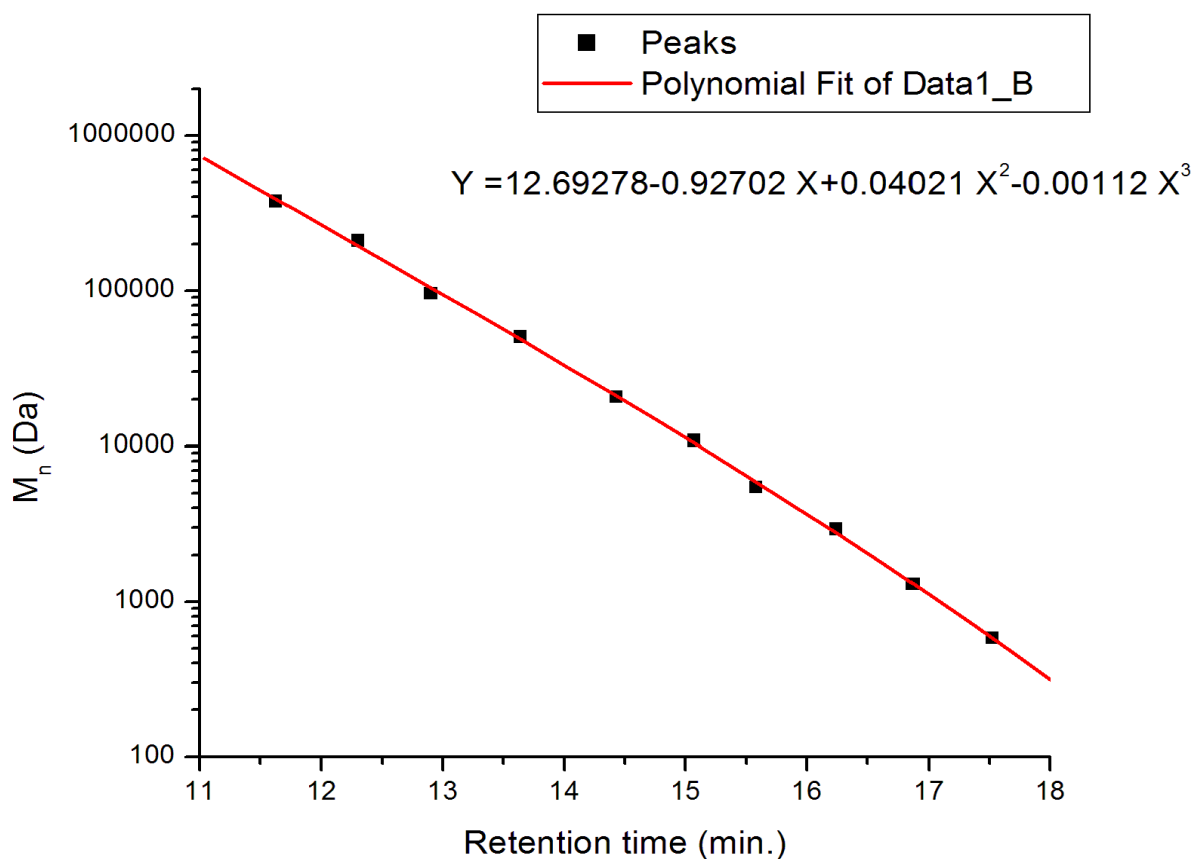


Figure A.4. Calibration curve for column Set 01.

Set 02: two columns of the PLGel Mixed-D type.

This kind of column has a smaller molecular weight range than the Mixed-C columns of Set 01. This set also does not separate as well as Set 01. The calibration curve shown in **Figure A.5** reveals that the retention times are not as long, and the resolution of the chromatograms was not as good for Set 02. The molecular weight range of this column set, according to the manufacturer is up to 4×10^5 Da which just barely covers the molecular weight range of the set of standards used. This set of columns worked, but not as well as other sets.

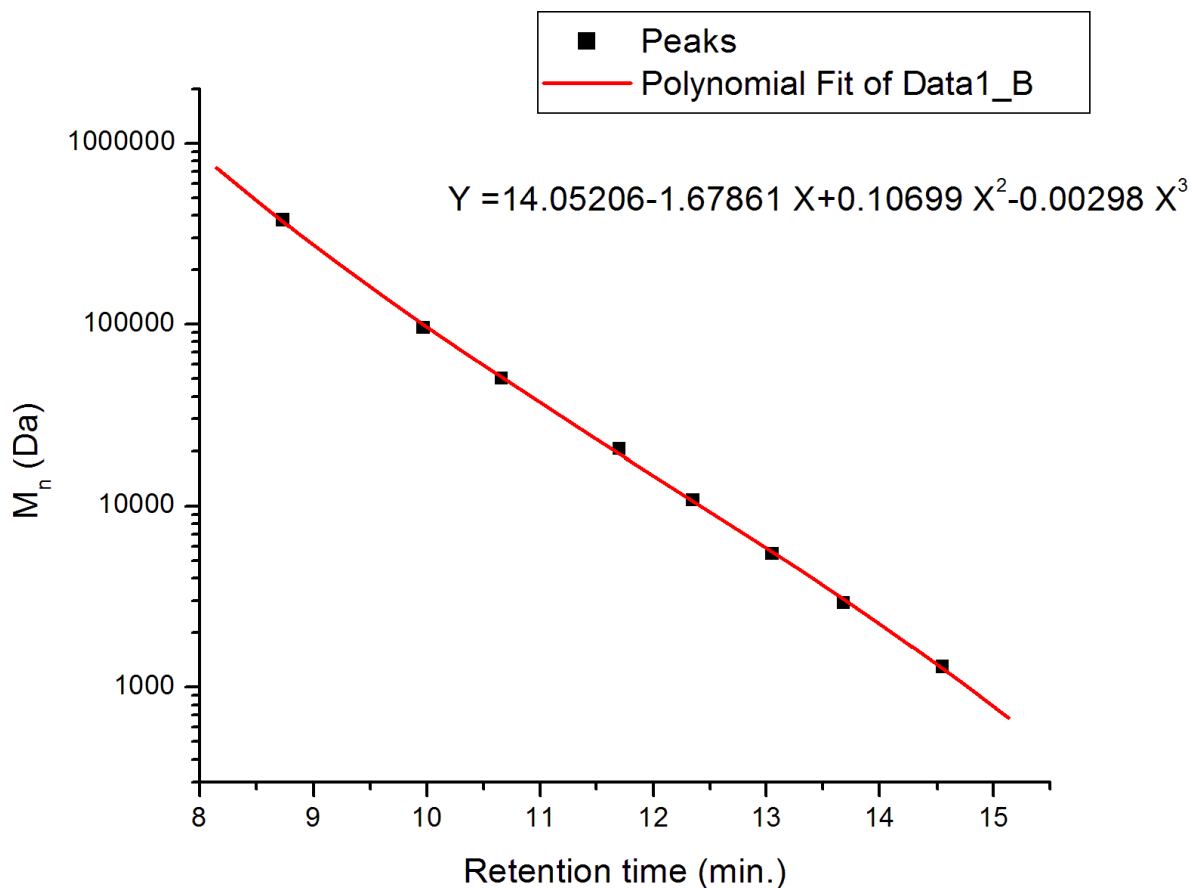


Figure A.5. Calibration curve for column Set 02.

Set 03: three-column set of PLGel columns.

Instead of being mixed bed columns like Set 01 and Set 02, Set 03 is classified by a larger particle size (10 μm instead of 5 μm), and pore sizes between 100 and 10^5 \AA . This should give the column set a molecular weight range of 500 to $2 \times 10^6 \text{ Da}$. The calibration curve is not linear, but does not suggest that the exclusion or total saturation limits are being approached by the calibration standards. Calibration and sample analysis also take longer due to the fact that this set has a third column. The calibration curve is shown below in **Figure A.6**.

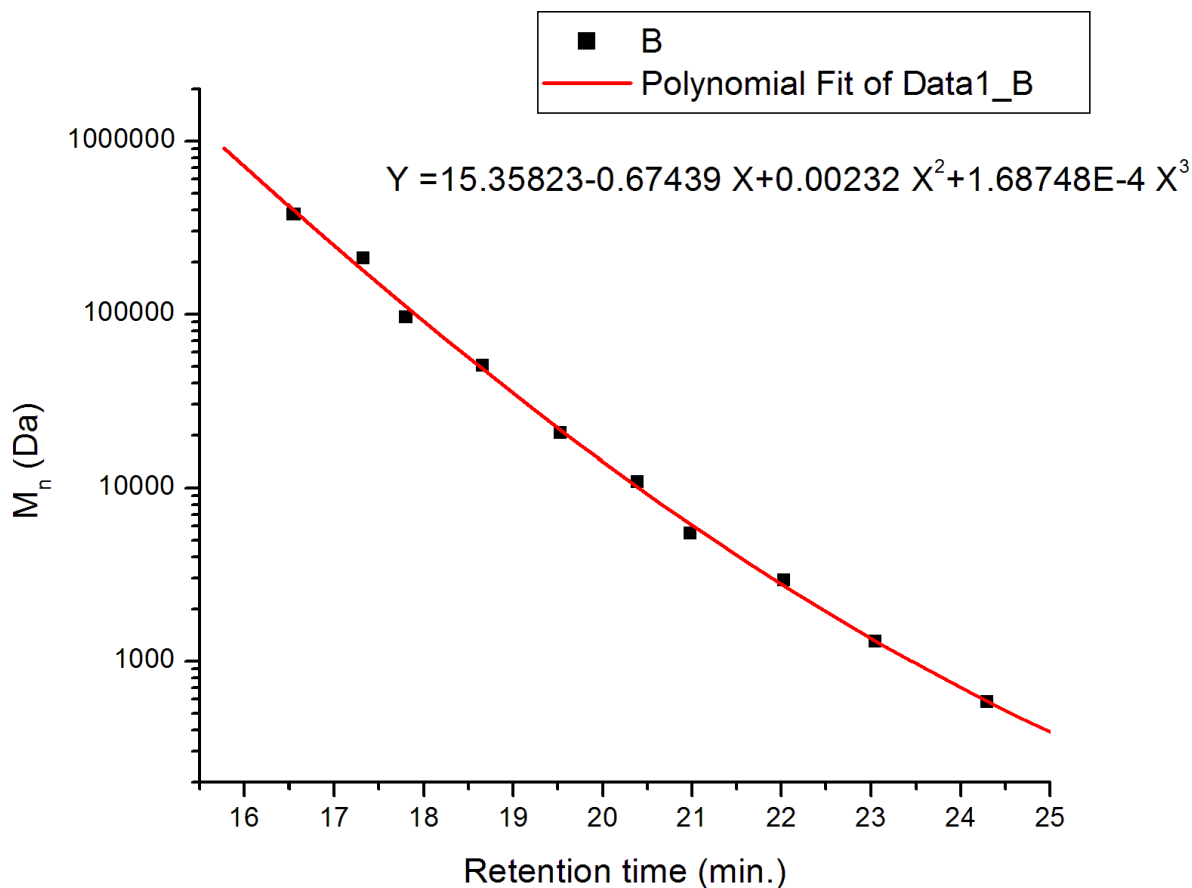


Figure A.6. Calibration curve for column Set 03.

Set 04: two column set of $\mu\text{Styragel HT } 10^3$ and 10^4 \AA

Column Set 04 was originally labeled as dead by a previous user; however, after conditioning, separation was achieved. The HT designation for these columns refers to their ability to function over a wider temperature range and a larger range of solvents than other Styragel type columns. The effective separation range for this two column set is from 200 to 6×10^5 Da.² The column set was conditioned using THF, and has also been used with a solution of lithium TFSI salt in THF. The separation of standards on this column set is slower than Set 05, which has the same manufacturer designation, but the resolution is acceptable. The calibration curve for Set 04 is shown below in **Figure A.7**.

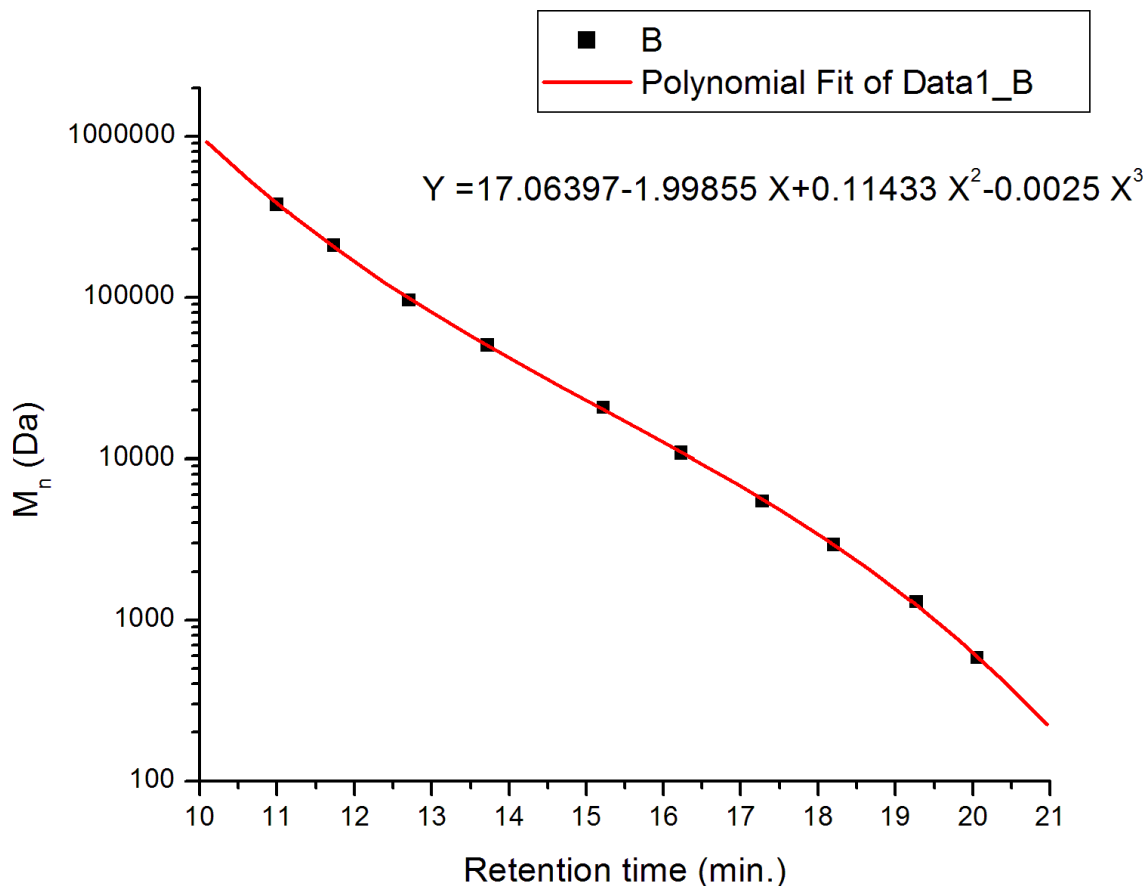


Figure A.7. Calibration curve for column Set 04.

Set 05; two column set of μ Styragel HT 10^3 and 10^4 Å

Sets 04 and 05 are labeled identically from the manufacturer. The calibration curve shown below is for Set 05. These two column sets have pore sizes from 10^3 to 10^4 Å.² The effective separation range is from 200 Da to 6×10^5 Da. The calibration curve shows some sigmoidal character that may be indicative of both the exclusion and permeation limits. These columns are fast though, and separate well enough to be used in the lab. The calibration plot is given in **Figure A.8**.

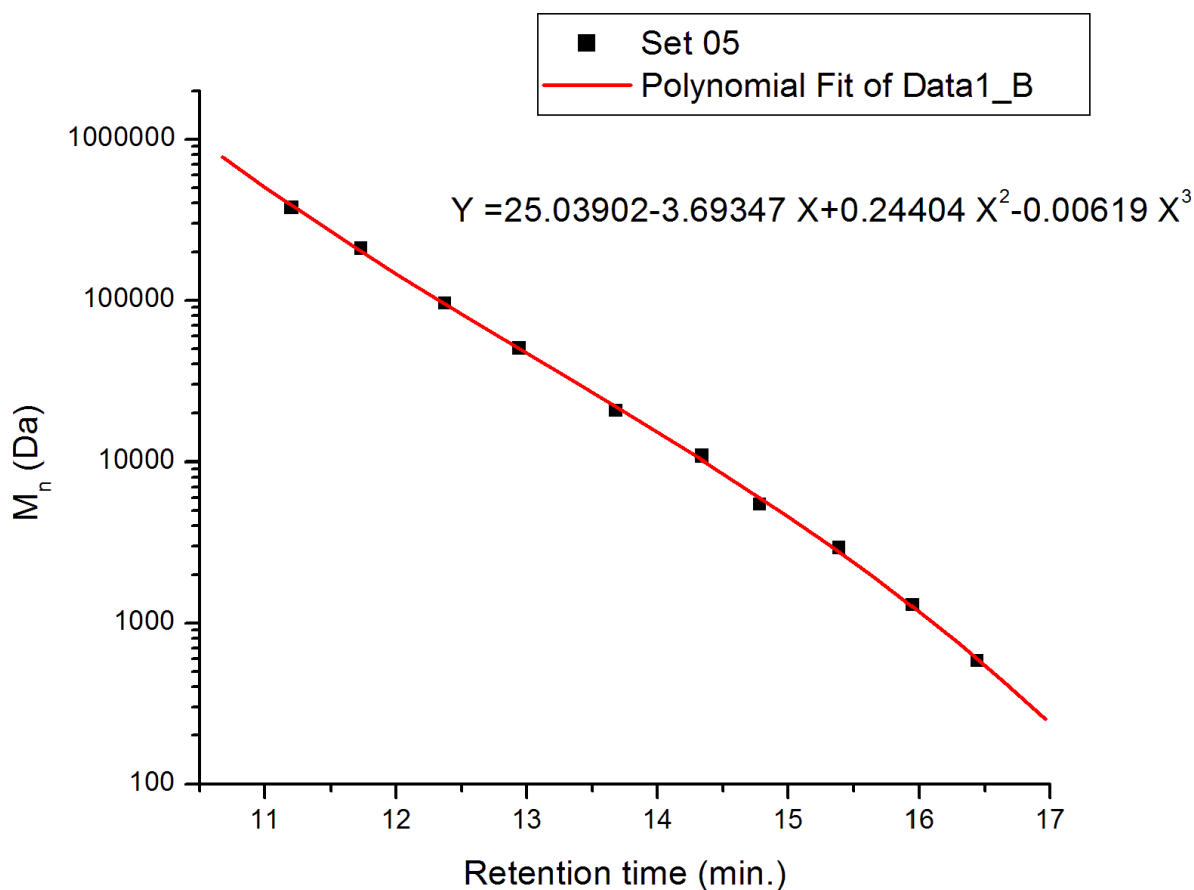


Figure A.8. Calibration curve for column Set 05.

Set 06: a three-column set designated HT 2, 3, and 4

Column Set 06 is intended for high temperature analysis. According to Waters they have a molecular weight range of 200 Da to 1×10^7 Da. The calibration curve shown in **Figure A.9** seems to show a sigmoidal shape indicative of the exclusion and permeation limits being approached. The column set is useful and works well enough; however, it may not have the full range that it originally possessed. Again, as this is a three-column set, the analysis takes longer than that of a two column set.

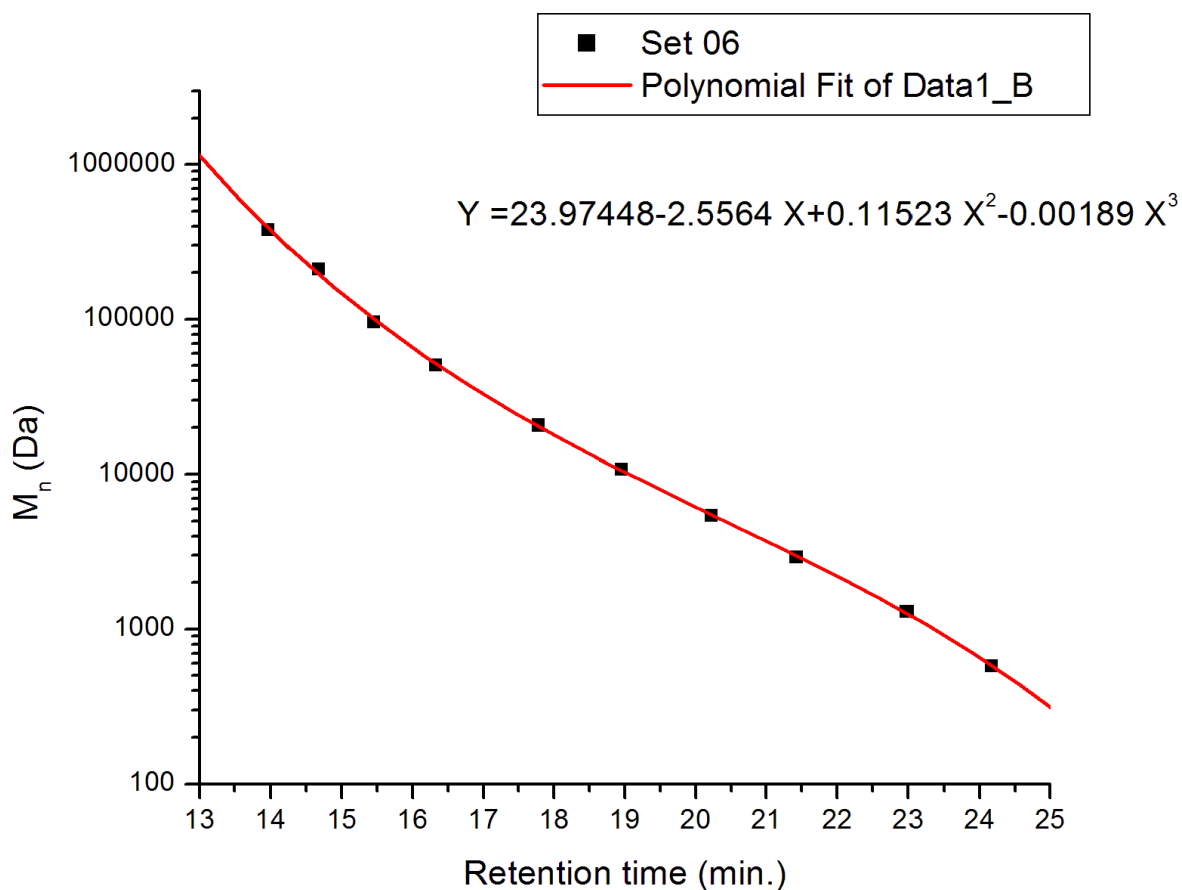


Figure A.9. Calibration curve for column Set 06.

Set 07: 5 columns in sequence that range from 100 to 10^5 Å pore size

Column Set 07 is the largest set. The columns are Ultra Styragel type, which indicates that they also have smaller particle sizes than comparable Styragel or Micro Styragel type columns. Waters suggests that the molecular weight range of this column set should be 50 Da to 4×10^6 Da. The inclusion of two smaller pore size columns (100 and 500 Å) suggests that this column set should be very good at separating smaller polymers and oligomers. The calibration curve, shown in **Figure A.10**, is more linear than the previous column set, and does show good separation for smaller polymers. Since this column set was so long, a flow rate of 1.5 mL/min was used instead of the standard 1 mL/min used for all the other analyses.

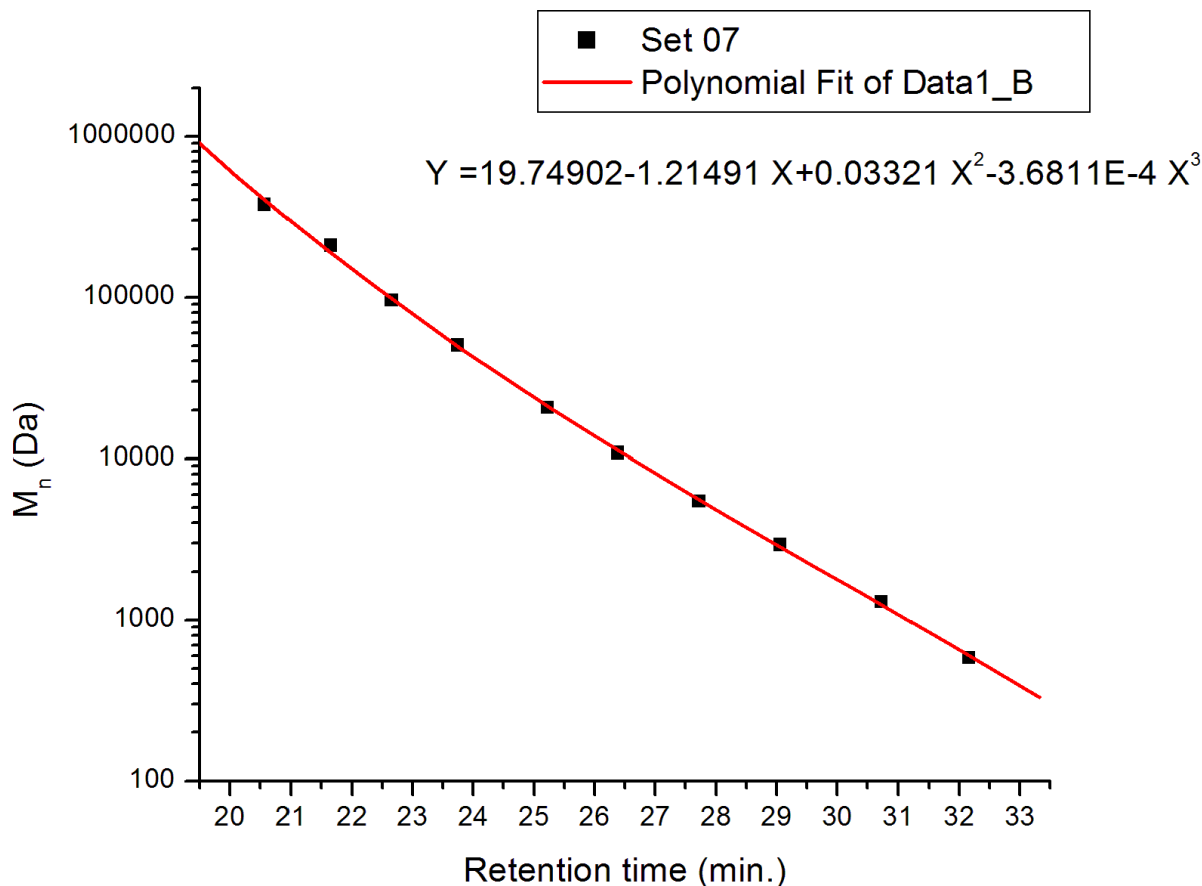


Figure A.10. Calibration curve for column Set 07.

Set 08: HR 4E and 5E

Finally, Set 08 was used with NMP and either LiBr or LiCl to separate charged polymers. This polar solvent and salt are used to mask the charges on ion-containing polymers so that standard SEC conditions can be used. These columns were also used with a column oven that was built for the purpose of analyzing ionic polymers at high temperatures. The designation HR means that these should be high resolution columns. The calibration curve, shown in **Figure A.11** is nearly linear; however, the resolution of the chromatograms was less than for other column sets. The calibration does not appear to change significantly at elevated temperatures either.

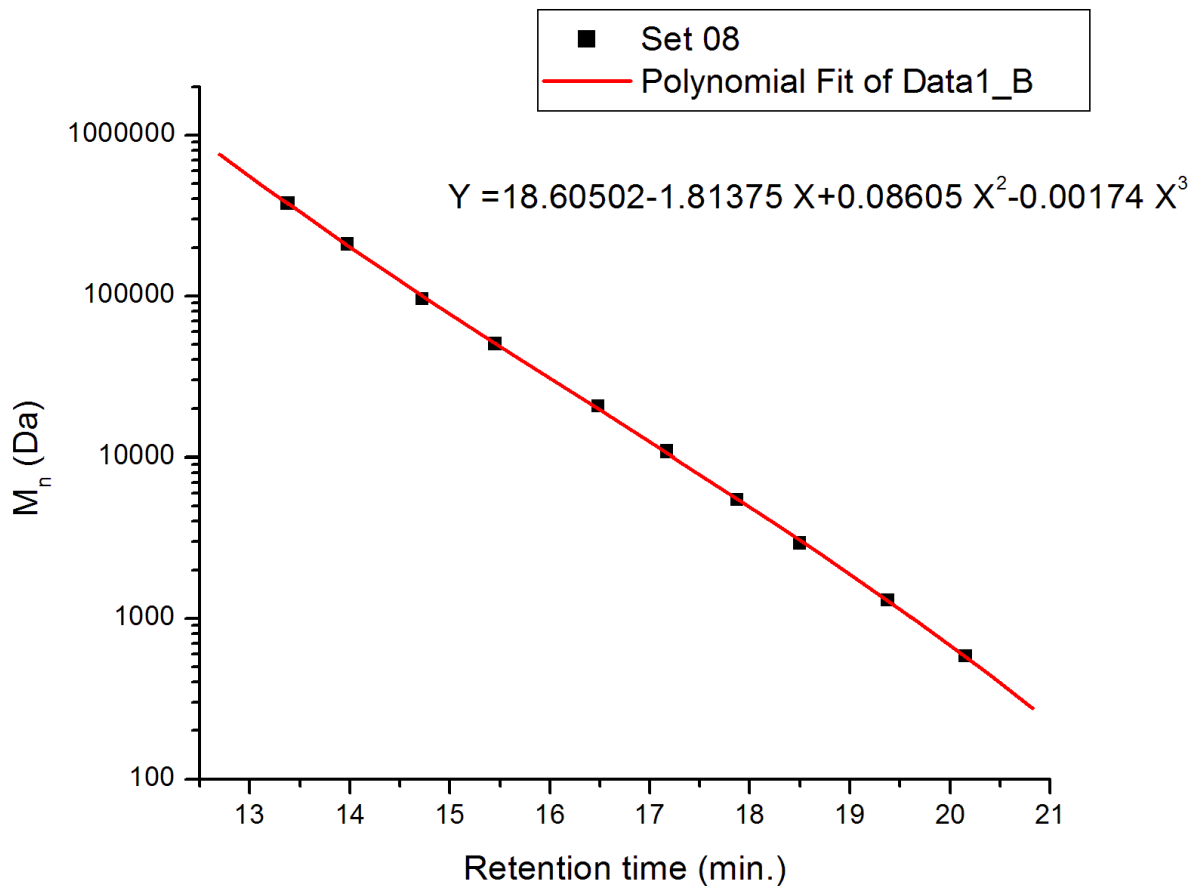


Figure A.11. Calibration curve for column Set 08.

Conclusions

A capable SEC instrument was constructed from several different components, made by at least four different manufacturers. The components were combined together to enable autosampling, and to allow several different solvents to be used. Eight different column sets were calibrated for use with the instrument and catalogued for their various uses. The resulting instrument is, within the bounds of its capabilities, accurate and precise.

References

1. Miller, J. M., *Chromatography Concepts and Contrasts*. Second ed.; Wiley Interscience: Hoboken, New Jersey, 2005.
2. Styragel Column Care and Use Manual. Waters Co.: USA, 1990.
3. Organic SEC/GPC Product Guide. Inc., A. T., Ed. Agilent Technologies Inc.: 2012.
4. HP 1050 Series Autosampler Instruction Kit. Hewett Packard Co. : FRG, 1990.
5. HP 1050 Series Multiple Wavelength Detector Instruction Kit. Hewett Packard Co.: FRG, 1990.
6. PL Caliber GPC/SEC Software User's Guide. Polymer Laboratories Inc.: Amherst, Massachusetts, 1995.